OPTIMIZING MANUFACTURING FACTORS IN MESENCHYMAL STROMAL CELL EXTRACELLULAR VESICLE PRODUCTION FOR APPLICATIONS IN NEURODEGENERATIVE DISEASE

by

COURTNEY CAMPAGNA

(Under the Direction of Leidong Mao)

ABSTRACT

Mesenchymal stromal cells (MSCs) offer significant therapeutic potential for neurodegenerative diseases, owing to their intrinsic immunomodulatory properties. However, several risks associated with MSCs, such as heterogeneity, thrombosis, uncontrolled differentiation, and the need for invasive application procedures, pose significant challenges to their use in clinical settings. Fortunately, MSCs secrete extracellular vesicles (MSC-EVs) that carry similar immunomodulatory potential as their parent cells. MSC-EVs are heterogeneous, non-replicating particles characterized by a lipid bilayer, and they are shed from the MSC plasma membrane. The immunomodulatory effects of MSC-EVs are driven by the bioactive cargo they carry, including proteins, RNAs, DNAs, enzymes, and other molecules. MSC-EVs offer advantages over their parent cells by avoiding many of the risks associated with MSCs, including the challenges posed by living cells. Additionally, MSC-EVs can be easily taken up by other cells and can cross the blood-brain barrier, making them an attractive therapeutic option for neurodegenerative diseases. However, challenges remain in the standardization of MSC-EV manufacturing processes and bioactivity assessment, limiting their clinical application. This

dissertation aims to address these challenges by examining how different manufacturing conditions affect MSC-EV characteristics, with the goal of identifying standardized methods for their production. We first investigated how different priming conditions influenced the generation of bioactive MSC-EVs, focusing on their potential use in neurodegenerative disease applications. To do this, we developed a human brain pericyte morphological assay to screen MSC-EVs. Using this assay, we identified optimal priming conditions (e.g., cytokines and oxygen levels) and culture platforms (flasks versus bioreactors) for producing immunomodulatory MSC-EVs. Additionally, we compared the physical and functional characteristics of MSC-EVs isolated using tangential flow filtration and ultracentrifugation from four different MSC lines derived from two tissue sources (bone marrow and adipose tissue). While we observed differences in the size and concentration of MSC-EV populations and their cargo, the functional properties (e.g., pericyte morphology, macrophage IL-6 secretion) of the vesicles were largely unaffected by the isolation method used. Overall, this work provides key insights into the manufacturing of MSC-EVs and highlights important considerations for developing standardized production methods for their use in neurodegenerative disease therapies.

INDEX WORDS: Mesenchymal Stromal Cell-Extracellular Vesicles (MSC-EVs), MSC-EV Manufacturing, Priming, Neurodegenerative Disease

OPTIMIZING MANUFACTURING FACTORS IN MESENCHYMAL STROMAL CELL EXTRACELLULAR VESICLE PRODUCTION FOR APPLICATIONS IN NEURODEGENERATIVE DISEASE

by

COURTNEY CAMPAGNA

BS, Worcester Polytechnic Institute, 2020

A Dissertation Submitted to the Graduate Faculty of The University of Georgia in Partial Fulfillment of the Requirements for the Degree

DOCTOR OF PHILOSOPHY

ATHENS, GEORGIA

2024

OPTIMIZING MANUFACTURING FACTORS IN MESENCHYMAL STROMAL CELL EXTRACELLULAR VESICLE PRODUCTION FOR APPLICATIONS IN NEURODEGENERATIVE DISEASE

by

COURTNEY CAMPAGNA

Major Professor:	Leidong Mao
Committee:	Kyung Sung
	Neil Grimsey
	Luke Mortensen
	Cheryl Gomillion

Electronic Version Approved:

Ron Walcott
Vice Provost for Graduate Education and Dean of the Graduate School
The University of Georgia
December 2024

ACKNOWLEDGEMENTS

This journey has been transformative, and I am immensely grateful to everyone who supported me along the way.

To my parents, thank you for your unwavering support and encouragement. You have shaped me into the person I am today, providing me with the guidance and resilience I needed to persevere, even during the most challenging times.

To my siblings, Paige, Michael, and Sara, thank you for always being there. Paige, your straightforwardness and drive to overcome obstacles have been inspiring. Michael, thank you for encouraging me to take breaks, step outside, and enjoy life (even if fishing wasn't my strong suit). Sara, your unmatched humor and adventurous spirit, even when on crutches, made every visit memorable. To my dog, Tucker, though you can't read, you taught me the value of curiosity and the importance of taking a moment to listen to the world around me.

To my friends in Georgia, thank you for enriching my life here. Kanupriya, our animated conversations, late-night lab sessions, and your encouragement to step outside my comfort zone have been invaluable. Andrew, thank you for all the adventures, last-minute hikes, listening to my rants, and always being there for Tucker. Thomas, thank you for your unique perspective and endless good times. To everyone else who filled my life with laughter and unforgettable experiences, I will always cherish our time together.

To my colleagues at the FDA, thank you for making my experience truly enriching. Kyung and Johnny, I am immensely grateful for your mentorship. You taught me the value of my scientific voice and encouraged me to steer my research with confidence. Mona, thank you for your

constant support, our daily lunch chats, weekend adventures, dance lessons, and your patience with my endless questions. I also want to thank everyone in the Sung Lab for the camaraderie, idea exchanges, and the sense of belonging you provided.

To my roommate, Morgan—thank you for making the transition to Maryland so much smoother. I'll always cherish our late-night talks, hiking adventures, and endless dog discussions.

This experience has had both its highs and lows. But without everyone mentioned here and many more that were not, I am so thankful for this experience and the influence you all imparted on me.

TABLE OF CONTENTS

Page

LIST OF TABLES

Page

LIST OF FIGURES

Page

CHAPTER 1

INTRODUCTION

Neurodegenerative diseases are currently the leading cause of disease burden worldwide, with their prevalence rising at an exponential rate [1]. According to the United States Food and Drug Administration (FDA), these diseases are defined as "a heterogeneous group of disorders characterized by progressive degeneration of the structure and function of the central or peripheral nervous systems" [2]. Neurodegenerative diseases result in the loss of neurons and axons, leading to significant physical and behavioral impairments.

Among the various neurodegenerative diseases, Alzheimer's Disease (AD) and Parkinson's Disease (PD) are the most common, affecting over 6.2 million people as of 2022 [3]. This burden is expected to grow, with AD projected to impact 75 million people by 2030 and PD expected to affect 1.64 million individuals globally by 2037 [4, 5]. Alzheimer's Disease is a progressive neurodegenerative form of dementia, characterized by the accumulation of amyloid-beta (Aβ) plaques, oligomers, and tau proteins [6]. These factors are thought to contribute to neuronal apoptosis, though the exact cause of AD remains unidentified [6]. Similarly, Parkinson's Disease is a progressive neurodegenerative disorder that primarily affects dopaminergic neurons in the substantia nigra, resulting in both cognitive and functional deficits [7]. Like AD and many other neurodegenerative diseases, the precise cause of PD remains unknown.

These diseases not only severely impact patients' quality of life but also place a heavy economic burden on society. In 2020, the annual cost of neurodegenerative diseases in the United States

reached $655 billion [8]. The healthcare costs associated with AD and PD alone were estimated at $305 billion and $51.9 billion, respectively, in the same year [9]. As the incidence of neurodegenerative diseases continues to rise, associated healthcare spending is expected to increase substantially.

Despite the rapidly increasing burden of neurodegenerative diseases, there are no cures, and current treatments only address symptoms rather than the underlying pathology [1, 9]. For Alzheimer's Disease (AD), available treatments include cholinesterase inhibitors (CIs) and N-methyl-D-aspartate (NMDA) antagonists [10]. CIs help preserve cholinergic function in the basal forebrain, which is among the first systems affected in AD, leading to cognitive decline through neuron loss and enzyme dysfunction [10]. NMDA antagonists aim to protect neurons from excitotoxicity associated with AD. While these treatments may improve cognition, they are not effective for all patients, and often fail to alleviate behavioral and psychological symptoms [10]. Parkinson's Disease (PD) is primarily treated with dopaminergic medications, including Levodopa, dopamine agonists, and monoamine oxidase B inhibitors. These therapies convert to dopamine in the brain, stimulate dopamine receptors, or inhibit dopamine metabolism, respectively [11]. However, like AD treatments, they do not address the root causes of the disease, allowing its progression and necessitating additional medications to manage various symptoms [11].

Although neurodegenerative diseases have distinct physiological mechanisms, they both exhibit neuroinflammation as a common characteristic [12]. Neuroinflammation involves a complex network of pro-inflammatory processes, including increased production of cytokines, chemokines, reactive oxygen species, and secondary messengers, as well as the activation of CNS cells such as microglia, astrocytes, endothelial cells, pericytes, and peripheral immune cells

[13, 14]. While neuroinflammation is intended to maintain CNS homeostasis by clearing debris, combating pathogens, and supporting regeneration, dysregulated inflammation can lead to tissue dysfunction and degeneration [14]. It has been identified as a key factor in the progression of neurodegenerative diseases [15].

Neuroinflammation is commonly studied at the blood-brain barrier (BBB), which forms the microvasculature of the central nervous system and serves as the interface between brain tissue and the bloodstream [16]. This barrier plays a critical role in maintaining homeostasis by regulating the trafficking of nutrients and waste to and from the brain [16]. However, during periods of heightened inflammation, the BBB often becomes compromised. The BBB is composed of various cells, including endothelial cells, pericytes, and astrocytes, which contribute to its formation, repair, and maintenance. Each cell type plays a specialized role in preserving BBB integrity. For instance, pericytes, located within the basement membrane of the endothelial tube, regulate vessel contractility, angiogenesis, and immune responses [16].

As neuroinflammation is a hallmark of neurodegenerative diseases, it has become a focal point for the development of therapeutic treatments. Stem cells, particularly mesenchymal stromal cells (MSCs), have gained attention due to their multipotent, neurotrophic, and immunomodulatory properties [17]. MSCs, which can be derived from various tissue sources (e.g., bone marrow, adipose tissue, placenta, umbilical cord, and dental pulp), have the capacity to differentiate into multiple cell types, including cartilage, adipose tissue, and bone[18, 19]. Preclinical and clinical studies have demonstrated the ability of MSCs to modulate the inflammatory response and facilitate tissue repair through direct and indirect cellular interactions [18, 19]. For example, in a diabetic cardiomyopathy (DCM) mouse model, the intravenous injection of human bone marrow MSCs significantly reduced cardiac injury by suppressing

NLRP3 activation, lowering inflammatory factors (IL-8, IL-1β, ROS), and downregulating pyroptosis-related proteins (NLRP3, Caspase-1, GSDMD [20]. Similarly, human umbilical cord MSCs administered to monkeys with acute liver failure reduced hepatic inflammation and monocyte activation, leading to improved liver function [21]. MSCs have also shown promise in treating neurodegenerative diseases. For instance, in a study of Alzheimer's disease, clinical-grade human umbilical cord MSCs administered to SAMP8 mice (a model of accelerated senescence) improved cognitive and behavioral outcomes by decreasing hyperphosphorylated tau expression, improving neurofibrillary tangles, reversing spine loss, and promoting synaptic plasticity [22]. Furthermore, a study by Jalali et al. demonstrated that Wharton's Jelly-derived MSCs significantly increased neuronal survival, enhanced the expression of brain-derived neurotrophic factor and nerve growth factor, and improved hippocampal function in a Parkinson's disease rat model [23].

Despite the therapeutic potential of MSCs, several challenges remain regarding their clinical application. Risks associated with MSC-based therapies include thromboembolism, tumorigenicity, and undesirable differentiation [24-26]. Additionally, the efficacy of MSC therapies can be influenced by manufacturing processes such as media composition, culture platforms, and storage conditions [24]. In the context of neurodegenerative diseases, the administration of MSCs directly into the brain is often required, which is an invasive procedure with significant risks [27]. Intravenous administration can also result in MSCs becoming trapped in the lungs, limiting their effectiveness [28]. Fortunately, MSCs secrete extracellular vesicles (EVs), which retain the same immunomodulatory properties as their parent cells and represent a promising alternative.

MSC-EVs are small membrane-bound particles that carry functional molecules, such as RNA, DNA, enzymes, and proteins, derived from their parent cells [29]. These molecules are believed to be responsible for the EVs' immunomodulatory potential. Unlike MSCs, EVs do not carry the risks of tumorigenicity or thrombosis since they are non-living and can be sterilized and stored [30]. Additionally, MSC-EVs can cross the BBB, allowing for intravenous administration [31, 32]. Preclinical studies have shown promising results for MSC-EVs in the treatment of neurodegenerative diseases. For example, Gschwendtberger et al. demonstrated that human MSC-derived exosomes had protective effects on ALS transgenic primary motor neurons, improving neuron survival and preserving healthy morphology [33].

Despite their potential, several challenges must be addressed before MSC-EVs can be widely used as therapeutics. The yield and functionality of MSC-EVs are greatly influenced by the characteristics of the parent cells, including cell confluence, passage number, oxygen concentration, cytokine exposure, medium composition, and culture platform (2D vs. 3D) [34]. Furthermore, storage conditions and isolation methods can significantly impact MSC-EV physiology [34-36]. Additionally, MSC-EVs are intrinsically variable due to the heterogeneity of their parent cell sources. While the International Society for Extracellular Vesicles provides recommendations for MSC-EV manufacturing and bioactivity assessment, these guidelines allow for significant flexibility, leaving many critical decisions to the individual researcher [34, 37]. This variability, combined with the lack of standardized manufacturing and assessment protocols, complicates efforts to identify MSC-EVs' mechanisms of action and contributes to batch-to-batch differences in bioactivity and therapeutic efficacy [38]. Therefore, the development of standardized MSC-EV manufacturing processes and bioactivity assessment protocols is crucial.

Many scientists have employed complex methods, such as *in vivo* animal models, to evaluate potential neurodegenerative therapeutics. However, these approaches are often expensive, require specialized training, and lack reproducibility. Utilizing model cells for therapeutic screening, such as investigating the potential of MSC-EVs in mitigating neuroinflammation, offers a cost-effective, rapid, and accessible alternative. Brain pericytes, with their multifaceted roles in maintaining homeostasis and responding to inflammatory conditions, offer a promising cellular model for this purpose, potentially contributing to the development of standardized methods to evaluate the role of MSC-EVs in mediating neuroinflammation.

Pericytes are multipotent, heterogeneous cells located throughout the basement membrane of brain vasculature within the BBB. Within the vasculature and central nervous system (CNS), they perform critical functions, including regulating blood vessel growth and maturation, maintaining structural integrity, controlling permeability, and modulating cerebral blood flow [39-42]. Beyond their role in vascular homeostasis, pericytes significantly influence immune responses during CNS neuroinflammation. They regulate leukocyte recruitment, facilitate phagocytosis and endocytosis, influence the polarization of parenchymal immune cells (e.g., microglia and astrocytes), and contribute to both innate and adaptive immune responses [43-46].

Given their pivotal role in mediating blood-brain barrier functions and interacting with various cells during inflammation, pericytes are uniquely suited for studying the BBB's overall response to neuroinflammatory conditions. Their diverse and integral functions in vascular regulation and immune modulation highlight their potential as a cost-effective, rapid, and reproducible cellular model. This makes them invaluable for advancing neurodegenerative research and standardizing the evaluation of MSC-EVs for therapeutic applications.

This project aims to contribute to the standardization of MSC-EV manufacture and characterization so that they may be widely sed as neurogenerative disease therapeutic agents. To achieve this, we investigated the effects of different manufacturing conditions, including cell priming and isolation methods, on MSC-EV bioactivity. This was accomplished using our developed pericyte-based morphological assay designed to quantify the bioactivity.

Chapter two provides an overview of current MSC-EV bioactivity assessment methods, including existing platforms (e.g., monocultures, in vivo models) and emerging technologies (e.g., microphysiological systems). This review evaluates how these models align with or fall short of the requirements for future FDA approval of MSC-EV therapeutics for neurodegenerative diseases.

Chapter three discusses an MSC-EV bioactivity platform that we developed using human brain pericyte morphological screening as a readout. We hypothesized that inflammatory pericytes (treated with TNF-α) would return to their basal morphology following MSC-EV treatment. This study explored how different priming conditions of the parent bone marrow MSCs resulted in MSC-EVs with varying bioactivities. We then compared the morphological changes in pericytes to proteomic changes in pericyte secretion before and after MSC-EV treatment to elucidate MSC-EV modulation of pericyte function.

Chapter four focuses on a key aspect of MSC-EV manufacturing: isolation methods. Using four MSC cell lines (two adipose-derived and two bone marrow-derived), we compared the physical (size and concentration) and functional characteristics (RNA and proteomic profiles) of MSC-EVs isolated via ultracentrifugation and tangential flow filtration.

Finally, chapter five summarizes the main findings of this dissertation, outlines future research directions, and discusses the potential contributions of this work to the scientific community.

1.1 REFERENCES

1. Steinmetz, J.D., et al., *Global, regional, and national burden of disorders affecting the nervous system, 1990–2021: a systematic analysis for the Global Burden of Disease Study 2021.* The Lancet Neurology, 2024. **23**(4): p. 344-381.
2. CBER, *Human Gene Therapy for Neurodegenerative Diseases* U.S. HHS, Editor. 2022. p. 1-16.
3. Sciences, N.I.o.E.H. *Neurodegenerative Diseases*. 2022; Available from: https://www.niehs.nih.gov/research/supported/health/neurodegenerative#:~:text=Neurodegenerative%20diseases%20affect%20millions%20of,Alzheimer's%20Disease%20Association%20in%202022.
4. Tay, L.X., et al., *Economic Burden of Alzheimer's Disease: A Systematic Review.* Value in Health Regional Issues 2024. **40**: p. 1-12.
5. Yang, W., et al., *Current and projected future economic burden of Parkinson's disease in the U.S.* npj Parkinson's Disease, 2020. **6**: p. 15.
6. *Addressing Unmet Needs in Alzheimer Disease: Implications of Delayed Diagnosis and Examing New and Emerging Therapies.* The American Journal of Managed Care 2020. **24**(8, Sup).
7. Foundation, T.P.s. *What is Parkinson's*. 2024; Available from: https://www.parkinson.org/understanding-parkinsons/what-is-parkinsons.
8. Thorpe, K.E., A.I. Levey, and J. Thomas *U.S. Burden of Neurodegenerative Disease*. 2021.

9. Hernando, S., et al., *Targeting the central nervous system: From synthetic nanoparticles to extracellular vesicles—Focus on Alzheimer's and Parkinson's disease.* WIREs Nanomedicine and Nanobiotechnology 2023. **15**(5): p. e1898.

10. Yiannopoulou, K.G. and S.G. Papageorgiou, *Current and future treatments for Alzheimer's disease.* Therapeutic Advances in Neurological Disorders, 2013. **6**(1): p. 19-33.

11. Rizek, P., N. Kumar, and M.S. Jog, *An update on the diagnosis and treatment of Parkinson disease.* Canadian Medical Association Journal, 2016. **188**(16): p. 1157-1165.

12. Kolliker-Frers, R., et al., *Neuroinflammation: An Integrating Overview of Reactive-Neuroimmune Cell Interactions in Health and Disease.* Mediators of Inflammation 2021. **2021**: p. 9999146.

13. Alexander, J.J., et al., *The complement cascade: Yin–Yang in neuroinflammation – neuro–protection and –degeneration.* Jornal of Neurochemistry 2008. **107**(5): p. 1169-1187.

14. DiSabato, D., N. Quan, and J.P. Godbout, *Neuroinflammation: The Devil is in the Details.* Journal of Neurochemistry, 2016. **139**: p. 136-153.

15. Zhang, W., et al., *Role of neuroinflammation in neurodegeneration development.* Signal Transduction and Targeted Therapy, 2023. **8**.

16. Daneman, R. and A. Prat, *The Blood-Brain Barrier.* Cold Spring Harbor Perspectives in Biology 2015. **7**(1): p. a020412.

17. Branscome, H., et al., *Use of Stem Cell Extracellular Vesicles as a "Holistic" Approach to CNS Repair.* Frontiers in Cell and Developmental Biology, 2020. **8**: p. 455.

18. Zhou, J. and Y. Shi, *Mesenchymal stem/stromal cells (MSCs): origin, immune regulation, and clinical applications.* Cellular and Molecular Immunology 2023. **20**: p. 555-557.

19. Zhou, T., et al., *Challenges and advances in clinical applications of mesenchymal stromal cells.* Journal of Hematology & Oncology, 2021. **14**: p. 24.

20. Yang, Q., et al., *Mesenchymal stem cells ameliorate inflammation and pyroptosis in diabetic cardiomyopathy via the miRNA-223-3p/NLRP3 pathway.* Diabetology & Metabolic Syndrome, 2024. **16**: p. 146.

21. Guo, G., et al., *Peripheral infusion of human umbilical cord mesenchymal stem cells rescues acute liver failure lethality in monkeys.* Stem Cell Research & Therapy, 2019. **10**: p. 84.

22. Jia, Y., et al., *HGF Mediates Clinical-Grade Human Umbilical Cord-Derived Mesenchymal Stem Cells Improved Functional Recovery in a Senescence-Accelerated Mouse Model of Alzheimer's Disease.* Advanced Science, 2020. **7**(17): p. 1903809.

23. Jalali, M.S., et al., *Transplanted Wharton's jelly mesenchymal stem cells improve memory and brain hippocampal electrophysiology in rat model of Parkinson's disease.* Journal of Chemical Neuroanatomy 2020. **110**: p. 101865.

24. Barkholt, L., et al., *Risk of tumorigenicity in mesenchymal stromal cell based therapies—Bridging scientific observations and regulatory viewpoints.* Cytotherapy, 2013. **7**(2013): p. 753-759.

25. Breitbach, M., et al., *Potential risks of bone marrow cell transplantation into infarcted hearts.* Blood, 2007. **110**(4): p. 1362-1369.

26. Tatsumi, J., et al., *Tissue factor triggers procoagulation in transplanted mesenchymal stem cells leading to thromboembolism.* Biochemical and Biophysical Research Communications, 2013. **431**(2): p. 203-209.

27. Boltze, J., et al., *The dark side of the force – constraints and complications of cell therapies for stroke.* Frontiers in Neurology 2015. **6**.

28. Kallmeyer, K., et al., *Fate of systemically and locally administered adipose-derived mesenchymal stromal cells and their effect on wound healing.* Stem Cells Translational Medicine, 2020. **9**(1): p. 131-144.

29. Seo, Y., H.-S. Kim, and I.-S. Hong, *Stem Cell-Derived Extracellular Vesicles as Immunomodulatory Therapeutics.* Stem Cells International, 2019. **2019**.

30. Toh, W.S., et al., *Immune regulatory targets of mesenchymal stromal cell exosomes/small extracellular vesicles in tissue regeneration.* Cytotherapy, 2018. **20**(12): p. 1419-1426.

31. Banks, W.A., et al., *Transport of Extracellular Vesicles across the Blood-Brain Barrier: Brain Pharmacokinetics and Effects of Inflammation.* International Journal of Molecular Sciences, 2020. **21**(12): p. 4407.

32. Matsumoto, J., et al., *Transmission of α-synuclein-containing erythrocyte-derived extracellular vesicles across the blood-brain barrier via adsorptive mediated transcytosis: another mechanism for initiation and progression of Parkinson's disease?* Acta Neuropathologica Communications 2017. **5**(1): p. 71.

33. Gscwendtberger, T., et al., *Protective effects of EVs/exosomes derived from permanently growing human MSC on primary murine ALS motor neurons.* Neuroscience Letters, 2023. **816**: p. 137493.

34. Lener, T., et al., *Applying extracellular vesicles based therapeutics in clinical trials – an ISEV position paper.* Journal of Extracellular Vesicles, 2015. **4**: p. 30087-30087.

35. Wiklander, O.P.B., et al., *Extracellular vesicle in vivo biodistribution is determined by cell source, route of administration and targeting.* Journal of Extracellular Vesicles, 2015. **4**(1): p. 26316.

36. Brennan, K., et al., *A comparison of methods for the isolation and separation of extracellular vesicles from protein and lipid particles in human serum.* Scientific Reports, 2020. **10**: p. 1039.

37. Welsh, J.A., et al., *Minimal information for studies of extracellular vesicles (MISEV2023): From basic to advanced approaches.* Journal of Extracellular Vesicles, 2024. **13**(2).

38. Lam, J., K.E. Sung, and S.S. Oh, *Science-based regulatory considerations for regenerative medicine cellular produces.* Current Opinion in Biomedical Engineering 2022. **21**: p. 100361.

39. Kang, T.-Y., et al., *Pericytes enable effective angiogenesis in the presence of proinflammatory signals.* Proceedings of the National Academy of Sciences, 2019. **116**(47): p. 23551-23561.

40. Dibble, M., et al., *The impact of pericytes on the stability of microvascular networks in response to nanoparticles.* Scientific Reports, 2023. **13**(1).

41. Winkler, E.A., et al., *Blood–Spinal Cord Barrier Pericyte Reductions Contribute to Increased Capillary Permeability.* Journal of Cerebral Blood Flow & Metabolism, 2012. **32**(10): p. 1841-1852.

42. Hall, C.N., et al., *Capillary pericytes regulate cerebral blood flow in health and disease.* Nature, 2014. **508**: p. 55-60.

43. Stark, K., et al., *Capillary and arteriolar pericytes attract innate leukocytes exiting through venules and 'instruct' them with pattern-recognition and motility programs.* Nature Immunology, 2013. **14**(1): p. 41-51.

44. Rustenhoven, J., et al., *Brain Pericytes as Mediators of Neuroinflammation.* Trends in Pharmacological Sciences, 2017. **38**(3): p. 291-304.

45. Matsumoto, J., et al., *TNF-α-sensitive brain pericytes activate microglia by releasing IL-6 through cooperation between IκB-NFκB and JAK-STAT3 pathways.* Brain Research, 2018. **1692**: p. 34-44.

46. Shibahara, T., et al., *Pericyte-Mediated Tissue Repair through PDGFRβ Promotes Peri-Infarct Astrogliosis, Oligodendrogenesis, and Functional Recovery after Acute Ischemic Stroke.* eneuro, 2020. **7**(2): p. ENEURO.0474-19.

CHAPTER 2

LITERATURE REVIEW: ASSESSMENT OF MSC-EV BIOACTIVITY FOR NEURODEGENERATIVE DISEASE

2.1 INTRODUCTION

Millions of people worldwide are affected by neurodegenerative diseases [1]. Neurodegenerative diseases encompass a range of neurological disorders characterized by diverse clinical and pathological features, leading to loss of neurons and axons within the central nervous system (CNS) and resulting in behavioral and functional deficits [2-4]. Despite the diverse pathologies of neurodegenerative diseases, they can all be characterized by the presence of acute or chronic inflammation [2]. Currently, there are several treatments available for managing neurodegenerative diseases; however, these treatments focus on alleviating symptoms rather than targeting the underlying pathology [3]. Neuroinflammation has been identified as a key factor driving neurodegenerative diseases, involving the production of cytokines, chemokines, reactive oxygen species (ROS), and secondary messengers, which are produced and utilized by cells of the central nervous system such as microglia, astrocytes, endothelial cells, and peripheral immune cells [2, 5]. The effects of neuroinflammation are dependent on the specific context, duration, and cause [5]. When properly regulated neuroinflammation aids in the protection of the brain by clearing debris, fighting pathogens, and aiding in regeneration. However, when inflammation becomes dysregulated or chronic it often leads to tissue dysfunction and degeneration [6]. This dysregulation has been shown to be an important contributor to the progression of neurodegenerative diseases [2]. For example, astrocyte secretion of apolipoprotein-4 (APOE4) has been seen to further promote the inflammatory response by

binding to pericytes inducing the secretion of proinflammatory cyclophilin A, resulting in the activation of nuclear factor kappa-light-chain-enhancer of activated B cells (NF-kB) and matrix metalloproteinase 9 (MMP9), leading to blood-brain barrier (BBB) breakdown (i.e., increased permeability and reduction in tight junction proteins) [7]. In a Parkinson's Disease (PD) model, toll-like receptors were observed activating microglia and increasing the infiltration of CD4+ and CD8+ T cells thereby altering the function of cellular immunity [8]. As inflammation is both a critical component and a common feature of neurodegenerative diseases, it is an attractive target for developing more effective treatments.

Currently treatment for neurodegenerative diseases usually uses a combination of pharmacotherapies that address both physical and psychological symptoms. The main drugs used include cholinesterase inhibitors, N-methyl-D-aspartate (NMDA) receptor antagonists, dopamine receptor antagonists, dopamine precursors, monamine oxidase inhibitors and antipsychotic medications [9]. However, many of these treatments have adverse side effects that limit their tolerability (e.g., gastrointestinal disturbances, bradycardia, dyskinesias, sedation), are not applicable to all disease stages, and are unable to halt disease progression [9]. Due to these limitations, researchers have been increasingly exploring cell-based therapies as a potential option for neurodegenerative diseases. Mesenchymal stromal cells (MSCs), in particular, have gained attention due to their multipotent nature and their neurotrophic and immunomodulatory functions, making them a promising candidate for targeted treatment approaches [10].

MSCs are heterogeneous, multipotent cells derived from multiple sources such as adipose tissue, bone marrow, dental pulp, and umbilical cord tissue [11]. MSCs have demonstrated the ability to migrate, engraft, and repair tissues, by exerting their immunomodulatory effects, making them a

promising candidate for treating a range of diseases, including Traumatic brain injury (TBI), graft-verse-host disease, and type 1 diabetes [12]. Studies have demonstrated that MSCs can interact with both the innate and adaptive immune systems, modulating inflammation by shifting macrophages from a pro-inflammatory M1 phenotype to an anti-inflammatory M2 phenotype, and by inhibiting natural killer cells, which increases Tregs expansion [13]. Nonclinical models, such as those for TBI, have shown that MSCs can promote neural stem cell proliferation and decrease proinflammatory cytokine expression [14]. The promising results of MSCs in in nonclinical studies have led to over 516 current ongoing clinical trials with 22 studies focused on the treatment of neurodegenerative diseases (https://clinicaltrials.gov/ ; October 2024) (Table 2.1).

While MSCs have shown significant therapeutic potential and are generally considered safe, certain challenges remain. These include rare but serious risks such as undesired differentiation, thromboembolic events, or ectopic tissue formation, particularly at higher doses or in more complex conditions [15-17]. In addition, MSC manufacturing processes, including culture conditions, duration of cell multiplication, and physiological stress, can increase the risk of chromosomal aberrations [15]. For the treatment of neurodegenerative disease, direct administration of cells into the brain significantly increases the risk of complications. However, when MSCs are administered intravenously, they have sometimes been reported to become trapped in the lungs [18, 19]. To mitigate some of these challenges, researchers are exploring MSC-derived extracellular vesicles (EVs) as a potential alternative. MSC-EVs carry similar immunomodulatory effects as their parent cells but may reduce risks like thromboembolic events and undesired differentiation. However, challenges remain regarding their manufacturing and long-term efficacy.

MSC-EVs are heterogeneous, non-replicating particles shed from the parent cells' plasma membrane and characterized by a lipid bilayer, which may contribute to their safety profile [20, 21]. They can be sterilized and stored without cryopreservatives, and are not associated with the same risks as transplanted cells (i.e., tumorgenicity, thrombosis) [22]. In addition, MSC-EVs can cross the BBB, allowing less invasive administration methods for neurodegenerative diseases. They encapsulate functional molecules, including transcription factors, small and large non-coding regulatory RNAs, lipids, enzymes, and proteins which can be transferred to recipient cells [23-28]. Currently, there are six MSC-EV treatment clinical trials listed on ClinitalTrials.gov (https://www.clinicaltrials.gov/ ; October 2024) - none of which focus on neurodegenerative disease (Table 2.1). However, nonclinical studies have shown promising results, with MSC-EVs for the treatment of many neurodegenerative diseases. In Alzheimer's disease (AD) models, MSC-EVs have been shown to increase neurogenesis, recover cognitive deficits, and decrease the activation of microglia in transgenic mice [29, 30]. In PD mice models, MSC-EVs were observed crossing the BBB into the brain parenchyma, where they promoted neuron recovery, reduced apoptosis, and inhibited oxidative stress [31, 32]. Additionally, MSC-EVs have been used in TBI swine and rat models, leading to increased angiogenesis and neurogenesis, as well as reduced inflammation [33, 34].

Despite their potential, MSC-EVs face significant manufacturing challenges. Their quality and bioactivity are influenced by factors such as parent cell conditions (i.e., cellular confluence, passage number, oxygen concentration, cytokines exposure, and medium composition), EV storage conditions (i.e., storage buffer, storage time and temperature), and isolation method (i.e., ultracentrifugation, tangential flow filtration, size exclusion chromatography) [35-38]. MSC-EV's intrinsic variability, due to their heterogeneous cell source, complicates their mechanism of

action [35] and leads to variability in batch preparations bioactivity [39]. Furthermore, most MSC-EVs are isolated from MSCs cultured in 2D environments, limiting scalability [35]. A major challenge is the absence of standardized protocols for producing MSC-EVs and assessing their bioactivity [35, 36, 39]. Although the International Society of Extracellular Vesicles (ISEV) provides recommendations for the definitions, isolation, and characterization of EVs comprehensive and standardized guidelines are still under development, which can pose challenges for consistent quality assessment [20, 35]. While the exact mechanisms by which MSC-EVs act in neurodegenerative diseases are still unclear, advances in systems biology, particularly in transcriptomics and proteomics, are beginning to clarify the functional components of EVs [40, 41]. To fully harness their therapeutic potential, standardized protocols and nonclinical *in vitro* and *in vivo* bioactivity assays must be established to reliably predict the efficacy of MSC-EVs in treating neurodegenerative diseases [35].

2.2 COMMON NEURODEGENERATIVE DISEASE MODELS

With the growing interest in MSC-EVs for neurodegenerative disease therapies, various nonclinical models have been developed to evaluate their therapeutic potential in both *in vivo* and *in vitro* settings (Figure 2.1). Since there is no standardization for assessing MSC-EV bioactivity, study parameters are Determined by individual researchers.

2.2.1 In Vitro Models for Neurodegenerative Disease

In vitro models, often paired with *in vivo* experiments, typically use simple monocultures to assess the therapeutic potential of MSC-EVs. Microglia and neuronal cultures are the most commonly used to model neurodegenerative diseases.

2.2.1.1 Microglia Cultures

Microglia, the central nervous system's resident immune cells, maintain homeostasis by clearing cellular debris, dying cells, misfolded proteins, and foreign substances while protecting neurons [42, 43]. However, they can also contribute to the progression of neurodegenerative diseases by releasing pro-inflammatory cytokines, chemokines, and ROS, as well as activating other resident brain cells and disrupting the BBB [43]. Given their central role in neuroinflammation, microglia are often used to assess MSC-EV applications for these conditions.

In intracerebral hemorrhage models, BV2 murine microglia treated with adipose-derived (Ad) MSC-EVs demonstrated a shift from lipopolysaccharide (LPS) treated pro-inflammatory M1 microglia to an anti-inflammatory M2 state [44]. Similarly, in PD models, bone marrow-derived (BM) MSC-EVs reduced the pro-inflammatory activation of LPS stimulated microglia [45]. In a microglial amyotrophic lateral sclerosis (ALS) model, Ad-MSC-EVs shifted microglia from a proinflammatory M1 phase to an anti-inflammatory M2 phase and reduced their metabolic activity [46].

2.2.1.2 Neuron Cultures

Neurons are highly specialized cells within the nervous system that are responsible for sending and receiving signals for the regulation of movement, sensory input, and consciousness [47]. Neuronal cell death is a shared characteristic for all neurodegenerative diseases, however determining the exact cause of neuronal death has proved challenging [48]. As neurons are key indicators of neurodegenerative disease progression, they serve as an ideal cellular model for assessing the therapeutic efficacy of MSC-EVs.

In a PD study, SY5Y neurons were stimulated with 1-methyl-1-phenylpyridinium (MPP+) as an inflammatory model and treated with BM-MSC-EVs which were shown to attenuate SY5Y cell damage and apoptosis [45]. Another study explored MSC-EV bioactivity on hippocampal neurons after H_2O_2 stimulation to mimic seizures. They found that the MSC-EVs restored the neuronal structure and function and were able to decrease ROS generation and stress-associated molecular patterns [49]. In an AD study, Wharton's jelly-derived MSC-EVs were shown to protect hippocampal neurons from damaged induced by amyloid beta oligomers [50].

2.2.1.3 Challenges of in vitro monocultures

In vitro models offer several advantages, including cost-effectiveness, the ability to be performed in a controlled environment and ease of reproducibility [51]. Both microglia and neurons have important roles in neuroinflammation and neurodegenerative disease, making them promising targets. However, culturing these cells *in vitro* lacks physiological relevance, as it removes both the 3D environment and complex tissue interactions that influence the mechanism by which MSC-EVs would be processed by these cells. Therefore, *in vivo* animal models are used to capture these complex interactions when assessing MSC-EV therapeutic potential.

2.2.2 In Vivo Models for Neurodegenerative Disease

Mice and rats are commonly used *in vivo* models for the assessment of MSC-EVs for neurodegenerative diseases, but porcine models are gaining popularity due to their closer genetic and anatomical similarities to humans (Figure 2.1).

2.2.2.1 Rodent Models

Rat and mouse models have been extensively used in biomedical research due to their physiological and genetic similarities to humans, combined with practical advantages such as their small size, short life cycle, and cost-effectiveness [52]. Additionally, their well-characterized genetic resources and ability to genetically engineer them for specific disease models make them valuable for studying neurodegenerative conditions [52].

In an AD model, Female Wistar albino mice were treated with LPS for one week, followed by BM-MSC-EVs [53]. The BM-MSC-EVs improved cognitive function in the AD mice, as shown by better performance in open-field and Y-maze tests, and reduced brain inflammation, evidenced by decreased tumor necrosis factor alpha (TNF-α), and increased interleukin 10 (IL-10) levels, and reduced levels of Aβ1-42 and tau proteins [53]. In a SOD1(G93A) ALS murine model, Ad-MSC-EVs improved cognitive deficits, reduced glial cell activation, and provided neuroprotection to lumbar motor neurons and neuromuscular junctions [54].

Wistar rats with ouabain-induced focal brain injury were treated with BM-MSCs, which reduced microglia, macrophage, and astrocyte activation, decreased leukocyte extravasation, and lowered pro-inflammatory cytokine and chemokine levels [55]. In another study, BM-MSC-EVs were administered to PD rat models induced by rotenone over 35 days. After 3 weeks of treatment, the rats showed improved cognitive function, neuronal recovery, and reduced oxidative stress compared to the PD group [56]. A different study, Sprague-Dawley rats with Aβ1-42-induced AD were treated with BM-MSC-EVs, leading to reduced Aβ deposition, plaques, and inflammatory cytokines, increased Aβ decomposition-related factors expression, improved cognition, enhanced neuron viability, and reduced apoptosis [57].

2.222 Porcine Models

While rodent models are commonly used, porcine models are gaining preference due to their genetic proximity to humans and the close similarity of their central nervous system (CNS), making them valuable for studying neurodegenerative diseases [58, 59]. Female Yorkshire swine were utilized as a model for severe TBI to evaluate the efficacy of a single-dose treatment of BM-MSC-EVs. The study demonstrated that MSC-EV treatment significantly reduced brain edema, lesion volume, and intracranial pressure, while also attenuating the expression of pro-inflammatory proteins [34]. In a separate TBI study using swine models, MSC-EV treatment was shown to enhance neurogenesis, promote neuron survival and differentiation, and reduce inflammation [60]. Additionally, in a study involving spinal cord injury in swine, the intrathecal administration of autologous MSC-EVs resulted in the restoration of motor function, reperfusion of neural tissue, and remyelination of axons [61].

2.2.2.3 Challenges of Animal Models

Although the use of *in vivo* models allows for the modeling of complex systems that are more physiologically relevant and translatable to humans than basic 2D models, they present several challenges. Animal studies are significantly costly in time and resources, and require high-level training [62]. In addition, although there have been great advances in the genetic modification of many animal models, many therapeutics that show promise in animal fail to translate to human trials [63]. Ethical concerns regarding animal research have also led to a growing movement towards developing more physiologically relevant *in vitro* models when possible. In 1959 the Universities Federation for Animal Welfare published the Principles of Human Experimental Technique which proposed the Three Rs; Replacement, Reduction and Refinement [64]. These

principles state that when possible animals must be replaced with insentient material, the minimal number of animals must be used, and the least harmful procedures must be applied [64].

2.3 MICROPHYSIOLOGICAL MODELS ADVANCING MSC-EV THERAPEUTIC RESEARCH FOR NEUROGENERATIVE DISEASES

Microphysiological systems (MPS) are increasingly recognized for their potential to simulate complex *in vivo* conditions in a controlled, reproducible manner. These microscale cell culture platforms can replicate key physiological parameters such as temperature, pH, mechanical forces, and biochemical stimuli, while incorporating elements like co-cultures, tissue explants, or organoids to model healthy and diseased tissues [65]. There are various types of MPS including but not limited to transwell, organoid, and microfluidic models (Figure 2.2). The flexibility of MPS models makes them especially useful for studying neurogenerative diseases, where they allow for a more accurate representation of cellular interactions and tissue responses than traditional 2D cultures.

2.3.1 Transwell Models

Transwell systems are simpler MPS setups that utilize permeable membranes to separate different cellular environments. They are often used to study cellular permeability and interactions across barriers, such as the BBB and neurovascular unit (NVU), which are critical in neurodegenerative disease like AD, PD, and Huntington's disease (HD). Although transwell models are useful for initial studies, they typically lack the full physiological complexity of other MPS types. For example, Stone et al. developed a human primary cell blood-brain barrier model using astrocytes, pericytes, endothelial cells, and neurons seeded on either side of a permeable membrane to mimic the neurovascular unit. Using this model, they found that their four-cell

model showed increased transendothelial electrical resistance (TEER) in response to dexamethasone, outperforming simpler two- or three-cell models [66]. Other transwell models aid in establishing interactions that cannot be discerned from basic 2D cultures. In an Alzheimer's model, brain endothelial cells were on the apical side, astrocytes on the basolateral side, and with neurons or neurons genetically modified to overexpress amyloid precursor proteins in the well. This model revealed significant decreases in tight junction proteins (ZO-1, claudin-5, occludin-1) in the AD model compared to the control aiding in the understanding of AD pathology [67]. Other transwell models are created with future therapeutic drug assessment in mind. For example, Cai et al., PD was modeled using primary endothelial cells from PD rats on the apical side and astroglia cells on the basolateral side showed irregular morphology, decreased TEER, and increased permeability, suggesting it could be useful for future drug testing in Parkinson's disease as the cellular phenotype and function was closer to *in vivo* conditions [68]. In another PD transwell model, neural stem cells effect on the activation of microglia under different treatments was used to determine the mechanism of action (MOA) finding that the overexpression of nuclear receptor-related protein 1 (Nurr1) may increase grafted NSC survival by attenuating microglia activation [69]. Transwell models have also been used to test different mechanical stimuli. Bolden et al., recapitulated the NVU using astrocytes, BM-MSCs and neurons whereby they moved the transwells into pressurized compartments to create distinct blood/brain environments and tested mechanical stimulus (wall sheer stress) for more accurate *in vitro* therapeutic testing for TBI [70].

2.3.2 Organoid Models

Organoids are another common model of MPS and are 3D structures that mimic the architecture and function of the specific tissue they are modeling. The ASTM International defines organoids

as an "*in vitro*, self-assembled, 3D micro-tissue or organ developed from stem cells that recapitulated tissue or organ micro-anatomy and functionality of *in vivo* tissues or organs" [71]. Organoids have been used to model various neurodegenerative diseases including AD, PD, and HD as the self-organization inherent in the creation of these models is believed to better recapitulate *in vivo* architecture and cell-cell interactions [72]. In AD models, induced pluripotent stem cells (iPSCs) or ReN cells (neural progenitor cell line with the ability to differentiate) derived from AD patients or treated with familial Alzheimer's Disease (FAD) mutations respectively were cultured to self-organize into neural organoids that had similar phenotypes and protein expression to AD [73, 74]. These models were able to recapitulate AD phenotypes such as amyloid and tau pathology with minimal external manipulation [73, 74]. Organoids in PD models have been able to recreate LRRK2-G2019S disease phenotypes allowing for the exploration of PD relevant pathophysiology [75, 76]. For HD, organoids have resulted in new insights into the disease pathology and physiological mechanisms. In one study researchers found that adding healthy cells interactions to a diseased model significantly improved HD cell phenotype and function, likely through receptor-ligand interactions facilitating cell-cell communication [77]. The study highlighted key pathways (e.g., NCAM1, CADM1) and underscored the importance of communication between healthy and diseased cells in HD pathology [77]. In another HD organoid study, the self-organization aspect allowed for the discovery that the Huntington mutation (muHTT) effects the development of neural progenitor cells leading to altered maturation and organization of neuronal tissue [78].

2.3.4 Microfluidic Models

Microfluidics are defined by the ASTM International as "the engineering or use of devices that apply fluid flow to channels generally smaller than 1mm but not smaller than 0.1µm, in at least

one dimension" [71]. Microfluidic devices are advantageous because they include increased complexity (biochemical, cellular, mechanical stimuli), repeatability, and controllability. MPS have been used in various neurodegenerative disease models. In an AD study, a 3D microfluidic triculture model, consisting of astrocytes, AD neurons, and microglia, was developed to investigate microglia accumulation mechanisms by isolating the initial locations of microglia and the neurons and astrocytes [79]. The model was further enhanced by integrating AD and inflammatory physiology to better mimic neural-glial interactions [79]. Cavaliere et al., used a microfluidic device with two compartments to study the transport and propagation of α-synuclein between neurons and astrocytes which is characteristic of AD [80]. With this model they were able to determine α-synuclein's effect on neurons and astrocytes [80]. Another study developed a microfluidic channeled device to create a concentration gradient of rapamycin to determine its therapeutic effect on TDP-43 aggregates associated with ALS [81]. They found that the optimal rapamycin concentration for treating an ALS phenotype ranged from 0.4-1.0 μM [81]. This culture system was extremely advantageous because it allowed for the testing of multiple rapamycin concentrations within the same culture experiment, increasing throughput and repeatability [81].

2.3.5 MSC-EV Evaluation in MPS

Although there are no published studies, we are aware of, that are exploring the bioactivity of MSC-EVs in the context of neurodegenerative disease in MPS models, the potential is clear. MSC-EVs have shown bioactivity in other MPS applications, such as liver and lung disease models. For example, liver spheroids and organoids are being used to assess both human umbilical cord derived MSC-EVs and placenta derived (Pl) MSC-EVs for hepatic fibrosis [82, 83]. Chiabotto et al., found that both BM-MSCs and umbilical cord (UC)-MSCs suppressed

fibrosis in their liver spheroids reflected by the suppression of TGF-β1 cellular activation and fibrotic marker expression [82]. Similarly, another study found that Pl-MSC-EVs rescued fibrotic phenotypes in transforming growth factor beta (TGF-β1) stimulated organoids consisting of hepatocytes, hepatic stellate cells, Kupffer cells, and liver sinusoidal endothelial cells through decreasing hepatic stellate cell activation, inhibiting epithelial-mesenchymal transition and stabilizing E-cadherin [83]. MSC-EV therapeutic effects have also been explored in both liver and lung microfluidic models. Chen et al., developed a microchip device consisting of two microchannels separated by a polyethylene terephthalate membrane to assess perfusion between their engineered alveolar-capillary barrier under normal and inflammatory (LPS) conditions for the assessment of UC-MSC-EVs as a therapeutic [84]. They were able to determine that the UC-MSC-EVs restored the alveolar-capillary barrier function reflected in inhibition of cell death and preservation of junctional proteins including VE-cadherin and occludin [84]. In other models, combine both different model types in addition to multiple systems to recreate physiological conditions as closely as possible. In another study, liver organoids and a 2D kidney tubules were integrated into a microfluidic device to allow for constant media flow between the cellular models to determine MSC-EV systemic therapeutic application in an *in vitro* model [85]. During this study, they found that the MSC-EVs accumulated in both the kidney tubules and the liver organoids thereby mimicking the biodistribution seen *in vivo* [85]. Although not specific to neurodegenerative diseases, these examples demonstrate the potential of MSC-EVs as a therapeutic across various MPS platforms and offer valuable insight into the discoveries that could emerge from studying MSC-EVs in neurodegenerative MPS models.

2.3.6 Challenges and Benefits of MPS

MPS models offer several advantages over traditional 2D cultures and even some animal models. These systems allow for the integration of physical, mechanical, electrical and biochemical stimuli in a controlled environment [65]. This ability to reconstruct complex and dynamic pathophysiological environments in 3D provides MPS models with an advantage over 2D models when studying physiological interactions [86]. However, MPSs may not be able to recreate the full complexity of *in vivo* animal models but can address many of their challenges. For example, MPSs can often recreate regions of the brain that would be otherwise unreachable as well as create systems that are more biologically relevant for testing of human therapeutic products [87]. These models also provide researchers with the ability to specifically target MOAs of interest and discover mechanisms that would otherwise not be observable in simple *in vitro* models or *in vivo* models. MPS models are reproducible, efficient, include relevant tissue complexity able to replace animal studies making them an ideal model for testing therapeutics [87]. However, further validation and qualification are necessary before MPS can be widely adopted for therapeutic assessment.

2.4 REGULATORY CONSIDERATIONS FOR MSC-EVS

As MSC-EVs are derived from cells, they are classified as biological products. Although there is no standardized regulatory framework for EVs, existing guidance for cellular products is relevant to their development and bioactivity assessment. According to FDA recommendations, all cellular products must undergo thorough qualification and validation, with key factors like potency, safety, and efficacy evaluated in the context of their intended therapeutic use. As per 21 CFR 600.3(s), potency is defined “as the specific ability or capacity of the product as indicated by appropriate laboratory tests or by adequately controlled clinical data obtained through the administration of the product in the manner intended, to effect a given result” [88]. Potency

assurance must be achieved through a qualified and validated assay that measures parameters relevant to the biologic's intended purpose [89]. Critical quality attributes (CQAs), which are critical for achieving the desired therapeutic effect, are often used to consistently assess potency [88]. However, identifying these CQAs can be challenging when the mechanism of action (MOA) is either not fully understood or is highly complex, as is the case with MSC-EVs [90]. Because MSC-EVs' bioactivity and MOA are still in early stages of research, determining the appropriate assays to qualify and validate their potency remains an urgent need. Current nonclinical models aim to clarify the MOA of MSC-EVs and, in turn, identify relevant CQAs. However, due to the unique nature of EVs, many unknowns remain. Developing more sophisticated *in vitro* models may provide insights into the potential MOAs of MSC-EVs in neurodegenerative diseases and aid in establishing standardized assays for potency and bioactivity assessment.

2.5 CONCLUSION

The growing prevalence of neurodegenerative diseases underscores the urgent need for effective therapies that target the underlying pathology. MSC-EVs present a promising treatment option due to their immunomodulatory properties, which can address the shared neuroinflammatory conditions across neurodegenerative diseases. Moreover, MSC-EVs offer advantages over cellular therapies, such as overcoming many of the logistical and safety challenges associated with cell-based treatments. However, significant challenges remain, particularly in understanding the MOA of MSC-EVs, as well as establishing standardized protocols for their manufacturing and potency assessment. To move MSC-EVs closer to clinical application, there is a critical need to qualify and validate these products as neurodegenerative therapeutics. Currently, the field relies heavily on 2D monoculture and in vivo animal studies for bioactivity assessment. While

2D models are useful for isolating specific mechanisms, they fail to account for the complexity of cellular interactions in a more physiologically relevant environment (Figure 2.3). *In vivo* models, although more dynamic, often present difficulties when translating findings to human systems. MPSs offer a promising alternative by providing a complex and physiologically relevant environment, while still enabling high-throughput testing in controlled settings. MPSs allow scientists to investigate specific cellular interactions and MOAs that would be difficult to identify using traditional models. Given that MSC-EVs' MOA is still poorly understood, MPS will play a crucial role in uncovering relevant therapeutic mechanisms, guiding the development of assays for potency assessment, and contributing to eventual standardization (Figure 2.3). By advancing potency assessments and standardization efforts, MSC-EVs will be one step closer to becoming a qualified and validated therapeutic product for neurodegenerative diseases.

2.6 REFERENCES

1. *Neurodegenerative Diseases*. 2022; Available from: https://www.niehs.nih.gov/research/supported/health/neurodegenerative.
2. Zhang, W., et al., *Role of neuroinflammation in neurodegeneration development.* Signal Transduction and Targeted Therapy, 2023. **8**.
3. Lamptey, R.N.L., et al., *A Review of the Common Neurodegenerative Disorders: Current Therapeutic Approached and the Potential Role of Nanotherapeutics.* International Journal of Molecular Sciences, 2022. **23**(3): p. 1851.
4. Amor, S., et al., *Inflammation in neurodegenerative diseases.* Immunology 2010. **129**(2): p. 154-169.
5. DiSabato, D., N. Quan, and J.P. Godbout, *Neuroinflammation: The Devil is in the Details.* Journal of Neurochemistry, 2016. **139**: p. 136-153.

6. Daneman, R. and A. Prat, *The Blood-Brain Barrier.* Cold Spring Harbor Perspectives in Biology 2015. **7**(1): p. a020412.

7. Bell, R.D., et al., *Apolopoprotein E controls cerebrovascular integrity via cyclophilin A.* Nature, 2012. **485**: p. 512-516.

8. Heidari, A., N. Yazdanpanah, and N. Rezaei, *The role of Toll-like receptors and neuroinflammation in Parkinson's disease.* Journal of Neuroinflammation, 2022. **19**(1).

9. Kharat, S., et al., *Navigating Neurodegenerative Disorders: A Comprehensive Review of Current and Emerging Therapies for Neurodegenerative Disorders.* Journal of Neuroscience and Neurological Disorders 2024. **8**: p. 33-46.

10. Branscome, H., et al., *Use of Stem Cell Extracellular Vesicles as a "Holistic" Approach to CNS Repair.* Frontiers in Cell and Developmental Biology, 2020. **8**: p. 455.

11. Ullah, I., Raghavendra, and Gyu, *Human mesenchymal stem cells - current trends and future prospective.* Bioscience Reports, 2015. **35**(2): p. 1-18.

12. Merimi, M., et al., *The Therapeutic Potential of Mesenchymal Stromal Cells for Regenerative Medicine: Current Knowledge and Future Understandings.* Frontiers in Cell and Developmental Biology 2021. **9**(2021).

13. Chiossone, L., et al., *Mesenchymal Stromal Cells Induce Peculiar Alternatively Activated Macrophages Capable of Dampening Both Innate and Adaptive Immune Responses.* Stem Cells, 2016. **34**(7): p. 1909-1921.

14. Galindo, L.T., et al., *Mesenchymal Stem Cell Therapy Modulates the Inflammatory Response in Experimental Traumatic Brain Injury.* Neurology Research International 2011. **2011**(1): p. 564089.

15. Barkholt, L., et al., *Risk of tumorigenicity in mesenchymal stromal cell based therapies—Bridging scientific observations and regulatory viewpoints.* Cytotherapy, 2013. **7**(2013): p. 753-759.

16. Breitbach, M., et al., *Potential risks of bone marrow cell transplantation into infarcted hearts.* Blood, 2007. **110**(4): p. 1362-1369.

17. Tatsumi, J., et al., *Tissue factor triggers procoagulation in transplanted mesenchymal stem cells leading to thromboembolism.* Biochemical and Biophysical Research Communications, 2013. **431**(2): p. 203-209.

18. Boltze, J., et al., *The dark side of the force – constraints and complications of cell therapies for stroke.* Frontiers in Neurology 2015. **6**.

19. Kallmeyer, K., et al., *Fate of systemically and locally administered adipose-derived mesenchymal stromal cells and their effect on wound healing.* Stem Cells Translational Medicine, 2020. **9**(1): p. 131-144.

20. Welsh, J.A., et al., *Minimal information for studies of extracellular vesicles (MISEV2023): From basic to advanced approaches.* Journal of Extracellular Vesicles, 2024. **13**(2).

21. NeGisela, v., G. D'Angelo, and G. Raposo, *Shedding light on the cell biology of extracellular vesicles.* Nature Review Molecular Cell Biology, 2018. **19**: p. 213-228.

22. Toh, W.S., et al., *Immune regulatory targets of mesenchymal stromal cell exosomes/small extracellular vesicles in tissue regeneration.* Cytotherapy, 2018. **20**(12): p. 1419-1426.

23. Andaloussi, S.E., et al., *Extracellular Vesicles: biology and emerging therapeutic opportunities.* Nature Reviews Drug Discovery 2013. **12**: p. 347-357.

24. Brennan, M.A., P. Layrolle, and D.J. Mooney, *Biomaterials functionalized with MSC secreted extracellular vesicles and soluble factors for tissue regeneration.* Advanced Functional Materials, 2020. **30**(37): p. 1909125.

25. Morad, G., et al., *Tumor-Derived Extracellular Vesicles Breach the Intact Blood-Brain Barrier via Transcytosis.* ACS Nano, 2019. **13**(12): p. 13853-13865.

26. Matsumoto, J., et al., *Transmission of α-synuclein-containing erythrocyte-derived extracellular vesicles across the blood-brain barrier via adsorptive mediated transcytosis: another mechanism for initiation and progression of Parkinson's disease?* Acta Neuropathologica Communications 2017. **5**(1): p. 71.

27. Banks, W.A., et al., *Transport of Extracellular Vesicles across the Blood-Brain Barrier: Brain Pharmacokinetics and Effects of Inflammation.* International Journal of Molecular Sciences, 2020. **21**(12): p. 4407.

28. Seo, Y., H.-S. Kim, and I.-S. Hong, *Stem Cell-Derived Extracellular Vesicles as Immunomodulatory Therapeutics.* Stem Cells International, 2019. **2019**.

29. Reza-Zaldivar, E.E., et al., *Mesenchymal stem cell-derived exosomes promote neurogenesis and cognitive function recovery in a mouse model of Alzheimer's disease.* Neural Regeneration Research 2019. **14**(9): p. 1626-1634.

30. Losurdo, M., et al., *Intranasal delivery of mesenchymal stem cell-derived extracellular vesicles exerts immunomodulatory and neuroprotective effects in a 3xTg model of Alzheimer's disease.* Stem Cells Translational Medicine, 2020. **9**(9): p. 1068-1084.

31. Ma, J., et al., *MicroRNA-181a–2–3p shuttled by mesenchymal stem cell-secreted extracellular vesicles inhibits oxidative stress in Parkinson's disease by inhibiting EGR1 and NOX4.* Cell Death Discovery, 2022. **8**(1).

32. Chen, H.-X., et al., *Exosomes derived from mesenchymal stem cells repair a Parkinson's disease model by inducing autophagy.* Cell Death & Disease, 2020. **11**(4).

33. Zhang, Y., et al., *Systemic administration of cell-free exosomes generated by human bone marrow derived mesenchymal stem cells cultured under 2D and 3D conditions improves functional recovery in rats after traumatic brain injury.* Neurochemistry International 2018. **111**: p. 69-81.

34. Williams, A.M., et al., *Early single-dose treatment with exosomes provides neuroprotection and improves blood-brain barrier integrity in swine model of traumatic brain injury and hemorrhagic shock.* Journal of Trauma and Acute Care Surgery 2020. **88**(2): p. 207-218.

35. Lener, T., et al., *Applying extracellular vesicles based therapeutics in clinical trials – an ISEV position paper.* Journal of Extracellular Vesicles, 2015. **4**: p. 30087-30087.

36. Wiklander, O.P.B., et al., *Extracellular vesicle in vivo biodistribution is determined by cell source, route of administration and targeting.* Journal of Extracellular Vesicles, 2015. **4**(1): p. 26316.

37. Brennan, K., et al., *A comparison of methods for the isolation and separation of extracellular vesicles from protein and lipid particles in human serum.* Scientific Reports, 2020. **10**: p. 1039.

38. Zheng, X., et al., *Characterization and bioassays of extracellular vesicles extracted bytangential fl ow fi ltration.* Regenerative Medicine, 2022. **17**(3): p. 141-154.

39. Wang, C., et al., *Mesenchymal Stromal Cell–Derived Small Extracellular Vesicles Induce Ischemic Neuroprotection by Modulating Leukocytes and Specifically Neutrophils.* 2020. **51**(6): p. 1825 - 1834.

40. Eirin, A., et al., *Integrated transcriptomic and proteomic analysis of the molecular cargo of extracellular vesicles derived from porcine adipose tissue-derived mesenchymal stem cells.* PLOS ONE, 2017. **12**(3): p. e0174303.

41. Li, S., et al., *Proteomic characterization of hUC-MSC extracellular vesicles and evaluation of its therapeutic potential to treat Alzheimer's disease.* Scientific Reports, 2024. **14**: p. 5959.

42. Gao, C., et al., *Microglia in neurodegenerative diseases: mechanism and potential therapeutic targets.* Signal Transduction and Targeted Therapy, 2023. **8**(1).

43. Nakaso, K., *Roles of Microglia in Neurodegenerative Diseases.* Yonago Acta Medica, 2024. **67**(1): p. 1-8.

44. Zhao, L. and J. Li, *Microglial uptake of hADSCs-Exo mitigates neuroinflammation in ICH.* Cellular Signalling, 2024. **119**: p. 111146.

45. Cai, Y., et al., *Bone Marrow-Derived Mesenchymal Stem Cell-Derived Exosomes Containing Gli1 Alleviate Microglial Activation and Neuronal Apoptosis In Vitro and in a Mouse Parkinson Disease Model by Direct Inhibition of Sp1 Signaling.* Journal of Neuropathology and Experimental Neurology, 2022. **81**(7): p. 522-534.

46. Dabrowska, S., et al., *A Cellular Model of Amyotrophic Lateral Sclerosis to Study the Therapeutic Effects of Extracellular Vesicles from Adipose Mesenchymal Stem Cells on Microglial Activation.* International Journal of Molecular Sciences, 2024. **25**(11): p. 5707.

47. *Brain Basics: The Life and Death of a Neuron*. 2024; Available from: https://www.ninds.nih.gov/health-information/public-education/brain-basics/brain-basics-life-and-death-

neuron#:~:text=Neurons%20are%20responsible%20for%20sending,sends%20and%20receives%20specific%20neurotransmitters.

48. Gorman, A.M., *Neuronal cell death in neurodegenerative diseases: recurring themes around protein handling.* Journal of Cellular and Molecular Medicine, 2008. **12**(6a): p. 2263-2280.

49. Luo, Q., et al., *Antioxidant activity of mesenchymal stem cell-derived extracellular vesicles restores hippocampal neurons following seizure damage.* Theranostics, 2021. **11**(12): p. 5986-6005.

50. Bodart-Santos, V., et al., *Extracellular vesicles derived from human Wharton's jelly mesenchymal stem cells protect hippocampal neurons from oxidative stress and synapse damage induced by amyloid-β oligomers.* Stem Cell Research & Therapy, 2019. **10**.

51. *National Research Council (US) Committee on Methods of Producing Monoclonal Antibodies. Monoclonal Antibody Production. Washington (DC)*. 1999, National Academic Press (US).

52. Bryda, E.C., *The Mighty Mouse: The Impact of Rodents on Advances in Biomedical Research.* Missouri Medicine 2013. **110**(3): p. 207-211.

53. Aboulhoda, B.E., et al., *Hydrogen sulfide and mesenchymal stem cells-extracted microvesicles attenuate LPS-induced Alzheimer's disease.* Cellular Physiology 2021. **236**(8): p. 5994-6010.

54. Bonafede, R., et al., *ASC-Exosomes Ameliorate the Disease Progression in SOD1(G93A) Murine Model Underlining Their Potential Therapeutic Use in Human ALS.* International Journal of Molecular Sciences, 2020. **21**(10): p. 3651.

55. Dabrowska, S., et al., *Human bone marrow mesenchymal stem cell-derived extracellular vesicles attenuate neuroinflammation evoked by focal brain injury in rats.* Journal of Neuroinflammation, 2019. **16**(1).

56. Mohamed, A.S., et al., *Biochemical study of the effect of mesenchymal stem cells-derived exosome versus l-Dopa in experimentally induced Parkinson's disease in rats.* Molecular and Cellular Biochemistry, 2023. **478**(12): p. 2795-2811.

57. Sha, S., et al., *Mesenchymal stem cells-derived extracellular vesicles ameliorate Alzheimer's disease in rat models via the microRNA-29c-3p/BACE1 axis and the Wnt/β-catenin pathway.* Aging 2021. **13**(11): p. 15285-15306.

58. Walters, E.M. and R.S. Prather, *Advancing Swine Models for Human Health and Diseases.* Missouri Medicine, 2013. **110**(3): p. 212-215.

59. Li, C., et al., *Genetically engineered pig models of neurological diseases.* Ageing and Neurodegenerative Diseases, 2022. **2**(13).

60. Bambakidis, T., et al., *Early Treatment With a Single Dose of Mesenchymal Stem Cell Derived Extracellular Vesicles Modulates the Brain Transcriptome to Create Neuroprotective Changes in a Porcine Model of Traumatic Brain Injury and Hemorrhagic Shock.* Shock, 2022. **57**(2): p. 281-290.

61. Shulman, I., et al., *Intrathecal Injection of Autologous Mesenchymal Stem-Cell-Derived Extracellular Vesicles in Spinal Cord Injury: A Feasibility Study in Pigs.* International Journal of Molecular Sciences, 2023. **24**(9): p. 8240.

62. Holen, I., et al., *In vivo models in breast cancer research: progress, challenges and future directions.* Disease Models & Mechanisms, 2017. **10**(4): p. 359-371.

63. Dawson, T.M., T.E. Golde, and C. Lagier-Tourenne, *Animal models of neurodegenerative diseases.* Nature Neuroscience, 2018. **21**(10): p. 1370-1379.

64. Russel, W.M.S. and R.L. Burch, *The Principles of Humane Experimental Technique*, UFAW, Editor. 1959.

65. FDA. *About Alternative Methods*. 2023; Available from: https://www.fda.gov/science-research/advancing-alternative-methods-fda/about-alternative-methods#:~:text=A%20microphysiological%20system%20uses%20microscale,their%20function%20or%20pathophysiological%20condition.

66. Stone, N.L., T.J. England, and S. O'Sullivan, *A Novel Transwell Blood Brain Barrier Model Using Primary Human Cells.* Frontiers in Cellular Neuroscience, 2019. **13**.

67. Park, J.S., et al., *Establishing Co-Culture Blood-Brain Barrier Models for Different Neurodegeneration Conditions to Understand its Effect on BBB integrity.* International Journal of Molecular Sciences, 2023. **24**(6): p. 5283.

68. Cai, P., et al., *New Blood–Brain Barrier Models Using Primary Parkinson's Disease Rat Brain Endothelial Cells and Astrocytes for the Development of Central Nervous System Drug Delivery Systems.* ACE Chemical Neuroscience 2021. **12**(20): p. 3829-3837.

69. Chen, X.-X., et al., *Nurr1 promotes neurogenesis of dopaminergic neuron and represses inflammatory factors in the transwell coculture system of neural stem cells and microglia.* CNS Neuroscience and Therapeutics, 2018. **24**(9): p. 790-800.

70. Bolden, C.T., et al., *Validation and characterization of a novel blood-brain barrier platform for investigating traumatic brain injury.* Scientific Reports, 2023. **13**: p. 16150.

71. International, A., *Standard Terminology Relating to Microphysiological Systems*, in *F3570-22*, A.N.S. Institutute, Editor. 2022.

72. Kim, J., B.-K. Koo, and J.A. Knoblich, *Human organoids: model systems for human biology and medicine.* Nature Review Molecular Cell Biology, 2020. **21**: p. 571-584.

73. Choi, S.H., et al., *A three-dimensional human neural cell culture model of Alzheimer's disease.* Nature, 2014. **515**: p. 274-278.

74. Raja, W.K., et al., *Self-Organizing 3D Human Neural Tissue Derived from Induced Pluripotent Stem Cells Recapitulate Alzheimer's Disease Phenotypes.* PLOS ONE, 2016. **11**(9): p. e0161969.

75. Smits, L.M., et al., *Modeling Parkinson's disease in midbrain-like organoids.* npj Parkinson's Disease, 2019. **5**(5).

76. Kim, H., et al., *Modeling G2019S-LRRK2 Sporadic Parkinson's Disease in 3D Midbrain Organoids.* Stem Cell Reports, 2019. **12**(3): p. 518-531.

77. Galimberti, M., et al., *Huntington's disease cellular phenotypes are rescued non-cell autonomously by healthy cells in mosaic telencephalic organoids.* Nature Communications, 2024. **15**: p. 6534.

78. Conforti, P., et al., *Faulty neuronal determination and cell polarization are reverted by modulating HD early phenotypes.* PNAS, 2018. **115**(4): p. 762-771.

79. Park, J., et al., *A 3D human triculture system modeling neurodegeneration and neuroinflammation in Alzheimer's disease.* Nature Neuroscience, 2018. **21**: p. 941-951.

80. Cavaliere, F., et al., *In vitro α-synuclein neurotoxicity and spreading among neurons and astrocytes using Lewy body extracts from Parkinson disease brains.* Neurobiology of Disease 2017. **103**: p. 101-112.

81. Chennampally, P., et al., *A microfluidic approach to rescue ALS motor neuron degeneration using rapamycin.* Scientific Reports, 2021. **11**: p. 18168.

82. Chiabotto, G., et al., *Mesenchymal Stromal Cell-Derived Extracellular Vesicles for Reversing Hepatic Fibrosis in 3D Liver Spheroids.* Biomedicines, 2024. **12**(8): p. 1849.

83. Zheng, W., et al., *Placenta mesenchymal stem cell-derived extracellular vesicles alleviate liver fibrosis by inactivating hepatic stellate cells through a miR-378c/SKP2 axis.* Inflammation and Regeneration, 2023. **43**: p. 47.

84. Chen, W., et al., *Screening Therapeutic Effects of MSC-EVs to Acute Lung Injury Model on A Chip.* Advanced Healthcare Materials, 2023. **13**(8): p. 2303123.

85. Nguyen, V.V.T., et al., *A human kidney and liver organoid-based multi-organ-on-a-chip model to study the therapeutic effects and biodistribution of mesenchymal stromal cell-derived extracellular vesicles.* Journal of Extracellular Vesicles, 2022. **11**(11): p. 12280.

86. Jensen, C. and Y. Teng, *Is It Time to Start Transitioning From 2D to 3D Cell Culture?* Frontiers in Molecular Biosciences 2020. **7**(33).

87. Miny, L., et al., *Modeling Neurodegenerative Diseases Using In Vitro Compartmentalized Microfluidic Devices.* Frontiers in Bioengineering and Biotechnology 2022. **10**.

88. CBER, *Potency Assurance for Cellular and Gene Therapy Products*, U.S. HHS, Editor. 2023.

89. CDER and CBER, *Analytical Procedures and Methods Validation for Drugs and Biologics*, U.S. HHS, Editor. 2015.

90. Lam, J., K.E. Sung, and S.S. Oh, *Science-based regulatory considerations for regenerative medicine cellular produces.* Current Opinion in Biomedical Engineering 2022. **21**: p. 100361.

Therapy Type	Disease/Condition	MSC Origin	Autologous or Allogeneic	Route of Administration	Trial Phase	Status	Location	Clinical Trials.gov ID	Study Title
MSCs	Alzheimer's Disease	Adipose Tissue	Allogeneic	nasal drip	Phase 1 and Phase 2	Unknown	China	NCT04388982	The Safety and the Efficacy Evaluation of Allogenic Adipose MSC-Exos in Patients With Alzheimer's Disease
		Umbilical Cord	Allogeneic	Intraventricular injection	Phase 1 and Phase 2	Completed	South Korea	NCT03172117	Follow-up Study of Safety and Efficacy in Subjects Who Completed NEUROSTEMÃ® Phase-I/IIa Clinical Trial.
			Allogeneic	Intraventricular injection	NA	Unknown	South Korea	NCT01696591	The Long-Term Safety and Efficacy Follow-Up Study of Subjects Who Completed the Phase I Clinical Trial of Neurostem
			Allogeneic	Intraventricular injection	Phase 1 and Phase 2	Completed	South Korea	NCT02054208	Safety and Exploratory Efficacy Study of NEUROSTEMÃ® Versus Placebo in Patients With Alzheimer's Disease
			Allogeneic	Intraveneous injection	Phase 1 and Phase 2	Unknown	China	NCT01547689	Safety and Efficiency of Umbilical Cord-derived Mesenchymal Stem Cells(UC-MSC) in Patients With Alzheimer's Disease
			Allogeneic	Intraventricular injection	NA	Unknown	South Korea	NCT04954534	Exploratory Efficacy Study of NEUROSTEMÃ® in Subjects Who Control Group of NEUROSTEM
	Amyotrophic Lateral Sclerosis	Adipose Tissue	Autologous	Intrathecal injection	Phase 2	Active, not recruiting	USA	NCT03268603	Intrathecal Autologous Adipose-derived Mesenchymal Stromal Cells for Amyotrophic Lateral Sclerosis (ALS)
		Adipose Tissue	Autologous	Intraveneous injection	NA	No longer available	USA	NCT04514952	Individual Patient Expanded Access IND of Autologous HBadMSCs for the Treatment of Amyotrophic Lateral Sclerosis
		Bone Marrow	Autologous	Injection into cerebrospinal fluid	Phase 1 and Phase 2	Completed	NA	NCT04821479	Repeated Mesenchymal Stem Cell Injections in ALS
		Bone Marrow	Autologous	Injection into cerebrospinal fluid	Phase 1	Unknown	NA	NCT02881489	Autologous Bone Marrow Mesenchymal Stem Cells in the Treatment of Patients With Amyotrophic Lateral Sclerosis
		Wharton's Jelly	Allogeneic	Injection into cerebrospinal fluid	Phase 1	Unknown	NA	NCT02881476	Therapeutic Treatment of Amyotrophic Lateral Sclerosis
		Not Specified	Autologous	Intrathecal injection	Phase 1	Completed	Brazil	NCT02987413	Escalated Application of Mesenchymal Stem Cells in Amyotrophic Lateral Sclerosis Patients
	Hereditary Ataxia	Umbilical Cord	Autologous	Intrathecal and intraveneous injection	Phase 1 and Phase 2	Unknown	China	NCT01360164	Safety and Efficacy of Umbilical Cord Mesenchymal Stem Cell Therapy for Patients With Hereditary Ataxia
	Multiple System Atrophy	Not Specified	Allogeneic	Intrathecal injection	Phase 1 and Phase 2	Active, not recruiting	USA	NCT02315027	Mesenchymal Stem Cell Therapy in Multiple System Atrophy
	Parkinson's Disease	Adipose Tissue	Autologous	Intravenous injection	NA	NA	USA	NCT04772378	Intermediate Size Patient Population Expanded Access IND for the Treatment of Patients With Parkinson's Disease.
		Bone Marrow	Allogeneic	Intraveneous injection	Phase 1	Completred	USA	NCT02611167	Allogeneic Bone Marrow-Derived Mesenchymal Stem Cell Therapy for Idiopathic Parkinson's Disease
		Bone Marrow	Autologous	Intravenous injection	Phase 1 and Phase 2	Unknown	China	NCT01446614	Mesenchymal Stem Cells Transplantation to Patients With Parkinson's Disease
		Bone Marrow	Autologous	Intra-arterial injection	Phase 1 and Phase 2	Unknown	Italy	NCT01824121	Clinical Trial to Evaluate Bone Marrow Stem Cell Therapy for PSP, a Rare Form of Parkinsonism
		Umbilical Cord	Autologous	Intrathecal and intravenous injection	Phase 1 and Phase 2	Unknown	Jordan	NCT03684122	Use of Mesenchymal Stem Cells (MSCs) Differentiated Into Neural Stem Cells (NSCs) in People With Parkinson's (PD).
		Umbilical Cord	Not Specified	Intravenous injection	Phase 1	Unknown	China	NCT03550183	Umbilical Cord Derived Mesenchymal Stem Cells Therapy in Parkinson's Disease
	Progressive Supranuclear Palsy	Not Specified	Allogeneic	Not Specified	Phase 2	Completed	USA	NCT04506073	Phase IIa Randomized Placebo Controlled Trial: Mesenchymal Stem Cells as a Disease-modifying Therapy for Idiopathic Parkinson's Disease
MSC-EVs	Acute Liver Failure	Not Specified	Allogeneic	Injection	Phase 1 and Phase 2	Withdrawn	China	NCT05940610	The Safety and Efficacy of MSC-EVs in Acute/Acute-on-Chronic Liver Failure
	Bronchopulmonary Dysplasia	Umbilical Cord	Allogeneic	Intratracheal administration	Phase 1 and Phase 2	Recruiting	Belgium, Italy	NCT06279741	Safety and Efficacy of MSC-EVs in the Prevention of BPD in Extremely Preterm Infants
	Covid-19	Umbilical Cord	Allogeneic	Nebulization therapy	Early Phase 1	Recruiting	China	NCT05808400	Safety and Efficacy of Umbilical Cord Mesenchymal Stem Cell Exosomes in Treating Chronic Cough After COVID-19
	Dytrophic Epidermolysis Bullosa	Not Specified	Allogeneic	Injection into wound site	Phase 1 and Phase 2	Not yet Recruiting	NA	NCT04173650	MSC EVs in Dystrophic Epidermolysis Bullosa
	Hearing Loss	Umbilical Cord	Not Specified	Added during cochlear implantation	Phase 1 and Phase 2	Not yet Recruiting	NA	NCT06545175	Intracochlear Application of VSF1.01 for the Reduction of Cochlear Implant Surgery Related Trauma
	Premature Ovarian Failure	Bone Marrow	Allogeneic	Intraovarian injection	Phase 1 and Phase 2	Recruiting	Iran	NCT06202547	Intra-ovarian Injection of MSC-EVs in Idiopathic Premature Ovarian Failure

Table 2.1 Current MSC and MSC-EV Clinical Trials. This table provides a comprehensive overview of ongoing clinical trials involving mesenchymal stem cells (MSC) for neurodegenerative diseases, as well as current clinical trials utilizing MSC-derived extracellular vesicles (MSC-EVs).

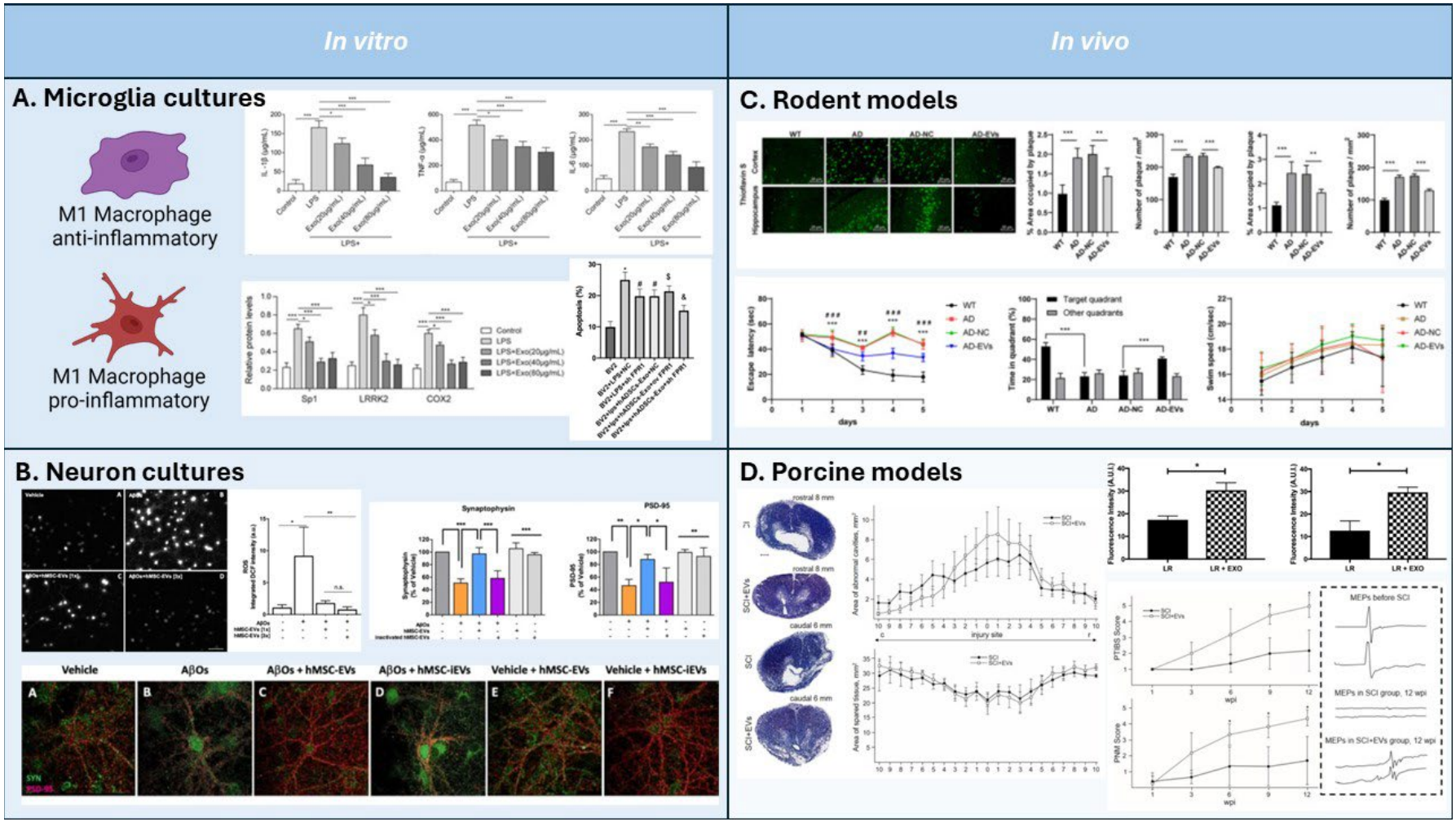

Figure 2.1 Current Common Current Common Neurodegenerative Disease Models. This figure illustrates commonly used *in vitro* and *in vivo* models for evaluating MSC-derived extracellular vesicles (MSC-EVs) **A)** Microglia monocultures stimulated with LPS to induce an inflammatory response were treated with MSC-EVs, which attenuated microglia activation, as evidenced by changes in protein secretion levels and decreased microglia apoptosis compared to untreated inflammatory conditions [44, 45] (Source: Reproduced and edited with permission, 2024 Elseiver and 2024 Oxford University Press, respectively) . **B)** In *in vitro* AD neuron monoculture models, MSC-EVs were internalized by neurons, reducing reactive oxygen species, increasing synaptic protein expression, and improving neuron morphology [50] (Distributed under a Creative Commons Attribution 4.0 International License (CC BY 4.0) http://creativecommons.org/licenses/by/4.0/). **C)** In an AD rat model, MSC-EVs significantly reduced plaque prevalence in both the cortex and hippocampus. Moreover, rats treated with MSC-EVs exhibited superior performance in behavioral tests compared to AD controls [57] (Distributed under a Creative Commons Attribution 4.0 International License (CC BY 4.0). **D)** In a spinal cord injury porcine model, MSC-EVs reduced the extent of damaged and abnormal tissue and restored neuronal motor evoked potentials [61] (Distributed under a Creative Commons Attribution 4.0 International License (CC BY 4.0).

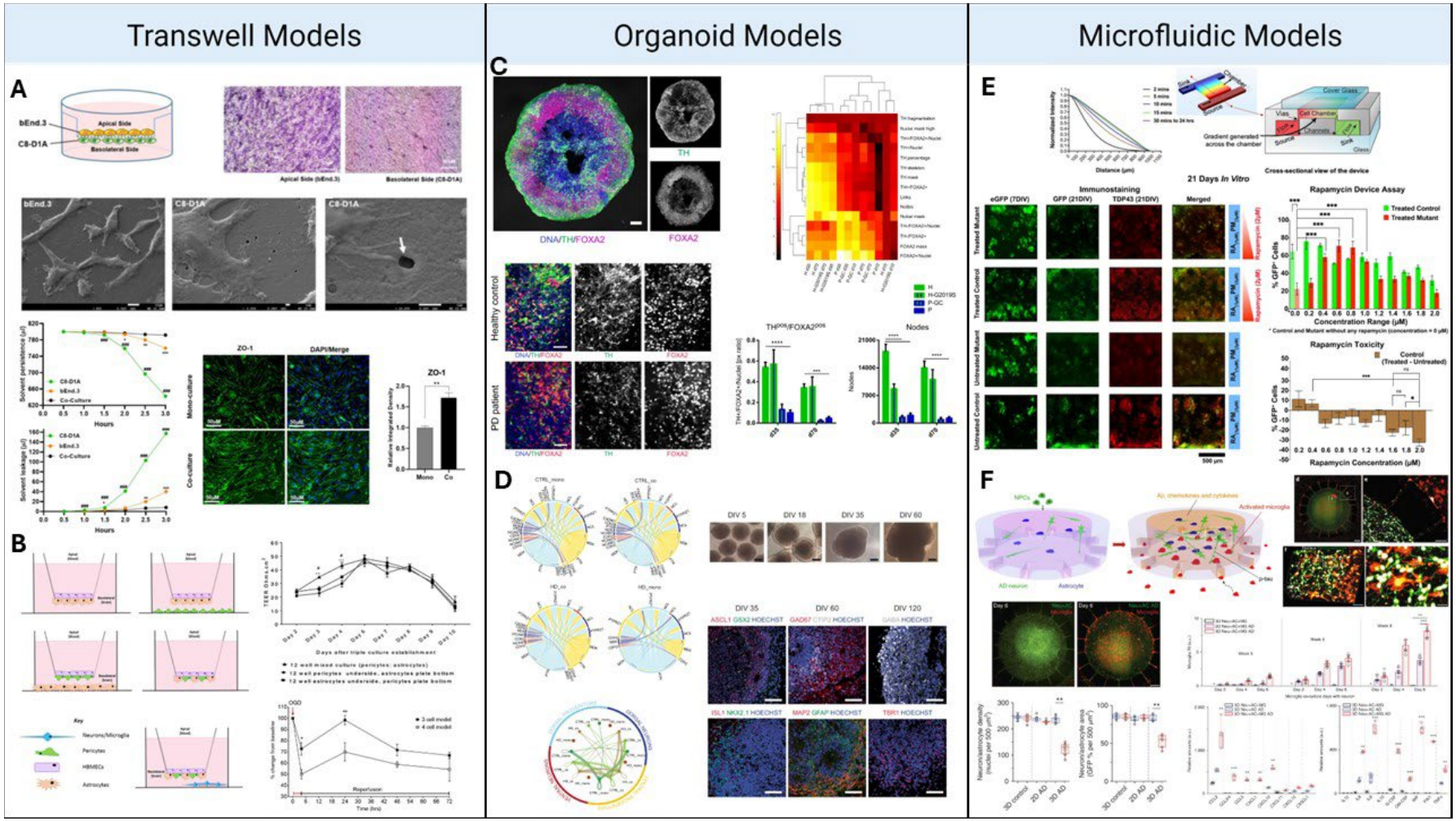

Figure 2.2. Microphysiological models for neurodegenerative diseases. A) Transwell model showing astrocytes co-culture decreasing barrier permeability and increasing ZO-1 expression [66]. **B)** Transwell co-cultures optimizing barrier model seeding configurations under normal and OGD conditions [67] (Distributed under a Creative Commons Attribution 4.0 International License (CC BY 4.0) http://creativecommons.org/licenses/by/4.0/). **C)** Midbrain organoid model of Parkinson's disease, revealing phenotypic and genotypic differences in LRRK2-G2019S mutation lines and isogenic controls [75] (Distributed under a Creative Commons Attribution 4.0 International License (CC BY 4.0)). **D)** Telencephalic organoid for Huntington's disease, demonstrating cellular interactions in different growth conditions [77] (Distributed under a Creative Commons Attribution 4.0 International License (CC BY 4.0)). **E)** Microfluidic model testing rapamycin concentration gradient on ALS-related TDP-43 aggregates [81] (Distributed under a Creative Commons Attribution 4.0 International License (CC BY 4.0)). **F)** Microfluidic device studying neural-glial interactions in Alzheimer's disease, showing microglial activation and migration [79]] (Source: Reproduced and edited with permission, 2018 Springer Nature America).

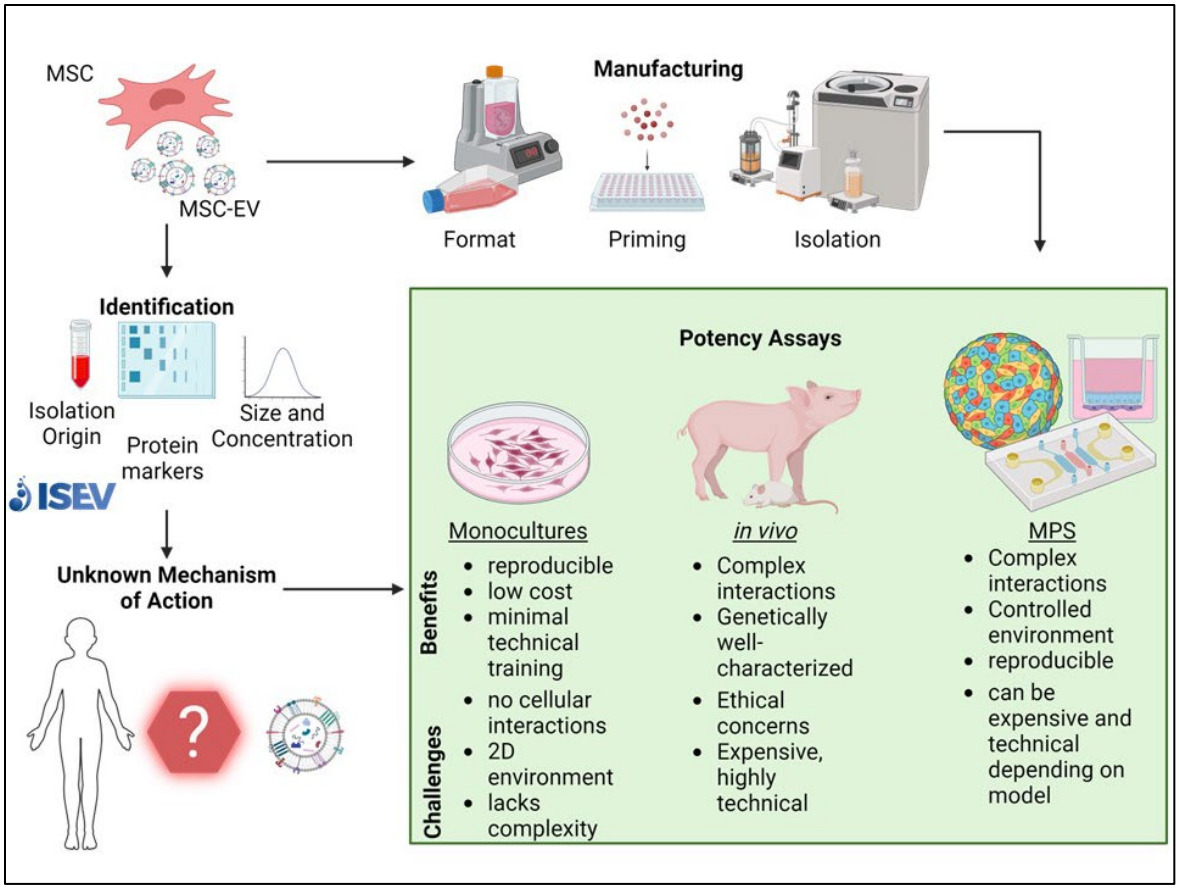

Figure 2.3. Potency Assays for MSC-EV Clinical Approval. The inherent heterogeneity of MSCs and MSC-EVs poses challenges in meeting regulatory requirements. Potency assays are critical for assessing both their mechanism of action and manufacturing processes. Each approach—monocultures, in vivo animal studies, and microphysiological systems (MPS)—offers distinct advantages and challenges.

CHAPTER 3

DEVELOPMENT OF A HIGH THROUGHPUT MORPHOLOGICAL ASSAY TO ASSESS MESENCHYMAL STROMAL CELL EXTRACELLULAR VESICLE MODULATION OF PERICYTE SECRETION OF CHEMOKINES AND CYTOKINES[1]

[1]Courtney E. Campagna, Andrew M. Larey, Kanupriya R. Daga, Morgan Roos, Sneha Ghosh, Neil Grimsey, Jin Han, Ross A. Marklein. To be submitted to Cytotherapy.

3.1 ABSTRACT

Mesenchymal stromal cell-derived extracellular vesicles (MSC-EVs) are a promising therapeutic that could help treat various neurodegenerative diseases. Neuroinflammation plays a major role in many of these diseases through an orchestration of interdependent processes that lead to the breakdown of the blood brain barrier (BBB), infiltration of immune cells and neuronal death. MSC-EVs have shown preliminary evidence of modulating neuroinflammation, but their mechanisms of action (MOA) are still unknown. We therefore explored the ability of MSC-EVs to modulate human brain pericytes, a cell-type that plays a critical role in BBB maintenance but has not been previously investigated as a therapeutic target of MSC-EVs. Brain pericytes are multifaceted cells that modulate neuroinflammation through their involvement in BBB homeostasis, as well as the innate and adaptive immune response. Pericyte morphology has been shown to change *in vivo* and this behavior was used to inform development of a quantitative morphological profiling approach to assess MSC-EV bioactivity in a rapid, high-throughput, low-cost manner. Using this assay, we were able to demonstrate that MSC-EVs manufactured in different conditions (flasks, bioreactors, and in response to priming) could induce distinct pericyte morphological responses indicative of changes in secretion of chemokines and cytokines relevant to neuroinflammation.

3.2 INTRODUCTION

Neurodegenerative diseases result in the loss of functional and cognitive abilities due to neuronal death [1]. While these diseases present diverse underlying pathologies, each presenting a unique challenge for therapeutic development, neuroinflammation is a common hallmark of many of them [2]. Neuroinflammation is an immune system response to inflammation located in the

central nervous system and includes interaction of various cell types and signaling molecules [3]. During homeostatic conditions, neuroinflammation serves a beneficial role to protect and maintain normal brain function. However, when neuroinflammation becomes chronic and/or dysregulated this results in tissue damage and the onset/progression of disease pathology [4]. Neuroinflammation maintains neuronal health by regulating the recognition, trafficking, and elimination of pathogens and unwanted host material. Neuroinflammation can include the release of pro-inflammatory cytokines and chemokines, activation of immune cells, the breakdown of the vasculature, and neuronal death [5]. Neuroinflammation is often associated with the breakdown of the blood-brain barrier (BBB), which is the interface between the blood and brain parenchyma [5]. The BBB's main role is to maintain homeostasis through the regulation of the passage of molecules across the blood-brain interface [6]. The BBB is made of multiple cell types including pericytes, astrocytes, and brain endothelial (BMEC) cells [6].

Mesenchymal stromal cells (MSCs) are a promising therapeutic for inflammatory diseases due to their established immunomodulatory function. In terms of neuroinflammation, MSCs have shown promise in treating neurodegenerative diseases such as traumatic brain injury (TBI), Alzheimer's disease (AD), Parkinson's disease (PD), and stroke [7-10]. However, due to the tightly regulated nature of the BBB, MSCs cannot readily enter the brain parenchyma when administered intravenously into blood circulation with most injected MSCs becoming trapped in the lungs [11]. Additionally, local intracranial administration of MSCs comes with inherent risks such as harmful MSC differentiation or formation of ectopic tissue [12, 13]. Finally, MSC functional heterogeneity has posed significant challenge in comprehending both their mechanism of action (MOA) and any associated safety concerns.

MSC-derived extracellular vesicles (MSC-EVs) can overcome many of the challenges associated with MSCs. MSC-EVs are lipid-membrane bound structures secreted by MSCs that contain bioactive molecules such as proteins, metabolites, lipids, and nucleic acids [14]. Because they are non-replicative and small size (~30-1000s of nm in diameter), MSC-EVs do not have the inherent risks of tumorgenicity, or thrombosis associated with MSCs [15, 16]. Importantly, MSC-EVs can readily cross the BBB and their cargo (e.g., tetraspanins, receptors, integrins, lipids, miRNA, etc.) has been shown to possess similar immunomodulatory functions as their parent MSCs [14, 17, 18]. Like MSCs, MSC-EV immunomodulatory function can be controlled through priming whereby MSCs are exposed to inflammatory-relevant signals (e.g. cytokines, hypoxia, low pH) for a short period of time (1-3 days) [19]. For example, one study found that MSCs primed with reduced serum and 1% oxygen for 48 hours induced cellular proliferation and increased secretion of proteins with mitogenic and neurotrophic functions [20]. Another study illustrated how priming bone marrow MSCs using hypoxia induced MSCs with increased angiogenic potential [21]. Although these studies provide promising preliminary evidence of the effects of manufacturing (priming conditions) on MSC-EV function relevant to neuroinflammation, there are no standardized approaches for assessing bioactivity. The current recommendations of the International Society of Extracellular Vesicles (ISEV) focus primarily on EV identification with no specific recommendations regarding bioactivity [22]. In some cases, EV bioactivity is assessed *in vivo* and using comprehensive multi-omics approaches, but these approaches can be high-cost, low-throughput, time-intensive, and difficult to standardize.

Pericytes are multipotent cells located throughout the basement membrane of the vasculature. Pericytes are heterogeneous in origin, tissue distribution, morphology, and play a critical role in the progression of neuroinflammation because of the regulation and proximity to the BBB. They

assist in the regulation of vasculature including angiogenesis and capillary blood flow, as well as the regeneration of function and structure in damaged parts of the CNS [23, 24]. They also regulate many aspects of the immune response including leukocyte extravasation, inflammation induced BBB distribution, clearance of waste products, propagation of peripheral and central inflammation, polarization of the inflammatory cells in the BBB and brain parenchyma, and the adaptive and innate immune response [25-30]. This multifaceted role makes pericytes and attractive cell-type for modeling neuroinflammation and screening potential therapies. Of note, no studies exist demonstrating the effects of MSC-EVs on pericytes although pericytes have been explored as a target for other drug therapies [31]. *In vivo*, pericytes morphologically respond to inflammation often becoming activated and migrating away from site of chronic inflammation. For example, in response to human penetrating cortical injury, pericytes were found to migrate away from the vessels [32, 33]. MSCs also morphologically response to inflammation (in the form of cytokine priming) and we have previously shown this morphological change can both predict a given MSC batch's bioactivity, as well as screen priming conditions to optimize MSC manufacturing [34]. For example, a morphological screen of MSCs primed with different combination of interferon gamma (IFN-γ) and tumor necrosis factor-alpha (TNFα) identified optimal IFN-γ/ TNF-α priming conditions that enhanced MSC function in terms of T cell suppression [35].

Previous work suggests pericytes and MSCs are phenotypically similar, and we hypothesized that a similar morphological profiling approach with pericytes could be used as an indicator of pericyte response to inflammation (*in vitro* model) and MSC-EV bioactivity [36, 37]. Therefore, we developed a high content imaging-based 2D pericyte based morphological assay to assess the effect of manufacturing conditions (flask vs bioreactor, priming, microcarrier density) on MSC-

EV bioactivity. TNF-α was used as a 'neuroinflammation relevant signal' to stimulate pericytes as it plays a role in neuroinflammation associated with many neurodegenerative diseases (i.e., AD, Ischemic stroke, TBI). Here we show comprehensive single cell morphological profiling of pericyte response to TNFα and multiple batches of MSC-EVs, as well as the association of these morphological responses to a targeted secretome panel of cytokines and chemokines.

3.3 MATERIALS AND METHODS

3.3.1 Pericyte Expansion and Cryopreservation

Human brain pericytes (gifted from the Grimsey lab at University of Georgia (ScienCell)) were expanded in Pericyte Complete Medium (Sciencell) on T175 flasks at 3500 cells/cm^2 coated with 1% (w/w) poly-d-lysine (PDL) (Sigma) for four passages with TryplE (Gibco) used to harvest cells at the end of each passage upon reaching 80-90% confluency. At passage four, pericytes were cryopreserved in alpha-MEM with 5% dimethylsulfide (DMSO) (Sigma-Aldrich).

3.3.2 MSC-EV Manufacturing

Human bone marrow derived MSC line RB71 was expanded according to the RoosterBio protocol previously described [35] and then cryopreserved at passage 2. One frozen vial containing 10^6 MSCs was seeded into T225 flasks at a seeding density of 4,444 cells/cm^2 in RoosterNourish-MSC-XF and cultured to 80% confluency. For flask MSC-EV manufacturing, the MSCs were passaged into T175 flasks at a seeding density of 714 cells/cm^2. For the bioreactor group, MSCS were passaged into 0.5L spinning wheel bioreactors (PBS Biotech) with 0.4g Corning Synthemax II polystyrene microcarriers. These MSCs were expanded in their respective vessels following protocols from PBS Biotech and RoosterBio. The MSCs were then

primed in RoosterCollect-EV with control and priming conditions. The MSC-EVs were collected from the supernatant using an adapted 2-step ultracentrifuge protocol[38]. The supernatant was first filtered through a 0.2µm filter and then centrifuged at 133,900 xg (Soorvall WX ultracentrifuge, ThermoFisher; Fiberlite F37L-8x100 Fixed-Angle Rotor, ThermoFisher, k factor=224; PC Bottle Assembly 70mL, ThermoFisher) for 1 hour at 4°C. The MSC-EV pellet was then resuspended in cold PBS-/- and then centrifuged again in micro-ultracentrifuge tubes (PC Thickwall 4mL, ThermoFisher) at 140,000xg (Sorvall MX 150+ Micro-Ultracentrifuge, ThermoFisher; S110-AT Fixed-Angle Rotor, ThermoFisher, k factor=76) for 1 hour at 4°C. The EV pellets were then resuspended at a 37.5X concentration in cold PBS-/-. The prepared EVs were then stored at -80°C until used.

3.3.3 Pericyte Morphological Assay

A T175 flask was coated with 1% (w/w) poly-d-lysine (PDL) for 24 hours at 4°C. After, the flask was washed with PBS three times to get rid of excess PDL and 35 mL of pericyte medium (Sciencell) was added. 10^6 previously frozen human brain pericytes (Sciencell) were thawed and seeded on the coated T175 flask. A flat-bottomed 96-well plate (Corning, Cat # 3599) was coated with 1% (w/w) poly-d-lysine (PDL) for 24 hours at 4°C. Once the pericytes reached 80-90% confluency (3 days) they were harvested using TrypLE (Gibco) and were seeded at 2,500 cells/cm^2 for 24 hours in 100 µL of pericyte complete medium in the prepared 96-well plate. After 24 hours, 50% of the media (50 µL) was aspirated from each well. Then 50 µL of pericyte medium only (‘unstimulated’) or 50 µL of pericyte medium containing 50 ng/mL TNF-α (Gibco, PHC3015) (‘stimulated’) were added to appropriate wells and pericytes incubated for an additional 24 hours. For MSC-EV treated pericyte groups, MSC-EVs were added concurrently with 100 ng/mL of TNF-α (50 ng/mL final concentration due to half media change) in pericyte

media to the appropriate wells. We fixed samples using 4% paraformaldehyde (Electron Microscopy Sciences) and stained with Hoechst [10µg/mL] (Invitrogen) and Fluorescein maleimide [20µM] (ThermoFisher) in PBS-/- (Gibco) for nuclear and cytoplasm morphology, respectively as done in Klinker et al [39]. Pericytes were imaged using Cytation 5 High Content Imaging system (Agilent) and a Ti-Eclipse (Nikon) with the imaging system indicated in each figure legend. We imaged 50% of every well using a 6x6 montage at 10X magnification. These images were processed on a single-cell basis for over 96 different nuclear and cytoplasmic morphological features using CellProfiler pipeline (Supplemental Figure 3.1), however, we focused primarily on the 21 features established in Klinker et al. A table summarizing and defining all morphological features quantified in this study can be found in Supplemental Table 3.1.

3.3.4 Pericyte Secretome

Pericytes were cultured on a PDL coated 96-well flat-bottomed plate at a density of 22,580 cells/cm^2 for 24 hours in pericyte media. After 24 hours, 50% of the media (50 µL) was aspirated from each well. Then 50 µL of pericyte medium only ('unstimulated') or 50 µL of pericyte medium containing 50 ng/mL TNF-α (Gibco, PHC3015) ('stimulated') were added to appropriate wells and pericytes incubated for an additional 24 hours. For MSC-EV treated pericyte groups, MSC-EVs were added concurrently with 100 ng/mL of TNF-α (50 ng/mL final concentration due to half media change) in pericyte media to the appropriate wells. Pericyte conditioned medium was collected from n=3 wells per experimental group and stored at -80°C. Frozen CM samples were shipped on dry ice to RayBiotech (Norcross, GA) for secretome analysis using the 200plex quantibody Array (Q400). Differentially secreted proteins of interest

were analyzed using STRING database (https://string-db.org/) to identify significantly enriched pathways.

3.3.5 Data Analysis and Statistics

Singe cell morphological data is presented on a median-per-well basis and summarizes data from at least 300 cells per well. All data and statistical analyses were performed using GraphPad Prism v10.

3.4 RESULTS

3.4.1 Stimulated Pericytes become larger and more complex with TNFα stimulation

Human brain pericytes (Supplemental Figure 3.2) were first identified using three known pericyte markers including nuclear factor-kappa-light-chain enhancer of activated B cells (NFκB), Alpha Smooth Muscle Actin (α-SMA), and platelet-derived growth factor beta (PDGFRβ). The pericytes were expanded until passage 4 and seeded into a 96-well plate coated with PDL and treated with and without [50ng/mL] TNF-α. Qualitatively, we observed that stimulated pericyte morphology is different than that of unstimulated pericytes (Figure 3.1A) as reflected in the significant and quantifiable change of multiple morphological features including perimeter, major axis length, compactness, form factor and aspect ratio (Figure 3.1B). The stimulated pericytes increased significantly in perimeter and major axis length illustrating an overall increase in size. In addition, pericytes decreased in form factor and increased in compactness that indicates an overall increase in complexity of morphology. An increase in aspect ratio is indicative of a more elongated morphology which coincides with the observed increase in major axis length. These were the only features that consistently changed over

multiple experiments. These characteristic morphological responses were observed over four independent experiments.

3.4.2 Change in pericyte morphology reflected by change in secretion

In addition to the morphological profiling, we performed quantitative secretome profiling on unstimulated and stimulated pericytes (Figure 3.2). Pericytes were cultured on a 96-well plate with and without TNF-α stimulation, after which the supernatant was collected and analyzed using the RayBiotech Array Q4000. 81 total proteins were detected as secreted by pericytes at levels above the pericyte medium only control and were used for further analysis. Hierarchical clustering illustrated the distinct secretion profiles of unstimulated (-CTL) and stimulated (+CTL) [50ng/mL] TNF-α pericyte groups (Figure 3.2A). STRING analysis of the 24 differentially expressed proteins highlighted several proteins that were highly connected (based on node degree) such as IL-6, ICAM1, and CXCL10 (Figure 3.2B). Of the 24 differentially expressed proteins, TNF-α resulted in increased production of 17 proteins and decreased production of 7 proteins (Figure 3.2C). Pathway analysis using STRING revealed these proteins were associated with distinct categories such as cell morphology (directly related to our initial hypothesis), regulation of cell activation/differentiation, regulation of chemotaxis, regulation of growth survival, and well-known signaling pathways. Notably, many of these processes included immune cell-types (T cells, B cells, glial cells) that play a role in the onset and progression of neuroinflammation.

3.4.3 MSC-EV treatment modulates pericyte morphology

After establishing the pericyte controls with and without TNF-α stimulation, we used this assay to assess bioactivity of 4 different MSC-EVs preparations produced in two different

manufacturing platforms (flasks and 500 mL vertical wheel bioreactors) and with and without 50 ng/mL IFN-γ/TNF-α priming. These MSC-EVs (from the same manufacturing run) were previously shown by our group to significantly modulate microglia morphology [34]. Although all MSC-EV manufacturing groups showed a general trend of increased size (perimeter, major axis length) and complexity (form factor, compactness, aspect ratio) in pericytes, there was consistent changes from treatment with MSC-EVs produced from MSCs primed in a bioreactor (Figure 3.3). This is contrary to what we observed previously with microglia where MSC-EV treatment resulted in a less pronounced morphological response of microglia to cytokine treatment (i.e., 'suppression' of morphological response) whereas pericytes treated with MSC-EVs had an even greater morphological response to cytokine treatment (i.e. 'enhancement' of morphological response). We chose to move forward with the bioreactor manufacturing platform for future studies based on several considerations: 1) The bioreactor primed group was the only MSC-EV group that consistently modulated pericyte morphology, 2) bioreactors are amenable to scaling necessary for clinical production, and 3) previous work from our group demonstrating MSC-EVs from bioreactor groups significantly modulated microglia morphology.

3.4.4 Priming and microcarrier concentration impact MSC-EV modulation of pericyte morphology

Based on the initial finding that MSC-Evs modulate pericyte morphology we then explored additional manufacturing conditions and their effect on pericyte morphology. MSC-Evs were manufactured in the same 500 mL vertical wheel bioreactor using three different priming conditions and two different microcarrier concentrations (Table 3.1 summarizing the specific conditions). The +CTL priming condition is the same IFN-γ/TNF-α priming condition shown in Figure 3.3 and the other 2 priming conditions (Hit 2 and Hit 4) were identified as 'Morphological

Hits' from a high throughput morphological screen detailed in Larey et al [34]. We assessed the pericyte morphological response to these six different MSC-EV preparations using our established analysis pipeline and observed significant differences in pericyte morphology between the stimulated control and all MSC-EV groups for compactness, form factor, and aspect ratio (Figure 3.4 *$p<0.05$). For perimeter and major axis length features, all EV groups (with exception of Priming +CTL at μC_{low}) enhanced the pericyte morphological response.

Furthermore, we were able to use pericyte morphology to identify differences in MSC-EV bioactivity due to priming and microcarrier conditions. For +CTL and Hit 2 priming conditions, MSC-Evs from μC_{high} enhanced pericyte morphological response to TNF-α more so than MSC-Evs from μC_{low} for perimeter, major axis length, compactness, form factor, and aspect ratio (Figure 3.4 \$$p<0.05$). For Hit 4 priming conditions, this greater morphological response was observed for perimeter, major axis length, compactness, and form factor. Analysis of MSC-EV groups manufactured using μC_{low} showed Hit 2 and Hit 4 priming conditions had a significant enhancing effect on pericyte morphological response compared to +CTL priming (Figure 3.4 #$p<0.05$). For MSC-Evs manufacturing using μC_{high} conditions, +CTL and Hit 2 priming groups were similar and Hit 4 had a less significant enhancement effect on pericyte morphology compared to +CTL (but still greater than the stimulated control).

3.4.5 Primed MSC-EVs modulate pericyte secretome

We analyzed how two specific EV groups (+CTL and Hit 2 at μC_{high}) affected pericyte secretion of a panel of 200 chemokines, cytokines, and growth factors as they had the most significant observed enhancement of pericyte morphological response to TNF-α (Figure 3.5). When analyzing the shift in pericyte secretome we observed many similarities between +CTL and Hit 2

MSC-EV treatment. In both treatments, we observed a decrease in the expression of various proteins that have roles in the regenerative response including angiogenin, HGF, LIF and BTC which have roles in angiogenesis, and neurogenesis and neuronal differentiation [40-43]. Pericytes treated with Hit 2 MSC-EVs increased production of various proteins including ALCAM, IL-13 R1, and CXCL10 which all have immunomodulatory roles including tight junction permeability, T cell suppression, macrophage and microglia activation, and migration of pericytes [44-47].

3.4.6 Comparison of secreted proteins from EV-treated pericytes and primed MSCs

Because the pericyte morphological response induced by MSC-EVs represented an enhancement of an inflammatory morphology (i.e. control pericytes stimulated with TNF-α) we sought to compare our secretome results with a previous study (Andrews et al) that demonstrated MSC stimulation with IFN-γ/TNF-α induced a similar morphological response, which was associated with enhanced immunomodulation of activated T cells [35]. Figure 3.6A illustrates schematically the secretome being compared across 3 experimental groups: 1 MSC group (Andrews et al) and 2 pericyte groups (new data from this work). Proteins from the same quantitative 200-plex secretome panel were categorized based on detection in different experimental groups and summarized in terms in Figure 3.6B. Individually MSCs secreted 31 proteins that were not detected in either EV treated pericyte group such as CCL21, IL1β, and IL6. Pericyte +CTL EVs alone expressed five different proteins, and pericytes treated with Hit 2 EVs expressed 12 proteins individually. When comparing MSCs to the EV pericyte groups there is no overlap between MSCs and either individual group. There were 20 proteins detected in both pericyte EV groups that were not detected in the MSC group. Primed MSCs, +CTL EV Pericytes and Hit 2 EV Pericytes all shared 32 different proteins including ANG, CXCL10, CCL2, and MIF which

have roles in vesicle mediated transport, positive regulation of T cell activation, Neurogenesis, blood vessel development and MAPK and ERK pathways as shown in Figure 3.6D.

3.5 DISCUSSION

To fully realize the therapeutic potential and accelerate translation of MSC-EVs for neurodegenerative diseases, there is a great need to develop robust assays that demonstrate bioactivity relevant to their proposed mechanisms of action. Here, we demonstrated how high throughput morphological screening can be applied on the target therapeutic cells of MSC-EVs (i.e., pericytes) and that this morphological response is associated with MSC-EV bioactivity relevant to the treatment of neurodegenerative diseases. Using this approach, we were able to screen the effects of different manufacturing conditions on MSC-EV and determine that MSC-EVs enhanced the morphological response of pericytes (beyond the stimulated control) promoted an immunomodulatory, pro-regenerative pericyte secretory profile like that of cytokine-primed MSCs.

Pericytes have been shown to have differing morphology depending on the state of the disease. During inflammation, pericytes are often seen to be migrating which is reflected in their extension (increase in size) and increased projections (complexity) [48]. We were able to identify consistent morphological and functional differences between unstimulated pericytes and TNFα-stimulated pericytes. Their morphology consistently becomes larger and more complex with stimulation reflected in their increase in perimeter, major axis length, aspect ratio, compactness, and a decrease in form factor. This change with TNF-α has been observed in other studies, for example, pericytes become more complex and elongated with 10ng/mL TNF-α stimulation that was then correlated with the increased migration of pericytes [49]. We believe this

morphological change is reflective of their function *in vivo* where they have been observed migrating away from locations of injury and hypoxia [32, 50]. The exact cause of this migration is unknown; however, it has been suggested that the thinning of the abluminal surface of the basal lamina is part of the physiological process to enhance endothelial cell plasticity during vascular remodeling, or to attenuate the cytotoxic effects between the synaptic terminals to protect the neural tissue [50]. In addition to morphological changes, pericyte secretion is altered *in vivo* in response to inflammation which was reflected in our *in vitro* results. We observed an increase in IL-6, ICAM-1 and CCL5 expression with the addition of TNF-α. In literature, pericytes treated with TNF-α increase their secretion of interleukin-6 (IL-6), intercellular adhesion molecule 1 (ICAM-1), and RANTES (CCL5). All three of these cytokines have been observed to increase their expression in pericytes treated with TNF-α [25, 51, 52]. IL-6 has been shown to induce BBB dysregulation through the activation of microglia and astrocytes leading to neuronal damage[25]. ICAM-1 and CCL5 both have roles in recruiting immune cells (i.e., monocytes, macrophages, NK cells, T cells) to the site of inflammation [53, 54]. However, CCL5 also has a regenerative role in promoting angiogenesis [55]. The TNF-α induced proteins primarily serve to regulate both adaptive and innate immune cells, facilitating their recruitment to the site of inflammation. Therefore, our work demonstrates TNF-α promotes a pro-inflammatory pericyte phenotype in our *in vitro* assay.

In terms of the effect of MSC-EVs on pericyte morphological parameters, we initially hypothesized that EV treatment would suppress the pericyte morphological response to TNF-α (i.e. preventing their increase in size and complexity); however, we observed an opposite/enhancing effect. Overall, MSC-EVs manufactured using 6 different conditions (Table 1) enhanced the stimulated morphology by increasing their size (increase in perimeter, aspect

ratio, and major axis length) and increasing their complexity (increase in compactness, and a decrease in form factor). This same response has been seen in cytokine-primed MSCs where either IFN-γ alone or a combination of IFN-γ and TNF-α stimulation the MSCs increase their immunomodulatory function (CD4+ and CD8+ T cell suppression) which is reflected by an increase in size and complexity [35, 39]. Although pericytes and MSCs can possess different functional properties *in vitro* (e.g. angiogenesis), they both share similar immunomodulatory functions in *in vitro* models [36, 56]. Considering the functional and phenotypic similarities observed between pericytes and MSCs both *in vitro* and *in vivo*, it is notable that they respond similarly to inflammatory signals (e.g. cytokines) in terms of their morphology. Therefore, we hypothesized this enhanced stimulated morphological response is indicative of pericytes having increased immunomodulatory function. We analyzed pericyte secretome in response to MSC-EVs as an indicator of MSC-EV bioactivity and found that MSC-EVs modulated pericyte secretion of proteins that have roles in the inflammatory response (Figure 3.6). For example, we observed a decrease in vascular endothelial growth factor A (VEGFA), macrophage inflammatory protein 3A (CCL20), and hepatocyte growth factor (HGF) with MSC-EV treatment. These proteins are involved in promoting angiogenesis, vasculogenesis and endothelial cell growth [41, 57, 58]. When comparing +CTL and Hit 2 MSC-EVs we observed a change in more proteins with immunomodulatory and angiogenic properties as well as a larger change in their morphological profile. Pericytes treated with Hit 2 MSC-EVs increased their expression of activated leukocyte cell adhesion molecule (ALCAM), MIG (CXCL9), IP-10 (CXCL10) and death receptor (DR6). ALCAM has been shown to increase the tight junctions of endothelial cells in the BBB as well as its association with leukocyte transmigration [44]. Both CXCL9 and CXCL10 are CXC receptor 3 (CXCR3) ligands that have been shown to increase

ERK activity resulting in an increase in cell transmigration of other pericytes [47]. DR6 has been shown in both zebrafish and mice to regulate angiogenesis through VEGF-mediated JNK activation of endothelial sprouting [59]. In addition, Pericytes treated with Hit 2 and +CTL EVs secreted proteins involved in the modulation of other neural cells. For example, AgRP and BTC have both been shown to activate dopaminergic neurons and induce neural stem cell proliferation and neurogenesis, respectively [43, 60]. TGF-β1 has been shown to induce an anti-inflammatory response from microglia as well as reduce pericyte proliferation and reduce pericyte phagocytic function [61]. Our pathway analysis demonstrates that these differentially regulated proteins are critically involved in BBB regulation and the overall brain immune environment which suggests the potential of MSC-EVs to indirectly modulate multiple cell-types in the BBB and brain parenchyma with pericytes serving as the mediator.

MSC-EV manufacturing conditions have been shown to change the functional outcomes of the EVs. In this work, we observed that the magnitude of the enhanced pericyte morphological response was manufacturing dependent. Compared to MSC-EVs produced by MSCs grown in flasks, MSCs grown in bioreactors produced EVs that had a more significant effect on pericyte morphology (Figure 3.3). In terms of manufacturing, bioreactors are better suited for large scale production of MSC-EVs which could address issues with consistency by enabling production of large batches of MSC-EVs. In addition, bioreactors allow for a dynamic environment that induces shear stress through stirring of the cell suspension that alters the topographical and surface environment the cells are exposed to which can influence their behavior such as migration, adhesion and morphology [62]. Multiple studies have shown that bioreactor systems have higher MSC-EV yield than flasks [62-64]. For example, a 38 times higher yield by volume of MSC-EVs was observed in a bioreactor system compared to MSC-EV production in flasks

[64]. We also found that the MSC-EVs that were produced by MSCs cultured on higher microcarrier densities had a greater effect on pericyte morphology, with a greater increase in size and complexity when compared to MSCs grown on lower microcarrier density. When culturing MSCs in bioreactors using microcarriers, there have been varying results on the effects of microcarriers depending on the microcarrier composition. Umbilical cord MSCs and adipose derived MSCs expanded on Cytodex 1 microcarriers were found to increase their angiogenic potency based on secretion of VEGF, FGF-2, MCP-1 and SDF-1 [64]. In addition to microcarrier composition, microcarrier density has also been shown to affect MSC yield. A study comparing three microcarrier densities with the same cell density found that an intermediate concentration of 1.25g yielded higher MSC proliferation than that of the lower 0.75g and higher 2.5g microcarrier densities [65]. In terms priming, regardless of microcarrier density, we observed that priming conditions 1 and 2 significantly induced a greater change in pericyte morphology than priming 3 conditions, which could be related to differences in EV composition due to priming. We have previously reported differences in the lipidomic profile of these same MSC-EV batches and these data align well with some of the enriched pathways observed based on the pericyte secretory response. Specifically, pericytes treated with +CTL and Hit 2 EVs secreted many proteins (e.g. CCL2, CXCL6, CXCL8, IL6, TNFRSF1B) that are associated with lipid response (Figure 3.6) [34]. This underscores the potential of our pericyte morphological assay to serve as a screening tool for MSC-EV manufacturing conditions in the future.

Our work provides preliminary evidence that MSC-EVs can shift pericyte secretome towards a ‘primed MSC’s immunomodulatory state. Overall, we observed that pericytes treated with MSC-EVs from +CTL and Hit 2 primed MSCs had a secretory profile that consisted of 31 shared proteins with primed MSCs. This is noteworthy as the pericytes in our study and MSCs from our

previous study were derived from different donors and were cultured using different media. These shared proteins are involved with pathways related to T cell proliferation, migration, and activation (CCL2, IL6, CXCL10), as well as positively regulated major signaling pathways such as MAPK and ERK1/ERK2 (MIF, CCL2, CCL20) [47, 66]. These proteins can regulate pericyte migration which is reflected in our observed change in pericyte morphology associated with TNF-α and MSC-EV treatment. In addition, proteins such as VEGFA and ANG are involved with neurovascular unit processes such as blood vessel development, endothelial proliferation, and neurogenesis. As primed MSCs have increased immunomodulatory function, we believe our work supports further investigation into the mechanisms driving pericytes towards a 'primed MSC-like' immunomodulatory state. Pericytes and MSCs share many of the same phenotypic markers - with some exceptions including desmin, PDGFRβ, and α-SMA - in addition to sharing similar immunomodulatory, and structural functions *in vitro* [37].

This is the first study demonstrating MSC-EV bioactivity in terms of modulating pericyte morphology and secretion. This novel approach provides a foundation for further exploring MSC-EV potential in treating neurodegenerative diseases by using pericytes as an *in vitro* model of MSC-EV bioactivity. In addition, we believe that this assay will aid in standardization efforts that aim to assess MSC-EV bioactivity. Morphology is a rapid, single-cell, high throughout analysis that provides comprehensive information on cellular responses to disease-relevant signals such as inflammatory cytokines. The capabilities afforded by morphological profiling will facilitate standardization of MSC-EV characterization, evaluation of the effects of manufacturing changes on MSC-EV bioactivity, and further contribute to eventual clinical translation. While this study demonstrates the potential of using pericytes as a model cell for assessing MSC-EV bioactivity relevant to treatment of neuroinflammation, it is important to note

that the studies were conducted using pericytes derived from one donor and MSC-EVs produced from a single MSC line. This morphological platform can therefore be applied in the future to evaluate whether pericytes from different donors respond differentially to MSC-EVs and whether MSC-EVs from different cell-lines (akin to different manufacturing conditions evaluated in this study) possess different bioactivity based on the pericyte morphological response. Additionally, this work provides a foundation for exploring MSC-EV modulation of pericytes in more complex *in vivo* disease models or 3D *in vitro* systems (i.e. microphysiological 'on-chip' systems) that could improve our understanding of not only MSC-EV modulation of pericytes, but indirect modulation of other cell-types mediated by pericytes. Finally, this pericyte morphological assay could be used to better understand MSC-EV (or other cell-based therapy) mechanisms of action, the knowledge of which could help further refine MSC-EV manufacturing and facilitate clinical translation.

3.6 REFERENCES

1. *Neurodegenerative Diseases*. 2022; Available from: https://www.niehs.nih.gov/research/supported/health/neurodegenerative.
2. Adamu, A., et al., *The role of neuroinflammation in neurodegenerative diseases: current understanding and future therapeutic targets.* Frontiers in Aging Neuroscience 2024. **16**.
3. Alexander, J.J., et al., *The complement cascade: Yin–Yang in neuroinflammation – neuro–protection and –degeneration.* Journal of Neurochemistry, 2008. **107**(5): p. 1169-1187.
4. Amor, S., et al., *Inflammation in neurodegenerative diseases.* Immunology 2010. **129**(2): p. 154-169.
5. Zhang, W., et al., *Role of neuroinflammation in neurodegeneration development.* Signal Transduction and Targeted Therapy, 2023. **8**.

6. Daneman, R. and A. Prat, *The Blood-Brain Barrier.* Cold Spring Harbor Perspectives in Biology 2015. **7**(1): p. a020412.

7. Matchynski-Franks, J.J., et al., *Mesenchymal Stem Cells as Treatment for Behavioral Deficits and Neuropathology in the 5xFAD Mouse Model of Alzheimer's Disease.* Cell Transplantation, 2016. **25**(4): p. 687-703.

8. QI, L., et al., *The Promising Effects of Transplanted Umbilical Cord Mesenchymal Stem Cells on the Treatment in Traumatic Brain Injury.* The Journal of Craniofacial Surgery 2018. **29**(7): p. 1689-1692.

9. Chen, D., et al., *Therapeutic effects of intranigral transplantation of mesenchymal stem cells in rat models of Parkinson's disease.* Journal of Neuroscience Research 2016. **95**(3): p. 907-917.

10. Chen, H. and L. Zhou, *Treatment of ischemic stroke with modified mesenchymal stem cells.* International Journal of Medical Sciences, 2022. **19**(7): p. 1155-1162.

11. Kallmeyer, K., et al., *Fate of systemically and locally administered adipose-derived mesenchymal stromal cells and their effect on wound healing.* Stem Cells Translational Medicine, 2020. **9**(1): p. 131-144.

12. Barkholt, L., et al., *Risk of tumorigenicity in mesenchymal stromal cell based therapies—Bridging scientific observations and regulatory viewpoints.* Cytotherapy, 2013. **7**(2013): p. 753-759.

13. Breitbach, M., et al., *Potential risks of bone marrow cell transplantation into infarcted hearts.* Blood, 2007. **110**(4): p. 1362-1369.

14. Colombo, M., G. Raposo, and C. Thery, *Biogenesis, Secretion, and Intercellular Interactions of Exosomes and Other Extracellular Vesicles.* Annual Review of Cell and Developmental Biology 2014. **30**: p. 255-289.

15. Tatsumi, J., et al., *Tissue factor triggers procoagulation in transplanted mesenchymal stem cells leading to thromboembolism.* Biochemical and Biophysical Research Communications, 2013. **431**(2): p. 203-209.

16. Welsh, J.A., et al., *Minimal information for studies of extracellular vesicles (MISEV2023): From basic to advanced approaches.* Journal of Extracellular Vesicles, 2024. **13**(2).

17. Morad, G., et al., *Tumor-Derived Extracellular Vesicles Breach the Intact Blood-Brain Barrier via Transcytosis.* ACS Nano, 2019. **13**(12): p. 13853-13865.

18. Weng, Z., et al., *Therapeutic roles of mesenchymal stem cell-derived extracellular vesicles in cancer.* Journal of Hematology and Oncology 2021. **14**: p. 136.

19. Miceli, V., et al., *Different priming strategies improve distinct therapeutic capabilities of mesenchymal stromal/stem cells: Potential implications for their clinical use.* World Journal of Stem Cells 2023. **15**(5): p. 400-420.

20. Yuan, O., et al., *Exosomes Derived from Human Primed Mesenchymal Stem Cells Induce Mitosis and Potentiate Growth Factor Secretion.* Stem Cells and Development, 2019: p. 398-409.

21. Yusoff, F.M., et al., *Implantation of Hypoxia-Induced Mesenchymal Stem Cell Advances Therapeutic Angiogenesis.* Stem Cells International, 2022. **2022**: p. 6795274.

22. Welsh, J.A., *Minimal information for studies of extracellular vesicles (MISEV2023): From basic to advanced approaches.* Journal of Extracellular Vesicles, 2024. **1**(13): p. 1-84.

23. Park, Y.S., N.H. Kim, and I. Jo, *Hypoxia and vascular endothelial growth factor acutely up-regulate angiopoietin-1 and Tie2 mRNA in bovine retinal pericytes.* Microvascular Research, 2003. **65**(2): p. 125-131.

24. Li, Q., et al., *Hemoglobin induced NO/cGMP suppression Deteriorate Microcirculation via Pericyte Phenotype Transformation after Subarachnoid Hemorrhage in Rats.* Scientific Reports, 2016. **6**: p. 22070.

25. Matsumoto, J., et al., *TNF-α-sensitive brain pericytes activate microglia by releasing IL-6 through cooperation between IκB-NFκB and JAK-STAT3 pathways.* Brain Research, 2018. **1692**: p. 34-44.

26. Stark K, E.A., Haidari S, Tirniceriu A, Lorenz M, von Brühl ML, Gärtner F, Khandoga AG, Legate KR, Pless R, Hepper I, Lauber K, Walzog B, Massberg S., *Capillary and arteriolar pericytes attract innate leukocytes exiting through venules and 'instruct' them with pattern-recognition and motility programs.* Nature Immunology 2013. **14**(1): p. 41-51.

27. Sun, Z., et al., *Reduction in pericyte coverage leads to blood–brain barrier dysfunction via endothelial transcytosis following chronic cerebral hypoperfusion.* Fluids and Barriers of the CNS 2021. **18**: p. 21.

28. Gundersen, G.A., et al., *Evidence that pericytes regulate aquaporin-4 polarization in mouse cortical astrocytes.* Brain Structure and Function 2014. **219**: p. 2181-2186.

29. Pieper, C., et al., *Brain capillary pericytes contribute to the immune defense in response to cytokines or LPS in vitro.* Brain Research, 2014. **1550**: p. 1-8.

30. Ayres-Sander, C.E., et al., *Transendothelial Migration Enables Subsequent Transmigration of Neutrophils through Underlying Pericytes.* PLOS ONE, 2013. **8**(3): p. e60025.

31. Beard, D.J., et al., *Rapamycin Treatment Reduces Brain Pericyte Constriction in Ischemic Stroke.* Translational Stroke Research 2024.

32. Gonul, E., et al., *Early Pericyte Response to Brain Hypoxia in Cats: An Ultrastructural Study.* Microvascular Research, 2002. **64**(1): p. 116-119.

33. Duz, B., et al., *The effect of moderate hypothermia in acute ischemic stroke on pericyte migration: An ultrastructural study.* Cryobiology 2007. **55**(3): p. 279-284.

34. Larey, A.M., et al., *High throughput screening of mesenchymal stromal cell morphological response to inflammatory signals for bioreactor-based manufacturing of extracellular vesicles that modulate microglia.* Bioactive Materials, 2024. **37**: p. 153-171.

35. Andrews, S.H., et al., *Morphological landscapes from high content imaging reveal cytokine priming strategies that enhance mesenchymal stromal cell immunosuppression.* Biotechnology and Bioengineering, 2022. **119**(2): p. 361-375.

36. Blocki, A., et al., *Not All MSCs Can Act as Pericytes: Functional In Vitro Assays to Distinguish Pericytes from Other Mesenchymal Stem Cells in Angiogenesis.* Stem Cells and Development, 2013. **22**(17).

37. Botelho de Souza, L.E., et al., *Mesenchymal Stem Cells and Pericytes: To What Extent Are They Related?* Stem Cells and Development, 2016. **25**(24).

38. Zhao, Z., et al., *Isolation and analysis methods of extracellular vesicles (EVs).* Extracellular Vesicles and Circulating Nucleic Acids, 2020: p. 80-103.

39. Klinker, M.W., et al., *Morphological features of IFN-γ–stimulated mesenchymal stromal cells predict overall immunosuppressive capacity.* PNAS, 2017. **114**(13): p. E2598-E2607.

40. Tello-Montoliu, A., J.V. Patel, and G.Y.H. Lip, *Angiogenin: a review of the pathophysiology and potential clinical applications.* Journal of Thrombosis and Haemostasis, 2006. **4**(9): p. 1864-1874.

41. Marui, A., et al., *Simultaneous application of basic fibroblast growth factor and hepatocyte growth factor to enhance the blood vessels formation.* Journal of Vascular Surgery, 2005. **41**(1): p. 82-90.

42. *LIP interleukin 6 family cytokine [Homo sapiens (human)]*. 2024, National Library of Medicine.

43. Gomez-Gaviro, M.V., et al., *Betacellulin promotes cell proliferation in the neural stem cell niche and stimulates neurogenesis.* PNAS, 2012. **109**(4): p. 1317-1322.

44. Lecuyer, M.-A., et al., *Dual role of ALCAM in neuroinflammation and blood–brain barrier homeostasis.* PNAS, 2017. **114**(4): p. E524-E533.

45. Cho, W.J., S.K. Mittal, and S.K. Chauhan, *Mesenchymal Stromal Cells Suppress T-Cell-Mediated Delayed-Type Hypersensitivity via ALCAM-CD6 Interaction.* Stem Cells Translational Medicine, 2023. **12**(4): p. 221-233.

46. Taj, S.H., et al., *argeted intracerebral delivery of the anti-inflammatory cytokine IL13 promotes alternative activation of both microglia and macrophages after stroke.* Journal of Neuroinflammation, 2018. **15**(174).

47. Bodnar, R.J. and A. Wells, *Differential Regulation of Pericyte Function by the CXC Receptor 3.* Wound Repair and Regeneration, 2015. **23**(6): p. 785-796.

48. Dore-Duffy, P. and K. Cleary, *Morphology and Properties of Pericytes*, in *Methods in Molecular Biology*. 2010, Humana Press. p. 49-68.

49. Tigges, U., et al., *TNF-α promotes cerebral pericyte remodeling in vitro, via a switch from α1 to α2 integrins.* Journal of Neuroinflammation, 2013. **10**(33).

50. Dore-Duffy, P., et al., *Pericyte Migration from the Vascular Wall in Response to Traumatic Brain Injury.* Microvascular Research, 2000. **60**(1): p. 55-69.

51. Persidsky, Y., et al., *Dysfunction of brain pericytes in chronic neuroinflammation.* Journal of Cerebral Blood Flow and Metabolism, 2015. **36**(4): p. 794-807.

52. Matsumoto, J., et al., *Tumor necrosis factor-α-stimulated brain pericytes possess a unique cytokine and chemokine release profile and enhance microglial activation.* Neuroscience Letters, 2014. **578**(22): p. 133-138.

53. Smyth, L.C.D., et al., *Unique and shared inflammatory profiles of human brain endothelia and pericytes.* Journal of Neuroinflammation, 2018. **15**(138).

54. Griffith, J.W., C.L. Sokol, and A. Luster, *Chemokines and Chemokine Receptors: Positioning Cells for Host Defense and Immunity.* Annual Review of Immunology, 2014. **32**: p. 659-702.

55. Vezzani, B., et al., *Higher Pericyte Content and Secretory Activity of Microfragmented Human Adipose Tissue Compared to Enzymatically Derived Stromal Vascular Fraction.* Stem Cells Translational Medicine, 2018. **7**(4).

56. da Silva Meirelles, L., et al., *Mesenchymal stem cells and their relationship to pericytes.* Frontiers in Bioscience, Landmark, 2016. **21**: p. 130-156.

57. Eiken, H.M., et al., *Pericytes regulate VEGF-induced endothelial sprouting through VEGFR1.* Nature Communications, 2017. **8**(1574).

58. Hung, C.F., et al., *Pericyte-like cells undergo transcriptional reprogramming and distinct functional adaptations in acute lung injury.* Federation of American Societies for Experimental Biology, 2021. **35**(4).

59. Tam, S.J., et al., *Death Receptors DR6 and TROY Regulate Brain Vascular Development.* Developmental Cell, 2012. **22**(2): p. 403-417.

60. Mikhrina, A.L. and I.V. Romanova, *The Role of AGRP in Regulating Dopaminergic Neurons in the Brain.* Neuroscience and Behavioral Physiology, 2015. **45**(5): p. 536-541.

61. Rustenhoven, J., et al., *TGF-beta1 regulates human brain pericyte inflammatory processes involved in neurovasculature function.* Journal of Neuroinflammation, 2016. **37**.

62. Hupfield, J., et al., *Modulation of mesenchymal stromal cell characteristics by microcarrier culture in bioreactors.* Biotechnology and Bioengineering, 2014. **111**(11): p. 2290-2302.

63. Fuzeta, M.d.A., et al., *Scalable Production of Human Mesenchymal Stromal Cell-Derived Extracellular Vesicles Under Serum-/Xeno-Free Conditions in a Microcarrier-Based Bioreactor Culture System.* Frontier Cell Development Biology, 2020. **8**.

64. Kink, J.A., et al., *Large-scale bioreactor production of extracellular vesicles from mesenchymal stromal cells for treatment of acute radiation syndrome.* Stem Cell Research & Therapy, 2024. **15**(72).

65. Lembong, J., et al., *Bioreactor Parameters for Microcarrier-Based Human MSC Expansion under Xeno-Free Conditions in a Vertical-Wheel System.* Bioengineering, 2020. **7**(3): p. 73.

66. Takata, F., et al., *Brain pericytes among cells constituting the blood-brain barrier are highly sensitive to tumor necrosis factor-α, releasing matrix metalloproteinase-9 and migrating in vitro.* Journal of Neuroinflammation, 2011. **8**(106).

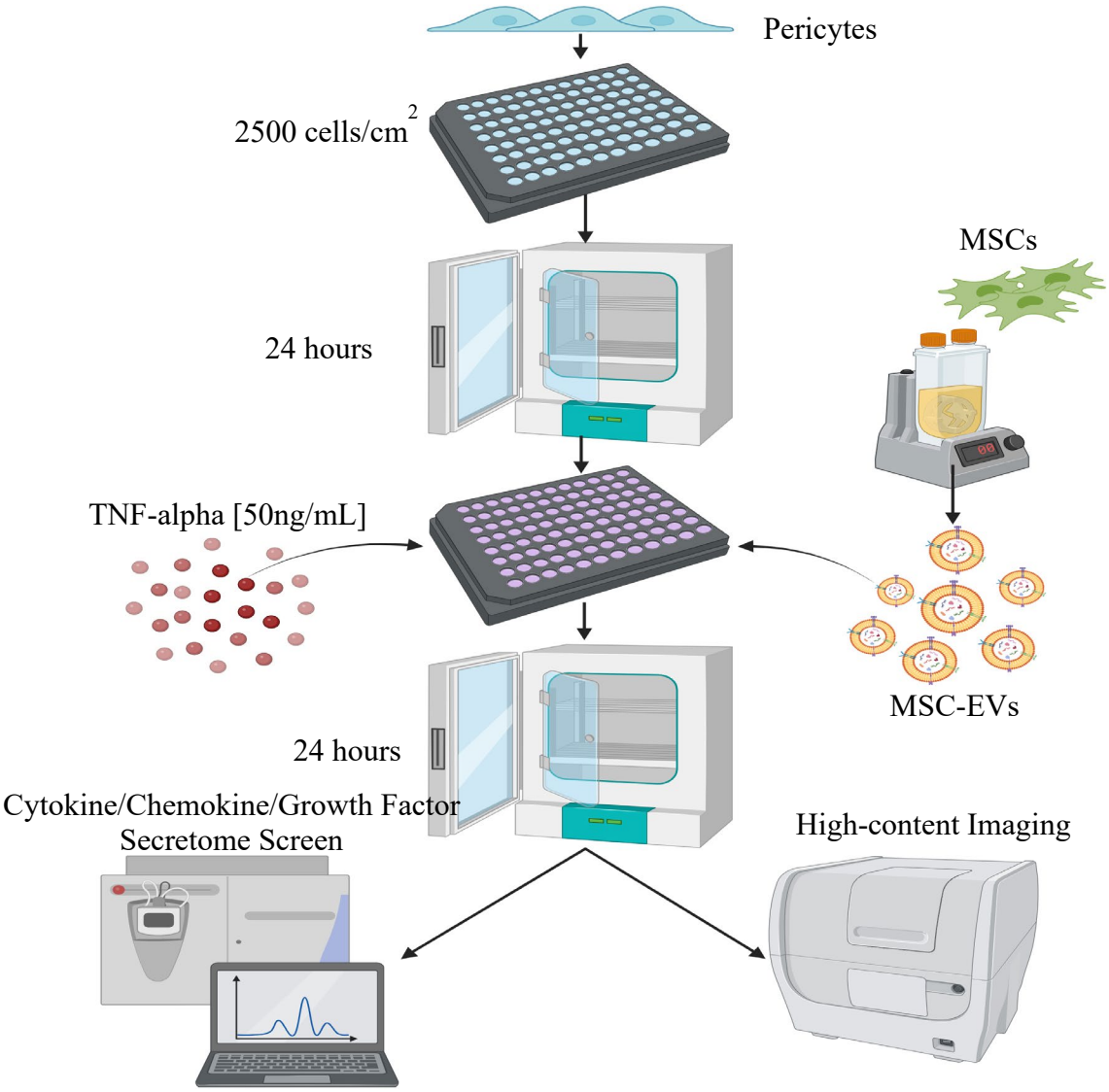

Figure 3.i Illustrative Abstract

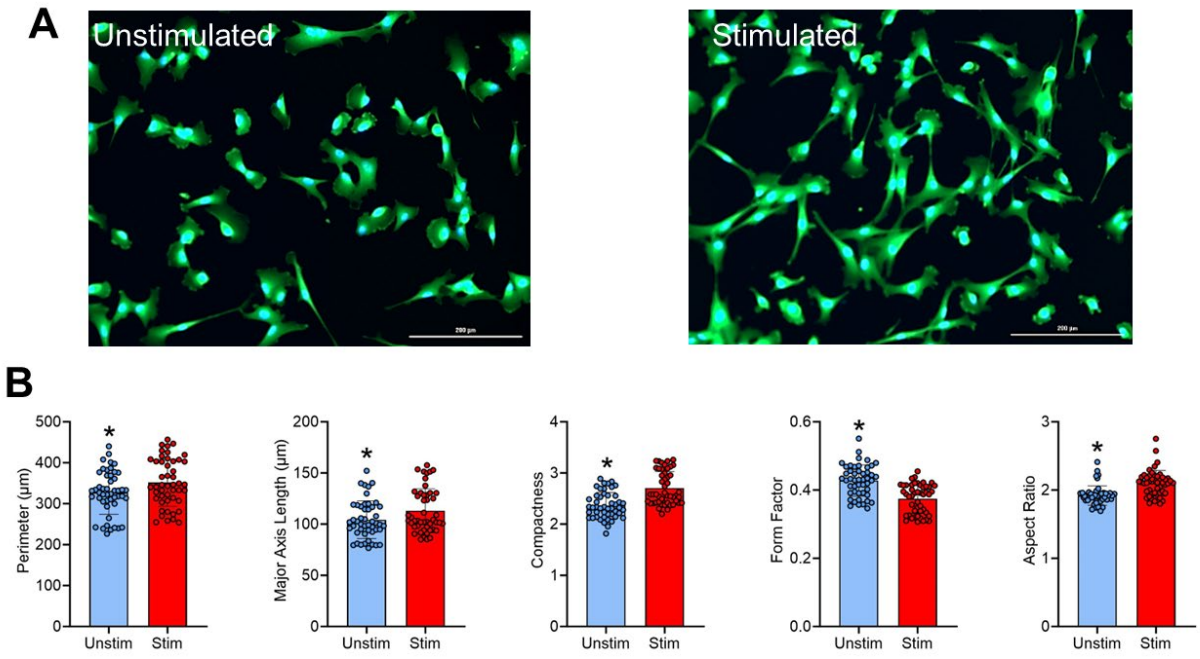

Figure 3.1. Pericytes become more complex and elongated with TNF-α stimulation. A. For each morphological feature, n=24 per condition. This data was gathered from four different experiments with 6 wells per condition. Unstimulated represents pericytes only in pericyte complete medium (ScienCell) and the stimulated group is pericytes treated with 50ng/mL of TNF-α in pericyte medium. *$p<0.0001$ different than unstimulated using paired T test. **B.** The left image represents unstimulated pericytes seeded in basal medium. The right image represents pericytes stimulated with TNF-α (50ng/mL). Pericytes were stained with Hoechst (blue) and fluorescein-maleimide (green) to show nuclei and cytoplasm, respectively. Scale bar = 200 µm.

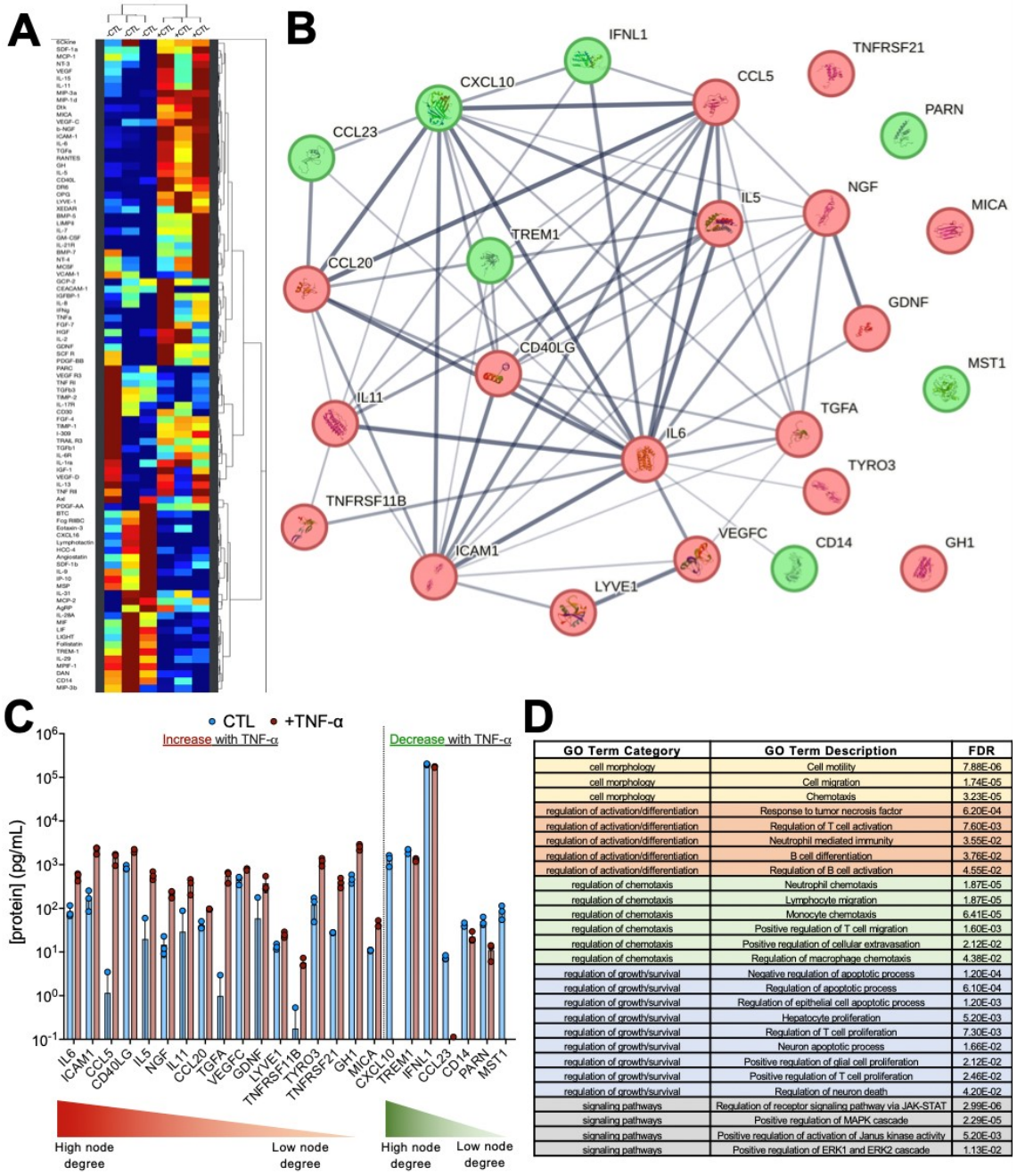

GO Term Category	GO Term Description	FDR
cell morphology	Cell motility	7.88E-06
cell morphology	Cell migration	1.74E-05
cell morphology	Chemotaxis	3.23E-05
regulation of activation/differentiation	Response to tumor necrosis factor	6.20E-04
regulation of activation/differentiation	Regulation of T cell activation	7.60E-03
regulation of activation/differentiation	Neutrophil mediated immunity	3.55E-02
regulation of activation/differentiation	B cell differentiation	3.76E-02
regulation of activation/differentiation	Regulation of B cell activation	4.55E-02
regulation of chemotaxis	Neutrophil chemotaxis	1.87E-05
regulation of chemotaxis	Lymphocyte migration	1.87E-05
regulation of chemotaxis	Monocyte chemotaxis	6.41E-05
regulation of chemotaxis	Positive regulation of T cell migration	1.60E-03
regulation of chemotaxis	Positive regulation of cellular extravasation	2.12E-02
regulation of chemotaxis	Regulation of macrophage chemotaxis	4.38E-02
regulation of growth/survival	Negative regulation of apoptotic process	1.20E-04
regulation of growth/survival	Regulation of apoptotic process	6.10E-04
regulation of growth/survival	Regulation of epithelial cell apoptotic process	1.20E-03
regulation of growth/survival	Hepatocyte proliferation	5.20E-03
regulation of growth/survival	Regulation of T cell proliferation	7.30E-03
regulation of growth/survival	Neuron apoptotic process	1.66E-02
regulation of growth/survival	Positive regulation of glial cell proliferation	2.12E-02
regulation of growth/survival	Positive regulation of T cell proliferation	2.46E-02
regulation of growth/survival	Regulation of neuron death	4.20E-02
signaling pathways	Regulation of receptor signaling pathway via JAK-STAT	2.99E-06
signaling pathways	Positive regulation of MAPK cascade	2.29E-05
signaling pathways	Positive regulation of activation of Janus kinase activity	5.20E-03
signaling pathways	Positive regulation of ERK1 and ERK2 cascade	1.13E-02

Figure 3.2. TNF-α stimulation significantly shifts pericyte secretome. A. Heat map representing all the proteins secreted by unstimulated (-CTL) and stimulated (+CTL) pericytes. Two-way clustering performed using Ward method. Red=high secretion, Blue=Low secretion. **B.** STRING pathway analysis relating secreted proteins. Those in green are decreased with TNF-α stimulation and those in red are increased with TNF-α stimulation. **C.** Shows the quantitative data of the proteins in B ordered from those with the most connections (node degrees) to the least number of connections within the network. **D.** Pathway enrichment analysis of the differentially regulated secreted proteins illustrates key pathways associated with pericyte function in homeostasis and disease. FDR: False Discovery Rate.

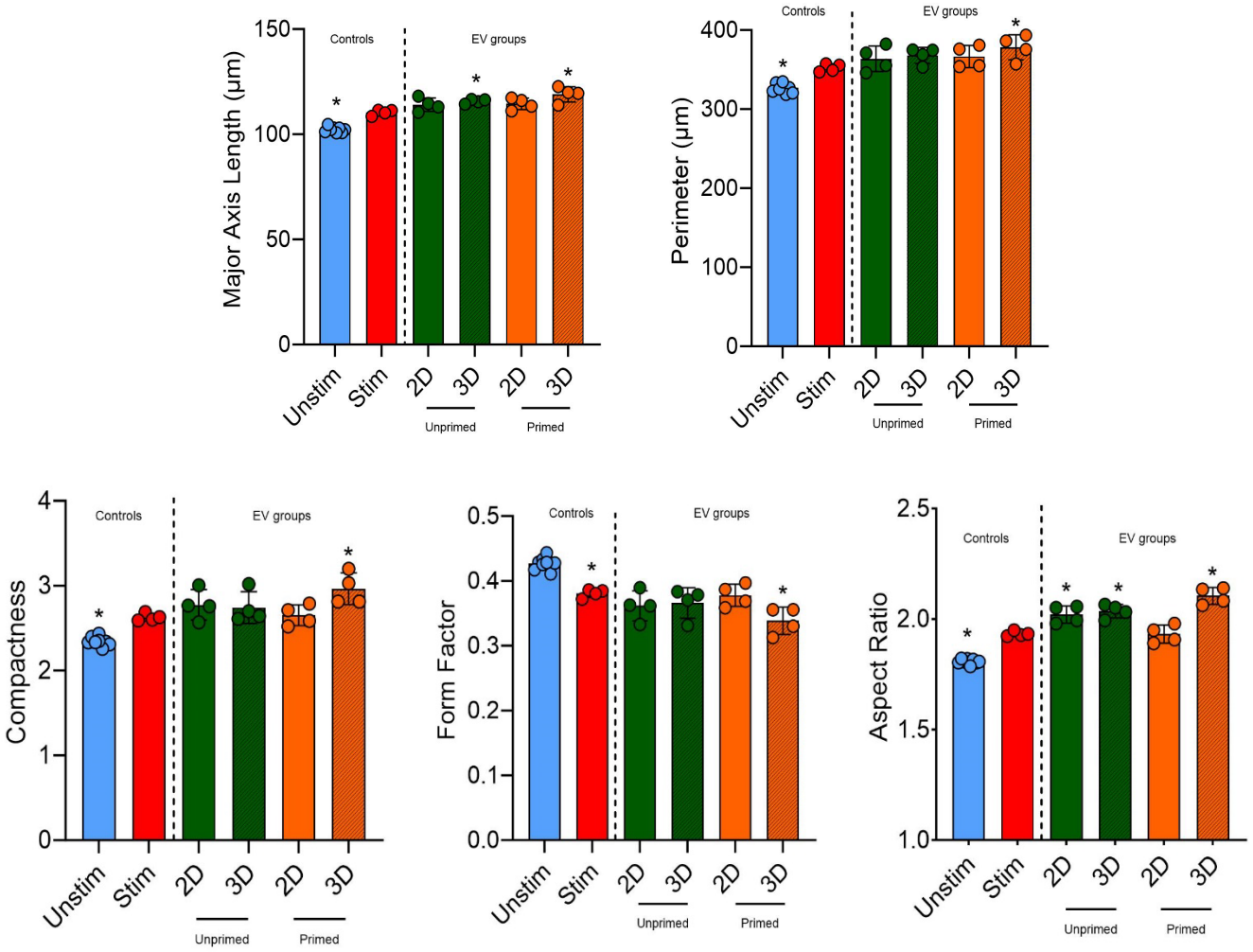

Figure 3.3. Primed bioreactor MSC-EVs increases pericyte morphological response. For each feature n=4. Unstimulated represents pericytes only in pericyte complete medium (ScienCell) and the stimulated group is pericytes treated with 50ng/mL of TNF-α in pericyte medium. 2D represents MSC-EVs derived from MSCs grown in T175 flasks and 3D represents MSC-EVs derived from MSCs grown in a vertical wheel bioreactor. Unprimed and primed are no treatment and 50ng/mL of TNF-α and 50ng/mL IFNγ, respectively.

Table 3.1 Tested MSC-EV Manufacturing conditions.

EV Group	Priming		Microcarrier Density
+CTL_low	1	+IFN-γ/TNF-α/20%O2	Low
Hit 2_low	2	+IFN-γ/TNF-α/2%O2	Low
Hit 4_low	3	+IFN-γ/TNF-α/IL-1β/20%O2	Low
+CTL_high	1	+IFN-γ/TNF-α/20%O2	High
Hit 2_high	2	+IFN-γ/TNF-α/2%O2	High
Hit 4_low	3	+IFN-γ/TNF-α/IL-1β/20%O2	High

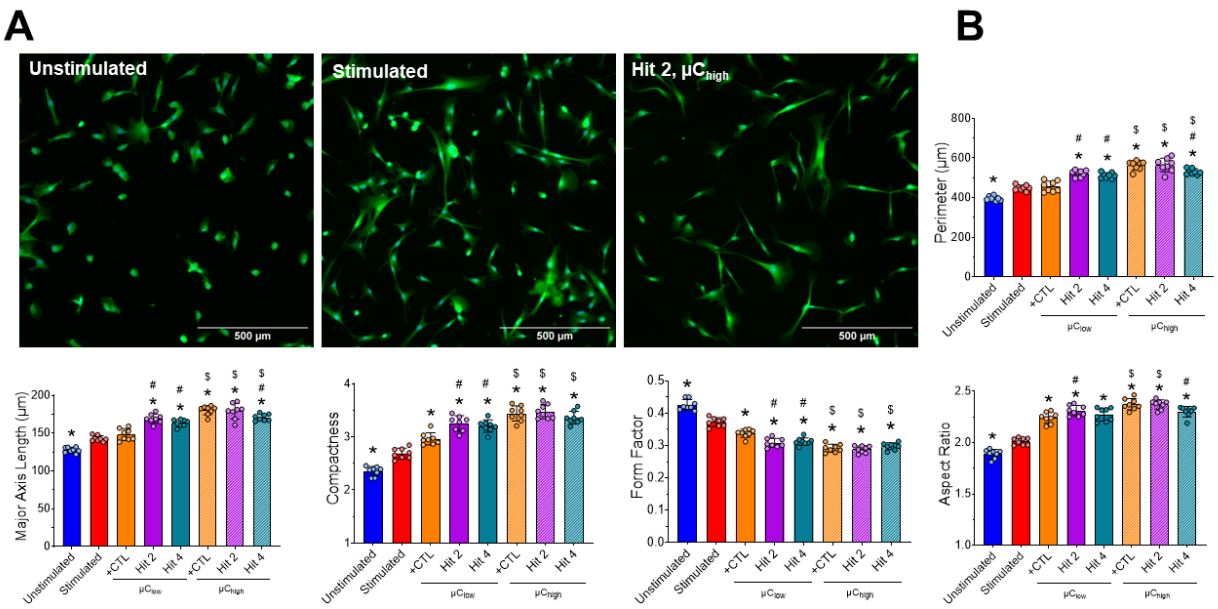

Figure 3.4. MSC-EVs affects pericyte morphology in a dose dependent manner. A. Illustrates (from left to right) Unstimulated, Stimulated, and EV group 5 at 1X. **B.** Describes differences between 5 different morphological parameters. ns represents insignificance from the stimulated group. Otherwise, all groups were significant compared to their stimulated control using a Brown-Forsythe and Welch's ANOVA test using Dunnet's T3 multiple comparison test where $p<0.0496$. * represents significance between dilution groups within an EV treatment using a Brown-Forsythe and Welch's ANOVA test using Dunnet's T3 multiple comparison test where $p<0.0487$. $ represents significance between microcarrier density groups between an EV treatment using a Brown-Forsythe and Welch's ANOVA test using Dunnet's T3 multiple comparison test where $p< 0.05$. # represents significance between EV treatment groups within a microcarrier density using a Brown-Forsythe and Welch's ANOVA test using Dunnet's T3 multiple comparison test where $p<0.05$. Scale bar = 500 microns.

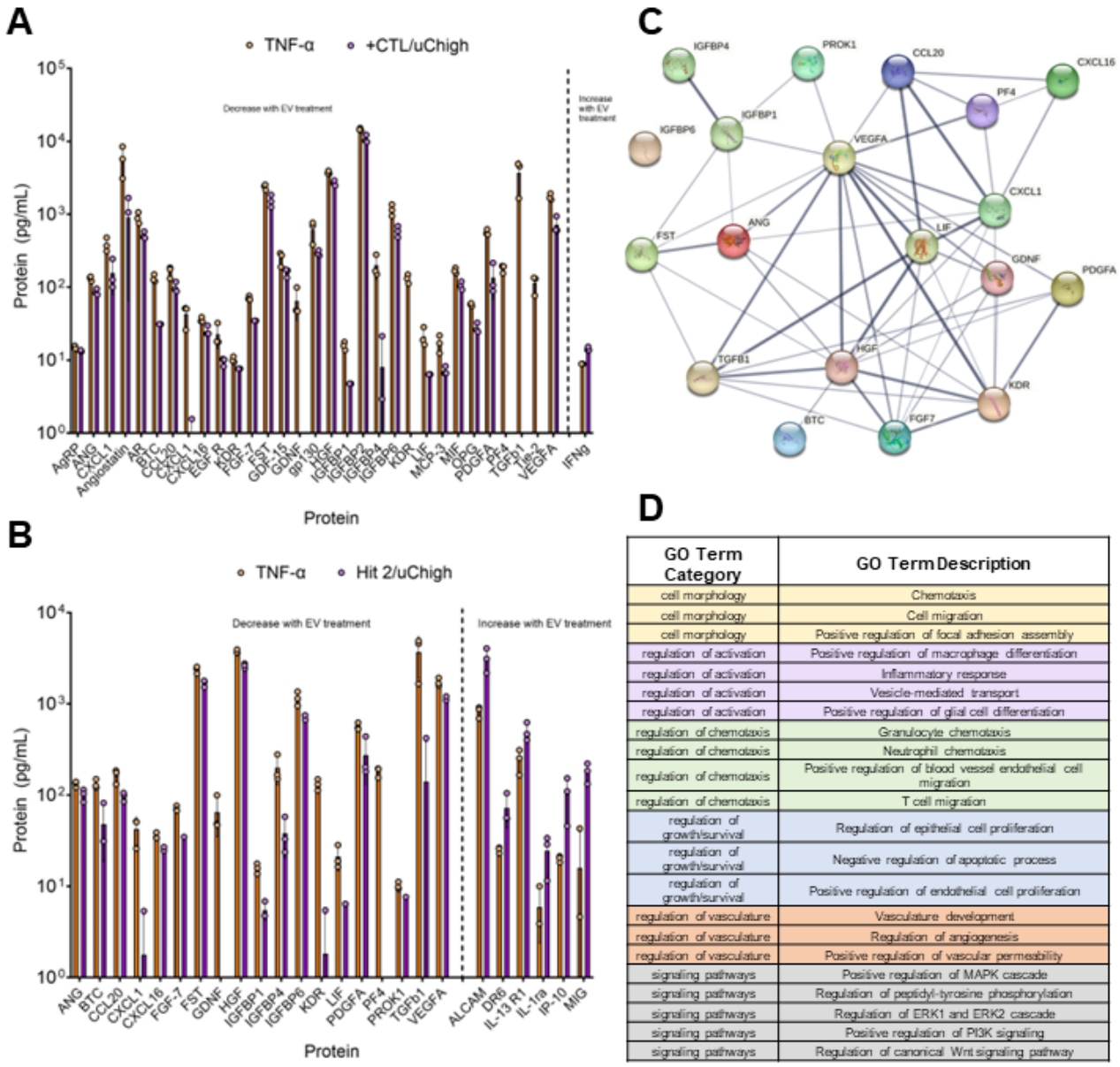

D

GO Term Category	GO Term Description
cell morphology	Chemotaxis
cell morphology	Cell migration
cell morphology	Positive regulation of focal adhesion assembly
regulation of activation	Positive regulation of macrophage differentiation
regulation of activation	Inflammatory response
regulation of activation	Vesicle-mediated transport
regulation of activation	Positive regulation of glial cell differentiation
regulation of chemotaxis	Granulocyte chemotaxis
regulation of chemotaxis	Neutrophil chemotaxis
regulation of chemotaxis	Positive regulation of blood vessel endothelial cell migration
regulation of chemotaxis	T cell migration
regulation of growth/survival	Regulation of epithelial cell proliferation
regulation of growth/survival	Negative regulation of apoptotic process
regulation of growth/survival	Positive regulation of endothelial cell proliferation
regulation of vasculature	Vasculature development
regulation of vasculature	Regulation of angiogenesis
regulation of vasculature	Positive regulation of vascular permeability
signaling pathways	Positive regulation of MAPK cascade
signaling pathways	Regulation of peptidyl-tyrosine phosphorylation
signaling pathways	Regulation of ERK1 and ERK2 cascade
signaling pathways	Positive regulation of PI3K signaling
signaling pathways	Regulation of canonical Wnt signaling pathway

Figure 3.5. MSC-EV treatment shifts stimulated pericyte secretome. A. Shows the quantitative data of the proteins effected by EV4 treatment. **B.** Shows the quantitative data of the proteins affected by EV5 treatment. **C.** STRING pathway analysis relating secreted proteins. Those in green are decreased with TNF-α stimulation and those in red are increased with TNF-α stimulation. **D.** Pathway enrichment analysis of the differentially regulated secreted proteins illustrates key pathways associated with pericyte function in homeostasis and disease.

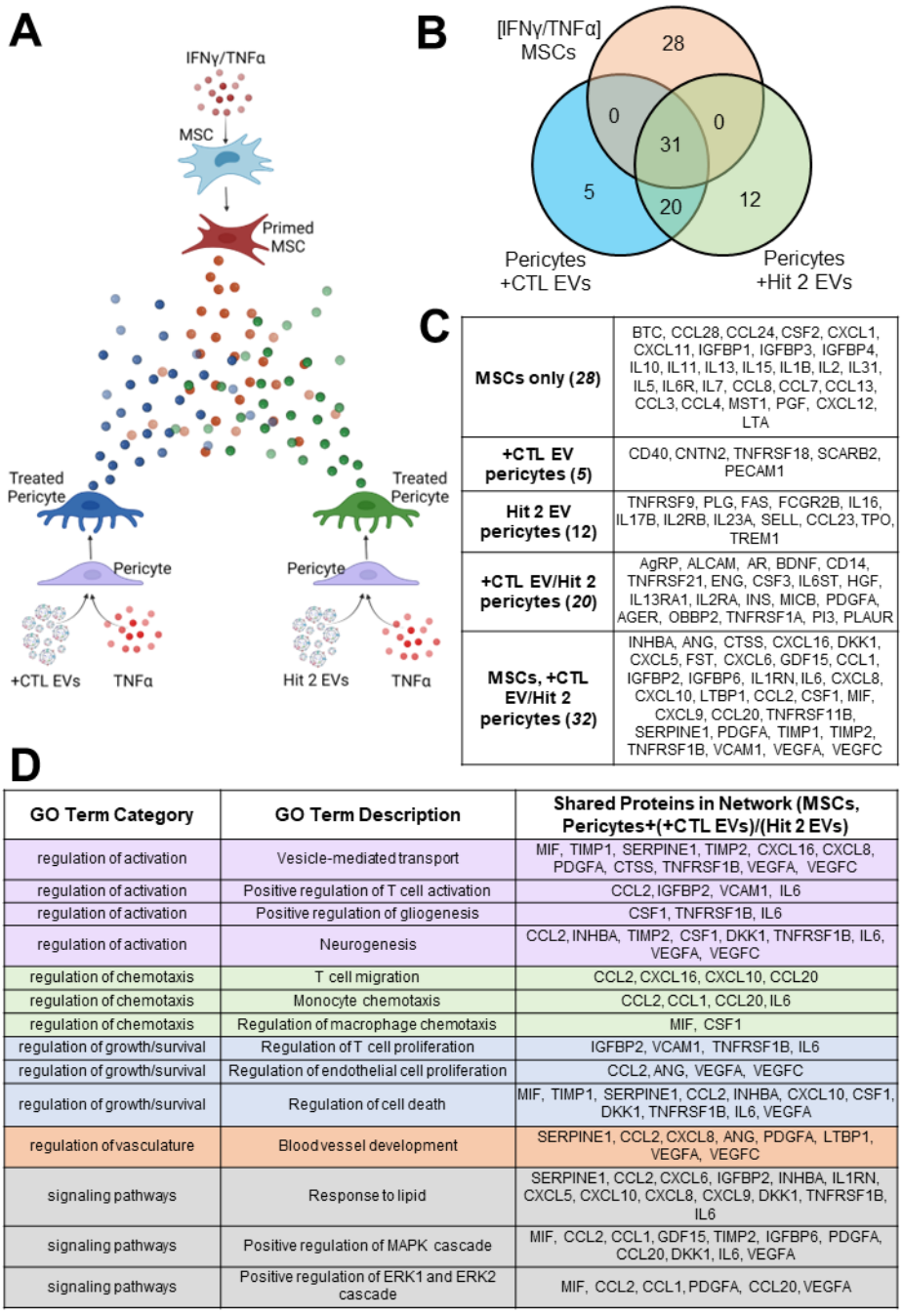

C

MSCs only (*28*)	BTC, CCL28, CCL24, CSF2, CXCL1, CXCL11, IGFBP1, IGFBP3, IGFBP4, IL10, IL11, IL13, IL15, IL1B, IL2, IL31, IL5, IL6R, IL7, CCL8, CCL7, CCL13, CCL3, CCL4, MST1, PGF, CXCL12, LTA
+CTL EV pericytes (*5*)	CD40, CNTN2, TNFRSF18, SCARB2, PECAM1
Hit 2 EV pericytes (12)	TNFRSF9, PLG, FAS, FCGR2B, IL16, IL17B, IL2RB, IL23A, SELL, CCL23, TPO, TREM1
+CTL EV/Hit 2 pericytes (*20*)	AgRP, ALCAM, AR, BDNF, CD14, TNFRSF21, ENG, CSF3, IL6ST, HGF, IL13RA1, IL2RA, INS, MICB, PDGFA, AGER, OBBP2, TNFRSF1A, PI3, PLAUR
MSCs, +CTL EV/Hit 2 pericytes (*32*)	INHBA, ANG, CTSS, CXCL16, DKK1, CXCL5, FST, CXCL6, GDF15, CCL1, IGFBP2, IGFBP6, IL1RN, IL6, CXCL8, CXCL10, LTBP1, CCL2, CSF1, MIF, CXCL9, CCL20, TNFRSF11B, SERPINE1, PDGFA, TIMP1, TIMP2, TNFRSF1B, VCAM1, VEGFA, VEGFC

D

GO Term Category	GO Term Description	Shared Proteins in Network (MSCs, Pericytes+(+CTL EVs)/(Hit 2 EVs)
regulation of activation	Vesicle-mediated transport	MIF, TIMP1, SERPINE1, TIMP2, CXCL16, CXCL8, PDGFA, CTSS, TNFRSF1B, VEGFA, VEGFC
regulation of activation	Positive regulation of T cell activation	CCL2, IGFBP2, VCAM1, IL6
regulation of activation	Positive regulation of gliogenesis	CSF1, TNFRSF1B, IL6
regulation of activation	Neurogenesis	CCL2, INHBA, TIMP2, CSF1, DKK1, TNFRSF1B, IL6, VEGFA, VEGFC
regulation of chemotaxis	T cell migration	CCL2, CXCL16, CXCL10, CCL20
regulation of chemotaxis	Monocyte chemotaxis	CCL2, CCL1, CCL20, IL6
regulation of chemotaxis	Regulation of macrophage chemotaxis	MIF, CSF1
regulation of growth/survival	Regulation of T cell proliferation	IGFBP2, VCAM1, TNFRSF1B, IL6
regulation of growth/survival	Regulation of endothelial cell proliferation	CCL2, ANG, VEGFA, VEGFC
regulation of growth/survival	Regulation of cell death	MIF, TIMP1, SERPINE1, CCL2, INHBA, CXCL10, CSF1, DKK1, TNFRSF1B, IL6, VEGFA
regulation of vasculature	Blood vessel development	SERPINE1, CCL2, CXCL8, ANG, PDGFA, LTBP1, VEGFA, VEGFC
signaling pathways	Response to lipid	SERPINE1, CCL2, CXCL6, IGFBP2, INHBA, IL1RN, CXCL5, CXCL10, CXCL8, CXCL9, DKK1, TNFRSF1B, IL6
signaling pathways	Positive regulation of MAPK cascade	MIF, CCL2, CCL1, GDF15, TIMP2, IGFBP6, PDGFA, CCL20, DKK1, IL6, VEGFA
signaling pathways	Positive regulation of ERK1 and ERK2 cascade	MIF, CCL2, CCL1, PDGFA, CCL20, VEGFA

Figure 3.6. MSC-EV treatment shifts pericyte secretome toward primed MSC secretome. **A.** Schematic of similaries between primed MSCs and EV treated pericytes. **B.** Venn diagram illustrating secretome similarities and differences between EV treated pericytes and primed MSCs **C.** Identifies the proteins that are similar and different between groups. **D.** Pathway enrichment analysis of the differentially regulated secreted proteins illustrates key pathways associated with pericyte function in homeostasis and disease and what proteins are associated with these functions.

CHAPTER 4

COMPARATIVE ANALYSIS OF MSC-EV POPULATIONS ISOLATED BY ULTRACENTRIFUGATION AND TANGENTIAL FLOW FILTRATION[1]

[1]Courtney E. Campagna, Lai Xu, Wells Wu, Kyung Sung. To be submitted to a peer-reviewed journal.

4.1 ABSTRACT

Mesenchymal stromal cell extracellular vesicles (MSC-EVs) hold great promise as therapeutics for inflammatory-related diseases, including Alzheimer's and Parkinson's. Despite this potential, standardized methods for MSC-EV manufacturing and analysis are lacking, with no established gold standard. As a result, researchers often employ their own protocols, contributing to variability in MSC-EV populations and making it difficult to define their mechanism of action. This variability, coupled with the inherent heterogeneity of MSC-EVs, presents challenges for translating these therapies into clinical applications. Previous studies have shown that isolation methods can influence the cargo profiles of MSC-EVs, potentially altering their therapeutic effects. In this study, we compare MSC-EV cargo and functional outcomes of MSC-EVs isolated by two widely used methods: tangential flow filtration (TFF) and ultracentrifugation (UC). Our findings reveal distinct differences in cargo profiles between these methods; however, these differences did not translate into detectable immunomodulatory functional variations.

4.2 INTRODUCTION

Mesenchymal stromal cells (MSCs) hold significant potential for treating inflammatory diseases such as multiple sclerosis, Alzheimer’s disease, and Parkinson’s disease, thanks to their strong immunomodulatory properties [1-3]. However, despite this promise, their use in clinical trials faces numerous challenges due to the need for invasive procedures and possible side-effects such as thrombosis and tumorgenicity [4-6]. MSC-derived extracellular vesicles (MSC-EVs) offer a cell-free alternative, carrying similar immunomodulatory benefits without cell associated risks [7, 8]. MSC-EVs are MSC-derived multivesicular bodies that fuse to the plasma membrane and are released into the extracellular space or shed directly from the plasma

membrane through outward budding. EVs include a lipid bilayer encapsulating various molecules (e.g., miRNA, tetraspanins, enzymes), allowing them to interact with other cells [9, 10].

Despite their potential, the heterogeneity of MSC-EVs and the variability in isolation methods make it difficult to standardize their production process. Although the international Society of Extracellular Vesicles (ISEV) provides guidelines for the manufacturing and analyses of EVs [11], no consensus exists on a standard method, leaving researchers to select methods based on their needs. As of 2016, ultracentrifugation is the most widely used EV isolation method but presents challenges in consistency and yield [12].

Ultracentrifugation (UC) uses centrifugal forces to separate particles from a mixture based on their size, shape, and density [13]. The samples for UC include particles suspended in a solution which is then spun at extremely high-speed creating strong centrifugal forces. This force pushes heavier and denser particles towards the bottom of the tube where, after centrifugation is complete, the separate components can be extracted [13]. UC is often the chosen isolation method because it is easy to use, requires little technical expertise, is affordable, and moderately time consuming [14]. However, UC is not the most reliable or efficient method. Crigna et al., performed an inter-laboratory comparison of extracellular vesicle UC isolations from colorectal cancer cells [15]. They found that all groups isolated EVs however, there were quantitative differences in EV yield that could be due to equipment, and operator-dependent variability [15].

Tangential flow filtration (TFF) is a filtration system that concentrates and filters particles using crossflow filtration. The media flows parallel across the filter membrane where particles smaller than the MWCO are discarded and those bigger, such as MSC-EVs, are retained and

recirculated and concentrated [16, 17]. TFF is an advantageous technique for isolating MSC-EVs because it produces a higher yield, preserves EV integrity, allows for size-based separation, and is both scalable and time efficient, however it requires technical training and is very expensive.

TFF operates with continuous flow and lower pressures exerting softer forces upon the MSC-EVs than UC [18]. The TFF process also allows for a more selective isolation of MSC-EVs as the separation is dependent on the pore size of the filter chosen. In addition, TFF can easily be scaled up for clinical or industrial production and is less time consuming than UC which is limited by the machine and accessories used in addition requiring hours to properly allow for the particles to precipitate in the tube [19]. These benefits have been reflected in experimental studies. For example, Visan et al., found that EVs murine cancer cell EVs isolated from TFF had a significantly higher concentration, yield, and purity than UC isolated samples [16]. Another study, found similar results finding that EV isolated by TFF significantly increased yield and was better at removing macromolecules than UC [20].

It is widely accepted that the parent cells and culture conditions MSC-EVs are derived from can greatly influence their functional abilities. However, there is little research exploring how isolation methods affect MSC-EV function outcomes. One study compared MSC-EVs isolated from conditioned culture medium using anion exchange resin (IEX) and Amicon filters with 100-kDA cut-off (UF) and found that these two methods yielded comparable size and concentration of particles and similar quantities of lipids. However, IEX had a 10-fold higher RNA quantity, larger number of proteins, and were more enriched in anti-inflammatory and immunomodulatory cytokines (i.e., IL-2, IL-10, TGF-B, VEGF) than UF isolated EVs [21]. When testing the EVs bioactivity, they used LPS stimulated macrophages and T cell proliferation assays and found that IEX significantly suppressed macrophage activation and T cell

proliferation compared to UF, respectively [21]. This illustrates how isolation methods can change the bioactivity of MSC-EVs. As TFF and UC have shown differences in the proteomic profile of their isolated EV populations we believe that these methods may also result in differences in bioactivity [16]. In this study, we compare MSC-EVs isolated by TFF and UC to assess how these methods impact EV characteristics and bioactivity.

4.3 MATERIALS AND METHODS

4.3.1 Cell Culture

Four MSC donors, two bone marrow and two adipose tissue, (RB14, RB30, RB61, and RB97) (RoosterBio; Frederick, MD) were thawed into a T175 culture flask with 25mL of MSC growth media and let to reach between 80-90% confluency over 96 hours. Once the cells had reached confluency, they were split into six T175 flasks at a million cells/flask. The cells were then grown for 72 hours after which the supernatant was discarded and replaced with RoosterCollect-EV (M2001; RoosterBio; Frederick, MD) supplemented with Interferon gamma (IFNγ) [50ng/mL] for 48 hours. After which, the supernatant was collected into 50mL conical tubes for EV isolation and the cells were trypsinized using TryplE (12604039; Gibco) for final count using Nexcelom Bioscience Cellometer.

4.3.2 EV isolation

The supernatant was first centrifuged at 300 xg for 10 minutes at 4C and then passed through a 0.022-micron syringe filter. The supernatant was stored on ice until it could be isolated. For TFF (KrosFlo KR2i, Repligen; Boston, MA) isolation the supernatant was passed through a 100KDa MWCO MidiKros mPES membrane with six diafiltration steps and a transmembrane pressure of

5 PSI to concentrate samples to a final volume of ~10-15mL in PBS-/-. For UC isolation, the supernatant was spun at 110,000xg for 90min at 4°C in a Beckman Coulter Optima MAX-XP Ultracentrifuge (Beckman Coulter; Brea, CA). After the supernatant was discarded, the remaining MSC-EV pellet was resuspended in a total of 6mL of PBS-/-. For both TFF and UC the samples were further concentrated using a 100kDA centrifugation spin concentrator (88524; ThermoFisher Scientific; Waltham, MA). The concentrated MSC-EVs were then resuspended in 1X PBS-/- for a final volume of 1mL. The MSC-EV samples were then aliquoted and stored at -80°C before being processed for characterization and functionality within 30 days of initial storage.

4.3.3 EV Characterization and Analysis

The size and count of the MSC-EVs were analyzed using a NanoSight LM10 (Malvern Instruments) using NanoTracking Analysis (NTA) software using the same settings (screen gain: 10, camera level: 10, number of captures: 3, Capture duration: 60s). The samples were diluted 20X and each sample was measured three times with 3 technical replicates. The protein concentration was analyzed using Bicinchoninic acid protein assay (23225; Thermo Scientific). The samples were diluted 8X with n=3 for each sample. Western blot was performed on all samples using MSC-EV markers CD81 (1:20,000; Proteintech), and CD9 (1:20,000; Proteintech) and CD63 (1:10,000; Proteintech), and secondary stain HRP (1:20,000; Abcam) using the Invitrogen system.

4.3.5 Next Generation Sequencing

Four MSC donors, two bone marrow and two adipose tissue cell lines, (RB14, RB30, RB61, and RB97) (RoosterBio; Frederick, MD) were thawed into about twelve T175 culture flask with

25mL of MSC growth media each and allowed to reach between 80-90% confluency over 96 hours. Once the cells had reached confluency, they were split into forty-eight T175 flasks at a million cells/flask. The cells were then grown for 72 hours after which the supernatant was discarded and replaced with RoosterCollect-EV (M2001; RoosterBio; Frederick, MD) supplemented with Interferon gamma (IFNγ) [50ng/mL] for 48 hours. After which, the conditioned media from twelve flasks was collected and isolated using either TFF and the other twelve using UC. The isolated MSC-EVs were then resuspended in 100uL of PBS-/-, aliquoted and frozen at -80°C. Within 2 weeks of freezing, the EV pellets were thawed, and the RNA was isolated using the PureLink RNA Mini Kit (12183018A; Invitrogen, Waltham, MA). The MSC-EVs were lysed using the kit's lysis buffer and the RNA was processed following the manufacturer's directions. The isolated RNA was then submitted to the FDA Analysis Core for next-generation sequencing.

4.3.6 Proteomic Profiling

For proteomic analysis, RB30 was thawed at passage 3 in three T175's containing 25mL of MSC culture media. The cells were then grown for 72 hours after which the supernatant was discarded and replaced with RoosterCollect-EV (M2001; RoosterBio; Frederick, MD) supplemented with or without Interferon gamma (IFNγ) [50ng/mL] for 48 hours. After which, the supernatant was collected into 50mL conical tubes for EV isolation. After isolating RB30 IFNγ and RB30 CTL MSC-EVs using the isolation methods explained above the MSC-EVs were aliquoted and stored at -80°C. The aliquots were then denatured by heating it to 95°C for five minutes and then sonicated for 30 seconds before being diluted in 1X RIPA buffer (89901; Fisher Scientific) at a ratio of 1:1 (v/v) and then submitted for Liquid Chromatography Mass Spectrometry (LC-MS) analysis at the FDA Proteomic Core.

4.3.7 Pericyte Morphology Assay

A T175 flask was coated with 1% (w/w) poly-d-lysine (PDL) for 24 hours at 4°C. After, the flask was washed with PBS three times to get rid of excess PDL and 35 mL of pericyte medium (Sciencell) was added. 10^6 previously frozen human brain pericytes (Sciencell) were thawed and seeded on the coated T175 flask. A flat-bottomed 96-well plate (Corning, Cat # 3599) was coated with 1% (w/w) poly-d-lysine (PDL) for 24 hours at 4°C. Once the pericytes reached 80-90% confluency (3 days) they were harvested using TrypLE (Gibco) and were seeded at 2,500 cells/cm^2 for 24 hours in 100 µL of pericyte complete medium in the prepared 96-well plate. After 24 hours, 50% of the media (50 µL) was aspirated from each well. Then 50 µL of pericyte medium only ('unstimulated') or 50 µL of pericyte medium containing 50 ng/mL TNF-α (Gibco, PHC3015) ('stimulated') were added to appropriate wells and pericytes incubated for an additional 24 hours. For MSC-EV treated pericyte groups, MSC-EVs were added concurrently with 100 ng/mL of TNF-α (50 ng/mL final concentration due to half media change) in pericyte media to the appropriate wells. We fixed samples using 4% paraformaldehyde (Electron Microscopy Sciences) and stained with Hoechst [10µg/mL] (Invitrogen) and Fluorescein maleimide [20µM] (ThermoFisher) in PBS-/- (Gibco) for nuclear and cytoplasm morphology, respectively as done in Klinker et al [22]. Pericytes were imaged using Cytation 5 High Content Imaging system (Agilent) and a Ti-Eclipse (Nikon) with the imaging system indicated in each figure legend. We imaged 50% of every well using a 6x6 montage at 10X magnification. These images were processed on a single-cell basis for over 96 different nuclear and cytoplasmic morphological features using CellProfiler pipeline (Supplemental Figure 4.1).

4.3.8 Macrophage Assay

RAW 264.7 murine macrophage cells (ATCC; Manassas, VA) were thawed and washed in 10mL of DMEM (Gibco; 11995-065) supplemented with 10% FBS, 1% penicillin and 1% streptomycin. The cells were centrifuged at 500 xg for 5 minutes and cultured in T75 flaks containing 20mL of DMEM supplemented with 10% FBS and 1% penicillin and 1% streptomycin for 24 hours at 37°C in 5% CO2. The cells were then trypsinized with TryplE Express Enzyme (ThermoFisher; Waltham, MA) and collected for centrifugation at 500 xg for 10minutes. The cells were counted and seeded on a 48-well plate at a density of 1 x 10^5 per well in 300uL of medium. After a 24 hour incubation, the macrophages were treated and placed in the incubator for another 24 hours. The conditioned medium was then collected and kept frozen at -80°C until analysis. The supernatant was then processed using IL-6 Murine ELISA (R&D Systems; M6000B) according to manufacturers' instructions.

4.4.9 Statistics and Data Analysis

All MSC-EV size and concentration data is presented as the average of three separate manufacturing's where each sample included three technical replicates of three biological replicates. All size and concentration data statistical analyses were performed using GraphPad Prism v10.

4.4 RESULTS

4.4.1 Tangential Flow Filtration isolated larger MSC-EVs at a higher concentration

Four MSC lines, two bone marrow (RB14 and RB30) and two adipose tissue (RB61 and RB97) cell lines were expanded until passage 3 and seeded into a T175 flask where they were expanded, split again, and then primed using RoosterBio RoosterCollect-EV and 50ng/mL of IFNγ for 48

hours. The conditioned media was collected from these flasks (total of 300mL) and MSC-EVs were then isolated from half the total media (150mL) using TFF or UC. The MSC-EVs were then resuspended in one mL of PBS-/- for a 150X dilution. These MSC-EVs were then frozen at -80°C and after one freeze thaw cycle were analyzed for size and concentration, and MSC-EV markers using NTA and western blot, respectively. We observed that all MSC-EV manufacturing groups were positive for MSC-EV markers CD9, CD63, and CD81 (Figure 4.1A). When observing the size distribution for each manufacturing method we found that all were within the accepted MSC-EV size range (30-1000nm) regardless of cell line or isolation method (Figure 4.1C). In addition to the size distribution and MSC-EV markers we looked at the size and concentration differences between batches, overall, and between manufacturing groups. When comparing concentration, we found that TFF isolated a higher concentration of MSC-EVs than UC for all three batches for all cell lines (Figure 4.1B and Supplementary Figure 4.2). We found that overall, the bone marrow lines produced a higher concentration of MSC-EVs than the adipose cells lines for both manufacturing conditions. We observed that within one batch there were not significant size differences (mean, median, or mode) between MSC-EVs manufacturing groups (Supplemental Figure 4.2) however, when taking the average, we found that TFF for RB14, RB30, and RB97 had a larger mean, median, and mode size, however for RB61, UC isolated MSC-EVs had a higher mean, median, and mode (Figure 4.1D and Supplementary Figure 4.2). We did observe batch-batch variability, however, none of the experiments were outliers.

4.4.2 Tangential Flow Filtration isolated MSC-EVs with a significantly different RNA profile compared to Ultracentrifugation

Both TFF and UC isolated MSC-EV RNA from all four MSC cell lines was analyzed using NGS. We first compared the differences between abundant genes (>5 RPKM) within a tissue source (bone marrow (left), adipose tissue (right)) and between isolation methods (Figure 4.2A). For RB14 and RB30 (bone marrow), we observed that TFF isolated MSC-EVs encompassed 1.53-fold more genes than UC MSC-EVs. Between the isolation groups they shared 894 genes that were related to cell death, intracellular transport, aerobic respiration, and neurogenesis. TFF isolated MSC-EVs included 1834 distinct genes that were related to catabolism, protein transport, mitotic cell cycle, ATP biosynthetic processes, and cytoskeleton organization. UC isolated MSC-EVs included 885 unique genes that are related to ribosome biogenesis, actin cytoskeleton organization, cell death, response to cytokines and cell migration. When comparing the adipose cell lines (RB61 and RB97), we observed TFF isolated MSC-EVs with 1.59-fold more genes than UC isolated MSC-EVs. Both TFF and UC shared 1596 genes that were related to ribosome biogenesis, actin cytoskeleton organization, cell death, protein transport, and response to cytokines. TFF isolated MSC-EVs contained 2963 unique genes that were related to catabolism, cell cycle, aerobic respiration, cell death and vesicle fusion and UC isolated MSC-EVs contained 1258 unique genes that were related to negative regulation of DNA-templated transcription, embryo development, cell cycle, regulation of secretion, and neural tube development. A full list of genes for each group can be found in Supplementary Table 4.1. When comparing isolation methods, we identified 55 genes that were upregulated 2-fold in TFF isolated MSC-EVs compared to UC isolated MSC-EVs (Figure 4.2B). Of these 55 genes, 27% have roles in immune suppression (i.e., LGALS1, RGP1, TPM3), while others have roles in

proliferation (i.e., LONP1, KPNA3, RND3), structure (i.e., RDX, PLEC, TUBB3), and tumor suppression (COX5B, DLC1, ERH) (Supplementary Table 4.2). Whereas only 2 identified genes (RNY1 and DUX4) were upregulated 2-fold in UC isolated MSC-EVs compared to TFF (Figure 4.2C). These genes have roles related to RNASE and transcriptional activation. Additionally, we observed a higher expression of key gene families known to aid in the regulation of the inflammatory response and aid in tissue regeneration (cell cycle, collagen, IFNγ, Fatty-acid oxidation, glycolysis and MMPs) (Figure 4.2D and Supplementary Table 4.3). These gene families were upregulated between 1.3- to 2-fold in TFF isolated MSC-EVs compared to UC isolated MSC-EVs.

4.4.3 Tangential Flow Filtration Isolates RB30 MSC-EVs with a distinct Proteomic Profile

We observed clear separation in the RB30 MSC-EV proteomic profiles between both priming conditions and isolation methods (Red TFF, Black UC) (Figure 4.3B) comparing 248 proteins using HCA. When identifying differences in isolation methods between priming conditions we found that in RB30 control groups there were 65 genes shared between TFF and UC isolated MSC-EV populations that were related to epidermis development (Figure 4.3A). In RB30 control TFF isolated MSC-EVs we identified 88 unique proteins that were related to cell adhesion and in RB30 UC isolated MSC-EVs there were 46 unique proteins related to epidermis development. We also found that in RB30 IFNγ groups there were 57 genes shared between TFF and UC isolated MSC-EV populations related to extracellular matrix and complement activation (Figure 4.3A). In RB30 IFNγ TFF isolated MSC-EVs we identified 86 unique proteins that were related to extracellular matrix and in RB30 UC isolated MSC-EVs there were 30 unique proteins related to cytoskeleton organization. When comparing isolation methods, we observed 19 proteins that were expressed 2-fold higher in UC isolated MSC-EVs than TFF isolated MSC-EVs that are

related to keratinization response, cytoskeleton development, and epidermis development (Figure 4.3C). We also found that there were 59 proteins expressed 2-fold higher in TFF isolated MSC-EVs than UC MSC-EVs (Figure 4.3D). These proteins are related to extracellular matrix, response to wound healing, complement activation, neurogenesis, and cell adhesion. Lastly, we observed a significantly higher expression of collagen, glycolytic and MMP proteins in TFF than UC (Figure 4.3E).

4.4.4 MSC-EVs influence macrophage activation and brain pericyte morphology

To evaluate the immunomodulatory effects of MSC-EVs, we focused on two assays: macrophage IL-6 secretion and human brain pericyte morphology. These assays were chosen because IL-6 is a key pro-inflammatory cytokine, and its regulation provides insights into the anti-inflammatory potential of MSC-EVs [23]. Similarly, human brain pericyte morphology is an indicator of vascular stability and regeneration, which are critical factors in tissue repair and inflammatory response [24, 25].

We treated RAW246.7 murine macrophages with 10μg of MSC-EVs for all manufacturing groups of MSC-EVs. We then measured the macrophages interleukin-6 (IL-6) secretion using an ELISA. We found that there were no differences in IL-6 secretion between isolation methods except for RB14 MSC-EVs where TFF isolated MSC-EVs significantly decreased IL-6 secretion compared to UC isolated MSC-EVs (Figure 4.4A). We also observed that RB30 MSC-EVs induced a significantly higher IL-6 expression than any of the other cell lines.

Using passage 4 isolated human brain pericytes we observed a larger morphological change with the addition of TFF isolated bone marrow (RB14, RB30) MSC-EVs than other manufacturing groups as seen in the images (Figure 4.4B). All MSC-EV TFF manufacturing groups became

more complex or stellated in phenotype as reflected by an increase in compactness and a decrease in form factor (Figure 4.4C). However, we only saw an increase in size (perimeter and major axis length) in RB14 and RB30 TFF groups. In addition, we only observed differences between isolation methods in RB14 and RB30 where we observed TFF isolated EVs inducing a more complex (decrease in compactness and form factor) and larger (increase in perimeter and major axis length) pericyte phenotype.

4.5 DISCUSSION

MSC-EVs present considerable therapeutic potential for neurodegenerative and other inflammatory diseases [26-28]. However, the absence of standardized manufacturing processes presents substantial challenges in meeting translational needs and advancing to clinical applications [29]. In this study, we evaluated two commonly used MSC-EV isolation methods-tangential flow filtration and ultracentrifugation-to demonstrate that different techniques can markedly impact the population characteristics of MSC-EVs. Our findings revealed that these methods produced two distinct MSC-EV populations with differences in physical characteristics and cargo composition, though these variations did not affect their functional outcomes.

Although UC is widely used for MSC-EV isolation, its scalability is often limited, prompting many manufacturers to explore alternative methods like TFF, which can process larger volumes [12]. Few studies have directly compared MSC-EV populations isolated by UC and TFF, though existing research confirms concentration differences between the two methods [20]. Based on previous reports, we anticipated that TFF would yield a higher concentration of MSC-EVs without affecting their size. However, using NTA, we found that TFF isolated larger MSC-EVs than UC. This size difference was observed when averaging across batches, not within individual

batches (Figure 4.1C, Supplemental Figure 4.2). Therefore, we attribute this variation to batch-to-batch variability rather than fundamental difference between isolation methods. Nonetheless, all MSC-EVs were within the acceptable size range of 30-1000nm (Figure 4.1B) [30]. It is also important to note that, while NTA is widely used for quantifying MSC-EVs, it is a non-specific method that may also count any aggregated proteins and lipoproteins present in the sample, potentially impacting the accuracy and reproducibility of results across batches [31].

We compared the RNA profiles of four IFNγ-primed MSC cell lines using next-generation sequencing (NGS) and analyzed the proteomic profiles of the RB30 cell line with and without IFNγ priming. MSCs were primed with 50 ng/mL of IFNγ, a concentration known to significantly enhance the immunomodulatory potential of MSCs and thereby the MSC-EVs they release [32, 33]. We hypothesized that the RNA cargo of MSC-EVs would contain similar immunomodulatory molecules, regardless of the isolation method. However, our findings revealed distinct differences in both RNA and protein expression between TFF- and UC-isolated MSC-EVs, with TFF-isolated MSC-EVs showing a higher correlation with immunomodulatory molecules. To our knowledge, this is the first study to compare the RNA and proteomic profiles of MSC-EVs isolated via UC and TFF, though other studies have examined differences in cargo profiles across alternative isolation methods [21, 34].

After normalizing for total RNA isolated, we found that TFF (tangential flow filtration) isolated 1.53-fold more genes than UC (ultracentrifugation) in the bone marrow groups and 1.59-fold more genes in the adipose groups (Figure 4.2A). Additionally, TFF isolated RB30 EVs (extracellular vesicles) with 1.38-fold and 1.76-fold more protein in the unprimed and primed groups, respectively (Figure 4.3A). These proteomic profiles not only illustrate clear separation between isolation groups but also between priming groups (Figure 4.3B and Supplemental Table

4.4). This difference could be due to TFF producing purer EV samples than UC, other studies have suggested that UC isolation may damage EV integrity resulting in impaired functionality and formation of aggregates [18, 20, 35]. In addition, we observed TFF isolated a higher concentration of larger MSC-EVs than UC, which may result in the isolation of a broader range of MSC-EV subpopulations or vesicles with larger cargo capacity. Future studies are required to discern the cause of increased proteomic and RNA in TFF compared to UC isolated MSC-EVs.

When evaluating the differences in upregulated RNAs between isolation methods, we found that 55 genes were upregulated 2-fold in TFF compared to UC, whereas only two genes were upregulated 2-fold in UC compared to TFF (Figure 4.2B, Figure 4.2C). Similarly, TFF isolated 59 proteins from RB30 EVs with a 2-fold higher expression compared to UC, which isolated only 19 proteins with a 2-fold higher expression than TFF (Figure 4.3D and Figure 4.3C). These findings align with previous studies, such as Tieu et al., which reported a 3.9-fold higher protein concentration in TFF-isolated EVs compared to UC-isolated EVs [16, 36].

Further analysis of the functions of these upregulated genes and proteins revealed that TFF-isolated MSC-EVs exhibited higher expression of genes involved in immunomodulation and tissue regeneration. Of the 55 genes upregulated by TFF, 27% play roles in immune suppression (e.g., LGALS1, PGAM1, TPM3) (Figure 4.2B, Supplemental Table 4.2). In contrast, genes upregulated in UC were predominantly involved in RNase activity and transcriptional activation (e.g., RNY1 and DUX4) (Figure 4.2C) [37-43].

Similarly, we observed clear proteomic profile separation between both UC and TFF isolation methods for RB30 MSC-EVs (Figure 4.3B). The 2-fold upregulated proteins in UC isolated RB30 MSC-EVs mainly had roles in epidermis development, keratinization, and cytoskeleton

development (Figure 4.3C) [44, 45]. Whereas the proteins 2-fold upregulated in the TFF isolated MSC-EVs had higher expression of immunomodulatory roles (e.g., ECM, wound healing, neurogenesis) (Figure 4.3D) [46-48]. In addition, we observed separation between the proteomic profiles of primed and unprimed and IFNγ primed RB30 MSC-EVs (Figure 4.3A and Figure 4.3B). The roles in the IFNγ primed MSC-EVs had roles in ECM, cytoskeleton organization, ECM and complement activation whereas the unprimed RB30 MSC-EVs included protein mainly focusing on regulatory functions such as cell adhesion and epidermis development (Figure 4.3A and Figure 4.3B). This is expected as various studies have shown that IFNγ significantly increased the immunomodulatory function of MSCs and illustrates how TFF may better preserve MSC-EVs and their intended function than UC [49-52].

A more in-depth analysis of the RNA profiles demonstrated that TFF-isolated EVs exhibited a 1.3- to 2-fold higher expression of gene families related to the cell cycle, collagen production, IFNγ response, fatty acid oxidation (FAO), glycolysis, and matrix metalloproteinase (MMPs) genes (Figure 4.2D, Supplemental Table 4.3). Correspondingly, the RB30 protein profile indicated higher expression of collagen and MMP2 proteins in TFF compared to UC (Figure 4.3E).

Key cell cycle genes, such as cyclin-dependent kinase-12 (CDK12) and cyclin A2 (CCNA2) are known to support the protection and long-term survival of brain neurons by promoting of DNA repair [53, 54]. Upregulation of collagen genes, including collagen 6A1(COL6A1) and collagen 4A (COL4A), plays a critical roles in the reparative process, as collagen is an essential extracellular matrix protein that is involved in cell growth, differentiation, and regeneration [55, 56]. FAO genes have been implicated in enhancing cell proliferation and DNA repair [57, 58]. Increased expression of glycolytic enzymes such as Enolase 1 (ENO1) and Phosphoglycerate

kinase 1 (PGK1), is linked to neuronal and microglia activation [59, 60]. Finally, MMPs, including MMP9 and MMP2, have been shown to have important roles in reducing inflammation through regulatory T-cell recruitment, activating astrogliosis for functional recovery, degradation of harmful aggregates (e.g., α-synuclein, associated with PD), and promoting angiogenesis [61-64].

Based off our cargo composition we hypothesized that TFF isolated MSC-EVs would have a higher immunomodulatory function than UC isolated MSC-EVs. However, these differences in cargo do not appear to have significant functional implications in our EV bioactivity assays. Murine RAW264.7 macrophages are known to produce pro-inflammatory cytokines such as TNFα, IL-6, and IL-1β in response to LPS treatment [65]. Previous studies have shown that LPS activated RAW264.7 macrophages respond to variations in EV manufacturing, making them a promising indicator of MSC-EV immunomodulatory potential [23, 66]. In our experiments, we measured IL-6 secretion from these macrophages but found minimal discernible differences between the manufacturing methods (Figure 4.4A). The only significant difference observed was in the RB14 group, where TFF-isolated EVs showed greater IL-6 attenuation compared to UC-isolated EVs. Overall, the trend suggests that TFF-isolated EVs from RB14, RB30, and RB97 were more effective at reducing macrophage activation, indicating an anti-inflammatory response. However, as this data is based on a single protein measurement, future studies should incorporate a broader profile of macrophage-secreted proteins for a more comprehensive understanding of MSC-EVs' effects on macrophage function.

In addition to the macrophage assay, we performed a screen of MSC-EV groups using our established pericyte morphological assay. In previous work, we demonstrated pericytes ability to discern manufacturing differences in terms of MSC culture platform and priming conditions

resulting in differing MSC-EV bioactivity (Chapter 3). In this study, we found that TFF-isolated MSC-EVs generally induced a more complex pericyte morphology, as indicated by increased compactness and decreased form factor (Figure 4.4B). Notably, only bone marrow-derived MSC-EVs increased pericyte size (in terms of perimeter and major axis length), which we believe reflects an enhanced immunomodulatory state in these pericytes based on previous work (Chapter 3). Consistent differences between TFF and UC were only observed in the RB14 group.

While the TFF-isolated MSC-EVs exhibited a cargo composition that suggests enhanced immunomodulatory potential, we found few functional differences between the isolation methods. Whether this is due to the limitations of our functional assays or because the observed cargo differences are not functionally significant requires further investigation.

This study represents the first in-depth evaluation of MSC-EV cargo differences between UC and TFF isolation methods. We believe this work will be instrumental in guiding the future standardization of MSC-EV manufacturing processes. Although multiple methods are currently used to isolate MSC-EVs, much attention has been placed on how conditions affecting the parent cells influence EV production, with less emphasis on the role of downstream processing. It is well understood, however, that these processing steps significantly impact the final MSC-EV populations [21, 29, 67]. Our findings provide initial evidence of cargo differences in MSC-EVs derived from the same cell source, though it is crucial to acknowledge the batch-to-batch variability and the limited scope of functional evaluations. Future studies will focus on optimizing the manufacturing process to minimize variability. This work lays a strong foundation for evaluating cargo differences across isolation methods, with future research aimed at clarifying these distinctions and determining their implications for the therapeutic potential of

MSC-EVs. Ultimately, our comparison of TFF and UC methods may help researchers choose the most effective isolation technique for MSC-EV production moving forward.

4.6 REFERENCES

1. Connick, P., et al., *Autologous mesenchymal stem cells for the treatment of secondary progressive multiple sclerosis: an open-label phase 2a proof-of-concept study.* Lancet Neurology 2012. **11**(2): p. 150-156.
2. Li, S., et al., *Proteomic characterization of hUC-MSC extracellular vesicles and evaluation of its therapeutic potential to treat Alzheimer's disease.* Scientific Reports, 2024. **14**: p. 5959.
3. Peng, H., et al., *Intranasal Administration of Self-Oriented Nanocarriers Based on Therapeutic Exosomes for Synergistic Treatment of Parkinson's Disease.* ACS Nano 2022. **16**(1): p. 869-884.
4. Kallmeyer, K., et al., *Fate of systemically and locally administered adipose-derived mesenchymal stromal cells and their effect on wound healing.* Stem Cells Translational Medicine, 2020. **9**(1): p. 131-144.
5. Barkholt, L., et al., *Risk of tumorigenicity in mesenchymal stromal cell based therapies—Bridging scientific observations and regulatory viewpoints.* Cytotherapy, 2013. **7**(2013): p. 753-759.
6. Breitbach, M., et al., *Potential risks of bone marrow cell transplantation into infarcted hearts.* Blood, 2007. **110**(4): p. 1362-1369.
7. Morad, G., et al., *Tumor-Derived Extracellular Vesicles Breach the Intact Blood-Brain Barrier via Transcytosis.* ACS Nano, 2019. **13**(12): p. 13853-13865.

8. Weng, Z., et al., *Therapeutic roles of mesenchymal stem cell-derived extracellular vesicles in cancer.* Journal of Hematology and Oncology 2021. **14**: p. 136.

9. Colombo, M., G. Raposo, and C. Thery, *Biogenesis, Secretion, and Intercellular Interactions of Exosomes and Other Extracellular Vesicles.* Annual Review of Cell and Developmental Biology 2014. **30**: p. 255-289.

10. Seo, Y., H.-S. Kim, and I.-S. Hong, *Stem Cell-Derived Extracellular Vesicles as Immunomodulatory Therapeutics.* Stem Cells International, 2019. **2019**.

11. Welsh, J.A., et al., *Minimal information for studies of extracellular vesicles (MISEV2023): From basic to advanced approaches.* Journal of Extracellular Vesicles, 2024. **13**(2).

12. Gardiner, C., et al., *Techniques used for the isolation and characterization of extracellular vesicles: results of a worldwide survey.* Journal of Extracellular Vesicles, 2016. **5**.

13. Thery, C., et al., *Isolation and Characterization of Exosomes from Cell Culture Supernatants and Biological Fluids.* Current Protocols in Cell Biology, 2006. **30**: p. 1-29.

14. Li, P., et al., *Progress in Exosome Isolation Techniques.* Theranostics, 2017. **7**(3): p. 789-804.

15. Crigna, A.T., et al., *Inter-Laboratory Comparison of Extracellular Vesicle Isolation Based on Ultracentrifugation.* Transfusion Medicine and Hemotherapy 2020. **48**(1): p. 48-59.

16. Visan, K., et al., *Comparative analysis of tangential flow filtration and ultracentrifugation, both combined with subsequent size exclusion chromatography, for*

the isolation of small extracellular vesicles. Journal of Extracellular Vesicles, 2022. **11**(9): p. 12266.

17. Liangsupree, T., E. Multia, and M.-L. Riekkola, *Modern isolation and seperation techniques for extracellular vesicles.* Journal of Chromatography A 2021. **1636**: p. 461773.

18. Linares, R., et al., *High-speed centrifugation induces aggregation of extracellular vesicles.* Journal Extracellular Vesicles, 2015. **4**: p. 29509.

19. Kawai-Harada, Y., V. Nimmagadda, and M. Harada, *Scalable isolation of surface-engineered extracellular vesicles and separation of free proteins via tangential flow filtration and size exclusion chromatography (TFF-SEC).* BMC Methods 2024. **1**: p. 9.

20. Busatto, S., et al., *Tangential Flow Filtration for Highly Efficient Concentration of Extracellular Vesicles from Large Volumes of Fluid.* Cells, 2018. **7**(12): p. 273.

21. Malvicini, R., et al., *Influence of the isolation method on characteristics and functional activity of mesenchymal stromal cell-derived extracellular vesicles.* Cytotherapy, 2024. **26**(2): p. 157-170.

22. Klinker, M.W., et al., *Morphological features of IFN-γ–stimulated mesenchymal stromal cells predict overall immunosuppressive capacity.* PNAS, 2017. **114**(13): p. E2598-E2607.

23. Kronstadt, S.M., et al., *Assessment of anti-inflammatory bioactivity of extracellular vesicles is susceptible to error via media component contamination.* Cytotherapy, 2023. **25**(4): p. 387-396.

24. Dore-Duffy, P. and K. Cleary, *Morphology and Properties of Pericytes*. 2011, Humana Press. p. 49-68.

25. Dibble, M., et al., *The impact of pericytes on the stability of microvascular networks in response to nanoparticles.* Scientific Reports, 2023. **13**(1).

26. Cai, Y., et al., *Bone Marrow-Derived Mesenchymal Stem Cell-Derived Exosomes Containing Gli1 Alleviate Microglial Activation and Neuronal Apoptosis In Vitro and in a Mouse Parkinson Disease Model by Direct Inhibition of Sp1 Signaling.* Journal of Neuropathology and Experimental Neurology, 2022. **81**(7): p. 522-534.

27. Zhang, Z., et al., *Human umbilical cord mesenchymal stem cell-derived exosomal miR-146a-5p reduces microglial-mediated neuroinflammation via suppression of the IRAK1/TRAF6 signaling pathway after ischemic stroke.* Aging, 2021. **13**(2): p. 3060-3079.

28. Lee, M., et al., *Adipose-derived stem cell exosomes alleviate pathology of amyotrophic lateral sclerosis in vitro.* Biochemical and Biophysical Research Communications, 2016. **479**(3): p. 434-439.

29. Lener, T., et al., *Applying extracellular vesicles based therapeutics in clinical trials – an ISEV position paper.* Journal of Extracellular Vesicles, 2015. **4**: p. 30087-30087.

30. Al-Sharabi, N., et al., *Osteogenic human MSC-derived extracellular vesicles regulate MSC activity and osteogenic differentiation and promote bone regeneration in a rat calvarial defect model.* Stem Cell Research & Therapy, 2024. **15**: p. 33.

31. Williams, S., et al., *Comparison of extracellular vesicle isolation processes for therapeutic applications.* Journal of Tissue Engineering 2023. **14**: p. 20417314231174609.

32. Noronha, N.d.C., et al., *Priming approaches to improve the efficacy of mesenchymal stromal cell-based therapies.* Stem Cell Research & Therapy, 2019. **10**: p. 131.

33. Bulati M, M.V., Gallo A, Amico G, Carcione C, Pampalone M, Conaldi PG, *The Immunomodulatory Properties of the Human Amnion-Derived Mesenchymal Stromal/Stem Cells Are Induced by INF-γ Produced by Activated Lymphomonocytes and Are Mediated by Cell-To-Cell Contact and Soluble Factors.* Frontiers Immunology, 2020. **12**(11): p. 54.

34. Brennan, K., et al., *A comparison of methods for the isolation and separation of extracellular vesicles from protein and lipid particles in human serum.* Scientific Reports, 2019. **10**: p. 1039.

35. Mol, E.A., et al., *Higher functionality of extracellular vesicles isolated using size-exclusion chromatography compared to ultracentrifugation.* Nanomedicine: Nanotechnology, Biology and Medicine, 2017. **13**(6): p. 2061-2065.

36. Tieu, A., et al., *Biodistribution of mesenchymal stromal cell-derived extracellular vesicles administered during acute lung injury.* Stem Cell Research & Therapy, 2023. **14**(1): p. 250.

37. Pedemonte, E., et al., *The molecular signature of therapeutic mesenchymal stem cells exposes the architecture of the hematopoietic stem cell niche synapse.* BMC Genomics 2007. **8**(1): p. 65.

38. Wagner, W., et al., *The heterogeneity of human mesenchymal stem cell preparations—Evidence from simultaneous analysis of proteomes and transcriptomes.* Experimental Hematology 2006. **34**(4): p. 536-548.

39. Ruvolo, P.P., et al., *LGALS1 acts as a pro-survival molecule in AML.* Biochimica et Biophysica Acta - Molecular Cell Research 2020. **1867**(10): p. 118785.

40. Wang, C., et al., *A phosphoglycerate mutase 1 allosteric inhibitor restrains TAM-mediated colon cancer progression.* Acta Pharmaceutica Sinica B 2024.

41. Zhao, Y.-C., et al., *TPM3: a novel prognostic biomarker of cervical cancer that correlates with immune infiltration and promotes malignant behavior in vivo and in vitro.* American Journal of Cancer Research 2023. **13**(7): p. 3123-3139.

42. MacIntosh, G.C., et al., *Characterization of Rny1, the Saccharomyces cerevisiae member of the T2 RNase family of RNases: Unexpected functions for ancient enzymes?* PNAS, 2001. **98**(3): p. 1018-1023.

43. Mocciaro, E., et al., *DUX4 Role in Normal Physiology and in FSHD Muscular Dystrophy.* Cells, 2021. **10**(12): p. 3322.

44. Kurashima, Y., et al., *Mucosal Mesenchymal Cells: Secondary Barrier and Peripheral Educator for the Gut Immune System.* Frontiers in Immunology, 2017. **8**.

45. Sémont, A., et al., *Mesenchymal stem cells improve small intestinal integrity through regulation of endogenous epithelial cell homeostasis.* Cell Death & Differentiation, 2010. **17**(6): p. 952-961.

46. Wang, N., et al., *Regulation of COL1A2, AKT3 genes, and related signaling pathway in the pathology of congenital talipes equinovarus.* Frontiers in Pediatrics, 2022. **10**.

47. Pascua-Maestro, R., et al., *Extracellular Vesicles Secreted by Astroglial Cells Transport Apolipoprotein D to Neurons and Mediate Neuronal Survival Upon Oxidative Stress.* Frontiers in Cellular Neuroscience, 2019. **12**.

48. Janciauskiene, S., et al., *Diagnostic and therapeutic value of human serpin family proteins.* Biomedicine & Pharmacotherapy, 2024. **175**(1): p. 116618.

49. Zhang, Q., et al., *Interferon-γ priming enhances the therapeutic effects of menstrual blood-derived stromal cells in a mouse liver ischemia-reperfusion model.* World Journal of Stem Cells, 2023. **15**(9): p. 876-896.

50. Wang, Q., et al., *Comparative analysis of human mesenchymal stem cells from fetal-bone marrow, adipose tissue, and Warton's jelly as sources of cell immunomodulatory therapy.* Human Vaccines & Immunotherapeutics, 2016. **12**(1): p. 85-96.

51. Chinnadurai, R., et al., *IDO-Independent Suppression of T Cell Effector Function by IFN-γ–Licensed Human Mesenchymal Stromal Cells.* The Journal of Immunology, 2014. **192**(4): p. 1491-1501.

52. Guan, Q., et al., *Interferon γ induced compositional changes in human bone marrow derived mesenchymal stem/stromal cells.* Clinical Proteomics, 2017. **14**(1).

53. Townsend, L.N., et al., *Cdk12 maintains the integrity of adult axons by suppressing actin remodeling.* Cell Death Discovery, 2023. **9**: p. 348.

54. Gygli, P.E., et al., *Cyclin A2 promotes DNA repair in the brain during both development and aging.* Aging, 2016. **8**(7): p. 1540-1564.

55. Yokomizo-Goto, M., et al., *Distinct muscle regenerative capacity of human induced pluripotent stem cell-derived mesenchymal stromal cells in Ullrich congenital muscular dystrophy model mice.* Stem Cell Research & Therapy, 2024: p. 340.

56. Kuo, D.S., C. Labelle-Dumais, and D.B. Gould, *COL4A1 and COL4A2 mutations and disease: insights into pathogenic mechanisms and potential therapeutic targets* Human Molecular Genetics, 2012. **21**(1): p. 97-110.

57. Alves-Fernandes, D.K. and M.G. Jasiulionis, *The Role of SIRT1 on DNA Damage Response and Epigenetic Alterations in Cancer.* International Journal of Molecular Sciences, 2019. **20**(13): p. 3153.

58. You, X., et al., *Loss of mitochondrial aconitase promotes colorectal cancer progression via SCD1-mediated lipid remodeling.* Molecular Metabolism 2021. **48**: p. 101203.

59. Jiang, W., et al., *Enolase1 Alleviates Cerebral Ischemia-Induced Neuronal Injury via Its Enzymatic Product Phosphoenolpyruvate.* ACS Chemical Neuroscience 2019. **10**(6): p. 2877-2889.

60. Cao, W., et al., *The Role of PGK1 in Promoting Ischemia/Reperfusion Injury-Induced Microglial M1 Polarization and Inflammation by Regulating Glycolysis.* NeuroMolecular Medicine 2023. **25**: p. 301-311.

61. Lavini-Ramos, C., et al., *MMP9 integrates multiple immunoregulatory pathways that discriminate high suppressive activity of human mesenchymal stem cells.* Scientific Reports, 2017. **7**(1).

62. Kim, C., et al., *Mesenchymal Stem Cell Transplantation Promotes Functional Recovery through MMP2/STAT3 Related Astrogliosis after Spinal Cord Injury.* International Journal of Stem Cells, 2019. **12**(2): p. 331-339.

63. Oh, S.H., et al., *The Cleavage Effect of Mesenchymal Stem Cell and Its Derived Matrix Metalloproteinase-2 on Extracellular α-Synuclein Aggregates in Parkinsonian Models.* Stem Cells Translational Medicine, 2017. **6**(3): p. 949-961.

64. Mira, E., et al., *Secreted MMP9 promotes angiogenesis more efficiently than constitutive active MMP9 bound to the tumor cell surface.* Journal of Cell Science, 2004. **117**(9): p. 1847-1857.

65. Yu, Y., F. Pei, and Z. Li, *Orientin and vitexin attenuate lipopolysaccharide-induced inflammatory responses in RAW264.7 cells: a molecular docking study, biochemical characterization, and mechanism analysis.* Food Science and Human Wellness, 2022. **11**(5): p. 1273-1281.

66. Wang, Y., et al., *Mesenchymal stem cell–secreted extracellular vesicles carrying TGF-β1 up-regulate miR-132 and promote mouse M2 macrophage polarization.* Journal of Cellular and Molecular Medicine, 2020. **24**(21): p. 12750-12764.

67. Brennan, K., et al., *A comparison of methods for the isolation and separation of extracellular vesicles from protein and lipid particles in human serum.* Scientific Reports, 2020. **10**: p. 1039.

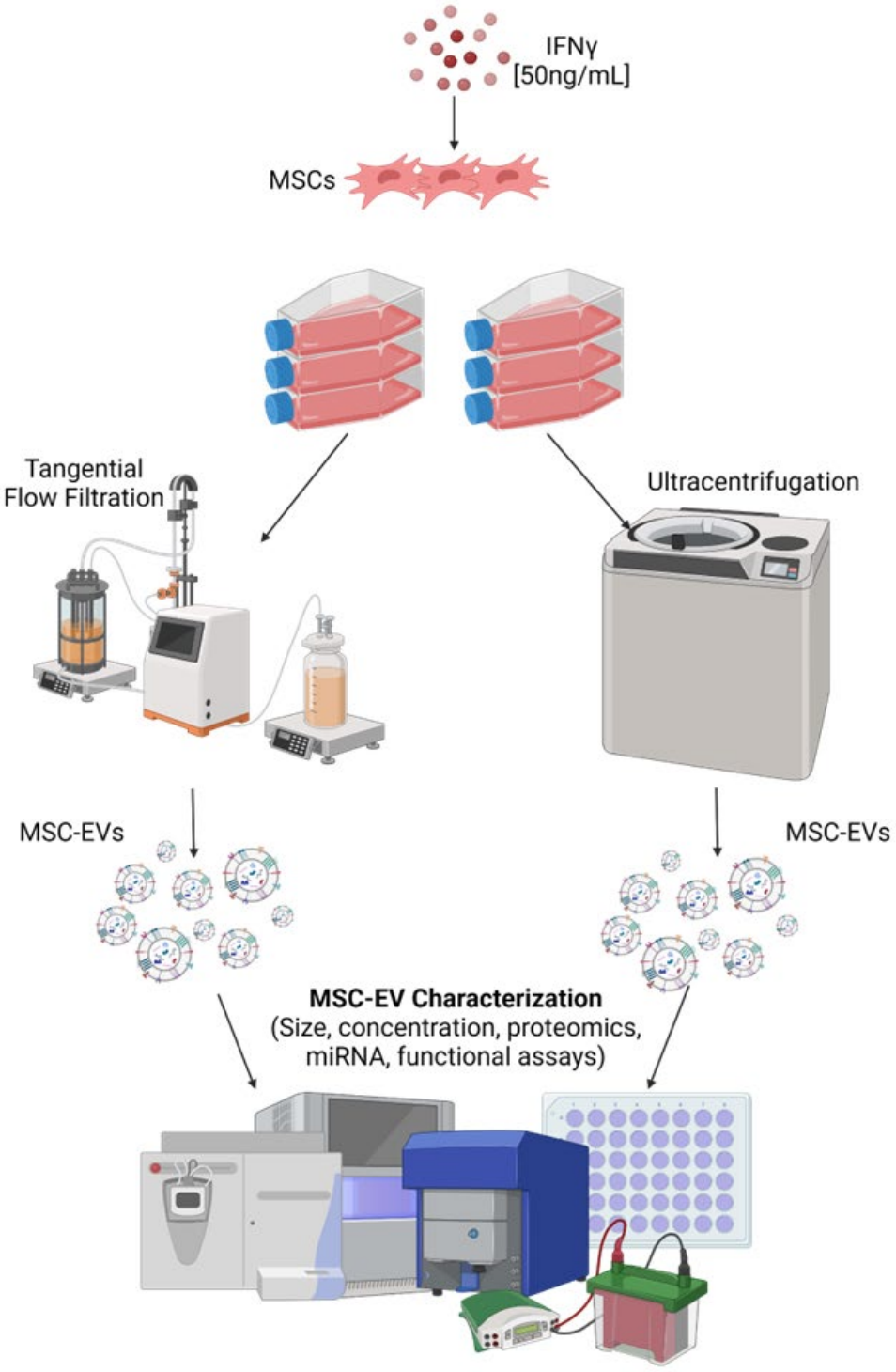

Figure 4.i Illustrative Abstract

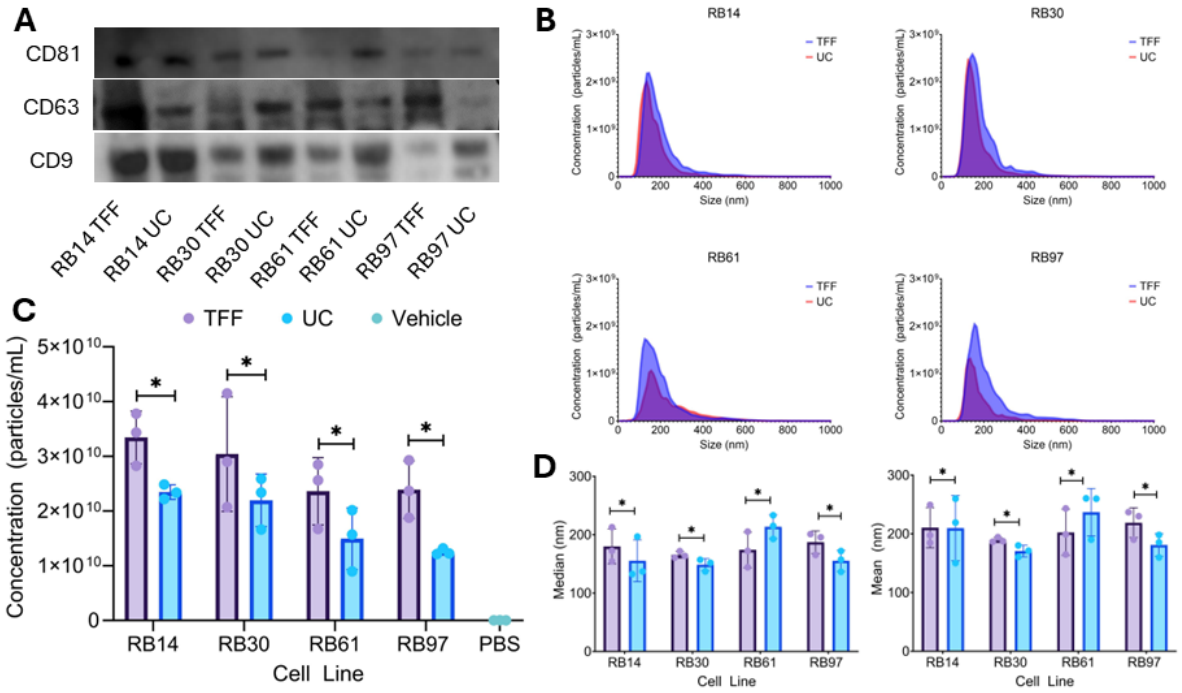

Figure 4.1. Characterization of MSC-EVs. A) illustrates the presence of 3 MSC-EV markers CD81, CD63 and CD9 for all MSC manufacturing groups using western blot. **B)** Illustrates the size average size distribution across 3 batches for each cell line. **C)** Represents the average concentration isolated for each manufacturing groups across 3 different batches. * represents $p<0.003$ using a ordinary one-way ANOVA and Sidak's multiple comparison test. **D)** Represents the average concentration isolated for each manufacturing groups across 3 different batches. * represents $p<0.0391$ using an ordinary one-way ANOVA and Sidak's multiple comparison test.

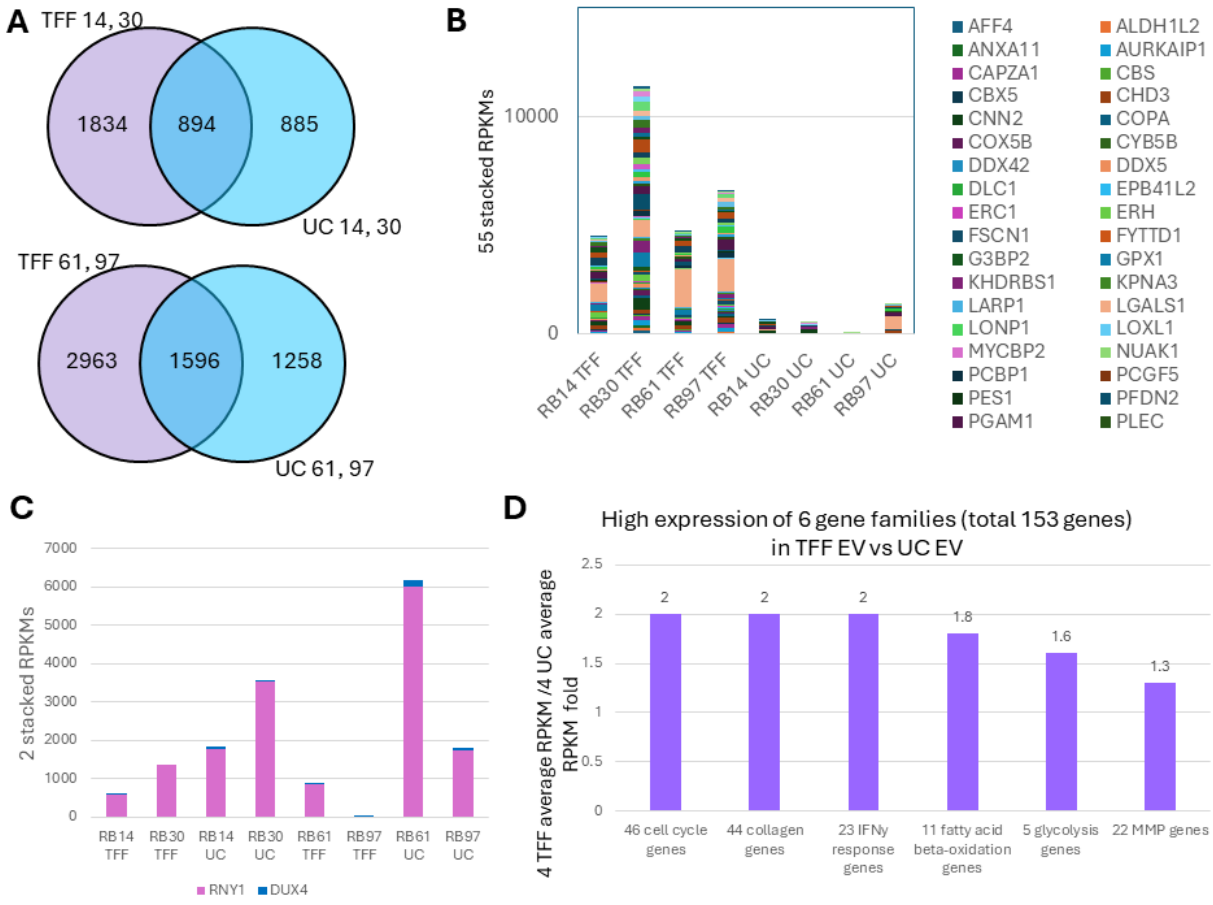

Figure 4.2. TFF and UC isolate MSC-EVs with distinct RNA Profiles. A) Illustrates the differences between the genes isolated by TFF and UC across bone marrow-derived MSCs (RB14 and RB30, top) and adipose tissue-derived MSCs (RB61, RB97, bottom). **B)** Is a stack plot of the genes 2-fold upregulated in TFF isolated MSC-EVs compared to UC isolated MSC-EVs. **C)** Is a stack plot of the genes 2-fold upregulated in UC isolated MSC-EVs compared to TFF isolated MSC-EVs. **D)** Illustrates the fold difference between TFF and UC between six gene families having roles in immunomodulation and regeneration.

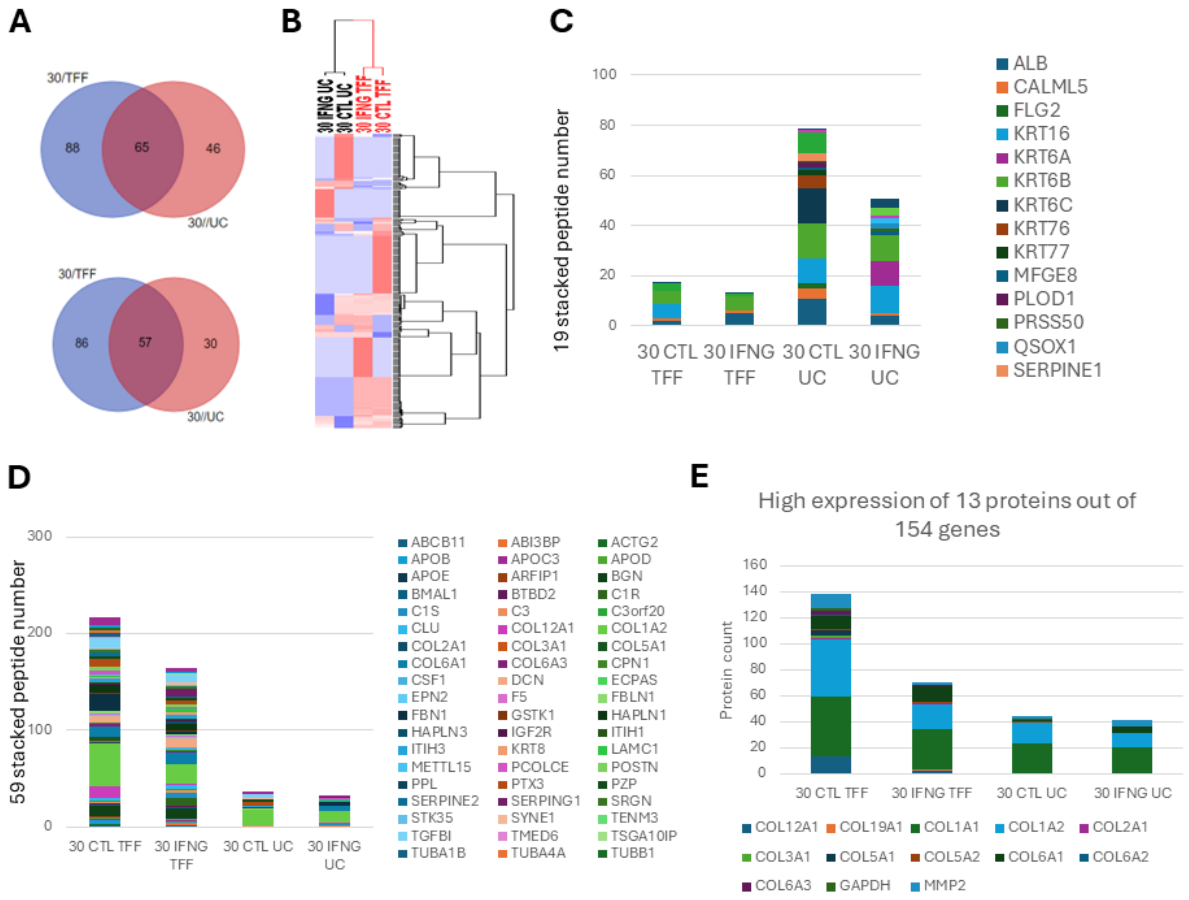

Figure 4.3. Isolation methods and priming induce distinct proteomic profiles in RB30 MSC-EVs. A) Venn diagrams of the differences and similarities between UC and TFF isolated MSC-EVs (unprimed-top and primed-bottom). **B)** Heat-map illustrating the distinct proteomic profiles between TFF (red) and UC (black) as well as with and without priming. **C)** Proteins 2-fold upregulated in the UC isolated MSC-EVs compared to the TFF isolated MSC-EVs. **D)** Proteins 2-fold upregulated in the UC isolated MSC-EVs compared to the TFF isolated MSC-EVs. **E)** Illustrates higher expression of protein in TFF that have immunomodulatory function than in UC.

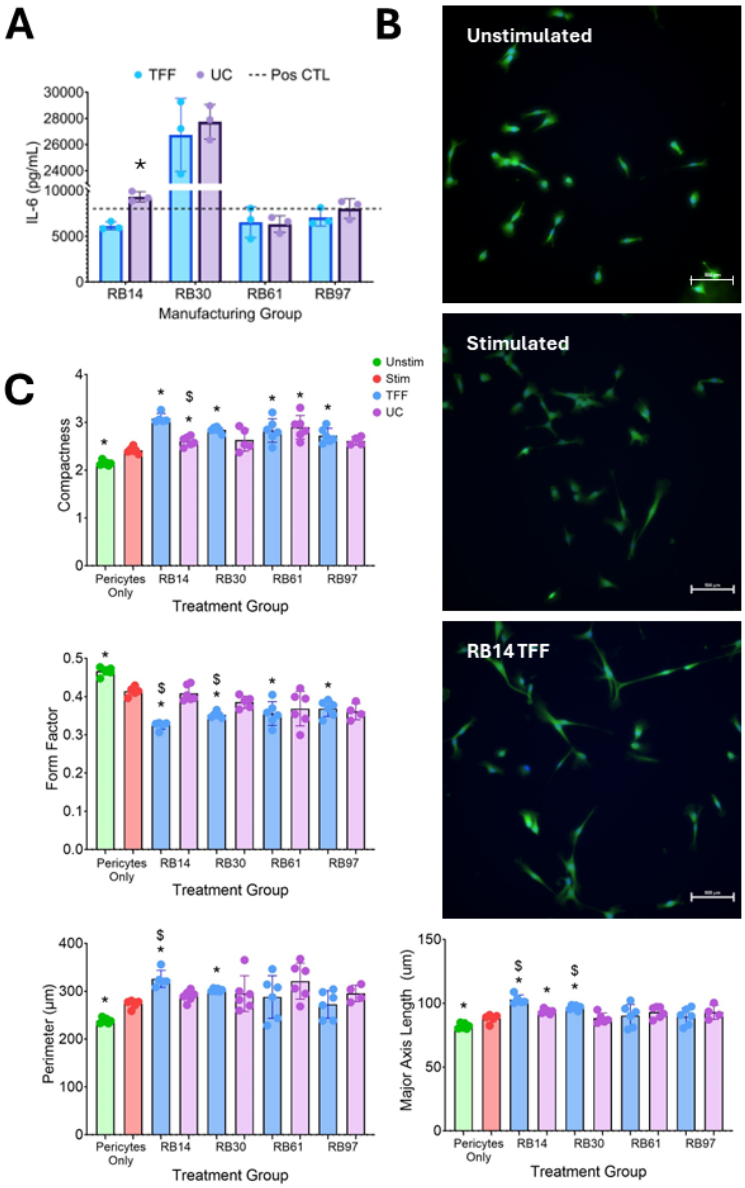

Figure 4.4. Isolation methods have minimal effect on MSC-EV bioactivity. A) IL-6 secretion of RAW264.7 macrophages after treatment with MSC-EVs. * represents $p<0.05$ between TFF and UC isolated MSC-EVs within the same cell line using a one-way ANOVA test using Tukey's multiple comparison. **B)** Images of pericyte from unstimulated, stimulated and Rb14 TFF manufacturing groups (top to bottom). Scale bar = 500µm. **C)** Pericyte morphological parameters including compactness, form factor, major axis length and perimeter. * represents $p<0.05$ compared to the stimulated group using a Brown-Forsythe and Welch's ANOVA and Dunnett's T3 multiple comparison. $ represents $p<0.03$ between TFF and UC within the same cell line using Brown-Forsythe and Welch's ANOVA and Dunnett's T3 multiple comparison test.

CHAPTER 5

CONCLUSION AND FUTURE DIRECTIONS

5.1 ACHIEVEMENTS

While MSC-EVs show great potential as a therapeutic for neurodegenerative diseases, the absence of standardized manufacturing practices hinders their ability to meet regulatory requirements for future clinical use. The variability in MSC-EV isolation, priming, and culture methods significantly impacts the consistency and bioactivity of the EVs, making it difficult to ensure reliable therapeutic outcomes. Therefore, through my thesis, I chose to investigate how different manufacturing practices influence MSC-EV populations, with the goal of identifying critical factors that affect their bioactivity and contributing to the development of standardized methods for more consistent and effective clinical applications. The overreaching goal was to study how MSC priming and isolation methods impact MSC-EV bioactivity and to develop a novel pericyte-based assay for assessing MSC-EVs in neurodegenerative therapies.

In Chapter 2, I conducted a comprehensive literature review on current evaluation methods for MSC-EVs in the context of neurodegenerative diseases. I found that no "gold standard" exists for either the manufacturing or assessment of MSC-EV bioactivity. By comparing existing MSC-EV evaluation models, I identified key challenges that could be addressed using newer evaluation platforms. This review provided a detailed overview of the current landscape of MSC-EV bioactivity assessment tools and their limitations in meeting regulatory requirements.

In Chapter 3, we developed a pericyte-based morphological assay for evaluating MSC-EV bioactivity and conducted an in-depth analysis of functional differences arising from various manufacturing methods. We identified key pericyte morphological features (i.e., perimeter, form factor, major axis length) that may offer insights into MSC-EV function and link these to corresponding secretome profiles, establishing pericytes as a reliable morphological assay. This assay also enabled us to evaluate MSC-EVs under different manufacturing conditions, including MSC priming and 2D versus 3D culture platforms and it was found that a 3D bioreactor platform produce more bioactive MSC-EVs than 2D flask produced MSC-EVs. Thus, through this approach, we identified differences between manufacturing methods and determined the most bioactive MSC-EV groups in the context of human brain pericytes for future therapeutic applications in neurodegenerative disease.

In Chapter 4, we further explored MSC-EV manufacturing techniques, focusing on EV isolation. Specifically, I compared MSC-EVs isolated by tangential flow filtration (TFF) and ultracentrifugation (UC) across four MSC donors (e.g., RB114, RB30, RB61, RB97). We evaluated physical (size, concentration, surface markers), compositional (RNA and proteomics), and functional (macrophage IL-6 secretion, pericyte morphology) characteristics. Our analysis revealed that TFF isolated a higher concentration of larger MSC-EVs with a distinct compositional cargo profile compared to UC. TFF-isolated MSC-EVs were enriched in RNA and proteomic cargo associated with modulating inflammatory responses. However, despite these compositional differences, functional distinctions were minimal, with TFF further promoting an immunomodulatory pericyte morphology, which we had previously established as significant.

5.2 LIMITATIONS

In Chapter 3, we developed a quick and easy assay for assessing MSC-EV bioactivity using a 2D system. While effective, this assay is best suited as a preliminary screening tool before transitioning to more complex and physiologically relevant 3D systems, such as microphysiological systems (MPS) or *in vivo* models, which can better capture intricate interactions. In addition, it is important to note that all studies utilize only one pericyte donor and one MSC donor. Nevertheless, I believe this assay represents a reliable method for MSC-EV bioactivity assessment, as demonstrated by the discernible differences observed across various priming and culture platform groups. However, further work needs to be conducted to efficiently qualify and validate this assay before it can be considered a proper MSC-EV potency assay. This qualification will require further studies assessing different donors of both pericytes, and MSC-EVs, known drug evaluation as a control, time-studies, and further specificity and reproducibility studies.

In Chapter 4, we encountered some challenges related to batch-to-batch variability, which impacted on the consistency of results. However, variability is expected due to the inherent heterogeneity of MSCs and the EVs they produce [1, 2]. Additionally, the limited culture platform restricted the volume of MSC-conditioned media produced, thereby limiting the number of MSC-EVs available for evaluation, particularly for specific miRNA analysis. Despite these constraints, the focused functional assessment assays provided valuable insights and lay the groundwork for further exploration in future research. While the limited availability of reliable MSC-EV assays is partly due to still-unknown mechanisms of action, I am optimistic that continued investigation will lead to advancements that enhance our understanding and evaluation of MSC-EVs.

5.3 FUTURE DIRECTIONS

Future experiments should prioritize a comprehensive investigation into the effects of manufacturing practices on MSC-EV bioactivity and their potential neurodegenerative therapeutic applications. Possible factors to explore development of potency assays and further exploration of manufacturing conditions (i.e., MSC priming, MSC culture platforms, and MSC-EV isolation methods).

5.3.1 Development of Physiologically Relevant Assays For MSC-EV Potency in Neurodegenerative Diseases

MSC-EVs hold great promise as a therapeutic for neurodegenerative diseases, but their potential will remain unrealized without a clearer understanding of their mechanism of action (MOA) and standardized potency assessments [3]. Thus, there is a critical need to develop, qualify, and validate potency assays for MSC-EV evaluation. Currently, no established potency assays exist, leaving bioactivity assessments to the discretion of individual researchers, which has hindered consensus within the MSC-EV field.

Current models for MSC-EV assessment are largely limited to 2D monoculture systems and in vivo animal studies [4, 5]. While 2D models are valuable, they often fail to capture the complexity of cellular interactions, limiting our ability to uncover more intricate mechanisms. In vivo models, though more complex, frequently lack translatability to human systems [6]. In this thesis, we developed a 2D monoculture assay capable of discerning differences between various manufacturing conditions. However, due to its simplicity, this assay will be most useful as a screening tool to identify promising conditions.

Once identified, more complex in vitro models will be necessary to further explore the mechanisms and deeper differences in MSC-EVs based on manufacturing variables. For example, future studies could include developing a blood-brain barrier (BBB) microphysiological system (MPS). This BBB MPS would provide a dynamic, physiologically relevant environment while maintaining high-throughput capabilities in a controlled setting [7-9]. Such a model could offer deeper insights into the MOA of MSC-EVs and enhance our ability to standardize potency assays, moving the field closer to realizing the therapeutic potential of MSC-EVs.

5.3.2 Further Evaluation of Manufacturing Methods Impacting MSC-EVs

5.3.2.1 Priming

In Chapters 3 and 4, we analyzed the differences in priming (using cytokines, chemokines, and oxygen), culture platforms (flask and bioreactor), and two different isolation methods (e.g., TFF and UC). While these parameters were the focus of our investigation, there are numerous other priming conditions, culture platforms, and isolation methods that remain unexplored.

In Chapter 2, we primarily focused on the combinatorial priming of MSCs with TNFα and IFNγ, while Chapter 4 concentrated solely on IFNγ priming, given its established role in enhancing MSC immunomodulatory potential. However, additional priming strategies—including hypoxia, other cytokines and chemokines, neurotrophic factors, and various bioactive molecules—are also pertinent to the preparation of MSCs for treating neuroinflammatory diseases[10-12].

For instance, priming bone marrow MSCs with interleukin-23 (IL-23) has been shown to increase the neuroprotective capacity of their secreted extracellular vesicles (EVs) in murine

models [13]. Another study demonstrated that priming MSCs with α-synuclein resulted in upregulation of transcriptional factors related to cell reprogramming, glycolysis, and autophagy, and when implanted, these MSCs improved the survival of dopaminergic neurons in a Parkinson's disease mouse model [14]. Additionally, MSCs primed with a combination of neurotrophic factors, such as B27, N2, dbcAMP, IBMX, EGF, bFGF, and valproic acid, produced secretome factors that promoted neurite growth, increased the expression of neuronal markers, and suppressed apoptotic markers [15].

These findings highlight the vast potential of alternative priming strategies to further enhance the therapeutic efficacy of MSCs, particularly in the context of neurodegenerative diseases. Exploring these untested priming conditions, as well as other culture and isolation methods, could significantly advance MSC-based therapies.

5.3.2.2 Culture Platforms

In Chapter 3, we compared MSC-EVs derived from MSCs cultured in both traditional cell culture flasks and vertical-wheel bioreactors, as well as different microcarrier concentrations within the bioreactor. Based on our findings and the need for large-scale MSC-EV production for future therapeutic applications, further studies should focus on MSC-EV production in scalable 2D and 3D culture platforms, including bioreactors and hydrogels.

Several 3D culture platforms are available, such as CellSTACK chambers, Hyperflasks, spinner flasks, stirred-tank bioreactors, vertical-wheel bioreactors, rotating wall bioreactors, and hollow-fiber bioreactors. In our study, MSC-EVs produced from MSCs cultured in a vertical-wheel bioreactor demonstrated enhanced immunomodulatory properties compared to those grown in T175 culture flasks. Similarly, Sun et al. found that MSCs cultured in 3D hollow-fiber

bioreactors produced a higher yield of EVs, which exhibited increased angiogenic potential, regulated macrophage transition, and reduced apoptosis compared to those grown in 2D conditions [16]. Fuzeta et al. further demonstrated that a scalable microcarrier-based bioreactor culture system significantly outperformed 2D flask systems in terms of MSC-EV production and productivity [17]. These studies collectively underscore the superiority of 3D bioreactor systems over traditional 2D platforms, both in terms of scalability and the enhancement of MSC and MSC-EV immunomodulatory potential.

Beyond bioreactors and flask systems, the choice of biomaterials used in MSC culture can influence the therapeutic potential of MSC-EVs. Factors such as pore size, mechanical properties, and material composition should be carefully evaluated to optimize MSC-EV production for neurodegenerative disease treatments [18]. For example, one study encapsulated umbilical cord-derived MSCs in an arginine-glycine-aspartic acid (RGD) hydrogel scaffold and demonstrated that, in a murine spinal cord injury model, the hydrogel slowly released the paracrine factor CCL2, leading to neuroprotective effects such as enhanced neuronal survival and growth [19]. Another study showed that bone marrow-derived MSCs cultured in collagen-pullulan hydrogels exhibited increased expression of angiogenic cytokines, such as vascular endothelial growth factor-A (VEGF-A) and monocyte chemoattractant protein-1 (MCP-1), as well as transcription factors associated with pluripotency and self-renewal [20].

In conclusion, exploring advanced 3D culture platforms and the impact of biomaterials on MSC and MSC-EV production holds significant promise for optimizing their therapeutic potential, particularly for neurodegenerative diseases. By refining these techniques, we can pave the way for more efficient and effective MSC-based therapies.

5.3.2.3 Isolation Methods

In our studies, we compared MSC-EVs isolated using TFF and UC. However, various other isolation methods may be better suited to different manufacturing applications. These include UC, size exclusion chromatography (SEC), immune-affinity capture, ultrafiltration (e.g. TFF), and microfluidics. Each method comes with its own challenges and benefits—some are more costly (UC, SEC, immune-affinity capture), others offer greater scalability (ultrafiltration, certain UC processes), and some may compromise EV integrity, such as UC [21-27].

The choice of isolation method must balance these factors based on the specific needs of the manufacturing process. However, it's important to recognize that different isolation methods can influence the characteristics of the resulting MSC-EV population, as we observed in Chapter 4. For instance, a study comparing MSC-EVs isolated using anion exchange resin (IEX) and ultrafiltration (UF) found that, while both methods produced EVs of similar size and particle concentration, IEX yielded 10 times more RNA, a higher protein count, and greater levels of anti-inflammatory cytokines. Additionally, IEX-isolated EVs more effectively suppressed macrophage activation and T cell proliferation compared to UF in bioactivity assays [28].

These findings highlight the need to carefully select the appropriate isolation method to optimize EV yield, quality, and functionality for specific applications.

5.4 BROADER IMPACTS

Neurodegenerative diseases are increasingly prevalent, underscoring the urgent need for effective therapeutic interventions [29]. Mesenchymal stromal cell-derived extracellular vesicles (MSC-EVs) hold significant promise as a potential treatment due to their ability to target

neuroinflammation, offering the possibility of a curative approach rather than merely symptom management [30-32]. Notably, MSC-EVs have demonstrated robust potential in attenuating inflammation and promoting regenerative processes in models of neuroinflammation [33]. For instance, in a rat model of minimal hepatic encephalopathy, adipose-derived MSC-EVs (AD-MSC-EVs) reduced neuroinflammatory responses and restored motor coordination. These effects were mediated through the modulation of microglia and astrocyte activation, ultimately restoring homeostatic GABAergic neurotransmission [34].

However, several challenges must be addressed before MSC-EVs can meet regulatory standards for therapeutic approval. These include the heterogeneity of MSC-EVs, limited understanding of their mechanisms of action (MOA), the absence of validated potency assays, and non-standardized manufacturing processes [3, 35-37].

In this dissertation, we developed a pericyte morphology-based bioactivity assay to screen MSC-EV manufacturing conditions and compared different MSC-EV isolation methods. Existing approaches predominantly rely on in vivo models and complex analysis techniques. While in vitro models offer initial insights, they often require time-intensive and resource-heavy methods, such as flow cytometry, polymerase chain reaction (PCR), and reactive oxygen species (ROS) assays, which also demand specialized training [38-40]. In vivo models, meanwhile, are costly, raise ethical concerns, and frequently exhibit poor translational relevance to humans [6, 41, 42]. Our assay provides a rapid and cost-effective screening method for evaluating MSC-EVs without the need for advanced training or complex techniques. Although often overlooked, morphology is a valuable metric for assessing cellular function, as demonstrated in previous studies [43, 44].

By employing this simple yet effective approach, we developed a platform that can be universally implemented, enabling the identification of promising therapeutics while conserving resources. This novel platform has the potential to standardize bioactivity assessments for neurodegenerative disease therapeutics and improve the understanding of MSC-EV bioactivity, MOA, and therapeutic efficacy.

Additionally, we conducted a comprehensive comparison of ultracentrifugation (UC) and tangential flow filtration (TFF) isolation methods, revealing significant differences in the cargo and bioactivity of resulting MSC-EV populations. To date, this is the first detailed analysis comparing the effects of UC and TFF on MSC-EV cargo composition and bioactivity. Our findings highlight the critical importance of evaluating manufacturing variables such as isolation methods, which are often overshadowed by a focus on priming conditions. While previous studies, such as Visan et al., demonstrated that TFF yields higher concentrations and purer MSC-EV populations than UC, these analyses primarily focused on physical characteristics like size and concentration, with limited exploration of cargo composition [45]. By performing a more thorough analysis of MSC-EV cargo (both full RNA and proteomic profiling) we supplied a greater indication of isolations methods effects on resulting populations. This is extremely important towards building a standardized methodology for MSC-EV manufacturing as we illustrated these methods significantly isolated MSC-EVs with different cargo compositions.

Interestingly, while these methods altered the MSC-EV populations, the observed differences did not consistently translate into significant therapeutic variations. Instead, donor source appeared to have a more pronounced impact. Previous studies identified differences in isolation methods

through macrophage functional assays and T-cell proliferation assays, often using an expanded panel of biomarkers such as IL-2, IL-10, TGF-β, and VEGF [28]. In contrast, the functional assays in our study (macrophage IL-6 secretion and pericyte morphology) may have lacked the sensitivity to detect these differences, emphasizing the need for validated and standardized MSC-EV potency assays. Alternatively, the findings may indicate that only a subset of cargo molecules plays a functional role, warranting further investigation into the functional relevance of MSC-EV cargo.

While this work only begins to explore the impact of different manufacturing conditions on the therapeutic potential of MSC-EVs for neurodegenerative diseases, it raises important questions and highlights areas that warrant further investigation. We hope that this research, along with contributions from other studies, will help advance the understanding of MSC-EV mechanisms of action, identify critical quality attributes (CQAs), manufacturing standards, and develop future therapeutic applications in neurodegenerative diseases.

5.5 REFERENCES

1. Chen, S., B. Liang, and J. Xu, *Unveiling heterogeneity in MSCs: exploring marker-based strategies for defining MSC subpopulations.* Journal of Translational Medicine, 2024. **22**: p. 459.
2. Almeria, C., et al., *Heterogeneity of mesenchymal stem cell-derived extracellular vesicles is highly impacted by the tissue/cell source and culture conditions.* Cell & Bioscience 2022. **12**(1): p. 51.

3. CBER, *Potency Assurance for Cellular and Gene Therapy Products*, U.S. HHS, Editor. 2023.

4. Zhao, L. and J. Li, *Microglial uptake of hADSCs-Exo mitigates neuroinflammation in ICH.* Cellular Signalling, 2024. **119**: p. 111146.

5. Bambakidis, T., et al., *Early Treatment With a Single Dose of Mesenchymal Stem Cell Derived Extracellular Vesicles Modulates the Brain Transcriptome to Create Neuroprotective Changes in a Porcine Model of Traumatic Brain Injury and Hemorrhagic Shock.* Shock, 2022. **57**(2): p. 281-290.

6. Dawson, T.M., T.E. Golde, and C. Lagier-Tourenne, *Animal models of neurodegenerative diseases.* Nature Neuroscience, 2018. **21**(10): p. 1370-1379.

7. FDA. *About Alternative Methods*. 2023; Available from: https://www.fda.gov/science-research/advancing-alternative-methods-fda/about-alternative-methods#:~:text=A%20microphysiological%20system%20uses%20microscale,their%20function%20or%20pathophysiological%20condition.

8. Jensen, C. and Y. Teng, *Is It Time to Start Transitioning From 2D to 3D Cell Culture?* Frontiers in Molecular Biosciences 2020. **7**(33).

9. Miny, L., et al., *Modeling Neurodegenerative Diseases Using In Vitro Compartmentalized Microfluidic Devices.* Frontiers in Bioengineering and Biotechnology 2022. **10**.

10. Gorin, C., et al., *Priming Dental Pulp Stem Cells With Fibroblast Growth Factor-2 Increases Angiogenesis of Implanted Tissue-Engineered Constructs Through Hepatocyte Growth Factor and Vascular Endothelial Growth Factor Secretion.* Stem Cells Translational Medicine, 2016. **5**(3): p. 392-404.

11. Lan, Y.-W., et al., *Hypoxia-preconditioned mesenchymal stem cells attenuate bleomycin-induced pulmonary fibrosis.* Stem Cell Research & Therapy, 2015. **6**(1).

12. Park, J., et al., *Additive effect of bFGF and selenium on expansion and paracrine action of human amniotic fluid-derived mesenchymal stem cells.* Stem Cell Research & Therapy, 2018. **9**(1).

13. Zhou, H., et al., *IL-23 Priming Enhances the Neuroprotective Effects of MSC-Derived Exosomes in Treating Retinal Degeneration.* Investigative opthamology and visual science 2024. **65**(10).

14. Shin, J.Y., et al., *Priming mesenchymal stem cells with α-synuclein enhances neuroprotective properties through induction of autophagy in Parkinsonian models.* Stem Cell Research & Therapy, 2022. **13**(1).

15. Teli, P., et al., *Priming Mesenchymal Stromal Cells with Neurotrophic Factors Boosts the Neuro-Regenerative Potential of their Secretome.* Regenerative Medicine, 2023. **18**(4): p. 329-346.

16. Sun, L., et al., *A 3D culture system improves the yield of MSCs-derived extracellular vesicles and enhances their therapeutic efficacy for heart repair.* Biomedicine & Pharmacotherapy, 2023. **161**: p. 114557.

17. De Almeida Fuzeta, M., et al., *Scalable Production of Human Mesenchymal Stromal Cell-Derived Extracellular Vesicles Under Serum-/Xeno-Free Conditions in a Microcarrier-Based Bioreactor Culture System.* Frontiers in Cell and Developmental Biology, 2020. **8**.

18. Hu, X., Z. Xia, and K. Cai, *Recent advances in 3D hydrogel culture systems for mesenchymal stem cell-based therapy and cell behavior regulation.* Journal of Materials Chemistry B, 2022. **10**(10): p. 1486-1507.

19. Papa, S., et al., *Mesenchymal stem cells encapsulated into biomimetic hydrogel scaffold gradually release CCL2 chemokine in situ preserving cytoarchitecture and promoting functional recovery in spinal cord injury.* Journal of Controlled Release, 2018. **278**: p. 49-56.

20. Rustad, K.C., et al., *Enhancement of mesenchymal stem cell angiogenic capacity and stemness by a biomimetic hydrogel scaffold.* Biomaterials 2012. **33**(1): p. 80-90.

21. Li, P., et al., *Progress in Exosome Isolation Techniques.* Theranostics, 2017. **7**(3): p. 789-804.

22. Mol, E.A., et al., *Higher functionality of extracellular vesicles isolated using size-exclusion chromatography compared to ultracentrifugation.* Nanomedicine: Nanotechnology, Biology and Medicine, 2017. **13**(6): p. 2061-2065.

23. Linares, R., et al., *High-speed centrifugation induces aggregation of extracellular vesicles.* Journal Extracellular Vesicles, 2015. **4**: p. 29509.

24. Wu, M., et al., *Isolation of exosomes from whole blood by integrating acoustics and microfluidics.* Proceedings of the National Academy of Sciences, 2017. **114**(40): p. 10584-10589.

25. Yaghoubi, Y., et al., *Human umbilical cord mesenchymal stem cells derived-exosomes in diseases treatment.* Life Sciences 2019. **233**(1): p. 116733.

26. Böing, A.N., et al., *Single-step isolation of extracellular vesicles by size-exclusion chromatography.* Journal of Extracellular Vesicles, 2014. **3**(1): p. 23430.

27. Popovic, M., et al., *Isolation of anti-extra-cellular vesicle single-domain antibodies by direct panning on vesicle-enriched fractions.* Microbial Cell Factories, 2018. **17**(1).

28. Malvicini, R., et al., *Influence of the isolation method on characteristics and functional activity of mesenchymal stromal cell-derived extracellular vesicles.* Cytotherapy, 2024. **26**(2): p. 157-170.

29. Steinmetz, J.D., et al., *Global, regional, and national burden of disorders affecting the nervous system, 1990–2021: a systematic analysis for the Global Burden of Disease Study 2021.* The Lancet Neurology, 2024. **23**(4): p. 344-381.

30. Kharat, S., et al., *Navigating Neurodegenerative Disorders: A Comprehensive Review of Current and Emerging Therapies for Neurodegenerative Disorders.* Journal of Neuroscience and Neurological Disorders 2024. **8**: p. 33-46.

31. Reza-Zaldivar, E.E., et al., *Mesenchymal stem cell-derived exosomes promote neurogenesis and cognitive function recovery in a mouse model of Alzheimer's disease.* Neural Regeneration Research 2019. **14**(9): p. 1626-1634.

32. Williams, A.M., et al., *Early single-dose treatment with exosomes provides neuroprotection and improves blood-brain barrier integrity in swine model of traumatic brain injury and hemorrhagic shock.* Journal of Trauma and Acute Care Surgery 2020. **88**(2): p. 207-218.

33. Jia, Y., et al., *HGF Mediates Clinical-Grade Human Umbilical Cord-Derived Mesenchymal Stem Cells Improved Functional Recovery in a Senescence-Accelerated Mouse Model of Alzheimer's Disease.* Advanced Science, 2020. **7**(17): p. 1903809.

34. Izquierdo-Altarejos, P., et al., *Extracellular Vesicles from Mesenchymal Stem Cells Reverse Neuroinflammation and Restore Motor Coordination in Hyperammonemic Rats.* Journal of Neuroimmune Pharmacology, 2024. **19**(1).

35. Lener, T., et al., *Applying extracellular vesicles based therapeutics in clinical trials – an ISEV position paper.* Journal of Extracellular Vesicles, 2015. **4**: p. 30087-30087.

36. Brennan, K., et al., *A comparison of methods for the isolation and separation of extracellular vesicles from protein and lipid particles in human serum.* Scientific Reports, 2019. **10**: p. 1039.

37. Zheng, X., et al., *Characterization and bioassays of extracellular vesicles extracted by tangential flow filtration.* Regenerative Medicine, 2022. **17**(3): p. 141-154.

38. Chen, H.-X., et al., *Exosomes derived from mesenchymal stem cells repair a Parkinson's disease model by inducing autophagy.* Cell Death & Disease, 2020. **11**(4).

39. Chen, H., et al., *miRNA-211-5p inhibition enhances the protective effect of hucMSC-derived exosome in Aβ1-40-induced SH-SY5Y cells by increasing NEP expression.* Journal of Biochemical and Molecular Toxicology 2023. **38**(1): p. e23624.

40. Che, J., et al., *Human umbilical cord mesenchymal stem cell-derived exosomes attenuate neuroinflammation and oxidative stress through the NRF2/NF-κB/NLRP3 pathway.* CNS Neuroscience and Therapeutics 2024. **30**(3): p. e14454.

41. Holen, I., et al., *In vivo models in breast cancer research: progress, challenges and future directions.* Disease Models & Mechanisms, 2017. **10**(4): p. 359-371.

42. Russel, W.M.S. and R.L. Burch, *The Principles of Humane Experimental Technique*, UFAW, Editor. 1959.

43. Klinker, M.W., et al., *Morphological features of IFN-γ–stimulated mesenchymal stromal cells predict overall immunosuppressive capacity.* PNAS, 2017. **114**(13): p. E2598-E2607.

44. Larey, A.M., et al., *High throughput screening of mesenchymal stromal cell morphological response to inflammatory signals for bioreactor-based manufacturing of extracellular vesicles that modulate microglia.* Bioactive Materials, 2024. **37**: p. 153-171.

45. Visan, K., et al., *Comparative analysis of tangential flow filtration and ultracentrifugation, both combined with subsequent size exclusion chromatography, for the isolation of small extracellular vesicles.* Journal of Extracellular Vesicles, 2022. **11**(9): p. 12266.

APPENDIX A.

CHAPTER 3 SUPPLEMENTARY FIGURES

CellProfiler Pipeline: http://www.cellprofiler.org
Version:5
DateRevision:424
GitHash:
ModuleCount:12
HasImagePlaneDetails:False

Images:[module_num:1|svn_version:'Unknown'|variable_revision_number:2|show_window:True|notes:['To begin creating your project, use the Images module to compile a list of files and/or folders that you want to analyze. You can also specify a set of rules to include only the desired files in your selected folders.', '', 'For a large screen, it may take a long time to read and collect all the images. E.g., for a screen of 830k files (images+thumbnails), it took ~2 hrs to process. However, this only needs to be done once as the file list is saved as part of the project file.', '', 'Recommended to save time: Drag/drop the images once for a single project (e.g, QC), save the project as a template and then copy/paste analysis modules from the other two by opening additional instances of CellProfiler, then save them as separate projects.']|batch_state:array([], dtype=uint8)|enabled:True|wants_pause:False]
    :
    Filter images?:Images only
    Select the rule criteria:and (or (extension does istif) (file does endwith ".npy")) (file doesnot contain "thumb")

Metadata:[module_num:2|svn_version:'Unknown'|variable_revision_number:6|show_window:True|notes:['The Metadata module optionally allows you to extract information describing your images (i.e, metadata) which will be stored along with your measurements. This information can be contained in the file name and/or location, or in an external file.', '', 'The settings here allow the user to extract (assuming an ImageXpress microscope is used):', '* The UserStem prefix, and the Well and Site IDs from the filename, as well as the channel number.', '* The 5-digit Plate ID, and optionally, the date of acquisition from the folder name. If needed, the regular expression can modified to collect the barcode ID as well.']|batch_state:array([], dtype=uint8)|enabled:True|wants_pause:False]
    Extract metadata?:Yes
    Metadata data type:Text
    Metadata types:{}
    Extraction method count:1
    Metadata extraction method:Extract from file/folder names
    Metadata source:File name
    Regular expression to extract from file name:(?P<Other>[a-z]{3})_(?P<Dilution>[0-9]{2}[A-Z]{2}[0-9]{1})_(?P<Well>[A-Z]{1}[0-9]{2})_(?P<read>[0-9]{4})_(?P<Useless>[A-Z]{3})_(?P<ChannelOut>[A-Z]{4})
    Regular expression to extract from folder name:(?P<Date>[0-9]{4}_[0-9]{2}_[0-9]{2})$
    Extract metadata from:Images matching a rule
    Select the filtering criteria:and (extension does istif)
    Metadata file location:Elsewhere...|

Match file and image metadata:[]
Use case insensitive matching?:No
Metadata file name:
Does cached metadata exist?:No

NamesAndTypes:[module_num:3|svn_version:'Unknown'|variable_revision_number:8|show_window:True|notes:['The NamesAndTypes module allows you to assign a meaningful name to each image by which other modules will refer to it.', '', 'The settings here match the channels by the channel number collected in the Metadata module.', 'Setting the image set matching method to "Metadata" has the advantage of omitting sites in which there is a metadata mismatch, i.e, missing files.']|batch_state:array([], dtype=uint8)|enabled:True|wants_pause:False]
Assign a name to:Images matching rules
Select the image type:Grayscale image
Name to assign these images:DNA
Match metadata:[{'DAPI': 'Dilution', 'FITC': 'Dilution'}, {'DAPI': 'Well', 'FITC': 'Well'}, {'DAPI': 'read', 'FITC': 'read'}]
Image set matching method:Metadata
Set intensity range from:Image metadata
Assignments count:2
Single images count:0
Maximum intensity:255.0
Process as 3D?:No
Relative pixel spacing in X:1.0
Relative pixel spacing in Y:1.0
Relative pixel spacing in Z:1.0
Select the rule criteria:and (metadata does ChannelOut "DAPI")
Name to assign these images:DAPI
Name to assign these objects:Cell
Select the image type:Grayscale image
Set intensity range from:Image metadata
Maximum intensity:255.0
Select the rule criteria:and (metadata does ChannelOut "FITC")
Name to assign these images:FITC
Name to assign these objects:Cytoplasm
Select the image type:Grayscale image
Set intensity range from:Image metadata
Maximum intensity:255.0

Groups:[module_num:4|svn_version:'Unknown'|variable_revision_number:2|show_window:True|notes:['The Groups module optionally allows you to split your list of images into image subsets (groups) which will be processed independently of each other. Examples of groupings include screening batches, microtiter plates, time-lapse movies, etc.', '', 'No grouping is needed, so this module is not enabled.']|batch_state:array([], dtype=uint8)|enabled:True|wants_pause:False]
Do you want to group your images?:No
grouping metadata count:1
Metadata category:Plate

IdentifyPrimaryObjects:[module_num:5|svn_version:'Unknown'|variable_revision_number:15|show_window:False|notes:['Identify the nuclei based on the DNA image.', ' ', ' The settings here were chosen based on the image data and acqusition settings provided in Gustafsdottir et al', ' PLoS One 8', ' e80999', ' 2013. Changing the image acqusition settings may affect a number of these parameters:', ' * Typical diameter of

objects: From the display window menu', ' select Tools > Measure length. Click/drag to measure diameters of a few select nuclei.', ' * Thresholding strategy: Global works fine in most cases', ' but Adaptive may work better if the background has non-uniform illumination. However', ' the illumination correction in CorrectIlluminationApply should mitigate the latter.', ' * Thresholding method: Select the method which provides the best foreground/background separation. Adjust the threshold corrrection factor if the threshold is concistently above/below where you want it to be for most images tested. ', ' * Lower threshold bound: Mouse over the background region to see the intensity variation in the lower-right of the display window.', ' * Method to distinguish clumped objects: Use Intensity if the intensity gradient dividing touching nuclei are pretty clear', " even if clumpy. Use Shape if the nuclei are usually well-separated (and Intensity doesn't work).", ' * Method to draw dividing lines between clumped objects: Intensity usually gives more realistic-looking boundary lines.', ' * Size of smoothing filter/minimum distance between local maxima: Override defaults if nuclei are getting under/over-segmented.', ' * Fill holes in identified objects: Currently set to Never since holes in nuclei may represent a phenotype. ']|batch_state:array(b'', dtype='|S1')|enabled:True|wants_pause:False]
    Select the input image:DAPI
    Name the primary objects to be identified:Nuclei
    Typical diameter of objects, in pixel units (Min,Max):5,100
    Discard objects outside the diameter range?:Yes
    Discard objects touching the border of the image?:Yes
    Method to distinguish clumped objects:None
    Method to draw dividing lines between clumped objects:Shape
    Size of smoothing filter:8
    Suppress local maxima that are closer than this minimum allowed distance:8
    Speed up by using lower-resolution image to find local maxima?:Yes
    Fill holes in identified objects?:After both thresholding and declumping
    Automatically calculate size of smoothing filter for declumping?:No
    Automatically calculate minimum allowed distance between local maxima?:No
    Handling of objects if excessive number of objects identified:Continue
    Maximum number of objects:500
    Use advanced settings?:Yes
    Threshold setting version:12
    Threshold strategy:Global
    Thresholding method:Robust Background
    Threshold smoothing scale:1
    Threshold correction factor:1
    Lower and upper bounds on threshold:0,1
    Manual threshold:0.0
    Select the measurement to threshold with:None
    Two-class or three-class thresholding?:Three classes
    Log transform before thresholding?:No
    Assign pixels in the middle intensity class to the foreground or the background?:Foreground
    Size of adaptive window:10
    Lower outlier fraction:0.001
    Upper outlier fraction:0.001
    Averaging method:Mean
    Variance method:Standard deviation
    # of deviations:1
    Thresholding method:Otsu

IdentifySecondaryObjects:[module_num:6|svn_version:'Unknown'|variable_revision_number:10|show_window:False|notes:['Identify the cells using the nuclei objects plus an image representative of the cell body.

Several of the channels could suffice for this purpose, but we chose the RNA channel as optimal. Using the "Watershed-Image" option over the default "Propagate" methods seems to often better capture the cell boundaries, especially when the cells are confluent.']|batch_state:array(b'', dtype='|S1')|enabled:True|wants_pause:False]
Select the input objects:Nuclei
Name the objects to be identified:Cells
Select the method to identify the secondary objects:Propagation
Select the input image:FITC
Number of pixels by which to expand the primary objects:10
Regularization factor:0.0
Discard secondary objects touching the border of the image?:Yes
Discard the associated primary objects?:Yes
Name the new primary objects:FilteredNuclei
Fill holes in identified objects?:Yes
Threshold setting version:12
Threshold strategy:Global
Thresholding method:Robust Background
Threshold smoothing scale:1
Threshold correction factor:1
Lower and upper bounds on threshold:0.0,1
Manual threshold:0.0
Select the measurement to threshold with:None
Two-class or three-class thresholding?:Two classes
Log transform before thresholding?:Yes
Assign pixels in the middle intensity class to the foreground or the background?:Foreground
Size of adaptive window:10
Lower outlier fraction:0.01
Upper outlier fraction:0.01
Averaging method:Mean
Variance method:Median absolute deviation
# of deviations:1
Thresholding method:Otsu

GrayToColor:[module_num:7|svn_version:'Unknown'|variable_revision_number:4|show_window:False|notes:[]|batch_state:array([], dtype=uint8)|enabled:True|wants_pause:False]
Select a color scheme:RGB
Rescale intensity:No
Select the image to be colored red:Leave this black
Select the image to be colored green:FITC
Select the image to be colored blue:DAPI
Name the output image:PericyteColorImage
Relative weight for the red image:1.0
Relative weight for the green image:1.0
Relative weight for the blue image:1.0
Select the image to be colored cyan:Leave this black
Select the image to be colored magenta:Leave this black
Select the image to be colored yellow:Leave this black
Select the image that determines brightness:Leave this black
Relative weight for the cyan image:1.0
Relative weight for the magenta image:1.0
Relative weight for the yellow image:1.0

Relative weight for the brightness image:1.0
Hidden:1
Image name:None
Color:#ff0000
Weight:1.0

OverlayOutlines:[module_num:8|svn_version:'Unknown'|variable_revision_number:4|show_window:False|notes:[]|batch_state:array([], dtype=uint8)|enabled:True|wants_pause:False]
Display outlines on a blank image?:No
Select image on which to display outlines:PericyteColorImage
Name the output image:PericyteOutlineImage
Outline display mode:Color
Select method to determine brightness of outlines:Max of image
How to outline:Inner
Select outline color:yellow
Select objects to display:FilteredNuclei
Select outline color:red
Select objects to display:Cells

MeasureObjectSizeShape:[module_num:9|svn_version:'Unknown'|variable_revision_number:3|show_window:False|notes:[]|batch_state:array(b'', dtype='|S1')|enabled:True|wants_pause:False]
Select object sets to measure:Cells, FilteredNuclei
Calculate the Zernike features?:Yes
Calculate the advanced features?:No

ExportToSpreadsheet:[module_num:10|svn_version:'Unknown'|variable_revision_number:13|show_window:False|notes:['Use if not using database']|batch_state:array([], dtype=uint8)|enabled:True|wants_pause:False]
Select the column delimiter:Comma (",")
Add image metadata columns to your object data file?:Yes
Add image file and folder names to your object data file?:No
Select the measurements to export:No
Calculate the per-image mean values for object measurements?:Yes
Calculate the per-image median values for object measurements?:Yes
Calculate the per-image standard deviation values for object measurements?:Yes
Output file location:Default Input Folder sub-folder|OneDrive - FDA\\Research\\Experiments\\Experimental Data&Analysis\\Pericyte Morphology\\Pericyte EV Morphology September 2023\\25X_R2_Output
Create a GenePattern GCT file?:No
Select source of sample row name:Metadata
Select the image to use as the identifier:None
Select the metadata to use as the identifier:None
Export all measurement types?:Yes
Press button to select measurements:
Representation of Nan/Inf:NaN
Add a prefix to file names?:Yes
Filename prefix:PeriMorph_
Overwrite existing files without warning?:No
Data to export:Do not use
Combine these object measurements with those of the previous object?:No
File name:DATA.csv

Use the object name for the file name?:Yes

DisplayDataOnImage:[module_num:11|svn_version:'Unknown'|variable_revision_number:6|show_window:False|notes:[]|batch_state:array([], dtype=uint8)|enabled:True|wants_pause:False]
Display object or image measurements?:Object
Select the input objects:FilteredNuclei
Measurement to display:Number_Object_Number
Select the image on which to display the measurements:PericyteOutlineImage
Text color:white
Name the output image that has the measurements displayed:DataImage
Font size (points):10
Number of decimals:2
Image elements to save:Image
Annotation offset (in pixels):0
Display mode:Text
Color map:Default
Display background image?:Yes
Color map scale:Use this image's measurement range
Color map range:0.0,1.0
Font:Adobe Arabic
Use scientific notation?:No
Font weight:normal

SaveImages:[module_num:12|svn_version:'Unknown'|variable_revision_number:16|show_window:False|notes:[]|batch_state:array([], dtype=uint8)|enabled:True|wants_pause:False]
Select the type of image to save:Image
Select the image to save:DataImage
Select method for constructing file names:Sequential numbers
Select image name for file prefix:OrigDNA
Enter file prefix:PeriMorph_
Number of digits:4
Append a suffix to the image file name?:Yes
Text to append to the image name:_nuclei
Saved file format:tiff
Output file location:Default Input Folder sub-folder|OneDrive - FDA\\Research\\Experiments\\Experimental Data&Analysis\\Pericyte Morphology\\Pericyte EV Morphology September 2023\\25X_R2_Output
Image bit depth:8-bit integer
Overwrite existing files without warning?:No
When to save:Every cycle
Record the file and path information to the saved image?:Yes
Create subfolders in the output folder?:No
Base image folder:Default Input Folder
How to save the series:T (Time)
Save with lossless compression?:No

Supplementary Figure 3.1. CellProfiler Pipeline for Pericyte Morphological Analysis

Supplementary Table 3.1 Morphological features of interest adapted from Klinker et al. 2017.

Morphological Feature	
Cell area	Nucleus area
Cell perimeter	Nucleus perimeter
Cell compactness	Nucleus compactness
Cell form factor	Nucleus form factor
Cell solidity	Nucleus solidity
Cell major axis length	Nucleus major axis length
Cell mean radius	Nucleus mean radius
Cell perimeter/area	Nucleus perimeter/area
Cell aspect ratio	Nucleus aspect ratio
Nucleus area/cytoplasm area	

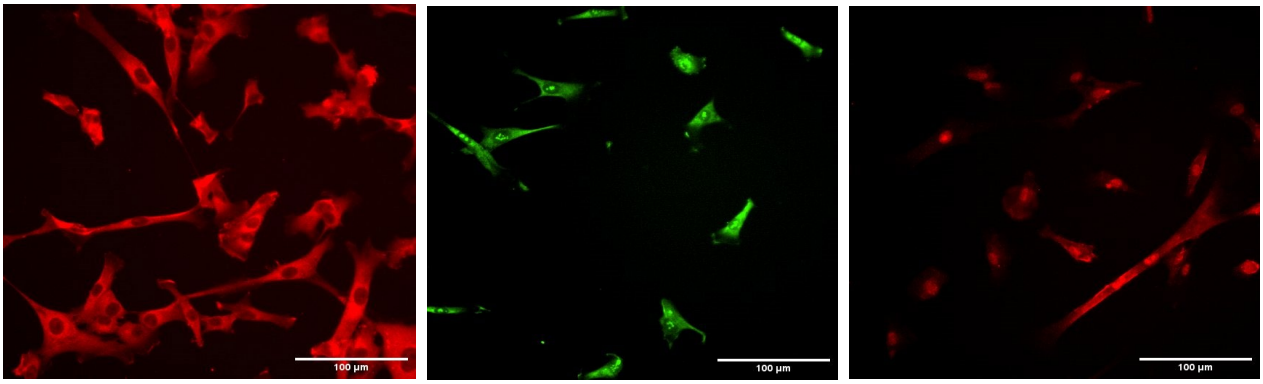

Supplemental Figure 3.2. Confirmation of pericyte identity. Pericytes were stained with **(A)** Neural/glial antigen 2, **(B)** α-Smooth Muscle Actin and **(C)** Nuclear factor kappa-B, from left to right respectively. Scale bar =100µm.

APPENDIX B

CHAPTER 4 SUPPLEMENTARY FIGURES

CellProfiler Pipeline: http://www.cellprofiler.org
Version:5
DateRevision:424
GitHash:
ModuleCount:12
HasImagePlaneDetails:False

Images:[module_num:1|svn_version:'Unknown'|variable_revision_number:2|show_window:True|notes:['To begin creating your project, use the Images module to compile a list of files and/or folders that you want to analyze. You can also specify a set of rules to include only the desired files in your selected folders.', '', 'For a large screen, it may take a long time to read and collect all the images. E.g., for a screen of 830k files (images+thumbnails), it took ~2 hrs to process. However, this only needs to be done once as the file list is saved as part of the project file.', '', 'Recommended to save time: Drag/drop the images once for a single project (e.g, QC), save the project as a template and then copy/paste analysis modules from the other two by opening additional instances of CellProfiler, then save them as separate projects.']|batch_state:array([], dtype=uint8)|enabled:True|wants_pause:False]
    :
    Filter images?:Images only
    Select the rule criteria:and (or (extension does istif) (file does endwith ".npy")) (file doesnot contain "thumb")

Metadata:[module_num:2|svn_version:'Unknown'|variable_revision_number:6|show_window:True|notes:['The Metadata module optionally allows you to extract information describing your images (i.e, metadata) which will be stored along with your measurements. This information can be contained in the file name and/or location, or in an external file.', '', 'The settings here allow the user to extract (assuming an ImageXpress microscope is used):', '* The UserStem prefix, and the Well and Site IDs from the filename, as well as the channel number.', '* The 5-digit Plate ID, and optionally, the date of acquisition from the folder name. If needed, the regular expression can modified to collect the barcode ID as well.']|batch_state:array([], dtype=uint8)|enabled:True|wants_pause:False]
    Extract metadata?:Yes
    Metadata data type:Text
    Metadata types:{}
    Extraction method count:1
    Metadata extraction method:Extract from file/folder names
    Metadata source:File name
    Regular expression to extract from file name:(?P<Other>[a-z]{3})_(?P<Platename>[A-Z]{1}[0-9]{1})_(?P<Well>[A-H]{1}[0-9]{2})_(?P<welllocation>[0-9]{4})_(?P<CLR>[A-Z]{3})_(?P<Channel>[A-Z]{4})
    Regular expression to extract from folder name:(?P<Date>[0-9]{4}_[0-9]{2}_[0-9]{2})$
    Extract metadata from:Images matching a rule
    Select the filtering criteria:and (extension does istif)

Metadata file location:Elsewhere...|
Match file and image metadata:[]
Use case insensitive matching?:No
Metadata file name:
Does cached metadata exist?:No

NamesAndTypes:[module_num:3|svn_version:'Unknown'|variable_revision_number:8|show_window:True|notes:['The NamesAndTypes module allows you to assign a meaningful name to each image by which other modules will refer to it.', '', 'The settings here match the channels by the channel number collected in the Metadata module.', 'Setting the image set matching method to "Metadata" has the advantage of omitting sites in which there is a metadata mismatch, i.e, missing files.']|batch_state:array([], dtype=uint8)|enabled:True|wants_pause:False]
Assign a name to:Images matching rules
Select the image type:Grayscale image
Name to assign these images:DNA
Match metadata:[{'DAPI': 'Platename', 'FITC': 'Platename'}, {'DAPI': 'Well', 'FITC': 'Well'}, {'DAPI': 'welllocation', 'FITC': 'welllocation'}]
Image set matching method:Metadata
Set intensity range from:Image metadata
Assignments count:2
Single images count:0
Maximum intensity:255.0
Process as 3D?:No
Relative pixel spacing in X:1.0
Relative pixel spacing in Y:1.0
Relative pixel spacing in Z:1.0
Select the rule criteria:and (metadata does Channel "DAPI")
Name to assign these images:DAPI
Name to assign these objects:Cell
Select the image type:Grayscale image
Set intensity range from:Image metadata
Maximum intensity:255.0
Select the rule criteria:and (metadata does Channel "FITC")
Name to assign these images:FITC
Name to assign these objects:Cytoplasm
Select the image type:Grayscale image
Set intensity range from:Image metadata
Maximum intensity:255.0

Groups:[module_num:4|svn_version:'Unknown'|variable_revision_number:2|show_window:True|notes:['The Groups module optionally allows you to split your list of images into image subsets (groups) which will be processed independently of each other. Examples of groupings include screening batches, microtiter plates, time-lapse movies, etc.', '', 'No grouping is needed, so this module is not enabled.']|batch_state:array([], dtype=uint8)|enabled:True|wants_pause:False]
Do you want to group your images?:No
grouping metadata count:1
Metadata category:Plate

IdentifyPrimaryObjects:[module_num:5|svn_version:'Unknown'|variable_revision_number:15|show_window:False|notes:['Identify the nuclei based on the DNA image.', ' ', ' The settings here were chosen based on the image data and acqusition settings provided in Gustafsdottir et al', ' PLoS One 8', ' e80999', ' 2013.

Changing the image acqusition settings may affect a number of these parameters:', ' * Typical diameter of objects: From the display window menu', ' select Tools > Measure length. Click/drag to measure diameters of a few select nuclei.', ' * Thresholding strategy: Global works fine in most cases', ' but Adaptive may work better if the background has non-uniform illumination. However', ' the illumination correction in CorrectIlluminationApply should mitigate the latter.', ' * Thresholding method: Select the method which provides the best foreground/background separation. Adjust the threshold corrrection factor if the threshold is concistently above/below where you want it to be for most images tested. ', ' * Lower threshold bound: Mouse over the background region to see the intensity variation in the lower-right of the display window.', ' * Method to distinguish clumped objects: Use Intensity if the intensity gradient dividing touching nuclei are pretty clear', " even if clumpy. Use Shape if the nuclei are usually well-separated (and Intensity doesn't work).", ' * Method to draw dividing lines between clumped objects: Intensity usually gives more realistic-looking boundary lines.', ' * Size of smoothing filter/minimum distance between local maxima: Override defaults if nuclei are getting under/over-segmented.', ' * Fill holes in identified objects: Currently set to Never since holes in nuclei may represent a phenotype. ']|batch_state:array(b'', dtype='|S1')|enabled:True|wants_pause:False]

Select the input image:DAPI
Name the primary objects to be identified:Nuclei
Typical diameter of objects, in pixel units (Min,Max):5,100
Discard objects outside the diameter range?:Yes
Discard objects touching the border of the image?:Yes
Method to distinguish clumped objects:None
Method to draw dividing lines between clumped objects:Shape
Size of smoothing filter:8
Suppress local maxima that are closer than this minimum allowed distance:8
Speed up by using lower-resolution image to find local maxima?:Yes
Fill holes in identified objects?:After both thresholding and declumping
Automatically calculate size of smoothing filter for declumping?:No
Automatically calculate minimum allowed distance between local maxima?:No
Handling of objects if excessive number of objects identified:Continue
Maximum number of objects:500
Use advanced settings?:Yes
Threshold setting version:12
Threshold strategy:Global
Thresholding method:Robust Background
Threshold smoothing scale:1
Threshold correction factor:1
Lower and upper bounds on threshold:0,1
Manual threshold:0.0
Select the measurement to threshold with:None
Two-class or three-class thresholding?:Three classes
Log transform before thresholding?:No
Assign pixels in the middle intensity class to the foreground or the background?:Foreground
Size of adaptive window:10
Lower outlier fraction:0.001
Upper outlier fraction:0.001
Averaging method:Mean
Variance method:Standard deviation
# of deviations:2
Thresholding method:Otsu

IdentifySecondaryObjects:[module_num:6|svn_version:'Unknown'|variable_revision_number:10|show_window:False|notes:['Identify the cells using the nuclei objects plus an image representative of the cell body. Several of the channels could suffice for this purpose, but we chose the RNA channel as optimal. Using the "Watershed-Image" option over the default "Propagate" methods seems to often better capture the cell boundaries, especially when the cells are confluent.']|batch_state:array(b'', dtype='|S1')|enabled:True|wants_pause:False]
    Select the input objects:Nuclei
    Name the objects to be identified:Cells
    Select the method to identify the secondary objects:Propagation
    Select the input image:FITC
    Number of pixels by which to expand the primary objects:10
    Regularization factor:0.0
    Discard secondary objects touching the border of the image?:Yes
    Discard the associated primary objects?:Yes
    Name the new primary objects:FilteredNuclei
    Fill holes in identified objects?:Yes
    Threshold setting version:12
    Threshold strategy:Global
    Thresholding method:Robust Background
    Threshold smoothing scale:0.5
    Threshold correction factor:1
    Lower and upper bounds on threshold:0.0,1
    Manual threshold:0.0
    Select the measurement to threshold with:None
    Two-class or three-class thresholding?:Two classes
    Log transform before thresholding?:Yes
    Assign pixels in the middle intensity class to the foreground or the background?:Foreground
    Size of adaptive window:10
    Lower outlier fraction:0.01
    Upper outlier fraction:0.01
    Averaging method:Mean
    Variance method:Median absolute deviation
    # of deviations:10
    Thresholding method:Otsu

GrayToColor:[module_num:7|svn_version:'Unknown'|variable_revision_number:4|show_window:False|notes:[]|batch_state:array([], dtype=uint8)|enabled:True|wants_pause:False]
    Select a color scheme:RGB
    Rescale intensity:No
    Select the image to be colored red:Leave this black
    Select the image to be colored green:FITC
    Select the image to be colored blue:DAPI
    Name the output image:PericyteColorImage
    Relative weight for the red image:1.0
    Relative weight for the green image:1.0
    Relative weight for the blue image:1.0
    Select the image to be colored cyan:Leave this black
    Select the image to be colored magenta:Leave this black
    Select the image to be colored yellow:Leave this black
    Select the image that determines brightness:Leave this black
    Relative weight for the cyan image:1.0

Relative weight for the magenta image:1.0
Relative weight for the yellow image:1.0
Relative weight for the brightness image:1.0
Hidden:1
Image name:None
Color:#ff0000
Weight:1.0

OverlayOutlines:[module_num:8|svn_version:'Unknown'|variable_revision_number:4|show_window:False|notes:[]|batch_state:array([], dtype=uint8)|enabled:True|wants_pause:False]
Display outlines on a blank image?:No
Select image on which to display outlines:PericyteColorImage
Name the output image:PericyteOutlineImage
Outline display mode:Color
Select method to determine brightness of outlines:Max of image
How to outline:Inner
Select outline color:yellow
Select objects to display:FilteredNuclei
Select outline color:red
Select objects to display:Cells

MeasureObjectSizeShape:[module_num:9|svn_version:'Unknown'|variable_revision_number:3|show_window:False|notes:[]|batch_state:array(b'', dtype='|S1')|enabled:True|wants_pause:False]
Select object sets to measure:Cells, FilteredNuclei
Calculate the Zernike features?:Yes
Calculate the advanced features?:No

ExportToSpreadsheet:[module_num:10|svn_version:'Unknown'|variable_revision_number:13|show_window:False|notes:['Use if not using database']|batch_state:array([], dtype=uint8)|enabled:True|wants_pause:False]
Select the column delimiter:Comma (",")
Add image metadata columns to your object data file?:Yes
Add image file and folder names to your object data file?:No
Select the measurements to export:No
Calculate the per-image mean values for object measurements?:Yes
Calculate the per-image median values for object measurements?:Yes
Calculate the per-image standard deviation values for object measurements?:Yes
Output file location:Default Input Folder sub-folder|OneDrive - FDA\\Research\\Experiments\\Experimental Data&Analysis\\EV miRNA Project\\EV Manufacturing\\Pericyte Morphology\\Output
Create a GenePattern GCT file?:No
Select source of sample row name:Metadata
Select the image to use as the identifier:None
Select the metadata to use as the identifier:None
Export all measurement types?:Yes
Press button to select measurements:
Representation of Nan/Inf:NaN
Add a prefix to file names?:Yes
Filename prefix:PeriMorph_
Overwrite existing files without warning?:No
Data to export:Do not use

Combine these object measurements with those of the previous object?:No
File name:DATA.csv
Use the object name for the file name?:Yes

DisplayDataOnImage:[module_num:11|svn_version:'Unknown'|variable_revision_number:6|show_window:False|notes:[]|batch_state:array([], dtype=uint8)|enabled:True|wants_pause:False]
Display object or image measurements?:Object
Select the input objects:FilteredNuclei
Measurement to display:Number_Object_Number
Select the image on which to display the measurements:PericyteOutlineImage
Text color:white
Name the output image that has the measurements displayed:DataImage
Font size (points):10
Number of decimals:2
Image elements to save:Image
Annotation offset (in pixels):0
Display mode:Text
Color map:Default
Display background image?:Yes
Color map scale:Use this image's measurement range
Color map range:0.0,1.0
Font:Adobe Arabic
Use scientific notation?:No
Font weight:normal

SaveImages:[module_num:12|svn_version:'Unknown'|variable_revision_number:16|show_window:False|notes:[]|batch_state:array([], dtype=uint8)|enabled:True|wants_pause:False]
Select the type of image to save:Image
Select the image to save:DataImage
Select method for constructing file names:Sequential numbers
Select image name for file prefix:OrigDNA
Enter file prefix:PeriMorph_
Number of digits:4
Append a suffix to the image file name?:Yes
Text to append to the image name:_nuclei
Saved file format:tiff
Output file location:Default Input Folder sub-folder|OneDrive - FDA\\Research\\Experiments\\Experimental Data&Analysis\\EV miRNA Project\\EV Manufacturing\\Pericyte Morphology\\Output
Image bit depth:8-bit integer
Overwrite existing files without warning?:No
When to save:Every cycle
Record the file and path information to the saved image?:Yes
Create subfolders in the output folder?:No
Base image folder:Default Input Folder
How to save the series:T (Time)
Save with lossless compression?:No

Supplementary Figure 4.1. CellProfiler Pipeline for Pericyte Morphological Analysis

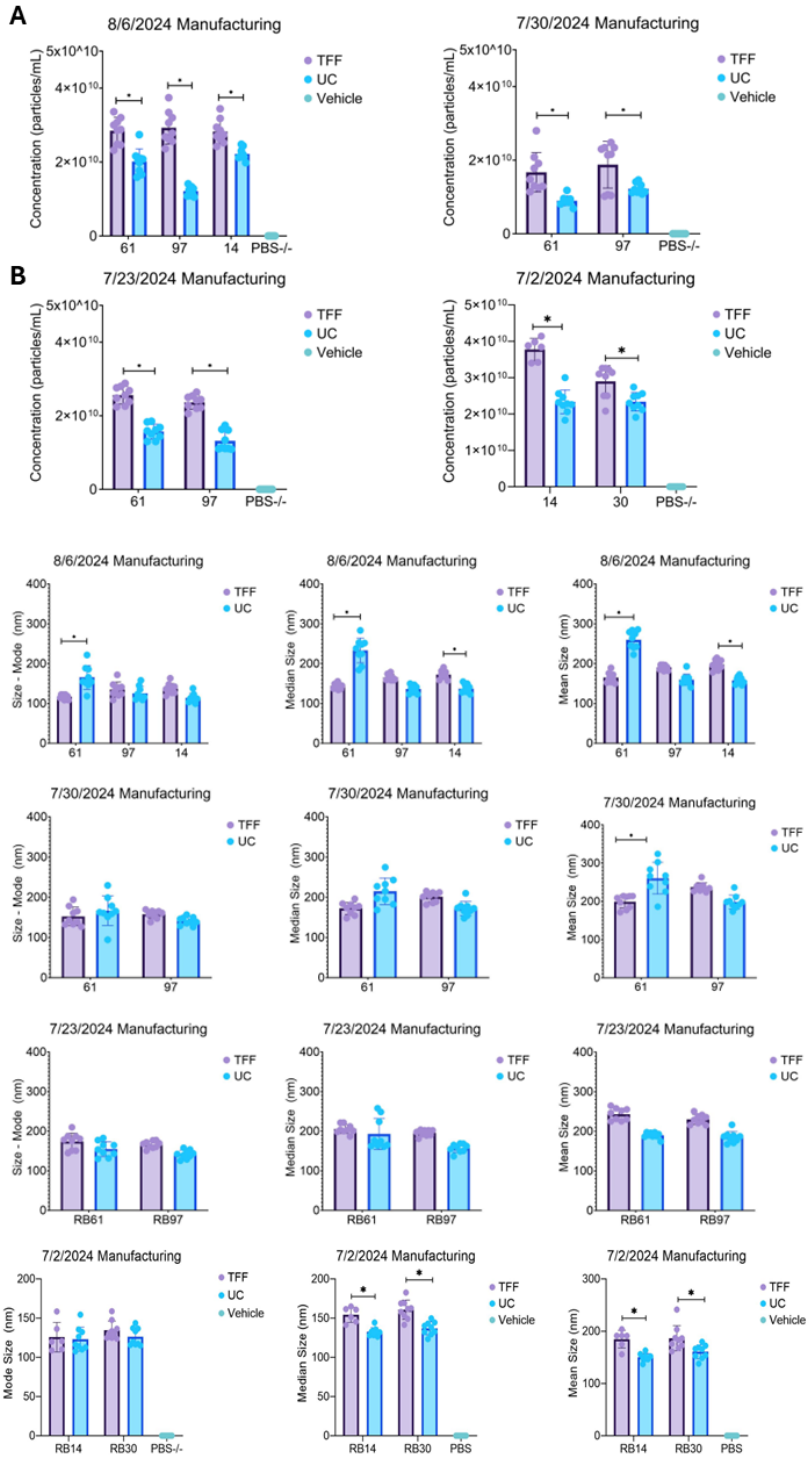

Supplementary Figure 4.2. Size and concentration data for each manufacturing batch. **A)** Concentration data for each manufacturing batch. **B)** Mean, median and mode size data for each manufacturing batch. For all, * represents $p<0.05$ using an ordinary one-way ANOVA and Sidak's multiple comparison test.

Supplementary Table 4.1. Genes found in each MSC-EV Manufacturing Group

Manufacturing Group	Genes
TFF RB14, 30/ UC RB14,30 shared genes (894 genes)	CLMP FSTL1 ACTN4 RPS11 CD44 RPS17 MMP2 SAMD4A PINK1 CMTR2 APOL2 FP236383.3 VPS4A HSPB1 PFKP DECR1 RPS18 TMSB10 G3BP1 RAB1B DDB1 CYCS SCAF8 MYO9B RPL19 CCNI TLN1 ZEB1 UBB CDK14 RPPH1 AES OSBPL8 TNS3 RPS5 SRPK1 RPL7A TCEANC2 ATXN10 PUF60 ATP5MG UTRN BAZ1B PALLD RPL35 COL1A1 RHOC GNAS DUX4 GOLGA3 STAU2 NCOR2 CTDSP2 MYL12A TPI1 DSTN BOP1 C1orf216 RPS28 RASA4B TUBB USP7 YWHAQ YME1L1 RPLP1 PTP4A2 C12orf75 PSMD3 COX8A NPM1 XRN2 COG1 CELF1 PSMD11 ASS1 ALAD TMEM59 SEC23IP SNX6 CCT8 NBPF19 SPTBN1 MFN2 LDHB TLCD2 RAB5B MAPRE1 BTF3 SARS ATAD3B USP32 EZR DYNC1H1 RPL32 GNG12 ASNSD1 NBR1 CD99 HSPA8 STK40 FP671120.3 ITPRIPL2 ARPC3 PJA2 GSTP1 CHMP7 TBC1D9B AHNAK FN1 RSU1 RPL4 RPS21 ALYREF PSMF1 SH3PXD2A YWHAZ RPL10 C6orf62 ASAP2 RNA5-8SN1 SPCS3 CD151 NDUFA13 TPT1 CUL4B FTH1 AC022150.4 CSRP1 ZFP36 EHBP1L1 PXN DCTN1 TTC3 C1orf198 IKBKG PGAM1 TCP1 CNDP2 PAWR ITGB1 RER1 RPN1 TUBA1A NOP10 PSMD8 SET EIF2S1 ANTXR1 BICD1 AKAP2 CORO1C IL13RA1 RPS29 CSNK2B RMRP_2 RF00019_485 EIF5A WBP11 EHD2 MAP1A TRIM56 HNRNPK CNOT7 KDELR1 FAM129B RIC8A CCND1 PDCD6IP NET1 ACLY NACA SMS VIRMA GPX4 CHMP3 PRMT1 PPDPF RPL39 ZBTB47 RBM3 SNRPG RPL17 FAM122B RNY3 SF3B2 HIPK3 WSB1 SOCS4 AP2S1 VAT1 TUFM RUFY1 MYC TMEM259 S100A16 SLC9A3R2 RUVBL2 RPLP2 RPS24 CALM2 SLC25A39 ZBTB4 AMOTL2 NUDT16 KLHDC2 CLIC1 STAT1 RBMXL1 SEC61A1 MRFAP1 CRTAP NME4 MT-RNR1 SMURF2 UCP2 EFEMP1 NAP1L1 PTDSS1 SEPT7 ARMCX3 YBX1 ANXA2 INPPL1 PTTG1IP CNN2 LMO7 HEBP1 PPP1R15A KPNA4 H3F3A GLO1 PRR13 RPLP0 HNRNPD EIF5B AXL LMNB1 MT-RNR2 MYL12B ZDHHC7 ELOA RPS6 IFT172 CTNNA1 AL139099.4 MZT2B ROMO1 GOLGB1 PDLIM1 HNRNPA2B1 PYGB RPS10 CLIC4 PPP1R14B SBF1 API5 TNRC6A EID1 DHX8 CAPNS1 COPE EIF3A ITGBL1 BOK NIPSNAP2 FP236383.2 ARHGAP1 PIP4K2A MYLK AFAP1 CAPN2 SNX9 PURA RPL15 TRAPPC11 RNU1-2 LNPK PRPF31 TRAK2 RPS3A MXRA7 LGALS3 CFL2 ZSWIM9 ABCF1 CFL1 SMARCA4 SEPT2 GBP1 BOD1L1 RPL34 AKAP12 PRPF8 PLEKHB2 RTRAF RPL28 SEC61G IARS RPL18A PHACTR2 TBL1XR1 NUDC DNAJC8 RPL3 THBS1 NCOR1 UBE2H NFE2L1 NT5DC2 PPP1CB NRDC ERBIN RNY4 HSP90AB1 CCT3 CABIN1 MTHFD1L NCL EIF4EBP1 NCOA1 GSPT1 GDF11 MRPS16 RNU1-28P ARPC4 RPL9 ATP2B4 TRIM28 PHLDA2 PSMD4 METAP2 HBB CYB5R3 MTPN ESYT2 CDC37 MT-CO1 KRT7 ODC1 SYNJ2BP DDX17 NACC1 SEC62 ENO1 ZMYM4 DDX1 ZNF532 ZNF106 RNPS1 GLS PEX5 RPL35A MX1 SH3BGRL3 LRCH1 VASP ANKRD13A SULF1 MYL9 CDKN1A CAT MARCH4 TBC1D15 NONO RN7SL5P NPM3 TPM2 NCBP3 AK5 CENPB RPL37A NREP ELAVL1 BNIP3L RNU1-1 PTPRJ SERF2 ZMAT2 EIF4H KLHL5 SRM PPM1G RPL11 NMT1 SNX8 HADHA TUBB4B CHURC1 SOD2_1 RPL8 SNX12 LDB1 PCBP2 GNB1 MBNL1-AS1 RPL23A SEPT11 UBE2V1 CALD1 BEX3 EIF3E RPL31 PSMB3 EXOC7 MPRIP DEK TAF15 UPF2 EIF3I SUCLG2 EPAS1 RAB18 UBTF OST4 ACTN1 NBPF14 ELOB MORF4L1 GAPDH COX7C PMP22 APC RNA5-8SN2 GALNT1 PSME2 RBM25 POLR2E WRB BICRA MAP1S GAS6 MAGED1 BCYRN1 MOCS2 AL135905.2 MTCH2 MT2A C9orf3 ACTG1 CALM1 C8orf33 FAM13B HNRNPU ATXN2L FLII RPS16 RPS9 RPL14 MAFF HNRNPA1 AKT3 RALBP1 KTN1 RANBP9 CAPZB SATB1 MLYCD UQCRH CYP1B1 COL12A1 PDLIM5 UQCRC2 HNRNPUL2-BSCL2 HDLBP IFIT3 ACTR2 RAP1GDS1 FAM50A PGK1 MAP4 MYO1B RPL10A MACF1 POLR2L ARHGAP11A ADD3 PTEN RASSF3 SLC25A37 HMGB3 SMARCC1 RNA5-8SN3 VCPIP1 DSP GABARAP DPYSL2 GOLM1 SSH2 C22orf46 SDHB MSN SMARCD1 GNAI2 RAB3GAP1 SMPD4 AIDA TGM2 TCAF1 TIMP3 RPL29 CIB2 SQSTM1 RPS23 SNRNP70 GABPB2 PTPN11 TAGLN2 HIST2H4A LGALS1 MYO1C YWHAE WDR1 RPL12 RPA2 DDAH1 DTX3L PARVA COPG1 KIF5B CCT2 CSDE1 MYH9 ANAPC13 MBTPS1 SUPT5H GPI LARS RPS4X SND1 CHD3 RPS3 RPS27A RAI14 DYNC1LI2 PRDX1 FLNC ARF1 PRAF2 BCL2L2 SPTAN1 CAVIN1 RHOA SERPINA1 RPS13 MYL6 RPSA ENAH SMC4 TMEM230 RPS8 TUBA1B ZFP36L2 RF00003_9 ZCCHC24 RNF20 USP9X FTL NEK7 IFITM2 HUWE1 EMP1 PPP1CC ZC3HAV1 RRAS2 RPS2 BNIP3 MAPK14 DYNLL2 MTHFD2 AP2M1 OAS3 ANXA6 RNY1 EIF2S3 AP2A1 RPL7 MYOF FURIN GSN AC120498.9 ZYX MAPRE3 SMOX SF3A2 MIR100HG CGGBP1 FHL2 VIM CALR UQCRB BZW1 RRAGA RPL22 SLC38A2 RPS26 DNAJA1 NDUFA4 MT-ND4 CAP1 PKP4 SEPT9 FAM168B BCAR1 SIPA1L3 MEGF8 MRC2 MTCH1 HK1 SZRD1 CDC42 UACA BAD TPM1 FLNB ATP5F1A SUMF2 WDR60 MAN2A1 SPECC1 TNS1 PPP1R10 PPIA VDAC1 TJP1 RNY3P1 TXNDC5 TOM1 MCRIP1 EEF1B2 RN7SL3 JCAD TUBB3 S100A6 RPL6 TCEAL4 DDX46 ILF3 GNB2 RPL30 ARRDC4 ADRM1 RAB31 DHRS3 ALDOA GAB2 LASP1 PLAA MCL1 ATAD3A RNA5S9 CCND3 S100A11 CLTC MAZ ECI2 ANXA5 KIF3B ANGPT1 KARS RAN SEC31A EEF1A1 EIF4G1 LINC00632 HSP90AA1 YWHAB RNF213 DHX9 EIF4B KCTD20 RPS15 FERMT2 SEC23A PRPF40A SLC35A4 AGO1 PSMA2 ROCK1 TAGLN RN7SK ARPC2 PTMA RPL26 NDUFV3 FOSL2 EEF2 RBM12 DENND5A ATP5F1E COTL1 IFITM3 MARCKS ANAPC11 RACK1 CD59 TPM4 OPTN AL135925.1 POMP NME2 RAI1 RPS20 PYGL RPL21 MLLT6 NFIX SLC7A5 CAPRIN1 PEA15 HNRNPF NQO1 RPL5 LSM5 RPS15A EIF4A1 MTURN TSPO TPGS2

	SRPK2 PTGR1 CMPK1 TUBB6 CCDC80 RHOB ENSA RPS12 DDX6 PPP2R1A HNRNPM COL2A1 SRSF1 FNDC3A NOTCH2NLA OS9 IGF2 1 MICAL2 UBA52 CAV1 RN7SL1 HECTD3 USP34 ACAA1 PLEC RNU1-4 SLC25A6 GLYR1 RPL18 WBP2 PSMB5 VAMP3 EIF3C TRIM44 KIF1C HIF1A DBN1 RPL27A RPS19 LRRC59 RNU1-27P ANPEP NKAPD1 EIF3L DST NFATC2IP CAB39 ZEB2 PKN1 MLF2 RAB13 NSA2 PRRC2A AAGAB RRM1 S100A10 RPL13 ZFAND3 ACTB CALM3 RPL23 RF00002_5 GBF1 FYTTD1 SERPINE1 MAP1B RARG RNF40 RN7SL4P PRELID1 SMG6 WWTR1 WDR41 NFX1 RPL13A AMOTL1 RPL41 DRAP1 PHF20L1 PPFIA1 RNVU1-18 ATP5F1B HLA-B CRK PKM ARHGDIA ZFR GSTO1 HNRNPA3 ULK2 RHOBTB3 CANX HIPK2 DAP CCND2 CUL4A UGP2 ANKIB1 EIF4A2 PABPC1 PLEKHA4 USP22 SERINC1 MALAT1 PPP1R3C MIF PFN1 SLFN5 ST13 ABLIM3 VOPP1 RARS P4HB SAE1 WDR55 COX4I1 OAZ1 HDGF SUPT6H ELL2 DDR2 SPARC BECN1 MAP4K4 EIF4G2 FAM208A IGFBP4 SYNPO LMNA KPNB1 ZNFX1 DCTN5 KHDRBS1 NORAD HIP1 WNK1 CHN1 LPAR1 TMSB4X PPA1 HMGA1 POPDC3 SERBP1 RANBP2 YTHDC1 STK38 RPS14 RNU1-3 FBXO32 TGFBI RNVU1-7 ANP32B PGD POLR3D CUTA FLNA BAX RPL37 NCOA4 NANS FKBP1A RN7SL2 PGPEP1 USP1 DPYSL3 PAK2 EEF1G INCENP RN7SL471P UBC HBA2 CBR1 NRSN2 HBA1 SHISA5 RPS27
TFF RB14, 30 unique genes (1834 genes)	RAB2A SLMAP PYROXD2 GNL3 GRAP2 APBB2 NDUFS6 ECHS1 CNBP BYSL AP003559.1 COX7A2L ABCC6 SNHG16 U2SURP GLTP SLC25A3 ADAM12 IRAK1 ZAR1 GAS5 RNU4-2 UBE2G1 MRPL10 DCAF5 GPSM2 KIRREL1 HIST1H4J DDX5 AL391422.4 EPN2 KCNK6 NDUFAB1 BAK1 AGPAT1 THRAP3 COX6C TOB2 GPR143 COPS7A WSCD1 LONP1 ARF6 C4orf3 ANP32E BET1L TEAD1 MNS1 HMGN1 UBA1 TSC22D1 POLR3K FAHD1 DARS SNORD3B-2 ARHGAP21 ACTR8 RIOK1 PUM3 LIMS2 SLK PRKCB CDK11A KRT1 LMNB2 ROCK2 MT-ATP6 IMPDH2 MCUB TERF2IP MAP3K20 KPNA2 PDIA3 DGUOK AP1S2 RBM17 VGLL3 ACBD3 ZNF83 KPNA3 DSCC1 ANLN SMYD3 CAVIN3 KATNB1 CCDC124 PPIL1 GPR55 RAD23B HIST3H3 CCNY LAMTOR2 RBPJ HIST1H1E USP14 GYPC ALDH2 GOLGA6L10 EMP2 IP6K1 SRSF6 TRIM41 QDPR TPM3 HSPD1 EIF1 CETN3 TMEM98 ADH5 NDUFA8 RARRES3 ATOH8 PLXNA1 KIAA0100 PMF1 ASCC1 CHMP1B COPS4 PMM1 LCMT1 FBXL19-AS1 PPM1A PCBP4 SRSF11 INTS1 ADI1 SCP2 ABHD2 MAFK TRAM1 METTL25 CHFR TAF12 MPP4 LINC02015 CDCA4 AVEN TSR3 ADAM19 AC026464.4 ADRA2A RGS4 UQCRC1 NIPBL TFR2 EIF3M SRP72 MICU1 NUCB1 SNAPC1 PTMS BRK1 PIP4K2B MRPS12 TAF10 RHBDF1 UPF3A LTBP1 TRIP12 DPYD DLGAP4 BACE2 ZBED1 NKAIN3 METTL21A PSMC3IP KDM2A H3F3B QKI EML3 ABHD12 FERMT3 LSM12 CFAP298 HABP4 FGF1 CST3 CD53 DHX16 ATP5PD NDUFC1 ARL2BP TTLL11 ZNF655 UBXN7 COG3 IMMT DHX15 PICALM PCCB MAK16 BRD8 GMFB SLAIN1 AL627309.1 NKTR ALDH1L2 TLE2 FKBP4 GPRC5C AP3B1 COP1 UBE2W STMP1 MTR UBL7 PPP1R37 CBX6 ASH1L EIF4A3 AC005261.1 CHMP2B DDX24 ACO2 IRX3 ATP1A1 MTSS1L LOXL1 CYSTM1 UBE2N NEK6 PRRX1 RBBP6 SCHIP1 OPA1 KRCC1 TRAF7 PFKL MOB1B IDS FAM189B DYRK4 NUAK1 ALG6 SSRP1 LINC01605 ETFA EXOC1 BAALC-AS1 PDAP1 CCDC6 ZNF146 CHAF1A IER3 KCTD10 YWHAH FAU PDGFRB ADRB1 ALDH6A1 RDX AL731577.2 FGD5-AS1 FOXL1 BCKDK SVIL AC073111.3 BOD1 ASAP1 TMEM248 PCBP1 HIST2H3D R3HDM2 SEC13 DLST OSER1 FYN YPEL5 RPS10-NUDT3 KLHL21 SCRN1 PARK7 PMVK PSMC4 COQ5 EIF3D SNRPC AL049543.1 DNAJB4 CYB5R4 MEMO1 ZNF827 SERP1 SH2B1 AURKAIP1 SPAG9 SLC39A9 FLJ13224 KRTAP1-5 ACADVL RASSF10 GPATCH11 MSANTD3 MCFD2 EIF2B2 WNT5A BDP1 RANBP1 THOC7 MKLN1 ENO2 SDHD B2M SPIDR SQLE PPFIBP1 KIAA1551 PARD6G CBS CTNNB1 NPIPB5 ANKRD17 SNTA1 CCNK MARCH3 EAF1 IGFBP2 USP11 NOL11 ADD1 PSMD2 FAM122A AP2B1 RRAS TOX IPO5 UBE2Q2 IK CDK4 RTL8C CCAR2 TYMS CEBPZ ZFAS1 BTBD10 PTPN14 ANKRD40 ACOT9 TSPYL5 CDK16 HRAS BSDC1 HOTAIRM1 ZNF677 UQCRQ SPRYD7 UBE2K PHPT1 CTU2 KAT5 XPOT ERH PSMB8 CRAT SREBF2 LIMS1 APOL1 MME SENP3 AD000090.1 CCDC14 EEF2K ARPC1A NAA15 ATP6V1E1 BIRC2 ACAA2 DNASE1L1 PLS3 TIMP1 RSPH3 AC087632.1 PTPN9 PLOD2 KLF9 RPL27 MT-ND6 ZFAND6 YES1 VCP MAGI1 BGN PWWP2A SMG1 SRSF3 SH3GL1 PIP5K1C RALB TSPAN31 ALAS1 MRPL37 AL162231.1 PANK3 PSMA5 WDR82 FUT8 MAGI2-AS3 CEP104 LRRFIP1 HIST2H2AC ZNF90 ALDH5A1 COL8A1 LINC02381 EPHB1 ADAMTS6 FBXO30 RPP30 DMAC2 BLVRB PEX11B METAP1 SMARCA1 ACOX3 ZNF846 BCL2A1 SPAST BANF1 ZFP91-CNTF ARHGEF5 RPS6KA2 TOR1A SMAP1 PES1 BBX PDE7B SRRM1 PPP1CA ZNF608 NDUFB3 FKBP8 B3GALT2 CCT7 MIPEP NDE1 MAGEF1 WDR45B ACSS3 EI24 DOCK1 PTPN23 HDDC2 PARVG GSR HIST1H4B FAM20B BUB3 COPB2 CDC27 COPS6 DCTN4 NEDD8-MDP1 EIF2AK2 PSMD9 ASNA1 IDO1 NUTF2 MSC-AS1 CITED2 FAM126A RABIF PKIG ATP11B PFAS AC067852.2 NUCKS1 IP6K2 CCDC74B RBM34 EXT1 YWHAG RMND5A CFAP36 MRAS EMB MAF1 SRP14 XPO6 SYNE3 AL360012.1 KDM7A KCTD4 CHMP2A C7orf50 USP15 GTF2H1 LSM14B PRAG1 RIPOR1 RAD23A GHITM HMGN2 FOXN3 MRM1 LCLAT1 ETV3 G3BP2 UTP18 AC004967.2 POSTN PPP3R1 PTBP3 ATP13A2 DCAF6 NAE1 STIM2 POTEF ZC3HC1 CD99L2 TAP2 SPOP BIVM PTPRF ICMT EGFR CYB5B TMED8 EEF1D BBOF1 RAB6A DOK1 SOD1 CDK13 PACS1 ITPRID2 BCR FSCN1 ZFP36L1 SH3BP5 TIAM2 ZNF317 CBR3 TRIM17 ST6GALNAC4 SIRPA IGFBP6 CREB1 RMDN1 DDX3Y NDUFV1 PDLIM4 STAG1 REXO4 ZNF142 SOGA3 CCPG1 AL118506.1 P3H2 FCF1 FAHD2A CLSTN3 PSMG1 CEP55 TAX1BP3 EYA3 CLPTM1L EML4 STAT5B SLAIN2 AMMECR1L SSB ARFIP1 DYNLL1 UBOX5 TCERG1 MPP6 SLC35E1 APOLD1 ZNF880 SLC25A11 PAOX SINHCAF EMP3 SYNCRIP RTCA MED13 RAB4A SNX11 GOLGA2 TMEM39B ESCO1 PHF2 PID1 FARSA VAMP5 TUBA1C PIK3R2 CMTR1 TXNRD1 CCDC9B

	TMBIM6 KLHL18 CCDC91 AKR1B1 STIP1 C16orf72 PSMB4 CYTIP SART1 PCMTD1 NDUFA1 RBM5 NOP14 RALGPS2 TUBGCP4 DPP9 ARPC1B SSR2 COPS3 ZNF616 VARS SUZ12 MED21 ZNF415 IL17RA SYF2 MCC WISP1 RNU4-1 CLPX MRPS36 ID2 NPLOC4 SLC24A1 ATXN1L ARHGAP5 DDX21 RB1 B3GALT6 HDAC11 SLC9A4 BZW2 HADHB HTATSF1 COL16A1 RNF24 TNIP1 GLRX TENT5B BPIFA3 MTA1 XRN1 NABP1 GOLGA6L4 IRF2 SNRNP35 INTS13 MAPRE2 ARFGAP3 CSNK1G1 GRINA ADIPOR1 CCZ1 DNAJB2 CDK11B TFPI SGCD CAMTA2 TMEM87A PDE4DIP DNM1P35 GFER DGKA PQLC1 DNTTIP2 ZNF559 PCBD1 TIPRL TAF3 ZNF263 SP3 AZIN1 SLC35C1 NDUFB11 VCAN UBE2A VTRNA1-1 NHS KANK2 DDHD1 BCL7B EPS8L2 C14orf119 PPP6C OTUB1 ARL6IP4 JUP RAB40C STK11 GINM1 CHP1 PSMC5 CLIP3 LOX KBTBD2 LAMB2 RPS27L ACP1 IQSEC3 PDIA6 GTPBP6 PPA2 TAB3 RAB11FIP5 GTF2I SCAF1 NCK1 KCTD8 BRD2 LAMP2 ZNF746 PRKCQ KIRREL3 RASA1 RNF10 JMJD8 FAT1 ITCH GOLGA6L22 ZC3H4 TCEAL3 NCOA2 C20orf194 USP5 IGBP1 AJUBA CFAP97 GUK1 FAM210B CYB5D1 USP12 FAM66B STAMBP CENPI GTF2E2 KLHL20 CD47 CCNF DLC1 LAP3 PRKACA SOCS5 WDR37 XRCC5 TBRG4 RBM39 POU5F1 RAB1A IMP3 SELENON SH3RF1 RNU2-2P USO1 RAB9A BLZF1 ZHX1 PCDHGC3 SWI5 SHLD2 HDGFL2 ARHGAP35 PREX1 MINOS1 MAPKBP1 CTSA HIST1H2BD ELP2 VGF TIMM17B WIPF1 ADNP MMADHC NSMAF AGBL5 SKIL HOXA11 SLC25A51 RAB28 TGFB1I1 SNRNP200 RAB10 RPS25 PRXL2B CNOT3 CLEC11A AL591623.1 TXN2 TRAPPC3 AP5S1 RNF11 MLH1 GYG1 POLR3GL DEXI VAMP7 PHB IFNAR2 R3HDM1 ZNF91 SLIT2 MKRN1 CLTB AKR1A1 ANXA7 AC004846.1 MLLT11 ERRFI1 HMGXB3 ZC3H15 WDR83 ANKRD13D COMMD6 ENGASE COMMD9 GPX1 STX6 HIST1H1C GNA12 LIMK1 MAP1LC3B2 CDC42EP1 TPR HIGD2A HIST1H2BO SNORA73B TNPO2 IRF9 PGS1 BMP2K TBC1D23 FP671120.4 SAMD4B HINT1 USP39 PLAUR CHCHD2 FKBP11 SCAP RPL38 SMAP2 CWF19L2 SIVA1 BABAM2 AC008735.2 APRT SELENOT PEBP1 AOX1 PCSK7 CYR61 COL1A2 LY96 IL1R1 HGS UBR4 CTTN PROCR PHF11 CCT6A LAPTM4B PYCARD TMEM256 NEK2 AC090204.1 ERC1 YPEL3 SHMT2 AP1S1 NCLN TMEM206 PIP4P1 BTAF1 ZNF280D ROS1 GPR108 C1orf43 RNPEPL1 ALPK2 B3GNT2 LTA4H SAFB FANCG CCDC24 CKAP4 PITPNM1 HMGB1 UCK2 CDYL KLF3 KHNYN MTFR1 ESPL1 RCN3 GMPR2 DBNL CHPT1 ERGIC1 ARHGEF10L ATOX1 STT3A LPP EIF4EBP2 ATRX NDUFB1 RTL8A TNIK MEF2D RCBTB1 COX5A SEC24D KMT2E RAC1 MAST2 ANXA1 MTA2 GTF2A1 TRIO SETD2 ID3 UGGT1 IQCK TOPBP1 CTNNBL1 NDUFA6 HMG20B PTRHD1 NDUFAF3 NAXE NOSIP TPD52L2 ZNF248 PELP1 CDK5RAP2 NXNL2 C5orf24 RPL36A AK3 CHID1 SERINC3 C8orf58 NRP1 TRIM22 LYRM2 ZNF347 C19orf53 GJA1 PKD1 ZFP3 CCDC50 METTL8 MRPS14 LAPTM4A PRDX6 KIAA1522 CRYZL1 FARSB PSMA3 BASP1 ZNF202 RXRA TMEM60 PDLIM7 MSL3 SLC44A2 PAIP2 ZNF879 ABHD4 RAC2 SEPT10 SCYL1 MTHFR PTOV1 CSGALNACT2 EML1 RALY SMAD3 KDM5C RSL24D1 TMEM45A YIPF4 MRPS34 PLCG1 CHMP5 ZDHHC16 ST3GAL1 PHF3 NEDD4 ATP8B2 RFTN1 RBBP9 TAPBPL DICER1 PSMC2 APEH FYCO1 FBLIM1 RAPH1 PCYT1A C5orf38 SRPRA CYFIP1 TAF1B UBQLN4 NPAS1 EXOC6B GAN HLA-E EVC2 KIFAP3 SWAP70 GSTA4 ZNF596 CDKN1B SLC15A4 MRPL12 AL359643.2 TRIR VWA8 REP15 WIZ YEATS2 RBM4 FGG CSF1 SLC35B2 FNIP1 TRNAU1AP MRPL47 COPA SYNC PSMB6 MAP3K14 TRMT112 FEM1B GNG5 TNFRSF11B STOML1 KIAA1143 TWF1 NUP153 TMEM233 FSCN3 ZNHIT1 EFHD1 XRCC6 COPZ2 MEF2A ASF1B USP16 GPCPD1 COPZ1 ANKRD28 FOXD3 LRFN3 RNF145 GDI1 ZMYND8 TSC22D3 KIF16B PTGES3 CS IFFO2 IGFBP7 ZNF609 NACC2 HYI COX17 CASC3 ARID5B TCF12 ZRSR2 ATXN7_2 ZNF641 NECAP2 ACTR1A CNN3 ORMDL3 HIST1H2AL HSPA4 NUPR1 EMC3 SMC1A SLC1A5 VPS41 NDUFB4 RBMS2 IFT80 PSMG2 TP53INP2 C11orf58 NAGA RBM19 SMIM10L1 CBSL AHCY RPL22L1 KCTD5 ECM1 DYM ZNF410 TMEM8A CDR2 PSMC6 ABCC4 ZNF343 SSR3 CC2D1A CHST13 PIM1 GOLGA1 IFIT2 PARP11 ARNTL2 PFN2 CHCHD7 SERINC2 TARS LTBP2 SH3BGRL ARPC5 ADGRL1 ANKRD42 PITPNA PRPF4B STUB1 SLC2A8 DELE1 ILK NBPF20 PEAK1 STK38L CUEDC2 DDX42 PRR14L RNF113A PHETA2 NHP2 CDK6 TEAD2 LIMA1 TSPYL2 VBP1 COL6A2 FBLN1 MRRF HIST1H2BN MARVELD1 ADGRL4 LCK AFF4 RAF1 DLG4 KIF20B FRMD6 HOGA1 SH3KBP1 SELENOW FKBP10 COPS2 GGPS1 VEGFC LARP1 SRBD1 SDC4 INVS PSMB2 WARS NCAPG2 PHOX2A ABCE1 GPATCH4 PPP2CB TWF2 B4GALT6 PRKAR1A LDHA MRPL20 SCD ARMH3 YDJC B4GALT2 C1orf122 SHANK1 PHC2 GPN3 CAPG TRIM26 AK9 ATN1 MPZL1 PEX7 CLVS2 DDX52 KXD1 INTS10 INPP1 DENND4A ANKRD11 CEP83 ASCC2 DUSP1 DDAH2 RAB11FIP3 CYTH2 VPS11 HBD MYO5A REV1 NAP1L4 TGFBR1 RNF187 SLIRP CDC26 GRK2 NPIPA1 PTER ACO1 CRLF1 SNX2 RBX1 PYCR1 MYO18A PRRC2C EDF1 LTN1 ARHGEF18 WDR78 ARRB1 HSPA1A PFKFB3 LIG4 SELENOM TXNL1 RNF168 RNF115 CISD2 TNFAIP8L1 PPIB RND3 ESD PNRC1 ATP5MC2 RRBP1 RBL2 MAT2B PRDX5 CSNK1D ASRGL1 PTX3 ARFGAP2 CDC20 FTSJ3 TAF4 ATG13 LYPLA2 CINP NMT2 C8orf88 ERI2 SLC4A7 STAT6 GNL1 PRPSAP1 RIOK3 SEC22B TTC7A TFRC VARS2 CAMK2N1 NFIC AK2 LHPP SH3TC1 PFDN5 H2AFZ MEIS3 H2AFX MED16 BCL2L13 CCDC30 PLOD3 DYNC1I2 DYNC2H1 DRG1 KDELR3 UROS RPS6KB2 TRAPPC10 KLHL25 ATP5ME TXLNA DYNLRB1 GTF3C2 MT-ND1 MAP4K5 HNRNPH3 ATF4 SPIN1 KCTD9 WDFY1 EMC7 HEG1 ZNF696 SIGMAR1 EHBP1 SNTB2 TXNIP PSMC1 NUDT3 COASY DOT1L SRP9 GABPA ALKBH4 CCDC93 CTGF TFG PTBP1 SSNA1 KRTAP1-1 FBXO44 PCNX1 CCDC8 IVD UFC1 PSMD14 NAA35 FOXK1 H1F0 ETF1 KCNJ14 BCL7C HNRNPC ARHGEF40 ISG15 FXR1 SF1 IDH3A RANBP3 PARP1 SUCLG1 NCKAP1 CLK1 TNFAIP1 GOLGA7 LGALSL PSMA4 ZNF213 DTD1 BLOC1S1 PACRG-AS3 MCTS1 ZC3H13 P3H4 CREB3L2

	ZNF45 RTN4 COL3A1 TK1 PRKCSH ENG MOB3A NAPA NDUFB10 SELENOK SAP30L SMIM4 KCNK2 DNAJC14 GLUD1 HMGN5 R3HCC1L AARS2 EDIL3 NIP7 DFFA CARM1 MYD88 SCYL2 AC100810.1 SESN3 HIST1H3H OSTC ZC3H7B PPP1R12B WDR11 TUBB2A DAB2 ZNF580 RPL36 LRP6 SERPINH1 RBCK1 EZH1 LAYN OCIAD2 MOSPD3 PNRC2 TRAPPC12 RNU5A-1 EXOSC1 CAPZA1 ERP29 GLRX3 ARHGAP18 NFASC PSMG3 PSAP NCS1 COPS5 STX1A PRSS12 TGFB3 ELK1 INHBA SP100 AC004069.1 UGDH NUP188 NTMT1 NOP56 HIVEP2 UBE2R2 CPEB2 SUMO2 LOXL2 SDCBP NPEPPS NUCB2 DENR DDRGK1 XPNPEP1 FPGS EPB41L2 PCGF5 BCL2L2-PABPN1 NUBP1 ADAMTS1 RAP1B SBF2 EIF5 AIFM2 AAMP ZSWIM2 RREB1 PABPC1L AC026271.3 TRIM13 AC080112.1 LIFR CDK2AP1 CBL HSPA9 FAM66E GTPBP4 KCNAB2 GTF2F1 TAF1 GSTK1 CIC FBXW5 PPME1 TRAPPC1 DCAF15 TNPO3 MAP3K2 NBPF10 JMY CLINT1 RAB3B MBNL1 REEP5 TSR2 BRI3 STX12 ZNF844 PLCL1 ABI1 HNRNPDL NECTIN3 MUL1 NUP58 DHX57 SPG21 PSAT1 TUT7 PTPN21 CALU EMC4 TBC1D1 FOS IQGAP1 MRPS5 MYCBP2 SAP18 COX18 ZKSCAN5 XPO1 Z95115.1 LATS1 CAMK2A F8A2 FGF2 PAMR1 ETHE1 MED1 CLU R3HCC1 PABPC4 SASH3 ING4 ABCB10 GLUL LAMTOR1 DIAPH1 ESF1 SPIRE1 AP3M1 ANAPC16 RRM2 COG5 METRNL CD63 C19orf48 BFAR TOP2A UBE2E1 DNAJC2 GADD45GIP1 FEN1 HSPBP1 SF3B1 CALCRL IPO7 RECK BCL2L1 NAV1 CRBN PSMA7 TUBG1 ABCF3 STK4 ADK TMEM164 CYTOR HDAC2 NEXN SMG5 ATP5PB ZNF319 TIMMDC1 TTI2 AC007036.3 ASNS WASHC2A UBAP2L HSP90B1 KRR1 ABCB4 SLF2 PC WDHD1 NIT1 RABEP1 DNTTIP1 CHD4 ELF2 AP3D1 ATP6V1G1 OTUD5 KHSRP DDX54 FBL ALG1L9P KIF15 KRTAP2-3 FAM43A ZNF280B ARMCX6 PTPRA LAS1L HSF1 DR1 NFATC2 UBXN1 RAB5C HOXA9 RIT1 GDI2 WTAP MED9 DKK1 USP48 SURF6 COX5B APOBEC3C BAZ1A CADM1 NSRP1 AC008878.3 CDC16 IL7R SRSF2 XKR8 ANKRD12 RAB12 SDHC ATF6 HIST1H2AH YLPM1 ZC3H11A TXNDC11 AL512791.2 LINC01925 BACH1 DOCK5 PSMD1 DGCR6L STAT2 COPB1 MATN2 PDCD11 FAM162A PEX10 KLC1 UBXN6 AKAP13 CBY1 MEG3 C6orf132 CTNNAL1 GXYLT1 BCCIP TMEM219 OXSR1 CLEC16A DLD RGP1 MCM3AP RAB11A SNX1 NCAPH2 BRPF3 OGA WSB2 RPS7 C6orf106 TBC1D25 JAK1 LY6E ARFGEF1 TRAPPC4 PARP3 CDV3 AUP1 VANGL1 FLOT1 NOLC1 SLC35E3 PPP2R3C AKT1 CDC42BPB CYB561D1 CDC34 PLD3 COL6A3 APOBEC3G NDUFS5 POFUT1 MLNR SNRPD3 AC244100.2 TSR1 WDR18 HIST1H2BM SUDS3 FAM114A1 SCRIB SPCS2 EGLN3 LINC01578 RALGAPA1 YAP1 ITPKC RAD21 EIF2S2 CKAP5 SMIM15 TAPT1 ZNF253 SLC16A8 TIMP2 MARS GTF3C6 MAP7D3 CCDC22 STC2 COL6A1 ANAPC15 FOXD1 TMEM141 YIPF5 NAA25 GSK3A ARID4B GIPC1 GKAP1 ZNF330 PSMB1 YKT6 TXN CBX5 NRAV UBE2V2 COL5A1 BOLA1 ASB7 PAF1 ACTA2 SPATC1L GMPS IFT57 ANKRD1 RIPOR2 ATP6V1D DCTD ZNF37A CTSZ STX16 DLAT FEZ2 VTI1B CDC5L HOXC6 IGIP NDUFA10 RNF13 ARAF FOXO3 LKAAEAR1 PPP1R18 PSME3 NME3 EPS15L1 HIST1H3A PARD3B OLA1 SMG7-AS1 AC005943.1 CSRNP2 MAGED2 RTF2 REXO2 NANOS1 GTF2H3 UAP1 SHKBP1 NAGK ECI1 APBB1IP RFLNB NF2 MZT2A TOMM7 DDX41 CEP57 MTMR3 UBE2D2 PSMB10 PGM3 PAM16 DDX3X NUP62 RASA3 EPB41L5 MPG ZMYM6 UBE2Q1 JPH3 E2F3 HDC PXK GOLGA4 IWS1 ATPAF2 PCGF1 MIR4458HG GORASP1 TDP2 STXBP3 EIF3G SMARCAL1 ARHGAP22 FUNDC1 PRKCA INPP5A CCDC115 SMARCE1 HIPK1 MAD2L2 SUSD1 PITPNB AARS SEMA4C RNF44 ATMIN BOLA2B SMIM29 AC125807.2 ANXA11 VDAC2 PPIAL4G TMA7 AC073508.3 WASF2 GARS AC011511.1 PNPLA2 PFDN2 PLSCR3 SNCB KLHL24 NDUFB9 HCLS1 PMS2 ITPR3 AC061992.1 DNAJC19 ATP5MC3 RAB8A ZNHIT6 SPOCK1 HIST1H2BF MPST
UC RB14, 30 unique genes (885 genes)	CREB3L1 AC133785.1 FARP1 FAM219A KCNMA1 TKT ITPK1 ADCY7 SUMO1 EP300 HIC2 GYS1 ZBTB12 AC004908.1 PAIP1 REEP6 IMP4 SH3BP4 ANAPC4 NDUFS1 SLC38A5 ARRDC2 DIRAS1 PAPOLA MSRB3 COX15 SLC16A14 MET PDLIM2 SPECC1L LYAR TTC37 PIKFYVE EVC MRPL1 LY6K SERPINF1 SHC1 IRX5 UNC45B CDC25B USE1 HCST OR8D4 NASP ZNF623 SDAD1 PPP1R15B VKORC1 INTS6 FOXK2 NECTIN2 SEL1L3 ELOA3C AC009275.1 LTBP4 BCLAF1 DNAJC15 MTRR LRRC8D SMUG1 ALDH18A1 DNAJC5 PF4 RFXAP PIN1 HIST1H2AD POLR1E N4BP2L2 CCAR1 SORT1 RFX3 EIF1AX TMEM120B AC136628.1 SAMSN1 ALCAM RWDD4 PLCL2 SEC14L1 THADA UBXN4 PXDN RHEB C9orf16 PCK2 FUS CXorf56 MMP15 F7 CNOT1 TMEM200A CAPN1 DDHD2 LAGE3 APPBP2 OXTR SDC2 USP19 NOMO1 MEG8 NQO2 QRICH1 HP1BP3 ADAMTS2 SF3A3 MT-ND2 MIR3648-1 HEATR5B FHL1 DHFR RTCB ARID5A SERTAD2 IGSF8 KLF4 PGM2L1 HDAC3 UIMC1 LSM3 NCOA3 ARFRP1 MTHFD1 UBTD1 SEC63 PACSIN3 FBXO46 ITSN1 POC1A DDX39A TIMM17A ANKRD26 TRAM2 HARS LCE2D TLK1 LRRC42 KIF4A RNF7 MAP1LC3B THY1 SVIP DCAF11 KANK3 XAF1 PHGDH ARHGAP25 C19orf47 AL136373.1 GPS1 FDFT1 CBX1 TALDO1 UBE2D3 GLIPR2 NEGR1 SCRT2 GALNT2 TRAPPC5 UBE2J1 C11orf49 DNMT3A SAFB2 SLC16A2 THAP5 CD93 PSIP1 ATXN2 KDM6B ANP32A ZFPL1 ARHGAP12 SURF4 CCNDBP1 SCCPDH BCAS2 NUB1 IRS2 ALG9 ANAPC1 SPATS2L CDKN2B TXNL4A XRCC1 NYAP1 PAK1IP1 PPP6R2 KANK4 SF3B5 UBE2L3 NRXN1 WDR26 TXNDC12 SCART1 ASB1 SAR1A BCL11B SUPT16H ARID1B RPL24 RNA5SP506 MIR3648-2 GSK3B KIF1B PDXP GNA13 ATG3 NDUFV2 RF00019_618 AC104134.1 MAPK1IP1L NNMT PIAS1 SNX29 CA12 ERGIC3 TRIM16 STMN1 GALNT10 CCZ1B TRIM6 SSR4 MRPL22 GPBP1 DAAM2 TDP1 ARMC2 BIN1 PLXNA4 COX6A1 MYO1E DUSP23 ZFX KCNH1 KDM4A AK1 AC004951.1 STK24 VPS26B SDS CHGB ATP6V1F DIAPH3 SP7 CCSER2 RHOD SIKE1 HNRNPH1 HAS3 COX16 C1S BPGM UBASH3B C12orf49 SIRT7 EIF4E RPE U2AF2 FCGRT BATF2 WDR70 CENPE URGCP METTL14 GATA3 CSNK1E ENTPD6 FOXC2 RNASEH2C NDUFB7 PFKFB2 GSTM1 WDR33 HIST2H3A

	UQCR10 KC6 ZNF16 SLC8A2 SH3PXD2B PSD APOPT1 SF3A1 IQCE ZDHHC3 IKBKB LINC01694 CLASP1 BACE1-AS AL355075.4 GPR161 FXYD5 FZD5 HIST1H4D POLDIP2 RAB3GAP2 BTBD1 NOP53 BAZ2B NISCH BBS4 BLCAP TTL ATP6V0C TTC39B FKBP3 SKI ARHGEF4 AC092807.3 UBE2O G6PD FEZ1 CTPS1 EHD4 ZFHX2-AS1 PPP2R2A CPEB4 SCLT1 ABCC5 KIF1BP LACC1 CRIP2 MYDGF HSPE1 SYNE1 GOLGA6L6 PPP1R9B FER LINC00598 WDR27 ROBO3 RAB34 CHMP1A POLE4 MT-ND5 ADAR MPIG6B PLXNB2 PAN3 CELF2 HIST1H2BK SUCLG2-AS1 SBK1 TENT2 SLC25A36 INTS2 PPP2CA KIF13A SNF8 NADK CBWD2 LINC01413 CRIP1 LCP2 FBXL16 GLI2 ALDH1A3 ZFAND5 NAV3 RNH1 CBX3 MAP4K2 YARS ZNF782 MCUR1 ZNF768 PLPP1 RPS6KA1 ICE2 KDM1B PAK4 CTNND1 MRPS21 FKBP1C PPP1R11 RF00019 676 CFLAR PIK3R1 CIAPIN1 CSTB ZNF668 TCF20 MLKL ANKRD33B CNIH1 FNDC3B NUDT4 ERI3 NFKB1 FOSB MRPL51 LINC01341 NDUFB2 MFAP1 KDM2B UBFD1 RNF181 DMWD NHSL2 ZNF689 KDELR2 TLE4 ALAS2 RPN2 DHRS1 RNF114 CLBA1 RAD54L2 ZNF207 TSPAN4 SFT2D2 PSMA6 SCMH1 LTK SFXN4 ALKBH6 JDP2 ELK3 ZBTB25 MTX2 BRD3 INO80 AC007906.2 ZFAND2B MAP2K3 SESTD1 ESR2 LACTB CSNK2A1 CALCOCO1 HACD2 DEPP1 SRRM2 AAK1 MSANTD4 RMND1 AANAT ATP5IF1 TP53RK MYBBP1A SF3B3 LRRC75A-AS1 XPO7 ARHGAP11B HIST2H2BE COMT CHST3 BRWD1 RBMS1 APC2 CPSF2 ZNF304 RNASEH1 BLOC1S4 SLC30A9 ACTR3 CCDC25 FIBP IL12RB1 RGMB SOS1 MRPL4 MDFIC CHMP4A NFE2 DBET ATP6V0D1 APOBEC3D MALT1 MSC HLTF SMARCC2 ZBTB34 AC090340.1 GNAI3 IRF1 PTK2B EXOC5 IRF2BP2 DNAJB1 L3MBTL2 PLEK RC3H1 RAB8B MED29 DDOST FGF12-AS2 CHSY1 SLC39A7 FAM129A SFPQ ILF2 CLN8 DIP2C MAP3K5 FUBP3 CRLS1 CCL4L2 SNORD3A NFATC1 UAP1L1 SCOC CMIP UCHL1 PLK1 DAP3 FAM192A EVI5L THAP11 MDH1 PRKAR2A BTG1 YTHDF3 DPH3 RPL7L1 ZNF148 CNOT4 ZBTB38 TBC1D5 BRMS1 SLC25A1 SLC25A5 AL358781.1 ARNT REEP3 PI4KA BTRC STEAP3 MGAT1 DYNLT1 PHC3 WDR43 PPP1R8 GOLPH3 ARF4 SH3GLB1 URI1 MYEF2 NEFM MAGI3 SNORA63 USP10 BCAP31 FKBP14 TMCC2 KRAS LSG1 HIRA VPS36 ISL2 DMPK CYP4F8 NEAT1 DCTN3 ZWILCH LPXN TRIM65 BCL9L TAPBP AL031777.3 MT-CYB PPTC7 HDAC9 LINC00963 FOXJ2 DLG3 TADA3 PLAGL1 ZBTB43 FNDC11 ZSCAN10 MTOR MCM3 NDUFS2 UBR5 NRBP1 FBXW4 TENM1 RASA4 MORF4L2 PRKAB2 SGSM1 AKIP1 ZBTB45 CPSF3 TCP11L1 DCDC2B MAP2K2 CDC42BPG SMIM7 UNK CSNK1G2 CYC1 PHF19 SGTB CD2AP MYH10 CTBP1 ALDH1B1 POMK USP25 ZNF124 CCSAP ADO CTRB2 SIPA1L1 GBP2 ZNF217 MIDN VTN LRPPRC CRIM1 DNAJC25-GNG10 GTF2H4 PARP2 SLC12A9 MINDY3 ZNF134 CCNYL1 KIAA2026 PCGF2 SRGN EIF3F VDAC3 CSE1L LENG8 SNHG7 UTP14A RRP1B THOP1 GLI3 PTPA GREM1 GABRR3 BCOR ZNF444 FBN1 WASF3 LONP2 SPCS1 CCNC KPNA5 TNFRSF12A MARCH9 POPDC2 FAM149B1 HIST1H4K RAP2B PBX3 PSME4 ELOVL4 ZMAT3 RF00003_5 ATP5PF KANSL1L GAR1 MTX3 AL157944.1 ISY1 GZF1 WDR47 C2CD5 INTS11 ASB16-AS1 PGM2 RGS2 FOXP4 PHRF1 GFM2 ARHGAP31 GIT1 TUBA4A MSL2 CHCHD3 ODF2 SLC11A2 H2AFJ NUP98 AL139349.1 LATS2 NOCT PTPN1 PML LINC02531 TTLL12 AFF2 SIK1B AL627309.5 PLCG2 DDIT4 PGRMC1 DNAJA2 EIF1B OR2A12 CDO1 DCDC2C MYO1A AC009779.2 SRXN1 MYRF BPTF DNMT1 KCNJ4 WIPF2 FAM136A SUV39H1 PCF11 MED17 NFIB NLN AC010198.2 SNHG5 FNBP4 TOX4 SEMA6C DAB2IP ARRDC3 AL118508.1 SLC1A4 AC009041.2 PLAG1 ZNF226 HSPA5 APH1A JUNB WIPI1 RWDD1 NPEPL1 TP53INP1 KCNN1 CKAP2 PDZD8 HK2 COMMD10 COPS8 SLC30A10 EHD3 ERO1A SOX8 EFEMP2 AC022098.1 FANCI MAPK3 JARID2 PLBD1 SLC16A3 APLP2 RETREG3 CELSR1 CORIN CA2 RANBP17 PRSS23 ANK1 ETS1 SPATA20 ANKRD29 PRPF18 LINC00926 MOB1A USB1 FAH PAPSS1 GRN SMIM14 OGFR JPT2 AP3S1 STOML2 FTSJ1 ALPI ADSL ANAPC5 FLAD1 HIF1AN ETAA1 EIF4E3 AKT1S1 MTMR2 PHF14 ERCC6 NEDD8 NAA30 PRDX2 TEX26-AS1 TRIM10 MAP9 RNF214 ACVR2B TCF3 UBQLN1 AC104964.1 PPP2R5D AKAP5 GGNBP2 BRWD3 LINC01133 DNAJB5 ARHGEF6 LLPH TGFBR2 OAF RNF121 SLC9A3-AS1 SLC38A1 BX088651.4 MMD MYO1F DENND4C MORC4 MT-CO2 SETD7 GALNT11 NDUFA3 LAPTM5 SDR42E2 QSOX1 KRT10 CUX1 YBX3 ANKRD27 EIF3K SNRPB DLGAP2 ENC1 HIVEP3 PTP4A1 CALHM6 PSMC3 ZNF613 CERS2 COL10A1 HIST2H2BF BLOC1S6 NBPF9 GMDS FKBP9 TBCD ZNF250 PEG10 SLC25A38 AC021078.1 UHRF1 HGSNAT GATAD2B CASP2 ANXA4 MLPH ATIC AL671762.1 STRN ESPN TXNDC17 GABARAPL2 ATP1B3 AP4E1 HNRNPL DHX36 SMG9 APOL3 NDFIP1 ATP6V0E1 WHRN GCNT1 IDH3B GGA2 TTC1 AHSP SRF STK17B VRK1 RASSF1 ARHGAP27 TRIM8 SAR1B PEPD APP LANCL1 CDK10 DNAJC13 CCDC9 GNL2 NDN PUM1 BIRC3 PCIF1
TFF RB61, 97/ UC RB14,30 shared genes (1596 genes)	FSTL1 RPS11 KRTCAP2 CD44 RPS17 MMP2 SAMD4A PFKP DECR1 SLC25A3 IRAK1 RPS18 TMSB10 SUMO1 RPL19 CCNI ZEB1 DIRAS1 KCNK6 THRAP3 INIP MAX OSBPL8 TNS3 IPO9 TEAD1 RPL7A UBA1 ITGA3 RABGGTA NOL8 BAZ1B ROCK2 COL1A1 VGLL3 ACBD3 RBM10 FAM98A EXOC3 RAD23B NCOR2 HIST1H1E CORO2A DSTN FBXO11 RNF4 GMPR TPM3 EPB42 DUS3L HSPD1 EIF1 BX890604.2 RPS28 TUBB GCLM PPM1A PTP4A2 PLCL2 PXDN COX8A XRN2 FUS PSMD11 ALAD TMEM59 CNOT1 SNX6 SPTBN1 CDC42EP3 MFN2 BTF3 USP32 QKI GNG12 HIST1H2BJ AGPS GSTP1 FKBP4 ZNF350 SF3A3 AHNAK FHL1 RSU1 RPL4 ACO2 RPS21 PSMF1 SH3PXD2A LMO4 KRCC1 MOB1B PARG GOT2 POLD2 CCT4 BRD4 RNA5-8SN1 VMP1 MANF UBTD1 CASC4 PDGFRB RDX DCTN1 C1QBP TTC3 NDUFB8 DLST TCP1 TRAM2 SCRN1 RPN1 TAB2 EIF3D TANC2 PGM1 SET SERP1 RFNG AKAP2 ACADVL PHGDH RPS29 RMRP 2 B2M IMPAD1 PPFIBP1 EIF5A NEGR1 PLRG1 EHD2 FIS1 HNRNPK KDELR1 FAM129B OXA1L ACLY SMS TAF1D STRN3 PEF1 PPDPF CSNK2A2 RPL39 ZBTB47 HRAS AP2S1 MME VAT1 TUFM MYC

	WDR26 MAPK8IP2 ARHGAP10 RUVBL2 RPLP2 RPL27 EPN1 VCP BGN EIF3H RALB MAPK1IP1L SFXN3 ZSWIM4 CRTAP TRIM16 STMN1 STK39 CCZ1B SMURF2 BANF1 RPS6KA2 PABPN1 FBRS SEPT7 ARMCX3 YBX1 ANXA2 STK24 VPS26B DGCR8 GSR PLBD2 EIF2AK2 LMO7 HNRNPH1 NUTF2 SIAH2 RMND5A HEATR5A KMT2D MRAS CSNK1E SRP14 FMR1 DUSP3 C7orf50 ZDHHC7 ZPR1 RAD23A MT1E CTNNA1 GPR20 CBX4 GHITM FOXN3 MFGE8 HIST2H3A GOLGB1 ETV3 PDLIM1 RNF126 RPS10 CLIC4 CAPNS1 SDF4 NDRG1 GBE1 TNPO1 EEF1D SOD1 CAPN2 ZFP36L1 FXYD5 CHD2 PCNP PURA RPL15 TRAPPC11 TRAK2 RPS3A ZSWIM9 LPIN2 ABCF1 FCF1 APOOL SEPT2 MRPL14 ZDHHC20 PFDN1 TTL ATP6V0C PRPF8 FKBP3 SKI RPL28 RPL18A TBL1XR1 UBE2O G6PD UBL5 RTCA RPL3 THBS1 TAL1 ARMCX1 NCOR1 TXNRD1 UBE2H CRIP2 C16orf72 USP33 NRDC PPP1CB ERBIN CCT3 RAD50 NCL TSPYL1 SSR2 GDF11 FBXL17 RPL9 TARDBP SLC24A1 ADAR METAP2 RHOQ TNIP1 MAP3K4 HBB GNG11 MTPN INTS13 CDC37 MT-CO1 ATP5F1C SRPX PPP2CA DDX17 PDE4DIP RAP2A AZIN1 VCAN SYDE1 UBE2A PPP6R3 RNH1 ALKBH5 ARL6IP4 RPL35A CHP1 KBTBD2 ACP1 PDIA6 MYL9 EHD1 MARCKSL1 CDKN1A RNF10 NONO RN7SL5P FAT1 CENPB NREP PIK3R1 RNU1-1 ZMIZ2 CSTB DMD CENPI KLHL5 SRM SNX8 HADHA CHURC1 SOD2_1 DLG5 RNU2-2P FNDC3B VMA21 AREL1 MRPL51 ARHGAP35 NEK9 MAPKBP1 TOMM40 GNB1 RPL23A SEPT11 UBE2V1 MBOAT7 CALD1 SNRPB2 NSMAF EIF3E SKIL ADSS RPL31 KDELR2 WRNIP1 ALAS2 IGFBP3 DEK SORBS3 EFR3A OST4 VAMP7 ACTN1 HLA-C NBPF14 ELOB NCOA7 KCTD3 RNA5-8SN2 DOCK7 TPR MAGED1 BCYRN1 MYO1D FP671120.4 SAMD4B FAM13B HNRNPU CHCHD2 FLII RPS16 AP2A2 PEBP1 AOX1 RPL14 COL1A2 CYR61 AKT3 KTN1 CTTN HSBP1 PHKB CCT6A USP8 TMEM147 LRRC75A-AS1 XPO7 TRIM5 COL12A1 MEDAG HNRNPUL2-BSCL2 CPSF2 HDLBP HMGB1 RCN3 MAP4 ACTR3 LPP QARS RPL10A HSPB6 EIF6 MACF1 SEC24D POLR2L ADD3 MTA2 SLTM TRIO NID1 RECQL SMARCC1 DSP NDST1 IRF1 TPD52L2 IRF2BP2 MSN SERINC3 DERA TPP2 ECPAS LAPTM4A SFPQ NGRN URB1 DIP2C NFATC4 PDLIM7 TIMP3 MXRA8 ABHD4 ARHGEF12 RPS23 RALY PLP2 TAGLN2 CACNB3 MDH1 PRKAR2A YTHDF3 SKP1 KATNAL1 RAPH1 CTIF SLC25A5 MYO1C PI4KA RPL12 CRYAB COPA PARVA SLC40A1 GOLPH3 CCT2 SH3GLB1 XRCC6 SUPT5H NEFM BCL9 SND1 CHD3 DYNC1LI2 GDI1 PTGES3 N4BP2 CS LINC01116 TMCC2 BCL2L2 ARMC8 SMC1A TRIM65 TP53INP2 MYO10 RPS13 RUNX1 PRKAA1 ENAH ATP2C1 EGR1 ZFP36L2 FAM171A1 SSR3 CC2D1A FTL KLF6 ARNTL2 HUWE1 LTBP2 SRP68 ARPC5 ZDHHC4 KDM1A ILK LEF1 PEAK1 MAPK14 DYNLL2 TRPV2 ANXA6 RNY1 EIF2S3 MORC3 COL6A2 GSN FRMD6 ARPP19 MAP2K2 VIM SUMO3 RRAGA LDHA SLC38A2 ATN1 ANKRD11 CAP1 PKP4 SEPT9 GOLGA6L2 TMEM214 SIPA1L1 RNF187 MRC2 MTCH1 HK1 GRK2 CDC42 UACA SNX2 GRHPR TSNAX PRRC2C KLF12 DCAF7 MINDY3 TNS1 RBL2 ALDH7A1 EIF3F TOM1 CDC20 TMED2 SLC4A7 RN7SL3 PRPSAP1 DNAJB6 NFIC GREM1 PELI1 H2AFZ BUB1 MT-ND1 ATL3 LASP1 ARHGAP23 MCL1 EHBP1 TXNIP RPL36AL PTBP1 KIF3B SEC31A RF00003_5 H1F0 MVP HNRNPC LYPD1 SF1 RAB11B ISY1 KCTD20 PKN2 AGO1 PSMA2 RTN4 PTMA RPL26 UHRF1BP1 TUBA4A EPPK1 EEF2 LMAN2 DEDD IFITM3 SLU7 RCCD1 NT5C3A EZH1 UBE2S CD59 MRPL3 POMP KLF7 NME2 COX6B1 FRMD8 LGMN HIVEP2 PYGL SNRPA1 ID4 ZNF354B NFIX EIF5 HNRNPF NQO1 TFDP1 RPL5 TOX4 HSPA9 GTF2F1 RPS15A TAF1 PPME1 UTP3 TSR2 DAB2IP MBNL1 TPGS2 PSAT1 TBC1D1 IQGAP1 XPO1 TUBB6 CCDC80 ZNF777 FADS3 RPS12 PABPC4 DDX6 DIAPH1 ZDHHC5 CD63 HNRNPAB TOP2A EHD3 SF3B1 IPO7 CAV1 NAV1 PSMA7 RETREG3 HMGCL PLEC SMG5 SLC25A6 ASNS WASHC2A RPL18 USB1 RABEP1 CHD4 HIF1A DBN1 RPS19 LRRC59 KHSRP FBL IBTK EIF3L KMT2A GDI2 MLF2 RAB13 ERF S100A10 RPL13 ZFAND3 SIRT3 OTUD7B ACTB RF00002_5 UBQLN1 DOCK5 NOL9 SRSF9 UBXN6 MARK4 WWTR1 TNFAIP2 RPL41 DRAP1 SLC38A1 RGP1 NIT2 RNVU1-18 ATP5F1B OGA WSB2 JAK1 SETD7 ZNF800 ZFR CANX HIPK2 ZMIZ1 DESI2 DAP TIMM13 EIF4A2 COL6A3 PABPC1 USP22 PLEKHA4 TSR1 WDR18 SUDS3 NES CUX1 MALAT1 EIF2S2 MAP2K1 ZBTB44 TIMP2 ST13 PTP4A1 MARS SREK1 PPIE VOPP1 SAE1 COL6A1 OAZ1 COX4I1 YIPF5 RLIM HDGF RNF19A SPARC DDR2 WWP2 COL5A1 TNFSF9 MAP4K4 PLEKHM2 LMNA KPNB1 SRSF5 PPP1R18 CTHRC1 WNK1 OLA1 LPAR1 MEX3C MAGED2 KPNA6 SSBP1 SERBP1 SHKBP1 RFLNB NF2 RNU1-3 FBXO32 CRKL ANP32B HNRNPL GOLGA4 ECD TMED4 C17orf51 AARS RN7SL2 USP1 SAR1B DPYSL3 GPC1 PAK2 CENPF EEF1G GARS GNL2 HIST2H3C UBC FBLN5 HBA2 RANGAP1 PUM1 NDUFB9 CNOT6L SPOCK1 H2AFY ACTN4 RAB2A CEP250 PINK1 GRAP2 APOL2 CNBP TKT HSPB1 COX7A2L SNHG16 ADAM12 G3BP1 RNU4-2 GAS5 TLN1 KIRREL1 SH3BP4 UBB RPPH1 AES PAPOLA TTC37 HIST1H4E ARF6 ANP32E PCOLCE HMGN1 FADS1 EPS8 DARS SHC1 ARHGAP21 PAPSS2 CAND1 UTRN PALLD RPL35 IMPDH2 CLTA MAP3K20 PDIA3 OGDH ANLN RHOC ELOA3C GNAS TSPAN13 DUX4 BCLAF1 GOLGA3 MYL12A ALDH18A1 TPI1 PF4 IP6K1 SLC38A10 PTK2 YWHAQ YME1L1 RPLP1 SCP2 SON MAFK TRAM1 UBXN4 NPM1 TSR3 CELF1 NIPBL CCT8 EIF3M MICU1 LDHB PTMS TRIP12 DLGAP4 TMEM87B H3F3B ENDOG EZR ATF1 DYNC1H1 RPL32 MFAP5 DHX16 ATP5PD NBR1 CD99 TTLL11 HSPA8 PICALM ITPRIPL2 ADAMTS2 TCF4 MGST1 AP3B1 AHCYL1 FN1 PPP1R12A DDX24 ATP1A1 NEK6 YWHAZ PRRX1 OPA1 RPL10 C6orf62 SH3D19 IFI16 SSRP1 SPCS3 MTHFD1 CHAF1A TPT1 SEC63 FTH1 BCKDK CSRP1 CTSB ZFP36 PXN RILPL1 DDX39A GANAB DNAJC11 HNRNPA0 C1orf198 PGAM1 SEC13 LRRC42 GTF3C5 ITGB1 PARK7 COL5A2 MAP1LC3B THY1 SPAG9 ANTXR1 CRCP CORO1C PLIN3 IL13RA1 SPDL1 CBX1 UBE2D3 MAP1A CTNNB1 ANKRD17 CCNK CNOT7 ORMDL1 CCND1 PSIP1 PDCD6IP PSMD2 AP2B1 RRAS NET1 IPO5 UBE2Q2 IK SURF4 NACA CDK4 CHMP3

	PRMT1 PLCXD3 SRRT RBM3 RPL17 ZKSCAN1 RCN1 SF3B2 HIPK3 XPOT TGFB1 AD000090.1 CEP68 UBE2L3 SAR1A PLS3 SLC9A3R2 TIMP1 PLOD2 RPS24 RPL24 ZFAND6 YES1 HIST1H2BE CALM2 NUDT16 CLIC1 NNMT STAT1 COL8A1 MRFAP1 MT-RNR1 SSR4 ARHGEF5 BBX BIN1 PPP1CA NAP1L1 FKBP8 CCT7 MYO1E AC004951.1 IQGAP3 COPB2 BUB3 CDC27 COPS6 CNN2 ZNF664 HEBP1 TTC19 GFPT1 HMOX1 KPNA4 H3F3A TRPM7 TMED3 RPLP0 HNRNPD EXT1 U2AF2 MKNK2 SEC16A YWHAG IGF2BP2 EIF5B MT-RNR2 MYL12B ASL PUM2 CMSS1 SRSF7 RIPOR1 AL139099.4 HMGN2 MAPK1 HNRNPA2B1 PYGB TRIM34 POSTN EID1 DCAF6 EIF3A SPTY2D1 SPOP FP236383.2 PIP4K2A ARHGAP1 MYLK FSCN1 AL355075.4 TMEM203 POLR2F MCM7 RNU1-2 POLDIP2 NDUFV1 CCPG1 SORCS3 CFL1 NOP53 CPSF6 GBP1 RPL34 BOD1L1 AKAP12 BLCAP SLAIN2 IARS DYNLL1 PHACTR2 CTPS1 EHD4 EMP3 SYNCRIP DNAJC8 MED13 TUBA1C TMBIM6 NFE2L1 NT5DC2 SART1 RNY4 HSP90AB1 HSPE1 TBX18 RHOT2 RALGPS2 GSPT1 DPP9 ARPC1B COPS3 KCMF1 RNU1-28P ELOA3 YTHDF2 TRIM28 HTATSF1 NDUFA7 GPX8 CYB5R3 MAPRE2 KRT7 PPRC1 CDK11B RC3H2 NACC1 SEC62 ENO1 TAF3 DDX1 AKAP8L UBE2Z MKI67 GLS KANK2 ZFAND5 Z84488.2 OTUB1 SH3BGRL3 PSMC5 VASP BAG5 LAMB2 MED24 GTF2I BRD2 TPM2 CPNE1 RPL37A CPS1 NCOA2 USP5 BNIP3L PITRM1 TRAK1 ADM LSM2 SERF2 EIF4H IMPDH1 RPL11 ETFB TUBB4B RPL8 XRCC5 SNX12 LMF2 PCBP2 HAX1 NUP205 UBFD1 ELP2 RBM15B TGFB1I1 SNRNP200 C11orf96 RPS25 DNM1L RAD54L2 TRAPPC3 TAF15 R3HDM1 CLTB MKRN1 GAPDH ERRFI1 RSL1D1 GNA12 RBM25 ARCN1 CDC42EP1 SEC24A POLR2E RTL6 LDOC1 TRAFD1 MGRN1 ACTG1 CALM1 RPS9 SRRM2 HNRNPA1 GPS2 RALBP1 SF3B3 CAPZB ERC1 SATB1 COMT SYAP1 CKAP4 FAM50A PGK1 RNASEH1 MLXIP ANKS1A CLPB DONSON SLC30A9 CCDC25 NBAS YIF1B MYO1B WASL RGMB ARHGAP11A LINC01184 JPT1 RAC1 DBET MAST2 ANXA1 RASSF3 UTP4 MID1IP1 RNA5-8SN3 DPYSL2 C22orf46 EIF3B RPL36A DNAJB1 CHID1 GNAI2 METTL8 PRDX6 FAM129A FARSB BASP1 TCAF1 RPL29 HPS6 PTPN11 ZC3H7A PHF3 BTG1 LPGAT1 NDUFC2-KCTD14 MAPKAP1 CYFIP1 LGALS1 WDR1 YWHAE LSM14A REST GMCL1 WDR43 COPG1 GNG5 KIF5B USP24 NUP153 CPLX1 CSDE1 MYH9 CAMK2D RPS4X RPS27A RPS3 RAI14 TSC22D3 ARHGEF2 RCOR3 ARF1 FLNC KRAS SPTAN1 CAVIN1 HSPA4 RHOA SLC1A5 VPS41 C12orf10 MYL6 RPSA SMC4 ZNF771 SMIM10L1 MT-CYB CBSL FAM208B ECM1 C1orf21 RPS8 TUBA1B RF00003_9 PPP3CC PIM1 IFIT2 EMP1 PFN2 PPP1CC SERINC2 TARS MTOR RPS2 FBXW4 BNIP3 MTHFD2 AP2M1 CDK6 LIMA1 MORF4L2 RPL7 MYOF AFF4 PRPF6 ZNF281 CD248 ZYX SH3KBP1 SMOX SMAD7 CALR WARS BZW1 PCNA GPATCH4 ZRANB1 PRELID3B CYC1 EPRS SGTB C1orf122 RPS26 CTBP1 DNAJA1 ZSWIM8 BABAM1 HBD FAM168B NAP1L4 MIDN SZRD1 TPM1 CRIM1 ACO1 FLNB NOC2L SLC4A2 ATP5F1A SPECC1 GBA STRAP PNRC1 PRDX5 PPIA TRIB1 ERLEC1 TXNDC5 JCAD SEC22B GID8 S100A6 AK2 PFDN5 ILF3 FBN1 DYNC1I2 CSNK1A1 ADRM1 UBAP1 ALDOA GAB2 CEP89 VPS13D HNRNPH3 ABHD17C ATF4 HEG1 KPNA1 RNA5S9 FAM149B1 S100A11 MAZ CLTC SRP9 RPRD2 TFG ANXA5 ZMAT3 KARS RAN EEF1A1 KDM3B FOXK1 ETF1 EIF4G1 UBE4A ADGRA2 LINC00632 HSP90AA1 BAG6 RPS15 SEC23A PSMA4 ROCK1 RN7SK TAGLN ZC3H13 ARPC2 PRKCSH ENG TAX1BP1 ARHGAP31 VEZF1 GLUD1 APIP PHIP ODF2 EPB41 DENND5A NUP98 RNF220 CARM1 COTL1 PML ZC3H7B DAB2 RPL36 MARCKS TTLL12 SERPINH1 RBCK1 RACK1 MGLL MLLT1 BACE1 TPM4 OPTN PRSS12 ACAD9 ZFP91 INHBA S100A4 RPS20 LOXL2 NPEPPS DENR RPL21 DNMT1 RAP1B AAMP CAPRIN1 PEA15 SNHG5 EIF4A1 CLINT1 RAB3B SYMPK ZNF322 SPG21 CALU SAP18 JUNB RHOB GNPNAT1 PPP2R1A HNRNPM SRSF1 RPA1 GLUL NOTCH2NLA IGF2_1 MICAL2 ERO1A RN7SL1 BCL2L1 MAPK3 JARID2 USP34 SLC16A3 APLP2 CA2 RNU1-4 UBAP2L HSP90B1 SLF2 NOL6 CD81 EIF3C TRIM44 KIF1C AP3D1 RPL27A RNU1-27P AP3S1 SNX3 GOLIM4 DST DR1 CAB39 ZEB2 WTAP NECAB3 NSA2 PRRC2A STK35 AAGAB RRM1 NEDD8 NSRP1 RNF214 KLHDC10 CALM3 ACIN1 RPL23 YLPM1 VCL SERPINE1 EIF2AK1 MAP1B AL928654.3 LINC01133 SEPT8 RN7SL4P RNF40 EWSR1 ZMYND11 LRRFIP2 AKAP13 OAF RPL13A DLD PPFIA1 PKM RPS7 ARHGDIA AUP1 GSTO1 HNRNPA3 IARS2 RGS10 CCND2 CUL4A CDC42BPB NPTN SCAMP2 NDUFS5 SNRPD3 SERINC1 CCT5 KIF20A YAP1 YBX3 PSMD7 RAD21 PFN1 CLIP1 SF3B4 ABLIM3 PSMC3 SMARCA2 P4HB RBM27 COL10A1 WDR55 CERCAM SUPT6H TXN TRPC4AP LGALS8 EIF4G2 IGFBP4 SYNPO SNRNP40 NORAD PSME3 HIST1H3A NMD3 BCAT1 TMSB4X HMGA1 REXO2 RANBP2 RPS14 TGFBI RNVU1-7 SCAF11 FLNA RPL37 FKBP1A ANO6 GGA2 TTC1 HIPK1 MAT2A PGPEP1 TRIM8 KAT6B S100A13 ANXA11 VDAC2 DACT1 RN7SL471P JOSD2 XPO5 RPS6KB1 HBA1 RPS27
TFF RB61, 97 unique genes (2963 genes)	CLMP CREB3L1 DPY30 ZHX3 ATF6B APBB2 GCSH ECHS1 LRRC41 PDCL3 KCNG1 ZNF646 SLC35G3 ESYT1 CXCL3 RAB1B UQCR11 DDB1 SCAF8 EP300 RDH10 HS3ST3A1 HIST1H4J AL135960.1 ZBTB12 C2orf49 DDX5 REEP6 KBTBD8 CCNB1 ANAPC4 TMX4 MIER1 CCDC97 MSRB3 COX15 AGPAT1 TOB2 PDLIM2 COPS7A NR4A2 LONP1 PPCS C4orf3 SRPK1 MED13L ZFYVE1 DUS2 FIBCD1 NAT10 CHD1 LINC02601 C15orf41 DMC1 SERPINF1 C20orf27 ATXN10 ACTR8 CCDC34 STK25 PTPN22 CDC25B AC104109.3 AC034102.2 STX8 LUZP1 SLK EIF4G3 ATP5MG A2M TRIQK LMNB2 AC008403.1 BBS12 TERF2IP GTPBP1 DGUOK PRDM2 SEL1L3 PDCD4 SUPT4H1 CEP350 WDR45 C16orf45 GFPT2 MFF SLFN12 CNGA3 CTDSP2 FOXM1 BUD31 UFM1 PABPC5 GYPC FRS2 F8A1 ALG2 GRB2 CCAR1 POLR2B KLHL36 GPN2 COQ9 ADH5 DESI1 CDIPT PLXNA1 KIAA0100 HS2ST1 CHMP1B CBLL1 EIF1AX INTS1 ARL13B CAMTA1 MYO15B SAMSN1 GMPPA SNX19 SEC14L1 NAALADL1 C12orf75 TAF12 ID1 TBC1D17 ATP11C TIMM22 SF3B6 VIM-AS1 C9orf16 COG1 DNAL4 ELAC2 CDC42BPA SEC23IP UQCRC1 ZBTB11 CEP120

	RICTOR LUC7L2 LSM4 HSF2 SAMM50 MRPL34 SRP72 POMT1 NUCB1 LRRC8A ARL16 BRK1 TLCD2 CAPN1 NME1-NME2 SNX25 ZBED1 AL445685.3 SDC2 COX7A2 SARS KDM6A OFD1 PRDX4 PDP1 FERMT3 ABHD12 PEX16 HABP4 VPS25 ASNSD1 GLG1 FANCC L2HGDH CMTM3 TMEM11 RPUSD3 NEU1 SPACA6 UBE2L6 MED14 WASHC5 CENPX TSN DCUN1D5 LTBR GMFB GNB4 ALDH1L2 DOCK11 NOP58 WASHC3 OVCA2 HCFC1 NADSYN1 GATA1 TRMT6 PSMD5 AHR CHMP2B CAMSAP1 IRX3 RTCB COQ10B UBE2N IGSF8 NRF1 KLF4 HUS1 CHRM4 GPBP1L1 NFYC CEP131 EXOC1 AHRR PDAP1 NDUFA13 ZNF146 CD151 MRPL41 NENF CUL4B TNRC18 FAU TMEM271 JUND PHB2 EHBP1L1 TNKS2 MRTO4 TMEM248 R3HDM2 WNT6 SLC2A10 CENPL TLK1 MTMR12 ESPNL ZNF384 RER1 PROSER2 SIX2 KIAA0930 HPS1 KIF4A RNF7 TFE3 ZMYM5 HLA-DOA IRF7 FAM193A TMEM189 AP003419.1 FAM120A EIF2S1 RBM7 DPYSL4 TM9SF4 NKX2-8 TAF9 RAB5A TNFRSF1A DCAF11 GTF2H5 RAB15 HAUS4 GPS1 BDP1 MKLN1 NAA60 SDHD TALDO1 SQLE GLIPR2 TCF19 CBS ATP5PO NPIPB5 UBE2J1 ELF1 CLIP2 NT5E NCSTN UTS2R PARP4 ICE1 AC098818.2 NCK2 SLC16A2 NOTCH2 SULF2 ADD1 KDM6B PSMD12 HSCB ANP32A DNAJC1 MEX3D ERCC8 MAPK7 VIRMA RRAGC NFAT5 GPX4 RTL8C CCDC85B CMKLR1 FAM199X MCM5 ZFAS1 TMEM106C RABGGTB PODXL CALCOCO2 SPATS2L KMT2B RABAC1 CDK16 FBXL5 BSDC1 RABL6 ZNF536 ITGB2 UQCRQ STX5 PHPT1 TMEM263 EPB41L3 AC011228.1 KAT5 MAP3K6 ERH AC138811.2 SOCS4 SDR39U1 XRCC1 PARVB CSRNP1 APOL1 SETBP1 NDC80 ZBTB41 SCARNA16 AHCTF1 AC009486.1 SENP3 EEF2K SF3B5 CEP72 KCTD2 KRT34 NR4A3 DNAAF5 SUPT16H TOMM22 POP4 MRPS18C SPNS1 MFSD14B SRSF3 SH3GL1 MBD2 AMOTL2 ABHD14B TNFAIP3 C6orf120 MRPL37 CRLF3 TRIP10 NPHP3 FBXO7 NCOA6 PPP4R1 CNOT2 MAN1A2 SEC61A1 FKTN SNW1 RPP30 BLVRB GALNT10 SETD3 PQLC3 PRRX2 ELK4 LINC02193 CD109 ZNF846 TP53I3 SLC25A24 ACER3 PES1 UCP2 DAAM2 DNAJB11 NDUFB3 AC007787.1 FMNL1 KIF23 MAGEF1 ARHGDIB URB2 PHAX AK1 FH SYNPO2L ARMT1 ABCD3 PAQR7 CACNA1C FAM20B ATP6V1F CCSER2 INTS7 ZNF775 UCKL1 IDO1 THAP4 OGFRL1 PPP1R15A CITED2 C12orf49 METTL18 PYCR3 FNDC4 ATP11B FBXO34 PCDH12 EIF4E RPE ABHD5 EXOC4 TRMT1 LRRC32 ZFAND1 TRAF6 AXL MAF1 NRN1 SPAG5 CD276 F13A1 XPO6 CHMP2A UBN1 SDSL SLC31A1 MYO9A BLMH TXLNG WDR33 CEP290 RNF167 PRMT5 TSKU TLE3 AL121900.2 PSMB7 LRP1 API5 BIRC6 SAMHD1 SH3PXD2B EPC2 NELFA TRIM4 DYNC1LI1 NETO1 TAP2 C19orf70 EFHD2 AKT2 CYB5B APPL2 SNX5 METTL6 MAPKAPK3 AC114730.1 AFAP1 PACS1 SIRT5 DZIP1 SEC22C SNX32 HIST1H2AJ FZD5 NR4A1 NUDT8 TRIM17 PRC1 CREB1 NAA38 RMDN1 MXRA7 LGALS3 CFL2 STAG1 IQCJ-SCHIP1 DBI UFD1 SMARCA4 ZNF624 RNF152 TGFBRAP1 AGL HS6ST1 CLPTM1L TIMM23 RTRAF SHISA4 ELAC1 GLIS3 TCERG1 ATXN7L3 NUDC TMEM126A FBLN2 SCARA3 EIF3J CPEB4 CAMSAP2 HCFC2 ABL1 MOCOS CCDC9B TBX3 MPLKIP LRRCC1 ARF5 ZNF121 MTHFD1L HIST1H2AC KHDC4 AP005205.2 NCOA1 GUF1 CRELD1 NUDT16L1 RNPEP GCN1 MCM2 RBMX2 MCM4 SYF2 DCAF13 HTRA1 TOMM70 RNF111 ATP2B4 KANSL3 RAB22A AL807761.4 STAU1 ARHGAP5 CHMP1A DDX21 DHX29 PWP1 BAHD1 MPIG6B RN7SL687P TM9SF2 TOX2 RHOG NSFL1C MTA1 ZBED4 ITGAX AC093151.3 RUNX2 ZER1 POLR2A ODC1 TMEM218 ZNF730 SYNJ2BP HIP1R ZNF236-DT EMC6 GALT ZMYM4 FECH NPIPB4 IL10RA SLC35C1 RSPRY1 C16orf58 NOL7 ASH2L TM9SF3 RBM41 BCL7B BICD2 TOMM5 JUP CLIP3 SULF1 PPP4R2 GUCD1 NBL1 CYBC1 B3GNT6 RAB11FIP5 SCAF1 NCK1 TRAF3IP3 LPL PLPP1 PUDP EIF2B1 PAK4 TENT4A FAM168A EVA1A NPM3 ITCH NCBP3 ARPC5L TCEAL3 KLHL42 MAGOH GTF2H2C CCDC71L AL591684.2 STAM2 DOK5 ZNF668 PLEKHJ1 C22orf39 KRTAP2-4 STAMBPL1 TMEM50A GTF2E2 ANKRD33B PPM1G OTULIN NMT1 SOCS5 SARNP PER1 COL26A1 ELMOD3 ZFYVE27 HDAC1 ATG12 SH3RF1 MICAL1 ZHX1 PCDHGC3 RPAP2 FOSB WARS2 HARS2 MBNL1-AS1 CFAP300 ADNP POLD1 TIGD3 AIG1 ARHGEF25 POM121C HOXA11 HAUS7 RAB28 SLC25A51 PYGO1 RAB10 PKP3 ZBTB7B MRPL23 RPN2 CNOT3 SDF2L1 HIBADH SFT2D2 HSF5 PSPC1 GRAMD2B UPF2 EIF3I GSE1 EIF3CL NINJ1 COL11A1 MYL6B UBAP2 DEXI CDKN2AIPNL SLC13A3 TIMP4 HAUS3 ODF3B HMGXB3 PYCR2 STX6 CASP4 TSPAN17 BICRA BRD3 TTC4 NDUFS3 WDR3 AC016026.1 MCPH1 MT2A ZFAND2B BHLHE23 POMGNT2 HINT1 USP39 DYNLT3 ATXN2L MAP2K3 FKBP11 SLC4A4 BAIAP2-DT RPL38 NARS KAZN CSNK2A1 BABAM2 MTFR1L AAK1 FBXO2 TMOD3 EEA1 IL1R1 UBR4 LTBP3 UTP15 MYBBP1A EEF2KMT PROCR NDEL1 RBAK KMT2C CGB1 ITGB5 TYMP FKBP2 KCNE4 NEK2 ARHGAP11B HIST2H2BE ARFGAP1 SHMT2 UQCRH TMEM206 SMAD6 SAT1 RCBTB2 VEGFB UQCRC2 MAEA ZNF22 RNPEPL1 PSD3 SAFB ACTR2 SENP5 AC097359.2 RAP1GDS1 AFF3 CCDC51 FZR1 BAIAP2L1 DBNL ERGIC1 KIF26B ORC3 HIVEP1 HECA ATRX RAE1 EIF4EBP2 RYK COX5A NMB WWC2 TGFB2 MRPL4 HSPB8 NUFIP2 TMEM160 MBNL2 ATP6V0D1 RAP1A ID3 TM9SF1 NBEAL1 GPR107 AC036176.1 SLC25A37 SMARCC2 AMBRA1 LINC00384 USF2 NAXE C7orf55-LUC7L2 DOP1B PTK2B LINC01106 PELP1 SDHB NUDT10 SOX4 C5orf24 RNF41 MFSD6 MYO3B SMARCD1 USP20 SLX1B STRADB JAM3 DDOST CHSY1 DIRC2 ARHGAP17 KIAA1522 GFRA4 SLC39A14 DDX19B CRYZL1 PSMA1 AL020996.1 SNIP1 CLDN11 INTS14 STAG2 MAML2 TMEM127 RAC2 SEPT10 SCYL1 RPP40 LINC01127 YOD1 APCDD1L YIPF4 ZBTB22 DDX27 PVALEF CHMP5 NEDD4 ZRANB3 DCBLD2 DPH3 THYN1 PGRMC2 ZBTB38 PAFAH1B1 OSTF1 FYCO1 FLYWCH1 GLRX2 DNAJA4 SLC25A1 PELO RNASEK BTN3A2 ATP5F1D SPRN BORA PRKCI OSMR MRPL12 SOD3 R3HDM4 VWA8 REP15 WIZ DDAH1 ACBD5 SLC35B2 TIPARP RIOX2 CHEK1 CKB RTN3 IPO8 SYNC PSMB6 PTHLH SYNJ2BP-COX16 PPP1R8 TRMT112 TNFRSF11B CD36 PIBF1 TTLL1 ARF4 DCAF12

	ANAPC13 PPP6R1 MBTPS1 SPRTN MRPL48 FAM133B LARS ANKRD28 MRPL28 RAB14 APBB1 USP10 NIPSNAP1 ARHGAP45 B4GALT1 KNSTRN SLC25A44 MED8 WDR75 TEX261 STAT4 RNF145 ZNF81 SNRPA GATAD2A GSAP PDXK CCM2 EFTUD2 HSPB11 IFFO2 IGFBP7 PRMT2 PRDX1 POTEE EHMT2 STRIP2 COX17 ERMP1 THAP8 HACE1 LSG1 PLEKHG2 MYNN ORMDL3 CORO2B ALOX15 PAN2 Z93930.2 TECR KIFC1 MARCH5 CXorf67 NUPR1 LHX5 NDUFB4 LPXN ANTXR2 SMYD5 BCL9L LDAH AC091057.1 MASTL TENM3-AS1 RCC2 AC097381.1 RASEF RNF103 AHCY CROT MAPK9 PPTC7 RIPK2 PDCD7 CDR2 EXOSC9 PSMC6 PPP4R3B PLAGL1 RNF2 DNAJC7 IFITM2 ASAP3 PROSER1 MRPS18A ASPH TM7SF2 FLOT2 RRAS2 OXCT1 PITPNA NDUFS2 UBR5 SLC43A3 NRBP1 STUB1 TLNRD1 SERPINB2 GTF2F2 MYPN NHP2 TSPYL2 AP2A1 SMPD1 TMEM47 TBC1D2B EFCAB14 FMC1 SMARCA5 WWC1 YY1AP1 MAPRE3 AKR7A2 RIF1 GGPS1 LARP1 CGGBP1 RNF19B UQCRB ABCC3 NAA50 ANGEL1 CARS2 ARHGEF35 ARHGEF3 EXOC8 HLA-A FAM167A SCD MRPL20 YDJC COX20 CACUL1 HSPA6 ZNF518A STAT3 PHC2 WDR36 SPHK1 MBD4 MPZL1 ARSB RUVBL1 ZSCAN29 SLC36A4 GPR176 NEK1 UBA3 DPEP3 NDUFA4 EBF3 TBC1D20 EIF5A2 DUSP1 STX7 C5orf49 GATD1 H19 IRX1 GBP2 SLIRP NAA10 SETD5 EBF1 CRLF1 ABI3BP PYCR1 MYO18A SEMA7A MADD EDF1 CRYBG2 LINC00667 GTF2H4 HSPA1A PPIB ATP5MF GOLGA5 MTREX SRGN PPP1R10 AL138920.1 VDAC3 CSE1L RNY3P1 CRYGN AATF MCRIP1 CENPN C3orf80 FTSJ3 ATG13 GABPB1-IT1 G0S2 RRP1B EEF1B2 PFKM DKC1 STAT6 GNL1 GART THOP1 RIOK3 TRIAP1 ATG9A MRPS26 RPL6 VARS2 ATP6V0E2-AS1 ZNF787 CCNT2 UBE2B MT1X KEAP1 RFC4 H2AFX MED16 BCL2L13 GNB2 RPL30 CCDC30 PLOD3 ZBTB39 ARRDC4 DRG1 UROS AKAP17A LRP10 PLEKHF2 PIEZO1 POLQ DYNLRB1 FAM173A GTF3C2 DYNLRB2 MR1 MAP4K5 ACHE MIEF1 TNFRSF12A PLAA SEH1L IFRD1 KCTD9 PRR14 WDFY1 PRR11 ATAD3A SKA1 NUDT3 ZRANB2 CASC23 SRSF4 GABPA CTGF HMGB2 POLB ZNF335 SNX7 IVD HEATR1 NSDHL NAA35 ATP5PF LSS ZMYM1 BCL7C FP565260.3 PSTPIP2 TCEAL9 ISG15 FXR1 ZMYM3 ZBTB14 CREBL2 BCAS4 FAM200B PPAN ELOC YWHAB RNF213 ACAP1 CLK1 WDR47 TNFAIP1 PRPF40A MAGEH1 INTS11 BTBD6 DTD1 SKA3 RGS2 SH3RF2 CREB3L2 COL3A1 MOB3A NUDT2 IVNS1ABP LSP1P5 NDUFV3 PPP1R2 DNAJC14 FOSL2 PRDX3 CHCHD3 MOV10 NIPSNAP3A RBM12 H2AFJ AC008687.8 SMC2 ATP5F1E PRPF4 VPS26C LATS2 PTPN1 OSTC APCDD1L-DT ZNF580 WDR11 NIFK MAGED4B OCIAD2 CAPZA1 CDYL2 ARHGAP18 DDIT4 UVRAG NUS1 PSAP CHM NCS1 ELP5 TGFB3 TOMM6 ZNF732 SERPINE2 PIMREG POC1B-AS1 AC009779.2 SUMO2 SDCBP NUCB2 CHTF8 NOL12 FPGS TAF13 NUBP1 FAM136A RIN3 PERM1 TIMM10 NLN TPP1 RREB1 BRAT1 UBE2C CDK2AP1 SEC24C HCCS GTPBP4 RBM42 TRAPPC1 TNPO3 NBPF10 AC006455.5 HTT DCUN1D1 ZFC3H1 BRI3 AL118508.1 ATP6V1H HNRNPDL IFI44L NECTIN3 FOS FIGNL1 MRPS5 MYCBP2 EMD CCL8 DCTPP1 ZNF300 BAZ2A SECISBP2L FGF2 VPS28 RRM2 SLC4A1AP COMMD10 SACM1L KLHL12 NCBP2 GPSM3 SLC20A1 ENTPD3-AS1 GADD45GIP1 FEN1 FAR1 SNX30 PCM1 TSG101 TSNARE1 PIP4P2 FANCI BAG2 THNSL1 SHROOM3 SNRPN MRTFA ACAA1 IL6ST NCAPD2 ZNF319 SRD5A3-AS1 SMU1 PPP4R3A KRR1 MON2 RELA MRPL40 DUT TXNDC9 MAP2 EDEM1 C21orf91 MATN1 GSTM3 VSX1 NFATC2 ANAPC5 NPIPB13 PKN1 AKT1S1 SURF6 PHF14 NRIP3 COX5B EIF2AK4 FAM3A PRDX2 DGCR6 BAZ1A TRIM10 ARID3B MRS2 HSPH1 KIF13B RBM18 AZIN2 CBLN3 PPP2R5D WDR5 RANBP10 C11orf24 SLC41A3 PSMD1 FBXO4 CSNK1G3 RABL3 PRELID1 MRPL21 RBMX AC009163.4 TGFBR2 GLIPR1 GPR137 INAFM1 CIZ1 ITGA11 CTU1 CIB1 CTNNAL1 CIT AMOTL1 HERC4 MCM3AP POLR2J2 PLCD3 HLA-B MATR3_2 ARHGEF17 SNX1 CACYBP RBM8A CDV3 CATSPERE FLOT1 NDUFA3 UGP2 MCM6 RRM2B GNPAT MYPOP NDUFA9 SCRIB POLR2C PON2 UNC119 ANKRD27 EIF3K CKAP5 C11orf98 ULK3 PNO1 SLFN5 CNPPD1 GP5 RARS STC2 PGLS TMEM141 DIS3L STRN4 KITLG ZNF490 ARID4B YKT6 KCTD12 CBX5 ZNF326 PAF1 IFT57 CFP CNIH3 GTF3C1 FAM208A STX16 FEZ2 DLAT VTI1B CDC5L TMEM119 SEPHS2 AL356481.1 WNT5B PEG10 FOXO3 KHDRBS1 CRYBB2 ZBTB5 BRD3OS ZNF12 PANK4 UHRF1 GPC6 HIP1 GSDMD SGO2 RFX7 ZNF341 TFPI2 YTHDC1 JUN STK38 TMEM101 HIST1H4C VTA1 DMAC1 PNN CLPP MTMR3 TRNP1 DDX3X TRIM25 NUP62 AP4E1 EPB41L5 PGD CDKN3 ITPRIP DHX36 E2F3 RPL26L1 PHTF2 FGD6 CHCHD4 CUTA ADCY9 PTPN13 TMF1 PNPO CDKAL1 IDH3B EIF3G ARHGAP22 MIB1 ALDH9A1 TTC38 INPP5A TRAF3IP1 SMARCE1 B3GAT3 PITPNB URM1 LINC01964 MBOAT2 MTERF2 TRAP1 STARD7-AS1 APP TOB1 SLC25A43 WASF2 CDK10 AC005670.2 HLX C12orf73 MDM4 NBPF15 PATL1 PFDN2 NDN RAB7A SLC35B4 ITPR3 CBR1 NRSN2 CDCA8 ZNF638 RXRB EIF2B5 PIGX FIBIN WASF1 KLHL2 ITPK1 POLK PAK1 RBM15 AMZ2 PPP1R14A DCAF5 CYCS TPX2 PRKRA TPRG1L STK32C IMP4 TCF25 AC068533.4 ARL2 CD2BP2 FGFR1 COX6C SPECC1L GOT1 ZNF576 CASTOR2 RPS5 PI4KB OAZ2 BET1L NOC4L LBX1 ATG2B ELOVL5 TANGO2 BLOC1S2 DAD1 HOOK3 LIMS2 AC244197.3 ACTR10 GLT8D2 CDK11A CNN1 MCUB SMC3 KPNA2 GSS DCP1A TMCO3 KPNA3 ZCRB1 BIRC5 CES2 MRPL52 TMEM250 TRA2B ARHGAP39 GLE1 KNTC1 EXOSC2 NPC2 YTHDF1 AVPR1B CEP170 DNAJC5 ALDH2 AC007390.2 DAPK3 QDPR PIN1 BOP1 THAP12 NELFE DNM1 NOP9 SORT1 PLIN2 FAM98B LRIT1 USP7 MCU PCBP4 NFKB2 ADI1 IFT140 ALCAM PSMD3 TMEM151B AVEN AC026464.4 PPP2R5A HMGN4 NBPF19 AL079303.1 ZNF24 ZZEF1 PBDC1 FUCA2 RAB5B MRPS12 TAF10 GMFG PRRC2B MMP24OS MAPRE1 NDUFA2 ZMAT5 PHLDA1 USP19 ACOT7 PSMC3IP AL031985.3 TMEM14C LIN52 ARIH1 PTGES POLDIP3 CALHM5 WDR20 CDC6 NUP88 TEN1 VASH1 SLC35A5 MIS18BP1 HPS4 OCRL MEG8 ARL6IP6 UBXN7 CCDC18 AGGF1 ARPC3 CBARP TMED9 PJA2 CARS AGTRAP FRYL RHOBTB2 PNPLA6 FUBP1 MT-ND2

	STON1 RPP14 SCARNA12 MTR UBL7 DHFR ALPP ASH1L GANC MLIP DGKD TTC21B LOXL1 AP001931.1 NT5C3B FAM83H KLHL9 ZNF747 AC226119.1 MITD1 SNN CDHR1 PRPF39 YIPF6 USP4 HPF1 NUAK1 LSM3 MOGS NCOA3 SNAI1 IER3 KCTD10 YWHAH PAFAH1B3 AC022150.4 BOD1 COG4 TIMM17A ASAP1 SMG8 PCBP1 NSD1 HDGFL3 PDGFD BRCC3 CNDP2 ERCC1 YPEL5 AGO2 CREBBP DUSP14 DSTYK COQ5 TUBA1A TTC12 LINC02179 NOP10 IFT43 PSMD8 RARS2 CYB561 DCLK2 ZNF827 AURKAIP1 DSE SERTAD1 CREB3 RHCE MCFD2 CSNK2B RF00019_485 ARFGEF2 REXO1 RASAL3 COX7B ATP6V1A WNT9A REPS2 C6orf48 ANO10 NCKAP5L MTLN BAG3 RIC8A USP35 PRKDC NOL11 EXOSC3 ZCCHC10 MVD SCCPDH BCAS2 ACE2 AL138752.2 OLIG3 KCTD17 TEX10 CEBPZ IRS2 RHOV SH2D3C PTPN14 APTX BMS1 PDE4D NFATC3 GEMIN4 THEM4 RNY3 UBE2K GXYLT2 MDH2 BCL6 GATD3B LIMS1 SREBF2 ZWINT TRUB1 ENPP2 OR10H1 PITPNM2 ZNF780B APEX1 EOMES MRPL11 SLC5A3 ARPC1A AC073188.6 ZBED6 NATD1 ATP6V1E1 BLOC1S5 ASB1 EVX1 ACAA2 S100A16 GTSE1 KLF9 MAVS SDHAF1 EEF1AKMT1 FAM120AOS PWWP2A SMG1 RCC1 RGS18 BTBD8 AC099681.3 PIP5K1C GNA13 FUT8 ALKBH7 NUFIP1 SNX29 WWP1 HIST2H2AC ERGIC3 POLD4 ANAPC10 NME4 LIX1L MEGF6 IRF2BPL UBE2T CREM CD68 METAP1 SMARCA1 NR2F2 PLXND1 NLRX1 ZFP91-CNTF SMAP1 BSG TEAD4 PDE7B EFEMP1 TIMM8A SRRM1 COX6A1 LNX1-AS1 EEF1A2 DUSP23 ABCC9 NUP35 HACD1 VPS29 IFT74 HERC1 DOCK1 SHC2 SDS CRADD INPP5K LINC00921 CTR9 PTTG1IP UBR1 MCCC1 VPS35 VAC14 ASNA1 PSMD9 RHOD KDM5B SRCAP C1S TCF7L1 UBASH3B FAM207A ARHGAP32 GGACT GLO1 PRR13 NECTIN1 SERPINB8 PKIG INO80B NUCKS1 IP6K2 KRTAP10-12 NXN FOXJ3 UTP25 CRABP2 COL11A2 BPNT1 SASH1 IL17RD PPP3CB EMC2 LSM14B NAMPT SSBP3 HECTD1 TLN2 ELOA HDAC4 AC103691.1 RPS6 FAM102A CTNNBIP1 ROMO1 BRPF1 AMFR G3BP2 GADD45A RF00019_628 OARD1 DKK3 NARF UTP18 DDX31 PPP1R14B NHLRC2 SBF1 KAT14 GTF2A2 PPP3R1 FAM57A NAE1 RBM14 UBE3B COPE SF3A1 IQCE RPGRIP1L DAZAP2 BOK FXR2 ZNF808 TYK2 NIPSNAP2 SDHAF2 TMED8 BACE1-AS TFAP4 DOK1 MTMR4 AQP3 USF3 SIRPA IGFBP6 SAMD11 PRPF31 PRICKLE4 MRPL55 PLCD1 ACTL10 RAB3GAP2 CCNQ CLEC7A STX18 DCBLD1 BRD7 PSMG1 NISCH DTYMK TAX1BP3 AMMECR1L WDR77 SLC39A13 TUSC3 QTRT1 AP1B1 CD74 ARFIP1 HSPA12B SLC35E1 MGST2 FEZ1 ZNF880 ZFHX2-AS1 RBBP8 SRP54 OSBPL1A STARD4 ACVR1 GOLGA2 TRA2A JADE2 RFC1 ASMTL PIK3R2 SYTL2 SNRNP25 DNAJC21 AL121992.1 STIP1 PSMB4 CYTIP SPTA1 C11orf45 ZCCHC17 NDUFA1 GOLGA6L6 NOP14 EIF4EBP1 METTL26 NAIF1 SNRK DNM2 LSM8 VARS SUZ12 KRT18 PI4K2B HIST2H2AA3 MFAP2 MPP5 TCEA1 ARPC4 TNFRSF14 MRPS36 CLPX RAB34 RB1 FGF5 CNIH4 ANKLE1 BZW2 PSMD4 JMJD4 CHCHD10 TENT5B GLRX CELF2 ST3GAL4 SHOC2 PDXDC1 GOLGA6L4 NFS1 TIMELESS SLC25A36 TMED10 IDH3G ARFGAP3 YIF1A AK6 DLGAP5 PHF8 GRINA ADIPOR1 SNF8 H2AFV TMEM87A SMTN TWIST2 DNTTIP2 AC005785.1 GOSR2 ZNF106 LCP2 RNPS1 NDUFB11 AC079781.5 VPS54 IL4R TMEM123 SEC11A PEX5 TP53 CCDC69 CLSPN MAP1LC3A EPS8L2 TM4SF1 ZNF628 AC125232.2 ANKRD13A LOX YARS RPS27L GTPBP6 SRA1 AKR1C1 IMMP2L ZNF615 ZNF768 BAG4 ZNF469 CHURC1-FNTB ICE2 ZNF746 AGAP3 PRKCQ KDM1B LAMC2 SPSB1 CNOT8 FAM219B ZC3H4 PDZD11 PPP1R11 OLFML3 ELAVL1 PIAS4 RF00019_676 MESD IGBP1 RASSF8 FAM210B AC004922.1 USP12 FSBP DLC1 LAP3 SPRY4 RAP2C MXD1 TBRG4 RAB1A USO1 NUDT4 RAB9A SIRT1 LDB1 COMMD3-BMI1 HDGFL2 ADGRA1 TMEM167B SP8 RNF151 TPRKB RF01892 WIPF1 MMADHC RNF181 COLGALT1 BEX3 SIAE AGBL5 PFDN4 DDX39B PSMB3 DEDD2 TOP2B ZNF207 CLEC11A MPRIP KLF13 TOLLIP NLE1 MED19 RNF11 IDE CERS6 PWWP2B EPAS1 RAB18 GYG1 PHB ANXA7 JDP2 NXT2 MORF4L1 HSPB7 COX7C ZC3H15 ELK3 SEC61B AC005082.1 COMMD9 GPX1 SBNO1 PSME2 SNAPC3 PLEKHA5 LIMK1 IFITM1 B4GALT5 TRMT1L HIGD2A AKAP11 MCMBP GLB1 INO80 GAS6 CNOT11 TMTC1 CTTNBP2NL MTCH2 BACH2 MRPL30 MIEN1 C8orf33 KDSR MCM8 NME1 MAP3K11 CRYBG1 RBM28 APRT LRTM2 GIGYF1 CAAP1 ATP5IF1 HGS NOL10 KAT7 HNRNPA1L2 ERCC6L2 TCOF1 RANBP9 CPNE7 NUDT21 INSIG1 PYCARD ACSL4 HSPA12A REPIN1 NKIRAS2 PPM1D VPS45 TP53BP2 GINS2 CYP1B1 VGLL4 PIP4P1 C1orf43 LETMD1 STT3B LTA4H IFIT3 MYADM TRIM68 ZNF652 UCK2 RPL39L OAT CDYL ERVK3-1 PLOD1 MTFR1 PRCP RNF135 SUPV3L1 TBCB ANKRA2 TOMM20 PTEN AGFG1 GTF2A1 PNKP SETD2 MRPS35 PACSIN2 AASDH SEC23B HMGB3 HMG20B SMDT1 GPR180 NDUFAF3 GALK1 NUP214 SDCCAG8 CDK5RAP2 EXOC5 SYNPO2 KCTD15 AK3 NRP1 TRIM22 CDH13 B4GALNT4 RC3H1 FASN MRPS14 FGF12-AS2 CAMK1 VEPH1 ILF2 NSD2 AC108047.1 SNORA71A AIDA PSMA3 SMIM3 TGM2 ACTL6A SLC22A18 GRK6 PKD2 STX2 ARHGAP30 PIGZ VPS26A PHACTR3 CYP2U1 SQSTM1 PAIP2 SNORD3A SNRNP70 ZNF197 MAN2A2 PTOV1 CSGALNACT2 KDM5C RSL24D1 UCHL1 TMEM45A APOL6 MRPS34 PLK1 ZNF397 AL139260.2 MIS18A DDX47 DVL2 DICER1 GEMIN8 MTRNR2L1 DPP4 ZNF148 CNOT4 KLF16 SSBP4 PSMC2 AL133352.1 GGA3 BRMS1 SRPRA UBQLN4 PCMT1 PIAS3 HLA-E SGPL1 AFG3L2 SWAP70 GSTA4 CDKN1B PRPF19 GRIPAP1 NDUFS8 TRIR ACBD6 YEATS2 MXD4 EDC3 SMARCB1 FNIP1 MRPL47 DYNLT1 TEAD3 ATP13A3 FEM1B FOPNL TWF1 MACO1 CENPH BDKRB2 HSD17B4 COPZ2 GPI NOP2 TAF2 COPZ1 KATNA1 TSEN15 TMEM237 LINC02361 HOXB3 PLCB3 CFH TSC2 PINLYP TOLLIP-AS1 BNIP2 CDH2 GJA8 HYI CASC3 GTF3A METRN PRAF2 ARID5B NECAP2 ACTR1A CNN3 PAPPA MMAB DHX40 RRP9 NT5C ZWILCH AC016747.1 CIAO2B IFT80 ZNF639 MYBL2 POMZP3 NRAS CXCL8 DNAJC3 PARP14 ZW10 CRY1 AGAP9 PBRM1 FBXO33 UHMK1 VILL CEP162 ZCCHC24 LY6G6C RNF20 AL645728.1 USP9X ZBTB43

	VAPA MEA1 NR3C1 NEK7 CORO1B TRAPPC2L NR2C2AP MCM3 RTL5 THTPA NBPF20 SNRPE LEPROT STK38L DDX42 WDR24 KSR1 VAPB RAB27B TMTC3 MARVELD1 RAF1 INF2 UBE2M AKTIP FURIN UQCRFS1 SNX4 AC120498.9 SELENOF DNLZ FN3KRP COPS2 AC096921.2 GATAD1 SDC4 FHL2 LMOD1 PSMB2 LTB SNRPD1 LPCAT2 PHOX2A XRCC3 BTBD2 RBBP4 PTK7 REV3L RPL22 NYNRIN RAB6B ZCCHC7 CCDC86 THOC1 TMEM9B KXD1 USP25 H1FX-AS1 MT-ND4 PCYOX1 ASCC2 FBXO17 KBTBD11 MYO5A SERF1B PARP6 ADAM10 SPEN PRPS1 LIPA MT-CO3 MRPS22 PSG5 RSAD1 SNORA73A PDS5B DHTKD1 MPHOSPH8 ATF5 IQCG TULP4 TAF1L SUGP1 HNRNPUL1 PKNOX1 NSD3 SELENOM TXNL1 RNF168 DDA1 RND3 ESD MAT2B VDAC1 TJP1 ARFGAP2 RETREG2 ABCF2 2 RPH3AL CTSD MRPL17 TUBB3 OCIAD1 DDX46 TCEAL4 TES CMTM6 GOPC AP000813.1 ARAP3 POLR3C HAUS8 ATG101 LONP2 RPS6KB2 ATP5ME RAB31 AP003419.3 AIP MCEE PBK CPPED1 AZU1 PRRC1 DIS3 SKIV2L MARCH9 ZNF292 SENP3-EIF4A1 TBX15 FUZ DROSHA EMC7 ZNF696 SNTB2 PSMC1 FAF2 TMEM41B ADA COASY LAMC1 M6PR DOT1L ZNF521 SMYD2 MED30 MKRN2 ECI2 SSNA1 AC135050.2 AGAP2-AS1 UFC1 PSMD14 CHAC1 PDCD2 MRPL44 AL139082.1 GAR1 RPF2 HHAT ING2 EMX1 UBE2D1 NDUFC2 TRAPPC13 PLIN1 EIF4B GOLGA7 RIN1 FERMT2 LGALSL PGM2 ASB16-AS1 PHF5A WDR81 TK1 DPH5 PGP ID2-AS1 KCNK2 UHRF1BP1L GIT1 MSL2 MMP28 MARCH2 HMGN5 HIST1H1B MEN1 AL022069.1 STN1 SS18 SHCBP1 ITGB1BP1 CBFB SESN3 UROD AL355315.1 AC118549.1 COMMD4 TUBB2A ASPM ZYG11B RFC2 SIK1B ZDHHC8 DVL3 PNRC2 MOSPD3 TRAPPC12 NSF TBC1D13 PLK2 EIF1B LSM6 SMURF1 TVP23B HERPUD1 SCPEP1 CDCA3 METTL9 CPSF1 UGDH METAP1D PXDC1 NUP188 SRXN1 CPEB2 AC106881.1 KNL1 BPTF JKAMP XPNPEP1 EPB41L2 PCGF5 CDK5RAP1 RNF26 MRGPRG SMARCD2 WIPF2 ZNF283 CADM3 PPM1B PCF11 SLC7A5 CYP20A1 MBD6 UQCC2 FMNL3 CBL SNAP23 AC048382.2 MXI1 CLCN5 ZDHHC9 TTC28 MTURN AL137782.1 MAP3K2 CEP97 TSPO UBA6 REEP5 ARRDC3 TBPL1 STX12 NIN SRPK2 SLC1A4 ANKFY1 CREG1 HSPA5 RWDD1 ZKSCAN5 SSH1 GNAQ CKAP2 CCNG1 ETHE1 ACAT2 SASH3 EPG5 RAB29 FNDC3A ESF1 SPIRE1 LAMTOR1 MRPL2 C19orf48 BFAR KHDRBS3 DLX3 UBE2E1 SLC27A4 UBA52 PPIF KLHL22 MTRF1L CPNE3 PRKD1 LRRC4B EIF2A ZNF561-AS1 GBP6 ADK TMEM164 HDAC2 NEXN CTSL ATP5PB TGOLN2 DNAJB9 PAFAH1B2 ETS1 MRPS27 MLST8 GATA5 PRPF18 AC008012.1 MOB1A GTDC1 VAMP3 ZNF528-AS1 SLC30A6 SH2B3 TMCO1 BICC1 H1FX ELF2 TRIM32 SCAMP1 NIPAL3 SLFN13 SERHL2 OGFR CYP51A1 ANPEP ZFYVE26 FGFR1OP STOML2 FTSJ1 HSF1 ADSL UBXN1 GLRX5 HOXA9 FLAD1 AC011825.3 HIF1AN BUB1B NFKBIB MTMR2 TSC22D4 CAPN5 FAM189A2 APOBEC3C RUSC2 HJURP THUMPD1 ST6GALNAC6 SRSF2 AQP5 RAB30 CEP41 MPDZ SDHC ATF6 GBF1 ZC3H11A HAUS5 FYTTD1 SLC49A3 RNASEH2A SMC5 SMN1 NVL ARC NUP54 BRWD3 STAT2 PORCN CENPV SMIM20 PDCD11 CTBP2 LLPH INTS4 MLEC GALE NT5C2 TBC1D10B EFCAB2 WDR41 RNF121 ATP6V1FNB ZNF337 SNAP47 ALS2CL GXYLT1 MEG3 MTSS1 DYRK1A HTRA2 CDK5 KIAA2013 AC021016.2 DNAJB12 HBS1L PDS5A C6orf106 HSPA1B PSMD13 MORC4 LY6E ARFGEF1 TRAPPC4 LAPTM5 CETN2 LSM1 QSOX1 PKDCC NOP14-AS1 CCDC171 PPP1R35 KLHL17 SAP25 FAM114A1 RAB27A TXNRD3 TRAM2-AS1 RALGAPA1 ITPKC PPP1R3C RPUSD4 SLC5A2 MIF ELP1 TAPT1 AC125793.1 HIVEP3 ITGB3 MRPL16 AC008663.2 GATA6-AS1 NUDT5 MAP7D3 CABLES1 UBP1 ARPIN TTPAL CERS2 BLOC1S6 NBPF9 PDZD4 GSK3A GIPC1 ELL2 PSMB1 EXOSC6 ACTA2 FANCE GMPS FKBP9 ATP6V1D CARD19 PMEPA1 SPAG7 RPF1 UBE3C HOXC6 HNRNPH2 PDSS2 NDUFA10 CLIC2 RNF13 ZNFX1 CCDC92 SNRNP27 KLF10 MFSD14A CLNS1A NME3 PVT1 CHN1 AC135050.1 RRNAD1 CEBPB MALSU1 METTL3 RTF2 CAPN7 ANXA4 ZFYVE19 LIG3 UAP1 IRAK4 TULP3 ATP2A2 APBB1IP CAST TBC1D9 DDX41 FANK1 PGM3 UBE2D2 TAOK1 UNC45A GIT2 NCAPG HSPG2 APOL3 GCNT1 LRPAP1 G6PC3 NCOA4 RAB5IF NANS SMARCAL1 SCNM1 AMD1 AC024592.3 SCARNA5 AL160006.1 PRMT7 COQ2 SIN3B FMN2 SEMA3C RNF6 SMIM29 PDGFC RUBCN SEC22A RPS6KA3 SLC25A5-AS1 UBXN2A NUSAP1 PHF21A PNPLA2 DNAJC13 HNRNPA1P48 ERCC2 BET1 CCDC9 USP3 SNX17 SPART ZNF622 ATP5MD DNAJC19 TOP1 AC092139.1 SHISA5 SNRPD2 SLC39A6
UC RB61, 97 unique genes (1258 genes)	MSRB1 ELMO2 ERAL1 FP236383.3 AEN LMAN1 CHD8 GALNT3 MSL1 OR13C2 CHRNA10 MYO9B NIFK-AS1 AC022762.2 COL4A5 PNPT1 KCNK3 GDA MAP3K3 PRSS51 EVC PTCD3 SNX33 TMEM184A SUGCT UFSP1 CMPK2 SLC26A10 TIGAR USP6NL RELT UGT2B7 AC022148.1 SLC8A1 AP1S2 SMYD3 ABR STK17A HIST3H3 FOXE1 C2CD3 AC007666.1 CCNY PODN SSU72 GAS2L1 RARRES3 PMM1 TJAP1 CHFR DUSP5 C1QL1 LIMD1 THRB ASS1 GSTM4 B3GALT5 IRS1 TMEM104 ATR GNA11 PRR29-AS1 UPF3A PCDH18 RASIP1 UNC13B ZNF687 KDM2A ATF7 FGF1 NFIL3 CD53 ZNF655 ARAP1 AC092053.2 QRICH1 PCCB FP671120.3 KLHL7 AGTPBP1 PTGER1 IL17C EIF4A3 ELFN1 KCNA4 RBM6 ARID5A WAPL SKAP2 IDS UIMC1 KIN HIST1H4I CHMP6 ARFRP1 IL17D ZNF568 SVIL ERMAP TMED7 CFC1B ASTN2 ELAVL2 AL451123.1 SNRPC SYDE2 LAMTOR3 METTL5 HBP1 ICA1L XPO4 SECTM1 AC108704.1 HCFC1R1 SAT2 KIAA0753 GABRE MICA C11orf49 VPS16 FP565260.1 DVL1 FLI1 GPR157 TYMS MAB21L2 GPRIN2 CLIC5 AL008636.1 LINC-PINT JAGN1 PTPN4 VEGFA MAS1 AC090517.5 AIF1L PCNX2 GRIN2A COG8 MUS81 AGBL1 NLRP9 E2F7 LZTS3 FAM138F SP4 SLC25A39 KLHDC2 NDUFV2 MATN4 AMPD3 HRASLS MMP1 CFAP20 ZC3H14 TWSG1 DDX50 ADAMTS6 MKKS CCER2 HMBS TOR1A GADD45B ZNF287 TBC1D16 FIG4 BHLHA9 DCTN4 C10orf55 BMF NKAIN1 CFAP36 SLC35F5 TELO2 RINT1 ANKMY1 AKR1E2 RNASEH2C SCAMP4 CCDC3 MIER2 DCAF4 IRX4 CHD7 THUMPD3 PTBP3 ITGBL1 EGFR VPS4B SESN1 FBXO9 AC099811.2 AL139393.2 ACOT11 RAB6A

	RNF146 CCNB2 TMEM175 POLR2J3_1 TBCE_1 FAM225A DDX3Y PDP2 TMEM43 SGTA PSMD6 PLEKHB2 ARHGAP29 BCAT2 C5AR2 RAB4A COMP ZNF865 SCLT1 RBBP7 CMAS PRDM10 SLC30A1 AC010226.1 DUSP27 SWSAP1 C15orf39 SLC3A2 MBTPS2 LINC01833 LINC02223 AL391294.1 BHLHE40 MCC IFT88 SLC26A2 ID2 HADHB EN2 PDHX UNC50 HEATR6 LINC01648 POLE SYBU TBC1D22A AC015971.1 TMUB1 STK32B ZNF532 ATP6AP2 TPT1-AS1 LAMTOR4 ZDHHC21 GOLGA6L1 SHANK2 SLC41A1 FAM124A MAP4K2 ACAP2 PINX1_1 AL022322.2 DCXR AL157392.3 CDC23 TAB3 ZNF496 HS3ST2 SH3BP1 KLHL26 HIST1H4H GABRA5 CFAP65 PTPRJ NDUFA12 TPM1-AS MVB12A TAAR1 TMEM272 LINC02076 RNMT AL034399.2 NDUFB2 MINOS1 UPF3B HPSE PIGU TSTD2 OR2M3 TLK2 ARHGAP24 SUCLG2 ZNF703 AC008395.1 MLH1 RSF1 HIST1H1C MAP1S HIST1H2BO AC005332.3 LBH RHOBTB1 ADAMTSL1 LINC01553 SMAP2 MAP7D1 PAX5 MRPS18B HEPACAM ARID1A MBD1 RCN2 STARD7 NCLN RYBP DRG2 NLRC3 HOPX MEF2C EIF2D MYB KLF3 DNASE1 TNIK TVP23C IER2 WNK2 NUBP2 ZNF783 AP1G1 ECHDC1 GNAI3 KBTBD13 SLC37A3 MMRN2 ZNF248 FBXW8 SH2D1A PKD1 ATAD2B MYOM1 ZSCAN30 ABL2 LAMP1 ALKBH1 SP6 B3GNT9 FBXO27 SMAD3 SLC16A7 OTOR CFAP57 MYO6 MINK1 LRRC38 SYT5 POU2AF1 LRRC58 PRSS50_2 AC140479.5 URI1 AC099329.1 TRAF3 ZFAND4 LRRC4 MED10 FAM135A SNU13 GALR1 FBRSL1 SLC47A1 OR8A1 TUSC2 TAPBP SHCBP1L LINC00862 ISPD AC005332.5 IREB2 DLG3 EPPIN LLGL1 MTF1 USP54 THBD LINC01863 ZSCAN10 TMPO OR5M1 LINC01879 PRPF4B EPS8L1 WDR17 ABTB2 AP4B1 ANKS1B PPHLN1 HIST1H2BN CHL1 ZBTB45 SENP6 ZNF516 ELN RFX1 HPS3 KIF21A UNK MAML3 ARMH3 NR1H2 PPP2R5C AC009318.3 SLC25A29 SVOP ADAM9 AC006504.5 APAF1 ZNF296 NOP16 IFNGR2 PLPPR3 RABGAP1 PAK3 PPP1R16A MRPL35 ATM SUMF2 MGAT4D ZNF134 SSTR3 AC100793.2 SNHG7 ACP7 SLC26A11 CBWD5 NMT2 AC012291.1 FCHSD2 SGMS1 ARMC10 PPP1R12C TTC7A UBD ERVK13-1 AC243829.1 MST1 GOSR1 RAB7B NUP50 SHC3 LRRC73 PUS7L MRPS30 VPS35L EGR3 ZNF184 PRRT3 OSGIN2 TRIP13 HIST1H4K ERG28 KLK15 LYPLAL1-AS1 EIF5AL1 LPAR2 TRIM58 INAFM2 ZC3H18 TMEM202-AS1 FAAP20 AC093591.2 NCKAP1 PRKCE CCDC149 GLYATL1 NDUFB10 CACNA1D PIK3R4 C1QTNF4 SGPP2 PGAM5 SLC8A1-AS1 LINC02604 INSIG2 SRARP CC2D2A DSC3 ANAPC11 ATP6V1B2 GLRX3 DNAJA2 CLDN5 LRRC55 NAP1L3 ELK1 AL365204.1 AHSA1 GCC1 IFI6 MAPK6 NTMT1 SNX27 OTX2 SEPSECS BCORL1 FFAR4 TUBGCP2 LARGE1 CYB5R1 PLEKHN1 ERBB3 NAXD ORMDL2 AP5B1 TUT7 PTPN21 AP005263.1 APH1A OGFOD3 CYP27A1 KCNQ2 SPEM2 GRM5 CXCL12 GUCY1B1 C15orf53 CEP76 CORO1A EFEMP2 AC022098.1 NMNAT3 STRBP SHISA9 TUBG1 OR9Q1 TMEM109 PRSS23 GLYR1 ANKRD29 ABCB4 KIAA1191 PC SETDB2 UBE4B C19orf84 TMED7-TICAM2 SPECC1L-ADORA2A OTUD5 SPATA2L CBLN4 OR52I2 PPP4C CEBPA C2CD2 ERCC6 MEAF6 IL7R IFI35 XG ADAMTS13 AL512631.2 GLB1L3 NKAIN2 SMG6 DDX60L MDN1 IER3IP1 RASAL2 LINC00668 PAICS SOWAHC GPD2 QSER1 TOR1AIP2 SLC35E3 GPANK1 ANKIB1 RP1L1 CUEDC1 AL133279.3 CTPS2 LINC01578 FBXO45 RNF130 ENC1 POP5 GPR156 MORC2 AC137932.3 ZFP69 FASTKD1 ZNF37A ALS2CR12 CTSZ LINC01119 MIEF2 PRICKLE1 SLC25A38 CDKN2A PPA1 DPAGT1 POPDC3 ADGRF4 ADAMTS5 TOMM7 RASA3 HDC HEYL WAC NOTCH1 P3H3 NPC1 ATG14 STK17B CDKL1 SKA2 BTG3 PPIAL4G SMAD5 UBE2J2 CDX1 ATP5MC3 DLG1 KCNJ2 VPS33A SLC4A1 BYSL RNF38 GLTP CSPG4 UBE2G1 ATP9B DAZAP1 DDX11 NSMCE4A ZNF131 TRIM33 USP47 MRPL45 ENDOU PUF60 SPPL2B LINC02397 BAHCC1 CYP2C19 SMO APOBR MT-ATP6 DSCC1 PPP3CA KATNB1 AL137786.1 ATP5MC1 CCDC124 MT-ND4L SCUBE3 MGAT4B RTF1 MIB2 GUCY1A1 LRRC8D GATA6 SRSF6 POLE3 PRDM16 UBR3 MFSD11 ASCC1 SPPL3 HNRNPR MEIS2 RACGAP1 CDH15 PRPS2 RBM26-AS1 PEX11G AC012213.2 POGZ AC010969.2 LTBP1 KIAA0355 KDM5A PRXL2C ZBTB18 TMEM33 LSM12 SULT1C2 KIF2A NOMO1 AC138894.1 DIDO1 COG3 DRAM2 PIGP CBX6 RBM38 SERTAD2 ALYREF IQSEC2 ANKRD52 FAM229A FAM189B IL22RA2 TIAF1 CCDC6 CMYA5 CTAG1A PCBP3 GRM6 AMMECR1 HAGH USP17L2 RPS10-NUDT3 PAX1 SGK1 RIMBP2 MEMO1 KRT8 ABHD17A KANK3 LINC02605 ZNF442 EPS15 AC090527.2 EIF2B2 ASPSCR1 RANBP1 FDFT1 AC027682.4 WBP11 NELFCD EFCAB5 HAS2 TMEM229A ATP2B1-AS1 MARCH3 ITGA6 RUNX1T1 THAP5 SMCO4 AGAP4 ZNF740 CHTF18 BMP2 AL162731.1 GIGYF2 PIM3 SNRPG DMTF1 MXRA5 PRKACB C10orf143 AC007563.2 SPRYD7 GAL3ST1 TRIM14 MAIP1 AL606970.3 NAA15 FRMD4A BCL11B DCAF8L1 PYROXD1 ZBTB4 FAM104A AC074138.1 ARGLU1 PTTG1 POLR2M AC001226.1 CASP8AP2 TNFRSF25 OR13C5 FHOD3 SLCO6A1 DTX4 RERE MOCS1 ECT2 WDR45B VAC14-AS1 SLA2 SLC25A40 FOXD2 ADARB1 SIKE1 ZFP62 EGFL8 FLT1 C1orf229 GAREM1 RBM34 PPIH TSSC4 PALM RALGAPB AL356512.1 AL160408.3 C5orf63 GTF2H1 MZT2B ACP5 AC124312.1 AC120024.1 TSKS TNRC6A TACC3 STIM2 DHX8 SPI1 PTPRF SEC24B UNC5C AC091736.1 CBR3 TRIM52 TSC22D2 SMAD1 SRD5A1 ABHD13 ZNF142 TRDMT1 MUT CEP55 HLA-DPB1 LINC00877 LIPG NOX5 SCN1B LINC01544 PHF2 MAP2K7 LACC1 SP2 AKR1B1 HLA-G FER GSDMB LIG1 NID2 HYLS1 EHMT1 FUCA1 WWC3 IL17RA NPLOC4 FKBP15 NSMCE1 RNF24 HIST1H2BK VASN ZNF606 RBFOX2 KIF13A NLRP4 PCDH17 LUC7L3 SP3 COL4A1 ABHD17B DCAF10 C18orf32 EMILIN2 GDE1 CTAG1B EID2 PPIP5K2 KLHL34 LAMP2 DNAH3 CAT ANKRD53 PTPRM SLC7A1 ATXN1 CPOX IGSF9B USP36 CTNND1 GABRG2 AK5 N4BP1 WDR48 CDKN2C C12orf56 CTDNEP1 DOC2B ZMAT2 CD47 PPIC PRKACA GRAP AL050344.2 BOC RBM39 FBXO38 ABCC1 CAPN15 MFAP1 TDRD7 AC008760.2 PIP5K1B INPP4A SBF2-AS1 UBE3A TMEM192 LRRC57 AL034430.1 AC104809.1 UBTF HSDL2 BSPRY RRP15 ANKMY2 AC010980.2 AC007906.2 CYBRD1 ME1

	AC009804.2 TMEM56 SCAF4 EPM2AIP1 SELENOT ZNF883 AMIGO2 TP53RK EVPL ADARB2 TMEM256 AC023908.3 YPEL3 RGPD6 SCO1 AL359091.1 H3.Y ART5 FNBP1 TMTC2 MCTP1 CACTIN-AS1 NDUFB1 CNPY2 MICU3 ZNF837 TAF5L TSTA3 KMT2E MOB2 FBXL12 TBC1D14 DCK SLC6A4 MAFG-DT NDUFA6 AC090340.1 PTRHD1 ZNF843 KLHDC4 AC073342.2 SSH2 PROM2 UBE2E3 SLC39A7 SMPD4 ASCC3 SOX21 MTHFR ACAT1 GABPB2 ZNF274 PHKA2 C1QL3 RFTN1 HIF3A EXOC6B HDAC5 EVC2 SLC25A32 TMEM222 TGFBR3L DTX3L NABP2 MUC1 LINC00294 SLC2A3 POLM ZNHIT1 CIAO3 RNF215 SPOPL TBX2 LINC01632 AL162231.4 FAM216A CTSV NPAT RAB11FIP2 MRPL54 HIST1H2AL PRDM4 DCTN3 C11orf58 NAGA SMAGP FBXW2 AL031056.1 GOLGA1 USPL1 TPBGL MAP2K6 CHCHD7 UBL4A FAM230J CARD6 RALGAPA2 SLC27A1 P2RY1 PRKAB2 ADGRL4 SUB1 ZIC1 AKIP1 SLC16A9 RHNO1 SMIM12 PDE8A KCNE5 SF3A2 AL161772.1 AC091959.3 PIP5K1A PRKAR1A AP1M1 CHUK PDPK1 AK9 MYH10 ADAL OR10J1 INTS10 ZNF124 SIPA1L3 AC211476.6 TBKBP1 RGCC TIMM29 GALM GABARAPL1 PAPPA2 DIRAS2 HAR1A ABCG4 RRBP1 PTPRT LINC01132 UTP14A SEMA3B ZNF653 VAV2 TADA2A NEDD1 BCOR AL512506.3 UCKL1-AS1 HYDIN TXLNA PEX6 MAP3K1 CR769775.1 SPIN1 BMPER CCND3 TAF6L CHMP4B ZNF629 GRAMD1A ENKD1 PSME4 CORO6 MED23 PTGDR2 TEF MAST1 AC022916.1 ISYNA1 IDH3A ZNF316 AC005329.1 DYRK1B AC046168.1 LINC02600 KRT2 ITGA4 MLX AL161644.1 CEP57L1 RILPL2 KIFC3 MCTS1 AC005005.4 INAVA TMBIM4 KLF1 TBC1D4 ST3GAL2 PLA2G2F RMI1 TRABD RRP8 UNQ6494 TLE1 CD244 AC090116.1 MYH15 LINC01305 SCARA5 ZNF597 RAI1 LAMB1 ATAD2 ADM2 CHRNA1 GORAB-AS1 ADAMTS1 MMP21 TRIM7 ATRAID NDUFAF2 AC037441.1 WDR25 CHST9 FBXW5 DCAF15 AC021660.2 ZNF451 AC005100.1 FOXA1 GRIN2D TCAF2 HINT2 ZNF302 ITPA PTGR1 CMPK1 FIP1L1 ENSA RALA TBC1D10C TMEM245 COL2A1 TROVE2 HK2 CIAO2A METRNL EPHX1 IAH1 VPS18 ANKRD50 HECTD3 CRBN ZDHHC23 PRR18 ABCF3 CHIC2 TTC21A SLC9A1 THBS2 CRYZ ADAT3 TMEM138 TMEM131 SORD ALG1L9P WWC2-AS2 MED28 BAP1 MSH2 PET100 NEUROD4 JMJD1C CCNH SALL4 NOTCH4 ARID4A HOXC-AS2 DIPK1A SPATA5 SSSCA1 PRPF38A INKA1 CYTH3 OXSR1 RBBP5 DENND4C RNASET2 JAK3 DDX23 ETV5 FAM221A S1PR5 ENPP1 NOLC1 SDR42E2 RHOBTB3 P2RX4 COX11 HEMGN NPTX1 PLD3 CAPN10 CNP TTC17 DLGAP2 AL049629.2 ZNF654 MICALL2 SOX11 OCSTAMP IPO9-AS1 BMPR1B SYVN1 LTC4S PLAC4 LINC01896 TMEM254 CLUAP1 LINC00934 ZNF770 SP5 RNF157 ATE1 B3GALNT2 TSNAXIP1 AL132671.2 NUP43 CYB561A3 ETV6 AP003119.3 VPS13C DCP1B LINC01970 ATIC AL671762.1 MYH7B SNAI2 ZMYM6 JPH3 PXK BAX FCHO2 AJ239322.1 PRKCA AL157702.2 VAV1 ZNF358 AC079612.1 FAM49B TMCC1-AS1 TRMU MATR3_1 RPRML RAB8A EXOC6

Supplemental Table 4.2. The 55 genes upregulated by TFF isolated MSC-EVs and their functions.

Function	Genes
Anti-viral	DDX42
Apoptosis	RPS8, TP53INP2
Extracellular Matrix	RGP1
Immune infiltration	GPX1
Immune suppression	CAPZA1, CHD3, DDX5, G3BP2, LGALS1, PCBP1, PCGF5, PES1, RIOK3, RPS26, SHMT2, TPM3, UPF2, WIPF1, PGAM1
Innate immune response	WDFY1
Migration	ERC1, FSCN1
mRNA trafficking	FYTTD1
Oxidative stress	ALDH1L2
Proliferation	LONP1, ANXA11, AURKAIP1, KHDRBS1, KPNA3, LARP1, LOXL1, MYCBP2, NUAK1, PSMD1, RND3, TCEAL4
Protein trafficking	COPA
Redox equilibrium	CYB5B
Structure	AFF4, PFDN2, PLEC, RDX, RFLNB, TUBB2A, TUBB3
Tumor suppressor	CNN2, COX5B, CBS, CBX5, DLC1, EPB41L2, ERH, SAMD4A, SMAP1

Supplemental Table 4.3. The genes upregulated in each gene family of interest between TFF and UC.

Gene Family	Genes
Glycolysis	ENO1, GAPDH, GPI, PGK1, PGM3
Fatty acid beta-oxidation	ACO2, OGDH, IDH1, CS, FH, SIRT1, SIRT2, SIRT3, SIRT4, SIRT5, SIRT6, SIRT7
MMP	MMP1, MMP10, MMP11, MMP12, MMP13, MMP14, MMP15, MMP16, MMP17, MMP19, MMP2, MMP20, MMP21, MMP24, MMP25, MMP26, MMP27, MMP28, MMP3, MMP7, MMP8, MMP9
IFNγ response	IFIH1, IFIT2, IFIT1B, IFIT2, IFIT3, IFIT5, IFITM1, IFITM10, IFITM2, IFITM3, IFITM5, IRF2, IRF2BP1, IRF2BP2, IRF2BPL, IRF3, IRF4, IRF5, IRF6, IRF7, IRF8, IRF9
Cell Cycle	CCNA2, CCNB1, CCNB2, CCNB3, CCNC, CCND2, CCND3, CCNE1,CCNE2, CCNF, CCNG1, CCNG2, CCNH, CCNI, CCNI2, CCNJ, CCNJL, CCNK, CCNL1,CCNL2, CCNO, CCNQ, CCNT1, CCNT2, CCNY, CDK1, CDK10, CDK11A, CCDK11B, CDK12, CDK13, CDK14, CDK15, CDK16, CDK17, CDK18, CDK19, CDK20, CDK3, CDK4, CDK5, CDK6, CDK7, CDK8, CDK9
Collagen	COL10A1, COL11A1,COL11A2, COL12A1, COL13A1, COL14A1, COL15A1, COL16A1, COL17A1, COL18A1, COL19A1, COL1A1, COL1A2, COL20A1, COL21A1, COL22A1, COL23A1, COL24A1, COL25A1, COL26A1, COL27A1, COL28A1, COL2A1, COL3A1, COL4A1, COL4A2, COL4A3, COL4A4, COL4A5, COL4A6, COL5A1, COL5A2, COL5A3, COL6A1, COL6A2, COL6A3, COL6A5, COL6A6, COL7A1, COL8A1, COL8A2, COL9A1, COL9A2, COL9A3

Supplementary Table 4.4. List of proteins found in each RB30 manufacturing group [Figure 3A].

Group	Proteins
30/TFF CTL and 30UC CTL 65 overlapped proteins	KRT6B ACTB MMP2 SPARC ARHGAP20 ITIH3 ITIH1 ALB ANKRD20A3P VCAN APOA1 KRT14 GC KPRP PTX3 GAPDH CALML5 KRT9 FBLN1 KRT16 SCYL2 HBE1 AVPR1A PDE8A THBS1 COL5A2 TGFBI ITIH2 LGALS3BP THBS2 ABHD8 RHOBTB3 PZP SYNE1 ACACB COL1A2 IGHG1 SLC34A2 A2M SERPIND1 SLC17A8 KRT1 CLCN6 F2 COL1A1 BDP1 KRT10 C2orf74 AHSG NF1 IGKC KRT5 AFP FN1 VTN SPRR2D SBSN SPATA31F1 PCDH17 COL6A1 C3 HBA1 KRT2 HRNR DCD
30/TFF CTL 88 unique proteins	CEP250 ZC3H6 CCDC168 IQCJ-SCHIP1 COL5A1 PPL THBS3 DCN ABCC6 COL3A1 RRBP1 BMAL1 ADAP2 SRGN TENM3 PSD4 ITGB8 LAMA2 CLU ACTG2 TUBA4A PXDN TLN1 COL2A1 COL6A2 TEKT2 CMYA5 SVEP1 ARFIP1 APOD SETBP1 GVQW3 GSN KLHL22 EPN2 LRCH3 KMT2D TUBB2A ESRRA MAPRE1 FBN1 PCOLCE APOB ECPAS F5 ITPRID1 BTBD2 CPN1 BGN KRT8 LSM12 CROCC C3orf20 SPACA3 KCNJ3 EGLN1 SERPINE2 COL6A3 EVPL ERVK-18 ABCB11 POSTN LAMC1 RAP1B C1QTNF3 LINE-1 NEB PRDM2 NUP93 TUBB1 STAT5A ADAR COL12A1 EEF1A1 NEK4 METTL15 APOC3 TUBA1B TSGA10IP GSTK1 STK35 HAPLN1 IGF2R EXPH5 STC2 FRMPD3 APOE TMED6
30/UC CTL 46 unique proteins	FLG2 EP400 FABP5 NAPEPLD ZNF532 PRSS50 DHCR24 SERPINE1 KL SYTL4 WARS1 LOXHD1 JUP CLIP3 PPIL3 CST6 TP53BP1 SPTBN1 DSP SDCCAG8 KRT77 KRT76 SERPINF2 TEX13C SHISA6 SERPINF1 PLEC PIP CFB MFGE8 DMKN UGP2 HR DHX16 UBR4 PHGDH SLURP1 TUBA3D ANXA2P2 ACOT11 S100A7 JMJD1C TRIM68 BAZ1A KRT6C PLOD1
30/TFF CTL and 30UC IFNG 57 overlapped proteins	KRT6B ACTB MMP2 ARHGAP20 ITIH3 NAPEPLD ALB SERPING1 APOA1 KRT14 GC C1S C1R CALML5 KRT9 WARS1 CMYA5 FBLN1 HBE1 AVPR1A PDE8A SERPINF2 FBN1 PCOLCE ITIH2 LGALS3BP ABHD8 PWWP3B TAF11L2 SERPINE2 ACACB COL1A2 IGHG1 A2M KRT1 CLCN6 F2 COL1A1 LAMC1 KRT10 NUP93 AHSG NF1 IGKC KRT5 AFP FN1 HAPLN1 ABI3BP SPATA31F1 PCDH17 COL6A1 HBA1 C3 KRT2 HRNR DCD
30/TFF IFNG 86 unique proteins	ENO3 SPARC FABP5 ITIH1 CSF1 PPL LAMA4 DHCR24 ANKRD20A3P DCN VCAN BMAL1 SRGN TENM3 PTX3 CLU COL2A1 BOD1 ARFIP1 PFKM LAMA1 APOD RBM34 KLHL8 DOCK4 SCYL2 EPN2 SPTBN1 TUBB2A AGBL3 THBS1 GTF2I CEP112 COL5A2 TGFBI EFTUD2 APOB ECPAS PLCH1 F5 ZP2 PIP BTBD2 PCSK2 CPN1 BGN KRT8 RHOBTB3 POLDIP3 C3orf20 PZP SYNE1 HAPLN3 SLC34A2 SPC25 SLC17A8 MFSD13A DAPK1 LAMB1 COL6A3 ANKRD19P TRPM6 SMC1A ABCB11 ACAD10 POSTN C2orf74 STIM2 COL12A1 SLURP1 METTL15 TUBA3D APOC3 RNF150 AMN1 TSGA10IP S100A7 VTN GSTK1 COL19A1 STK35 BICRAL IGF2R SBSN APOE TMED6
30/UC CTL 30 unique proteins	FSTL1 C11orf96 SLC25A16 SRCIN1 PRSS50 INS-IGF2 TGIF1 SYTL4 MUC19 TEKT2 KRT16 SETBP1 FOXD3 CC2D2A AK2 MED8 AGAP3 SLC2A7 THBS2 RIOK1 MYO9A QSOX1 MFGE8 KRT6A CELF4 SRGAP2 SSC5D ZNF711 VILL TSPEAR